ADDIS ABABA UNIVERSITY

COLLAGE OF TECHNOLOGY AND BUILT ENVIRONMET

SCHOOL OF CHEMICAL AND BIO-ENGINEERING

Formulation and Characterization of Wood Polymer Composites (WPCs) from Ethiopian Lowland Bamboo Fibrous particles and Recycled Thermoplastic Polyblends

A Dissertation by Keresa Defa Ayana

Submitted to the School of Chemical and Bio Engineering in Partial Fulfilment of the Requirements for the Degree of Doctor of Philosophy (Ph.D.) in Chemical Engineering (Process engineering)

Advisors: Abubeker Yimam Ali (Associate Professor. Dr. Eng.)

Chang-Sik Ha (Prof. Dr. Eng)

September 2025

Addis Ababa Ethiopia

Statement of the Author

I declare that the content of this submitted dissertation is entirely my own original work, carried out independently. I further certify that Addis Ababa University is permitted to reproduce and publish this work without violating the rights of any third party. I also confirm that this dissertation has not been submitted, either fully or in part, toward the fulfillment of any academic degree or qualification at any other institution.

Keresa Defa Ayana

Signature and Date: Ayana K.Defa (November 28, 2025)

Copyright © 2025 Addis Ababa University All rights reserved

Approval of Dissertation

Addis Ababa University

School of Chemical and Bio Engineering

As a Ph.D. research advisor, I hereby attest that I have read and assessed this dissertation with the following title:

"Formulation and Characterization of Wood Polymer Composites from Ethiopian Lowland Bamboo Fibrous particles and Recycled Thermoplastic Polyblends" Hence, I recommend that it can be submitted as fulfilling the requirements of the degree of Doctor of Philosophy (Ph.D.).

Abubeker Yimam Ali (Assoc.Prof. Dr. Eng)	----------	----------
Advisor	Signature	Date

As members of the Board of Examiners for the Dissertation Open Defence Examination, we certify that we have read and evaluated the dissertation submitted by Keresa Defa Ayana and examined the candidate. We recommend that the dissertation be accepted as fulfilling the requirements for the Degree of Doctor of Philosophy (Ph.D.) in Chemical Engineering (Process Engineering Stream), with due consideration to its academic standards.

Dr. Anteneh Marelign Beyene (Ass.Prof.)	----------	----------
Chairperson	Signature	Date
Prof. Dr. Hirpa Gelgele Lemu	----------	Oct. 18, 2025
External Examiner	Signature	Date
Dr.Melakuu Tesfaye Alemea (Asso. Prof.)	----------	----------
Internal Examiner	Signature	Date

Executive Summary

Increasing global concerns over environmental sustainability and the responsible use of natural resources have increased efforts to develop eco-friendly materials derived exclusively or partly from renewable sources. One of these efforts aim to mitigate the environmental degradation and resource depletion caused by the widespread use and poor end-of-life management of petroleum-based synthetic polymers, which are non-biodegradable and accumulate in large volumes. Within this context, the valorization of thermoplastic waste through innovative recycling and repurposing strategies has emerged as a key solution under the circular economy framework. Concurrently, increasing urbanization and population growth, along with the environmental drawbacks of conventional construction materials, highlight the urgent demand for more sustainable alternatives. One promising alternative is the formulation of Wood Polymer Composites (WPCs), which effectively combine thermoplastic wastes as matrices with bio-based fibrous fillers, providing a sustainable pathway toward affordable building components and environmentally friendly construction materials.

In this doctoral study, a wide range of WPC formulations was developed using six recyclable thermoplastics sourced from post-consumer and electronic waste as matrices and fibrous particles from Ethiopian indigenous lowland bamboo (*Oxytenanthera abyssinica*, LLB) as a novel reinforcement. Key formulation variables—including reinforcement content, matrix composition, polymer blending, particle size, and interfacial modifications through coupling and crosslinking agents—were systematically investigated to evaluate multiscale reinforcement mechanisms and synergistic interactions within multipurpose thermoplastic matrices. Composite prototypes were prepared by compounding in an internal Haake mixer configured with a counter-rotating twin-screw, followed by compression molding into board panels. Their performance was comprehensively assessed through fundamental mechanical testing, thermal stability and dynamic mechanical analysis, water absorption, dimensional stability, and interfacial characterization. All formulations were benchmarked against commercial polyolefin-based WPCs to assess their viability as sustainable alternatives within the four main sub-studies outlined below.

The first sub-study investigated recycled polyethylene polyblends—comprising linear low-density (rLLDPE), medium-density (rMDPE), and high-density (rHDPE)—sourced from

municipal waste as matrix materials. Their chemical composition, heavy metal and polycyclic aromatic hydrocarbons (PAHs) content, and thermal degradability behavior were characterized including the compositions of LLB biomass. The ultimate tensile strength (TS) and flexural strength (FS) decreased as the LLB content increased from 40% to 60%; however, the best mechanical performance was achieved at 40% loading, primarily due to improved melt flow and better matrix encapsulation of the bamboo particles. Nevertheless, even at the higher LLB content (60%), the incorporation of MAPP effectively preserved substantial mechanical integrity by enhancing interfacial adhesion between the matrix and the reinforcement. In contrast, both Flexural modulus (FM) and tensile modulus (TM) show an increasing trend with increased with higher LLB loadings in all formulations, while the influence of MAPP on these properties was minimal. Equal-phase melt blends demonstrated distinct improvements over separate-phase blends, likely due to thermally induced crosslinking and enhanced compatibility despite inherent immiscibility. Furthermore, in situ compatibilization with maleic anhydride grafted polypropylene (MAPP), combined with balanced blending of rLLDPE, rMDPE, and rHDPE, yielded significant property enhancements while retaining desirable characteristics of the constituent polymers.

Next, WPCs were developed using an equal blend of recycled polystyrene (rPS) from electronic waste and rHDPE from post-consumer packaging based on the inherent properties of the polymers before blending. rHDPE may provide ductility and toughness, while rPS may contribute to rigidity, hardness, and dimensional stability. The LLB-reinforced blend composites were processed by incorporating both MAPP and dicumyl peroxide (DCP) to promote chemical level interaction. The study assessed the comparative effects of LLB particle size, equal polymer blend composition, and LLB content. Results demonstrated that reactive blending with MAPP and DCP substantially enhanced mechanical and thermal properties compared to uncoupled blends. Particularly, formulations containing LLB particles below 500 μm synergistically improved stiffness, toughness, and rupture properties, highlighting application of new insight to WPC formulations.

Subsequently, further investigations were conducted on a 50/50 blend of rHDPE and rPS reinforced with LLB particles below 500 μm, compatibilized using either MAPP or SEBS-g-MA (triblock copolymer of styrene–ethylene–butylene–styrene block copolymer (SEBS) grafted

with a maleic anhydride) in combination with 1% DCP for crosslinking. The study evaluated various compatibilizer loadings (3%, 5%, 7%, and 10%) to assess their effects on composite performance. Results demonstrated that SEBS-g-MA markedly enhanced water resistance, dimensional stability, and thermal degradation behavior, with impact strength and interfacial compatibility improving linearly across all loading levels. In contrast, MAPP combined with DCP contributed primarily to improvements in tensile and flexural properties as well as dynamic mechanical performance. Optimal composite performance was achieved at 5% MAPP or 3% SEBS-g-MA in combination with 1% DCP, yielding the highest overall strength while the remaining property remained significantly at all loading .

Finally, high-performance WPCs were developed using recycled acrylonitrile butadiene styrene (rABS) and high-impact polystyrene (rHIPS) matrices reinforced with 50% LLB particles. Ethylene propylene diene monomer (EPDM) and methyl methacrylate-butadiene-styrene (MMBS) were applied synergistically with maleic anhydride (MA) and DCP to enhance multipurpose toughening and interfacial compatibility. EPDM and MMBS contents (5–15%) were varied to optimize mechanical performance, while MA and DCP were fixed at 1% and 0.5%, respectively. Comprehensive evaluations showed that MMBS-modified rABS and rHIPS composites (10% MMBS, 1% MA, 0.5% DCP) achieved superior flexural strength (74.5 MPa), modulus of rupture (6.09 GPa), and dimensional stability (+65.65%) compared to uncoupled and unmodified composites. EPDM enhanced thermal stability and reduced water uptake in both systems, though excessive amounts slightly reduced stiffness and strength, while still outperforming unmodified matrices.

In conclusion, the formulated WPCs offer lightweight, eco-efficient, low-carbon, and sustainable construction materials that support circular resource utilization by valorizing waste thermoplastics and utilizing the untapped potential of indigenous Ethiopian LLB particles. These composites achieved performance comparable to or exceeding that of commercial polyolefin-based WPCs, without the need for fiber extraction or energy-intensive nanoreinforcement processes.

Keywords: *Wood plastic composite, Interfacial compatibility, Bamboo fibrous particles, cascading thermoplastic waste, Sustainable building materials, Postconsumer thermoplastic valorization, polyblend polymeric matrices*

Dedication

This dissertation is lovingly dedicated to my family—visionaries who recognized the transformative power of education long before its rewards could be seen. In times marked by hardship and uncertainty, they made countless sacrifices, giving all they had to ensure I received a formal education. Their unwavering commitment laid the foundation of my academic journey and shaped me into a better version of myself. This work is dedicated for enduring love, belief, and sacrifice of my family.

Acknowledgements

All praise and thanks be to Almighty God, whose boundless grace has sustained me throughout this journey.

I wish to express my profound gratitude to my advisors for their unwavering support. I am sincerely thankful to Dr. Ing. Abubeker Yimam Ali for his open-minded mentorship, and to Prof. Dr. Chang-Sik Ha for his kind guidance, constructive criticism, and continual encouragement. I am especially grateful to Prof. Ha for his generous support during my most challenging times and for kindly hosting me for a one-year research stay at the Polymer Composite Laboratory of Pusan National University. I am also thankful to the former BioHome project team—Prof. Andreas Krause, for hosting my three-month research stay at the Thünen Institute, Hamburg University, and providing invaluable feedback; and to Dr. Ing. Esayas Gebreyouhannes and Dr. Goran Schmidt, for their generous support . I also gratefully acknowledge the German Federal Ministry of Education and Research for partially funding my local studies and facilitating my research visits to Hamburg University.

I deeply appreciate the collaboration and kindness of the Polymer Composite Laboratory at Pusan National University, especially Dr. Siva Gangi Reddy Nagella, Mr. Joon Woo, and Mr. Siwoo. I also thank the Korea Institute of Materials Convergence Technology (Mr. Jong-Man Yoo and Dr. Kyung Man Choi) and KATRI Testing & Research Institute (Mr. Woohong Jeon) for their technical support. Similarly, I am very grateful to the staff of the School of Chemical and Bio Engineering, College of Technology and Built Environment, Addis Ababa University—particularly Mr. Hinsta Gebresillassie and Dr. Ing. Shimelis Kebede Kassahun—for their invaluable assistance. Additional my gratitude goes to LG Co. (South Korea) and NANODAS PLC (Ethiopia) for generously supplying recycled raw materials. Moreover, I am profoundly thankful for the one-year research stay made possible by the Global Korea Scholarship (GKS), funded by the National Institute for International Education (NIIED) of South Korea; your support was exceptional to this work.

Finally, I extend my deepest gratitude and love to my family, whose unwavering commitment laid the foundation for my academic journey and shaped me into a better version of myself. You are my deepest gratitude and love.

List of Peer Reviewed Publications

Paper I

K.D. Ayana, C.S. Ha, A.Y. Ali, Comprehensive Overview of wood polymer composite : Formulation and technology , properties , interphase modification , and characterization, Sustain. Mater. Technol. 40 (2024) e00983.
https://doi.org/10.1016/j.susmat.2024.e00983

Paper II

K.D. Ayana, A.Y. Ali, C.S. Ha, Wood Polymer Composites Based on the Recycled Polyethylene Blends from Municipal Waste and Ethiopian Indigenous Bamboo (Oxytenanthera abyssinica) Fibrous Particles Through Chemical Coupling Crosslinking, Polymers 16 (21) (2024).
https://doi.org/10.3390/polym16212982

Paper III

K.D. Ayana, J. Man, Y. Woohong, J. Kyung, M. Choi, C.S, Ha. A.Y. Ali, Wood polymer composite (WPC) formulation from Ethiopian indigenous lowland bamboo particles and post-consumer plastic blends: synergetic and dual effects of both coupling agent and organic crosslinking catalyst, Macromol. Res. 33 (2025) 479–496.
https://doi.org/10.1007/s13233-024-00347-6

Paper IV

K.D.Ayana, C.S. Ha, A.Y. Ali, Property optimization of wood polymer composites (WPC) formulated from recycled thermoplastic blends and bamboo particles reinforcements by cross-inking coupling agent and initiator catalyst, Compos. Interfaces (2025) 1–23.
https://doi.org/10.1080/09276440.2025.2467689.

Paper V

K.D Ayana, C.S, Ha, A.Y Ali, A Valorization of valuable Thermoplastic Waste from E-Waste for High-Performance Bamboo fibrous particles-Reinforced Composites via Chemical Compatibilization and Toughening agents **(under review)**

Table of contents

Keresa Defa Ayana

List of Figures

List of Tables

Acronyms and Abbreviations

ABS	Acrylonitrile Butadiene Styrene
ASTM	American Standard of Testing Materials
DCP	Dicumyl Peroxide
DSC	Differential Scanning Calorimeter
DTGA	Derivative thermogravimetric analysis
DTMA	Dynamic Thermal mechanical analysis
ELLB	Ethiopian Low land Bamboo
EPDM	ethylene propylene diene monomer
FS	Flexural strength
FTIR	Fourier Transform Infrared
HDPE	High Density Polyethylene
HIPS	high-impact polystyrene
HPAE	High-performance anion exchange chromatography
ISO	International standard organization
LLDPE	Linear Low-density Polyethylene
MAPP	maleic anhydride grafted polypropylene
MDPE	Medium Density Polyethylene
MFI	Melt flow index
MMBS	methyl methacrylate-butadiene-styrene
MOE	Modulus of elasticity (stiffness)
MOR	Modulus of Rapture
MSW	Municipal solid waste
PMC	Polymer matrix Composites
PS	Polystyrene
SEBS-g-MA	Styrene-ethylene-butylene-styrene grafted with maleic anhydride
SEM	Scanning Electron Microscopy
TGA	Thermogravimetric analysis
TS	Tensile strength
WPC	Wood Plastic Composites

CHAPTER ONE
INTRODUCTION

1.1 Background

The current critical sustainability challenge, resulting from resource constraints on a global scale, impacts both present society and future generations. This challenge has prompted the search for sustainable products and processes aimed at minimizing resource consumption and mitigating environmental deterioration [1,2]. As a result, a new concept of circular resources use involving low-carbon footprint through the maximum efficient utilization of renewable resources and the mitigation of non-renewable resource exploitation, involving a closed-loop resource flow have emerge [3]. The construction and plastic industries which use abundant non-renewable resources are significantly impacted by this shift and increasingly challenged by the rising demand for affordable building materials driven by the dynamic wave of urbanization and population growth [4,5].

Traditional construction materials such as cement, steel, and virgin plastics are not only resource-intensive but also associated with significant environmental drawbacks, including high energy consumption and carbon emissions [6]. At the same time, the growing accumulation of non-biodegradable plastic waste presents a major environmental burden, contributing to climate change, biodiversity loss, and inefficient resource use [7]. Polymeric plastic products have become essential to modern life, serving as vital materials in industries like construction, automotive, consumer goods, and electronics, etc. Their widespread use is driven by properties such as low weight, corrosion resistance, low density, design flexibility, ease of production and cost-effectiveness, all of which continue to drive global demand, consumption, and associated waste generation [8,9]. Much of these plastic wastes ends up infiltrating terrestrial, freshwater, and marine environments due to its extremely slow or no degradation rate. Consequently, there is a growing shift toward the cascading use of recycled plastics to reduce carbon footprints, limit single-use practices of linear economies, and address environmental challenges. This approach extends product lifecycles by reintegrating recycled materials into production, offering a more sustainable alternative to landfilling, incineration, and other disposal methods [4,10–12].

Recycling has become integral to many plastic life cycles, with Wood Plastic Composites (WPCs) emerging as an intermediary cascade chain for valorization of valuable thermoplastic waste into a promising affordable building materials for global housing deficit specifically in the packed communal housing units [13]. WPCs are one of such typical polymer-based composites that cover a wide range of thermoplastics matrix such as polyethylene (PE), polypropylene (PP), polyvinyl chloride (PVC), polylactic acid (PLA), and polyoxymethylene (POM) and variable amounts of lignocellulosic particles and/or fibers as the dispersed phase [3,14–17]. Plant-based fibers and particles offer renewable, low-cost, and non-toxic alternatives to synthetic reinforcements in WPCs, with advantages such as carbon sequestration, high specific strength, and reduced machine wear. Despite often being overlooked in favor of mineral fibers, their sustainability and environmental benefits make them promising for developing nearly climate-neutral WPC [18,19].

WPCs is mostly produced as low-cost social housing units used for non-load-bearing applications of building materials components which are suitable for use in humid environments preferably as hydrophobic matrix of WPCs encapsulates the fibers. They serve as potential substitutes for medium-density fiberboard (MDF) and high-density fiberboard (HDF) [10]. Furthermore, WPC use extends to both internal and external applications even though it is quite impossible to fully replace the best conventional constructions materials like steel and concrete cement within the current technologies. Internally, WPCs are applied in kitchen cabinets, wall and door panels, bathroom doors, window frames, decorative panels, office and household furniture, partition systems, roof tiles, sliding panels, and flooring [4,14]. Externally, they are used for decking, wall cladding, railings, decorative garden furniture. Beyond construction, WPCs formulated from short fibers and/or particles and produced via thermoforming are used in automotive parts, such as door panels, noise insulation panels, headliner panels, and electrical appliance packaging [4]

The dispersed phase in WPCs includes particles, flour, and nanosized cellulose-based reinforcements, derived from lignocellulosic biomass, agricultural residues, and industrial by-products through cutting, milling, grinding, or extraction. Common sources include kenaf, flax, hemp, jute, pine, poplar, hemp, spruce, sisal, maple, oak, and other [4,15,19]. While nanosized reinforcements fibers could potentially enhance stiffness and structural stability in WPCs, their production involves energy-intensive fine grinding and the addition of coupling agents which significantly elevate processing costs and carbon footprint. Moreover, the recovery of nanoscale

dimensions of highly fibrillated nanocellulose fibers remain challenging due to filtration difficulties, and complex structural characteristics, which hinder property control and scalability for commercial use in WPCs [20]. Similarly, larger reinforcing elements are susceptible to agglomeration, often resulting in composites with inferior surface quality. Consequently, flour- or particle-based morphologies are generally favored in commercial WPC production, as the retention of lignin and extractives in the biomass contributes to improved moisture resistance and durability, owing to their some of their inherent hydrophobicity [13,16,17]. However, WPCs have certain drawbacks, such as lower strength and stiffness compared to synthetic fibers based composites, as well as moisture sorption and swelling when compared to solid polymer matrices [21]. Similarly, limited interfacial adhesion results from the distinct chemistry of the hydrophilic lignocellulosic fibers and hydrophobic matrix requires coupling or crosslinking agents for effective compatibility at the interphase [22].

Moreover, WPC properties and their functional performance are influenced by several factors like the fractional composition, type of polymer matrix, and the characteristics of the filler or reinforcement such as species, particle size, and aspect ratio. The particle size and morphology of the dispersed phase affect WPC properties in multiple ways. Larger particles are typically used as reinforcements but may not be fully encapsulated within the plastic matrix, whereas smaller particles are often fully embedded in the matrix and significantly impact melt viscosity and flow behavior [23]. This is a key consideration in these studies, which explore the composition of both polyblend polymer matrices and dispersed phases at higher and lower loadings using two distinct size fractions to evaluate performance at both extremes. Furthermore, processing parameters such as temperature, pressure, mixing time, and screw rotation speed of the extruder critically influence the WPCs performance [21,24]. Temperature is a critical processing parameter in WPC production constrained by melting temperature of the thermoplastic and onset thermal degradation of the biomass which begins between 200–220 °C [19]. This limits the selection of thermoplastics to those with melting points below this range. Despite the complexity and interdependence of these influencing parameters, certain factors can be controlled prior to WPCs formulation.

A major limitation in WPC performance arises from the inherent incompatibility between hydrophobic thermoplastics and hydrophilic lignocellulosic biomass, which is rich in hydroxyl and carboxyl groups, resulting in weak interfacial bonding [25]. To overcome this, current research

focuses on enhancing interfacial compatibility by modifying fiber or polymer surface chemistry, improving wettability, removing weak boundary layers, and forming stronger interphases. Interface reinforcement relies on mechanisms such as inter-diffusion, electrostatic attraction, chemical bonding, mechanical interlocking, and secondary interactions including hydrogen bonding and van der Waals forces, achieved through chemical, physical, physiochemical, and nanotechnological strategies [18,26]. Among these, coupling agents and compatibilizers have proven particularly effective in improving WPC performance across multiple properties without the need for chemical surface treatments. In contrast, solvent-based approaches, while useful, add complexity and cost due to solvent recovery.

Coupling agents are bifunctional molecules that enhance interactions between polymer matrix chains and fibrous particles through in situ reactive compatibilization [27] or graft copolymerization with reactive polyfunctional monomers, such as maleic anhydride (MA) and its analogues [29]. A variety of coupling agents including silanes, titanates, zirconium aluminates, and maleic anhydride-grafted copolymers have been widely applied in WPC research [4,28]. Among these, maleated polyethylene (MAPE) and maleic anhydride-grafted polypropylene (MAPP) have shown effectiveness in polyolefin-based WPCs, forming covalent and hydrogen bonds that promote uniform microstructures, enhanced dimensional stability, and improved mechanical properties[19,29]. Urethane linkages can also form between isocyanate groups and the hydroxyl groups of natural fibers [4], while silanization—where silanes hydrolyze into reactive silanol groups—further facilitates strong bonding with fiber hydroxyl groups [30–32]. Additionally, various graft polymerization techniques [32,33] have been successfully employed to enhance interfacial adhesion and mechanical performance in WPCs.

Recent research on WPC formulations has primarily focused on neat polymeric matrices reinforced and various dispersed phases. Polyethylene variants, including LDPE [34] and HDPE [35,36], along with other polymers such as PP [37–39] and rarely PVC [40,41], have been widely studied. These investigations explored the influence of nano-reinforcement incorporation, matrix composition, compounding methods, surface treatments, and coupling agents on mechanical performance, thermal stability, water absorption, and durability of WPCs [4].

Driven by growing demand for wood fibers and neat polymer matrices, recent trends have shifted toward alternative natural fibers and recycled thermoplastic polyblends as secondary raw materials

form other alternatives sources. Municipal solid waste (MSW) represents a significant source of recycled plastics; however, only 7.6% of the roughly 31 million tons of annual plastic waste—12.4% of MSW—is currently recycled, highlighting the urgent need for more efficient recycling systems and sustainable material innovations [42]. Similarly, thermoplastic waste from electrical and electronic equipment (EEE), which generally contains 10–30% plastics depending on the specific stream or category, presents additional potential [43]. Within this category, general-purpose polystyrene (PS), high-impact polystyrene (HIPS), and acrylonitrile butadiene styrene (ABS) are especially promising due to their widespread use as engineering thermoplastics that bridge commodities and performance-grade recyclable engineering plastics. Findings across the literature clearly demonstrate that WPCs produced from recycled plastics can achieve levels of mechanical performance, dimensional stability, interfacial bonding, and durability comparable to, and in some cases exceeding those manufactured with virgin plastics. Such promising outcomes have provided strong motivation to valorize post-consumer plastics as secondary raw materials in WPC manufacturing, aligning with circular economy principles. In addition, ongoing research efforts emphasize improving performance through multifunctional polymeric coupling agents and versatile impact modifiers.

Considering these challenges and opportunities, this dissertation presents a comprehensive investigation of WPCs reinforced with underutilized indigenous Ethiopian lowland bamboo (LLB) fibrous particles, representing the first known application of LLB fibrous particles in such formulations. Thermoplastic matrices comprised thermomechanically recycled post-consumer polyolefins (LLDPE, MDPE, HDPE), used individually and in novel polyblends not previously reported in the literature. Equal melt blending was employed to explore synergistic effects from combining low-cost recycled LLDPE with MDPE and HDPE, potentially facilitated by thermal cross-linking and chemical interactions. Additionally, recycled polystyrene (rPS) from electronic waste was blended with rHDPE to examine their synergetic performance at varies compositions including the influence of LLB particle size while simultaneously MAPP, DCP and SEBS-g-MA introduced to evaluate their efficiency. The composites were systematically characterized for mechanical performance, water absorption, thermal stability, and degradation resistance. Further formulations employed rHIPS and rABS as matrices, incorporating multipurpose elastomeric impact modifiers (EPDM and MMBS) for the first time to enhance toughness and achieve balanced performance through in situ reactive melt compounding with MA and DCP. All composites were

produced using a pilot-scale Thermo Scientific HAAKE Reomix 3000 OS equipped with a counter-rotating twin-screw extruder, followed by hot-pressing into WPC panel prototypes. Processing parameters—such as temperature, screw speed, and residence time—were carefully controlled via PolyLab software. The resulting WPCs were then benchmarked against commercial products and existing literature to evaluate their suitability as sustainable building materials.

1.2 Statement of problem

Population growth and rapid urbanization have significantly increased the demand for building materials, placing substantial pressure on limited natural resources, many of which are produced through unsustainable and resource-intensive methods [2]. For example, the production of ordinary Portland cement (OPC) is highly energy-intensive and emits significant amounts of CO_2. On average, producing one ton of OPC results in approximately one ton of CO_2 emissions, contributing to a projected increase of 71 million tons of CO_2 by 2030 under current trends [3]. Similarly, the introduction of fossil hydrocarbons into modern society has triggered an irreversible shift, characterized by a rising global demand for energy and material goods—particularly plastics. [45]. Among these productions volumes 55% is discarded or land filled into open environments where it can take hundreds of years to decompose. Furthermore, 25% is incinerated which can reduce the volume of plastic waste and generate energy while simultaneously releasing harmful pollutants and greenhouse gases such as carbon dioxide, dioxins, and furans into the atmosphere, exacerbating climate change [26]. Finally, only 20% is recycled reflecting significant deficiencies in global recycling systems [45]. However, integrated waste management methods like source reduction, reuse, recycling, landfilling, and waste-to-energy processes were adopted long before to manage vast volume plastic waste. Recycling constitutes a central component of the circular resource utilization within the context of the contemporary circular economy approach, with both thermomechanical and chemical recycling routes extensively investigated[46–48]. Chemical recycling methods—such as glycolysis, pyrolysis, ammonolysis, hydrogenation, hydrolysis, gasification, methanolysis, and cracking—can complement mechanical recycling. Nevertheless, these processes are capital-intensive and still underdeveloped [49].

While there is no single universal solution to the complex issue of plastic waste, certain strategies have shown considerable promise. One such approach is the thermomechanical recycling of various thermoplastics. When this method is combined with improved polymer blending and

compounding using lignocellulosic fillers, it presents significant potential for the development of wood–plastic composites (WPCs). This strategy serves as a promising intermediate step in the cascade utilization of abundant and sustainable lignocellulosic biomass with recyclable thermoplastics, transforming them into valuable secondary materials for WPC formulations prior to final disposal through landfilling or energy recovery [3]. Moreover, the growing demand for sustainable, high-performance materials has intensified research into WPCs, which combine thermoplastic matrices with lignocellulosic reinforcements.

In this context, bamboo biomass constitutes a substantial but underutilized resource potential in Ethiopia. The country is home to two main bamboo species of *Oxytenanthera abyssinica* (Lowland Bamboo, LLB) and *Yushania alpina* (Highland Bamboo) which collectively cover over 1.47 million hectares, accounting for 67% of Africa's and 7% of the global bamboo coverage [50,51]. LLB has the solid cross-section and dominates 85% of national bamboo coverage, while HLB, which has a hollow cross-section accounts for the remaining 15% [26,52]. Globally, bamboo-related trade generates between USD 5–7 billion annually, a figure comparable to the USD 8 billion earned from tropical timber trade. Despite its potential, Ethiopia's indigenous LLB bamboo remains underutilized LLB is used in traditional ways with less value additions and with insignificant engineering applications because of their very limed diameter unlike conventional woody materials. Currently, bamboo contributes only USD 5.7 million annually to Ethiopia's GDP, representing about 0.43% of global bamboo imports [53,54] and resulting in a trade deficit. One pathway of contributing to the estimated USD 1.2 billion (2–3% of the national GDP) in annual revenue from the full utilization of Ethiopia's bamboo resources [53] is its integration with recycled thermoplastic materials for WPC production. This approach can simultaneously support socio-economic development, likely through the production of sustainable building materials and the valorization of secondary waste streams.

The performance of WPCs is influenced by numerous factors of which the compatibility between the matrix and fibrous filler, their compositions and particle size and the processing conditions are especially critical [7]. To address interfacial compatibility, several surface modification techniques have been explored. These include chemical treatments (alkaline treatment or mercerization, esterification via acetylation), the use of coupling agents (e.g., maleic anhydride-grafted polypropylene, silanes, acrylonitrile), grafting polymerization, and physical methods (e.g., corona

discharge, plasma treatment, and steam reforming) [4]. Moreover, monomers such as maleic anhydride (MA) and its derivatives are widely used for polymer modification with some applications already reaching commercial viability [55]. This is because simultaneous in situ melt reactive compatibilization and multimonomer graft copolymerization alternatives to solvent-based surface treatments, minimizing secondary waste and reducing the complexity and cost of solvent recovery and separation [56]. Similarly, performance of WPCs ware enhanced using recyclable multifunctional polymers, such as poly(styrene-b-butadiene-b-styrene), poly(styrene-b-ethylene-butylene-b-styrene), methacrylate-butadiene-styrene terpolymer, poly(styrene-b-isoprene-b-styrene), and poly(styrene-co-methyl methacrylate-co-glycidyl methacrylate) [57]. Notably, the use of polystyrene-block-poly(ethylene-random-butylene)-block-polystyrene grafted with maleic anhydride (SEBS-g-MA) has shown significant improvements in WPC properties[58]. SEBS contributes excellent UV and heat resistance, enhanced toughness, and better molecular entanglement with polyolefin matrices [59]. The MA groups further improve compatibility with natural fibers [60].

Additionally, recyclable thermoplastic elastomers (TPEs) enhance versatile properties of WPCs. Their dual-phase structure of rigid and flexible segments combines thermoplastic processability with rubber-like elasticity, counteracting the reduced impact strength and toughness often caused by natural fiber reinforcements, while reactive melt mixing or compatibilization, often involving maleic anhydride grafting [7], further can improve melt compounding, processability, and overall performance. Common such as TPEs includes EPDM, SEBS, acrylonitrile-butadiene rubber (NBR), chlorinated polyethylene (CPE), ethylene vinyl acetate (EVA), polyisobutylene (PIB), maleic anhydride-grafted EPDM, MMBS, and poly(styrene-co-methyl methacrylate-co-glycidyl methacrylate. Notably, EPDM—both neat and grafted with MA—is particularly valued for enhancing toughness through cavitation and shear-yielding mechanisms, while also providing exceptional resistance to chemicals, oxidation, ozone, heat, and harsh environmental conditions. However, few studies have focused on terpolymer PP/EPDM mixture or as the core matrix for WPCs, which often results in weak matrix performance, though EPDM shows better impact strength when combined with other WPC formulations [4,30,61].

Similarly, MMBS, featuring a soft butadiene-styrene copolymer core and a hard poly(methyl methacrylate) (PMMA) shell, is another impactful TPE category that offers high stiffness and

excellent miscibility with polymer matrices. While few related studies incorporating MBS as an toughening agents [62], available report indicate significant improvements. In this work, extensive investigations of both EPDM and MMBS as the multipurpose WPCs performance modifiers are conducted with new insights into WPC formulations.

In parallel, a wide body of research have investigated the use of polymeric thermoplastic matrices combined with various lignocellulosic fibers to produce WPCs using the different wide range of lignocellulosic dispersed phase reinforcements in the form of particles or flour [4,16,17]. Most of these polymeric thermoplastic matrices mostly neat but including their respective recycled one are LLDPE [34], HDPE [63,64] [8,65–68], PP [18, 30-32] and PVC [40,41] are utilized in the WPC applications. Similarly, More recently, studies have extended to thermoplastics recovered from electronic waste streams, particularly rHIPS and rABS which have been reinforced with conventional wood fibers to investigate their mechanical, thermal, and morphological performance [56,71–75].

Despite these advances, several areas remain uninvestigated. First, no prior studies have thoroughly characterized WPCs formulated from three potential recycled polyethylene (PE) waste fractions—specifically polyblends composed of rLLDPE, rMDPE, and rHDPE— either individually or in blended ratios as the polymer matrices. Moreover, the reinforcement potential of short, fibrous LLB particles with a wide size distribution has not been fully explored. Its integration into WPCs, particularly when compatibilized with commercially available coupling agents such as MAPP, could yield improved interfacial bonding, thermally induced crosslinking, and enhanced immiscibility balance in polyblend matrices. Furthermore, the influence of blending highly contaminated rLLDPE with rMDPE and rHDPE on composite properties has not been adequately investigated, nor has the retention of key performance properties in such blends.

Second, while rHDPE and rPS have been separately employed in WPCs, most studies focus on single waste streams with fixed compatibilizer concentrations. The synergistic performance of polyblends combining rHDPE from post-consumer waste with rPS from WEEE sources, particularly when reinforced with LLB particles is not investigated. Third, the optimization and comparative effectiveness of commercial MAPP and SEBS-g-MA, crosslinked with DCP, with

respect to the key mechanical, thermal, and interfacial properties of WPCs, remain largely uncharacterized.

Fourth, recycled engineering thermoplastics derived from WEEE—specifically rABS and rHIPS—are incorporated into WPCs to broaden application potential. The demand for these materials is growing due to industrialization in sectors such as electronics, automotive, and urban construction. However, no comprehensive studies have evaluated the effects of varying EPDM and MMBS ratios in rABS- and rHIPS-based WPCs reinforced with natural fibers. In particular, the influence of in situ melting reactive compatibilization using MA and crosslinking with DCP remains largely unexplored.

Considering these gaps, this work undertakes a comprehensive investigation of WPCs formulated from diverse recycled thermoplastic matrices, reinforced with fibrous LLB particles, and compatibilized using multifunctional coupling strategies. Specifically, the study addresses: (i) reinforcement of polyblends of rLLDPE, MDPE, and rHDPE with LLB particles, with a focus on mechanical, thermal, and interfacial properties; (ii) synergistic compatibilization of rHDPE–rPS blends based WPCs using MAPP, SEBS-g-MA, and DCP; (iii) optimization of compatibilizer compositions to enhance WPC performance; and (iv) evaluation of rABS- and rHIPS-based WPCs, toughened with EPDM and MMBS, reinforced with LLB particles and processed via in situ reactive compatibilization.

Across these investigations, the study focused on developing eco-efficient, low-carbon composites that valorize recycled thermoplastics and incorporate indigenous Ethiopian lowland bamboo, organized into sub-studies aimed at affordable WPC formulations for non-load-bearing and semi-structural building applications, with performance benchmarked against commercial WPCs.

1.3 Objective of the research Work

1.3.1 General objectives

The general objective of this study is to formulate, characterize, and evaluate WPCs reinforced with Ethiopian indigenous LLB particles dispersed in recycled thermoplastic polyblend matrices from post-consumer and electronic waste: enhancing interfacial compatibilization through cost-effective in situ melt processing, examining the synergistic effects of coupling and crosslinking

agents, as well as multipurpose copolymer impact modifiers, as specifically out lined as the following specific objectives.

1.3.2 Specific objectives

- To comparatively evaluate WPCs from recycled polyethylene polyblends (rLLDPE, rMDPE, rHDPE), including equal blends and MAPP, focusing on interfacial adhesion, mechanical strength, and thermal stability.
- To assess WPCs from rPS/rHDPE blends reinforced with LLB particles via in situ reactive blending with MAPP and DCP, evaluating the effects of particle size and composition on mechanical, thermal, and dynamic thermal properties.
- To investigate WPCs from rHDPE/rPS (1:1) blends reinforced with equal LLB particle content, compatibilized with varying MAPP and SEBS-g-MA levels in the presence of DCP, assessing mechanical, impact, thermal, water absorption, and dimensional properties.
- To formulate and evaluate high-performance WPCs from rABS and rHIPS reinforced with LLB particles, using MA and DCP with varying EPDM and MMBS content to optimize mechanical strength, dimensional stability, thermal properties, and morphology

1.4 Significance of the work

This research plays a vital role in advancing sustainable building materials by promoting circular economy practices and the valorization of locally available resources. Although the global WPC industry is progressing, Ethiopia still faces a shortage of eco-friendly construction materials, despite possessing Africa's largest and underutilized reserves of fast-growing indigenous bamboo biomass. By utilizing Ethiopian lowland bamboo reinforcements and recycled thermoplastics, this study supports sustainable material use, particularly in rural development, by encouraging local resource utilization and strengthening value chains for affordable construction. Converting abundant natural fibers and plastic waste into WPCs through cost-effective, low-tech processes not only helps reduce plastic pollution but also can create income opportunities for local micro-enterprises. In the long term, this approach can drive innovation, reduce dependency on imported materials, reduce the trade deficit in the construction sector, and open new markets for local recycled and bio-based materials.

1.5 Scope of the study and organization of the dissertation

The scope of this work is structured into four main parts (Chapters III to VI), following article-based dissertation format organized into seven chapters as follows.

Chapter I: Introduces the research context, outlining the background, problem justification, objectives, significance and scope of the work, and organization of the dissertation.

Chapter II: Reviews WPCs in terms of formulation, manufacturing technologies, properties, interphase modification, and characterization. Summarizes recent developments and benchmarks in WPC formulations using natural reinforcements and recycled plastics as secondary resources. The effects of polymeric matrices and reinforcements on mechanical performance are comprehensively examined to better comprehend research trends, challenges, and unresolved issues in advancing WPCs as sustainable green building materials (*Paper I*).

Chapter III: This chapter presents the results of WPC formulations developed from recycled LLDPE, MDPE, and HDPE polyblends obtained from municipal solid waste. The study involves characterization of the recycled matrices in terms of chemical composition, contamination levels (e.g., heavy metals and polycyclic aromatic hydrocarbons), and thermal properties. Concurrently, the indigenous Ethiopian lowland bamboo biomass is analyzed for its cellulose, hemicellulose, and lignocellulosic content. The mechanical performance of the resulting composites, including tensile strength, modulus of elasticity, flexural properties, and impact resistance, is evaluated. Furthermore, interfacial adhesion and overall composite performance with MAPP compatibilization was examined using FTIR, SEM, and TGA (*Paper II*).

Chapter IV: This chapter examines WPCs fabricated from blend hybrid matrices of rPS (derived from electronic waste) and rHDPE (post-consumer waste), melt-compounded with LLB particles through in situ reactive blending and in situ compounding. It emphasizes the effects of bamboo particle size and matrix composition on the mechanical and thermal properties of the composites, with reactive compatibilization achieved using MAPP and DCP. Additionally, a comparative analysis of uncoupled versus compatibilized blends were conducted, considering the influence of matrix composition, compatibilizer content, reinforcement level of wider particle size distribution, and their combined effects on strength, stiffness, and thermal stability (*Paper III*).

Chapter V: This chapter investigates WPCs based on a 50/50 weight blend of rHDPE/rPS reinforced with LLB particles, focusing on optimizing compatibilizer content (3%, 5%, 7%, and 10%) to maximize targeted properties. It provides a comparative evaluation of commercial MAPP and SEBS-g-MA in enhancing interfacial bonding, mechanical performance, water resistance, dimensional stability, and thermal degradation. Dynamic mechanical analysis is further employed to validate improvements in storage modulus and damping behavior, linking compositional and wide particle size ranges to overall composite performance (*Paper IV).*

Chapter VI: This chapter investigates WPCs based on high-performance engineering thermoplastics, rABS and rHIPS, reinforced with 50 wt.% LLB particles and compatibilized using MA, DCP, and varying levels of impact modifiers (EPDM and MMBS). The study systematically varies impact modifier content (5%, 10%, and 15%) to evaluate its effectiveness in achieving a balanced combination of mechanical, thermal, and water-resistance properties. Thermal and morphological analyses are conducted to assess retained storage modules and stiffness including internal damping behavior related to interphase modifications. Additionally, the study compares property enhancements across rABS and rHIPS matrices, emphasizing trade-offs between fundamental mechanical properties, thermal and dimensional stabilities (*Paper V*).

Chapter VII: Concludes the dissertation by synthesizing findings across all sub-studies, confirming the potential of recycled thermoplastic/bamboo composites as eco-efficient, low-carbon WPCs, and outlining directions for future research.

CHAPTER TWO

LITERATURE REVIEW

Comprehensive overview of wood polymer composite: formulation and technology, properties, interphase modification, and characterization

Abstract

Increasing global concerns regarding environmental sustainability and the responsible use of natural resources have led to global efforts to develop eco-friendly materials. These are driven by the desire to establish a circular and carbon-neutral economy and to reduce the environmental impact of non-renewable resources, particularly synthetic polymeric materials derived from finite petroleum fossil fuels. The adverse effects of the excessive use and waste accumulation of such materials have prompted the search for alternative routes for polymer production, emphasizing lower energy consumption and reduced emissions of pollutants such as greenhouse gases. Similarly, the growing population and negative environmental effects of conventional building materials demand more environmentally friendly building materials from sustainable untapped resources. Wood polymer composites, which combine synthetic thermoplastic polymers as a matrix and lignocellulosic fibers as a dispersed phase, have been developed as alternative materials. This critical review provides a comprehensive overview of current WPC formulations, comparative advantages, and critical properties based on the matrix and filler compositions. Progress in various applications, interface functionalization, and modification of both hydrophilic lignocellulosic fibers and hydrophobic polymer matrices including WPC interphase characterization were considered. This review also investigates the recent developments and benchmarks in WPC formulations achieved through natural reinforcement and the use of recycled plastics as secondary resources. The effects of the polymeric matrix (from non-polar to polar) and reinforcement (from nano to micro) on mechanical performance were comprehensively reviewed to better understand the research trends, challenges, and unsolved problems of WPCs as promising a sustainable transition to green building materials.

Keywords: *Wood Polymer composite, Interphase Characterization, Coupling agents, Mechanical Properties, Dispersed phase, Sustainable building materials, Carbon neutral economy*

2.1 Introduction

In the future society, there is a need to move to a circular, carbon-neutral economy to mitigate the exploitation of non-renewable resources while simultaneously minimizing waste by reusing, repairing, and recycling [1]. Similarly, relentless efforts for sustainable building materials are demanded due to population growth and urbanization which have led to an increased demand for conventional building materials which use a large proportion of the Earth's non-renewable resources in terms of material and energy consumption [5]. For instance, the annual production of 3.5 billion tons of ordinary Portland cement, a crucial construction material, requires significant energy for carbonate decomposition through coal burning, resulting in a notable 5–7% contribution to global CO_2 emissions. Projected trends indicate a potential increase to 71 million tons by 2033 [76].

Similarly, the large-scale production and consumption of petrochemical-based plastic materials, particularly thermoplastics, have increased more than 200-fold since 1950, exceeding more than 8 billion tons, equivalent to more than one ton per person living today [45]; this trend is expected to continue, given the indispensable role of synthetic organic polymers in the modern world [77]. Nevertheless, thermoplastics consume nearly 8% of global oil production for both raw materials and energy, primarily for short-term applications that ultimately result in plastic waste [78]. Removing such useful waste streams and integrating them into a circular economic chain requires cascading them into product life cycles with sustainable raw materials that can simultaneously substitute the urgent needs of building materials. These demands have led to the development of novel materials known as wood polymer composites, currently recognized as vital components of post-consumer cascade utilization [3].

WPC is a polymer matrix composite (PMC) mostly a thermoplastic matrix and a lignocellulosic dispersed phase in the form of short fibers, particles, and flour [79,80] both vary in composition from 10-90 % and small additives added to enhance the properties for their destined application. Thermoplastic polymer matrices of WPC are cost-effective commodity polymers capable of flowing easily when heated below the thermal degradation threshold of lignocellulose fibers (200-220°C) and regain their properties upon cooling. A particular example of common matrices are the PE varieties, PP, and PVC.

WPCs have been developed as a commercial and state-of-the-art innovative product over the last three decades and have subsequently penetrated the building and furniture markets in Canada, the USA, Asia, and Europe. In Europe, 30% of WPCs are currently used in construction, with 25% used in the automotive industry, while mining and shipping (6%), electronics (9%), sports (8%), aviation and space (3%), medical (1%), and railways (1%) sectors are among major other consumers [81]. While using plant-based dispersed phases in the polymer matrix can be justified undeniably by their ecological and economic benefits, they have been overlooked compared to mineral fibers [82,83]. Such bio-based fibers and their composites are environmentally friendly with high carbon dioxide sequestration, low production costs, and no toxic side products compared to conventional synthetic reinforcing fibers, such as polymers, carbon, and glass fibers [84], making WPCs almost climate-neutral, with an overall positive balance the longer it remains in application. Additionally, WPCs are easily produced and machined to the required color and shape using well-known thermoplastic manufacturing technologies, such as extrusion and injection molding [81].

Recent studies have explored the incorporation of entirely recovered and virgin polymers including LDPE, ABS, LLDPE, PVC, MDPE, polylactic acid (PLA), HDPE and PP in WPC formulations for alternative building materials [26], with the results indicating further reductions in pollution and increases in the valorization of lignocellulosic fibers [85] thus enabling the circularity of recycling valuable plastic waste which otherwise disposed as waste [86]. Similarly, WPCs can replace energy-intensive traditional construction materials, such as cement, steel, and various ceramic products [87] in some areas, which can simultaneously reduce the carbon footprint and CO_2 emissions, considering no alternative materials have been discovered to fully replace these excellent construction materials. WPCs can be applied in non-structural internal applications, such as modular kitchens, wall panels, bathroom doors, decorative wall tiles, curved components, office and household furniture, and partitioning systems and also cover exterior uses, such as railing, wall cladding, pavements in corridors, and various decking products [88,89]. However, monitoring WPCs poses a significant challenge and requires continuous effort, considering their performance relies heavily on formulation factors, including the nature of its ingredients (thermoplastic polymer matrix, dispersed phase, and additives), production methods, and processing parameters. Hence, understanding the key elements and factors, such as the polymeric type, filler or reinforcement characteristics, processing conditions, and additive amounts, is crucial for optimal formulation.

The quality of raw materials and, most importantly, interface modifications, are crucial in determining the ultimate performance of such products [21].

In WPCs, poor interfacial compatibility at the interphase results from the inherent hydrophobic polymers, and the hydrophilicity of the natural fibers results in discontinuities in the physical, mechanical, and chemical characteristics, weakening both the interphase and bulk properties of the material [41], thus necessitating the improvement of interfacial bonding mechanisms that result in molecular entanglement following interdiffusion, electrostatic adhesion, chemical reactions, and bonding [90].

Existing reviews [20,21,24,90] lack comprehensive insight into current formulations, mechanical properties variations, and interphase surface mechanisms with only a narrow scope, without in-depth discussions about the interphase modifications and characterizations, particularly the interrelated dynamics among lignocellulosic fibers morphologies, loading rate and polymer matrix including their collective impact on properties. These areas remain unclear and have not been adequately explored in previous studies. As a result, the specific aim of this review focused on the current formulation and technology essential to WPC production and its advanced applications, comprehensive mechanical properties, and variations due to morphologies, loading rate, and size of dispersed phases (particles, fibers, and nanoparticles).

This review also emphasizes in-depth interphase modification of hydrophilic lignocellulosic fibers and hydrophobic polymer matrices through coupling-agent reaction mechanisms, concise characterization techniques, well-known coupling additives, and crosslinking for strong interphase compatibility. Additionally, this review includes current research benchmarks of WPC produced from natural reinforcement and recycled plastics as secondary resources. Finally, it outlines future work and prospects to bridge the gap among diverse research results in these areas.

2.2 Wood Polymer Composite (WPC) as an Engineering Material

Composites comprise commonly solid multiphase, chemically and physically distinct components combined to form a new material that exhibits a significant characteristic difficult to obtain from a discrete material [21]. The two common parts of the composite are the matrix and dispersed phases [91]. The matrix is a continuous phase that binds the dispersed phases together, transmitting stress and loads within the material. The second phase is called the dispersed phase, in the form of

particles or fibers—a discontinuous phase. Composites can be classified based on their matrices and dispersed-phase components, as shown in Figure **2.1**. Matrix-based classification of composites includes ceramic, metal, and polymer-matrix composites (PMCs).

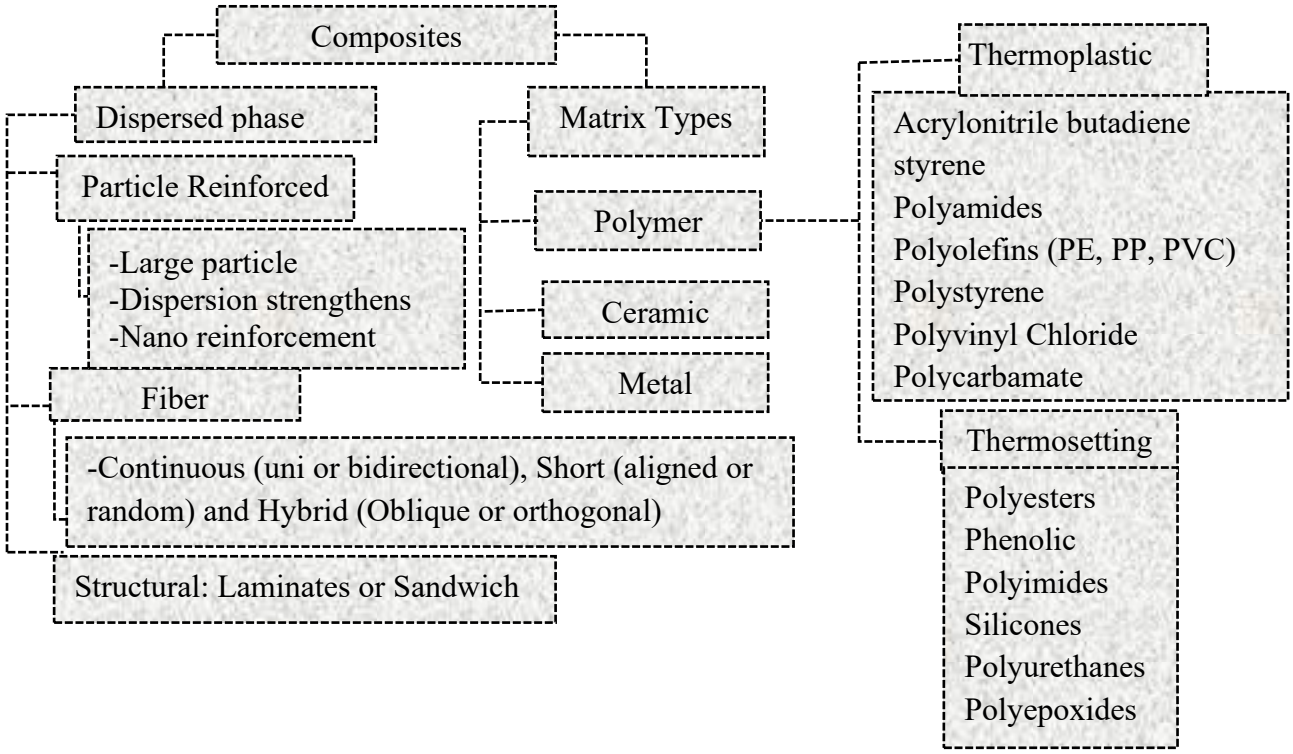

Figure 2. 1 Classification of engineering composite materials.

Currently, PMCs are gaining considerable interest owing to their light weight, stiffness, strength, and easy fabrication. Polymeric matrices used in the PMCs can be thermoplastic and thermoset polymers in origin. Thermoplastics can be molded with heat and remelted without losing their inherent qualities which differs them from thermosets known to undergo irreversible changes after their permanent hardening process [92]. Thermoset matrices such as phenolic, unsaturated polyester, vinyl ester, and epoxy polymeric resin, are utilized with long fiber reinforcements owing to their low processing temperature and viscosity, which prevents damage to the bio-fibers and enhances the interfacial properties, resulting in greater strength compared to that of thermoplastics [17]. However, a significant loss of properties may occur beyond the glass transition temperature [84]. This polymer variety is recognized for its strong intermolecular bonds, stiffening with increasing temperature, and stable molecular network that enhances stability under higher loads compared to thermoplastics. Nevertheless, thermoplastics offers a more economical option

compared to thermosetting polymers. They easily stretch their molecular orientation and flow upon melting, then reorient their molecular structure upon cooling restoring their stability and structure. This makes their composite-like WPC easily manufactured by integrating bio-based short particulate, fibrous, or flour fillers of varying dimensions into existing plastic manufacturing processes, particularly extrusion and injection molding with high possibility of recycling [93].

2.2.1 Formulation and composition of WPC

WPC is one of the PMCs whose polymer matrix phases are thermoplastic polymers and plant-based dispersed phases. The composition of both phases varies widely depending on the desired properties of the final product, specific application, and performance requirements. Accordingly, WPCs can be categorized into low-filled, high-filled, and liquefied WPCs, with bio-fibrous filler contents ranging from 10%-40%, 40%-80%, and 80%-90%, respectively [94,95]. The remaining additives include encompass coupling agents, biocides, antioxidants, UV stabilizers, flame retardants, and lubricants [92,96,97] added in small quantities for enhancing the properties and durability of WPC materials. Examples of the composition and formulation of WPCs that have a wider commercial footprint are shown in **Table 2.1.** The polymer matrices utilized in WPCs consist of affordable commodity polymers that exhibit easy flow when heated below the onset thermal degradation threshold of lignocellulose fibers (200-220°C), subsequently restoring their properties upon cooling [92]. Moreover, these thermoplastics are chosen based on factors such as availability, recyclability, high toughness, and exceptional resistance to moisture and microcracking. Common examples include PE, PP, and PVC. Additionally, other thermoplastics like polyoxymethylene (POM), polystyrene (PS), ABS, and PLA [92], as well as polyurethane [98], poly (ether-block-amide) or pebax®[99], polycaprolactone [100], micronized waste tires blended with a polymeric matrix [101,102] and polycarbonates [103] are considered potential future substitutes for polyolefin polymer matrices to impart hydrophilicity, better strength, toughness, stiffness, and elongation [22,82,100].

Table 2. 1 Composition and additives in WPCs formulated from PE, PP, or PVC matrix (compiled from Ref. [104]**)*.**

	PE core Polymer (wt.%)	*PP Core Polymer (wt.%)*	*PVC Core polymer (wt.%)*
Matrix	100- the rests	100- the rests	100- the rests
Fiber/flour	30–60%	30–60%	30–40%
Lubricant	Stearate/esters/EBS/ others 3–8%	Stearate/esters/EBS/ others 3–8%	Stearate/paraffin/esters/OPE/ EBS 3-8%
Coupling Agent	MAPE/MAPP 2-5%	MAPE/MAPP 2-5%	-
Heat stabilizer	-	-	Various 1-3%
Antioxidant	Phenolics/phosphites 0–1%	Phenolics/phosphites 0–1%	-
Acid scavengers	Stearates/hydrotalcites 0–1%	Stearates/hydrotalcites 0–1%	Stearates/hydrotalcites 0–1%
UV protection	HALS/ benzophenones/ benzotriazoles 0–1%	HALS/ benzophenones/ benzotriazoles 0–1%	HALS/ benzophenones/ benzotriazoles 0–1%
Mineral filler	Talc 0–10%	Talc 0–10%	Carbon filler 0–10%
Biocide	Zinc borate 0–2%	Zinc borate 0–2%	Zinc borate 0–2%
Co-stabilizer	-	-	Zeolite 0–3%
Density reduction	Microspheres/ chemical or physical blowing agent 0–5%	Microspheres/chemical physical blowing agent 0–5%	Microspheres/ chemical or physical blowing agent 0–5%
UV protection and pigments	as required	as required	as needed
Fire retardant	Various as required	Various as required.	Various as required.

* Ethylene bis stearamide (EBS), hindered amine light stabilizers (HALS), coupling agent (CA)

The dispersed phase in WPCs comprises a variety of morphologies, primarily sourced from lignocellulosic fibers such as kenaf, pine, oil palm, spruce, flax, beech, poplar, hemp, sisal, maple, oak, coir, and jute. Lignocellulosic particles or flour typically have nearly equal dimensions in all directions, whereas fibers have a high aspect ratio [16,17]. Comparatively, nanosized cellulose-based reinforcements exhibit improved elastic modulus, enhanced stiffness, and structural stability. However, the elevated energy input for fine-ground particles raises the preparation costs, including coupling agents (CAs) for functionalization and interphase modification, contributing to the overall cost and a high-carbon footprint process. Additionally, challenges arise in collecting highly fibrillated cellulose nano cellulose because of filtration difficulties, and monitoring its properties for full-scale commercial use is complicated owing to its small dimensions and complex

structure [20]. Similarly, larger reinforcing elements face agglomeration issues, resulting in a lower quality and rougher composite surface. Both extremes require optimization for WPC formulations, considering the availability and engineering constraints [23]. Other useful sources of construction and demolition waste [105,106] and by-products of industrial processes, such as sawdust waste, carton-cutting waste [107], and veneers were recently investigated to improve the impact properties. Additionally, functional fillers and reinforcements like micro- and nano-SiO_2, glass, Al_2O_3, $Mg(OH)_2$ [83,108], kaolin, carbon nanotubes, layered silicates [109], talc, wollastonite, modified Nano clay [110,111], nano boron nitride [112] and superparamagnetic magnetic wood flour nanoparticles [100,113] have been recently used in WPC formulations to enhance UV degradation resistance, dimensional stability and mechanical properties.

2.2.2 Manufacturing process and technologies for WPCs

The WPC manufacturing process consists of two main phases. The initial stage, referred to as compounding, includes feed-in, blending, and homogeneous mixing. The second stage involves forming or consolidation. In the feed-in phase, the introduction of polymer granulates, filler particles or fibers, and additives is determined based on the densities of the dispersed phase and polymers [88], achieved through continuous, discontinuous, or batch feeding by employing either volumetric or gravimetric feeding principles. Compounding is a uniform melt-blending process of wood particles, additives, and polymeric matrices, mostly in continuous screw extruders, helping in the homogeneous dispersion of filler particles and additives using the heat and shear generated by closely meshing screw elements to form a uniform melt blend called a compound. This compound is then consolidated into products through either a one-step route or pelletized via a two-step route via injection molding [21].

Polymer-based composites are typically produced using three primary methods: solution blending or casting (SBC), in-situ polymerization (ISP), and melt blending (MB). SBC composites—prepared by dissolving the fibers and polymer matrix in an appropriate solvent and subsequently evaporating the solvents [114]—are widely used commercially as polymer nanocomposites via processes such as sol–gel method, in situ polymerization, and intercalative polymerization involving nanosized particles [24]. However, the toxic, temperature-sensitive, and hazardous nature of organic solvents renders SBC environmentally unsustainable. ISP involves the

polymerization of a monomer in the presence of another polymer to enhance the compatibility of the polymer blends. This process involves the formation of covalent bonds between components, leading to the development of graft or block copolymers that establish a stable interface [115,116]. MB involves polymer matrix heating above its melting point within the 10–30°C range, with fibers subsequently incorporated into the molten polymer through consistent mixing under applied shear force. Most MB techniques for WPC fabrication include extrusion molding (EM), injection molding (IM), and compression molding (CM). The first two are recognized for achieving optimal homogenization and mechanical interlocking, thereby reducing the voids in the composites [104]. Extrusion is a high-volume longitudinal manufacturing process that primarily involves melting and homogeneous mixing of a thermoplastic matrix with fibrous fillers or particles.

Common technologies for WPC production include single screws (SSE), co-rotating twin screws (CoTS), counter-rotating twin screws (CTS), and WoodtruderTM (a combination of parallel CoTS and SSE). As shown in **Table 2.2**, different priorities can be determined depending on the target requirements [89]. Various post-extrusion operations, such as IM and CM, are also used, accompanied by extrusion, to produce WPCs with complex geometries and high production rates [117]. IM facilitates molecular orientation and improves tensile properties. However, extrusion has some benefits over IM because it burns wood fibers using the large heat produced by injection at a high-speed rate [82]. In comparison, hot CM has been employed to manufacture large-scale 3D components and high-density WPCs with low porosity. CM is used to fabricate composites of both thermoplastic polymer matrices such as HDPE, PP, polyamide (PA), and polyether ether ketone (PEEK), including thermosetting polymers such as unsaturated polyester, vinyl ester, and phenolic [84,118]. Moreover, CM can compensate for the decrease in impact strength resulting from a higher fiber content [104]. For full matrix impregnation with fibers during CM, the viscosity of the polymers, pressure, holding time, and temperature must be optimized considering the type of fiber and matrix. Recently, three-dimensional (3D) printing has become a cutting-edge technique for creating polymer–matrix composites. Through the deposition of composite materials, a solid object is printed layer by layer, starting with a virtual 3D model developed using computer-aided design (CAD). This method has potential for fabricating composite filaments made of natural fibers [92,119]. Nevertheless, using 3D printing technology for fabricating WPCs is constrained by notable reductions in mechanical properties owing to lower pressure during manufacturing, relatively high energy consumption, processing costs, material limitations, and

slow processing speeds. Overcoming these limitations critically requires further research and development [92].

Table 2. 2 Characterization of the different extruder systems tabulated from Ref. [104]

Properties for comparison	**Screw Extruder Systems**		
	SSE	CoTS extruder	CTS extruder
Conveying mechanism	Drag flow	Forced conveying solid flow	Drag flow (Forced flow)
Screw speed range	60-250 rpm	25-80rpm	100-1200rpm
Viscosity range	small	Large	large
Residence time range	Large	small	small
Mass and heat exchange	+	++	++
Dispersing	+	++	++
Mixing	+	+	+++
Self-cleaning	+	+++	+++
Degassing	+	++	+++
Pressure builds up	++	+++	+
Flexibility	+	+	++
+++- very good, ++- good, +- satisfactory			

2.2.3 WPCs from recycled thermoplastic as secondary resources

Polymeric plastic materials are successfully integrated into the daily life of human beings with exceeding 8 billion tons [120,121] of volume production. However, approximately three-quarters of these essential plastic polymers end up as waste in the environment, with 55% being discarded or sent to landfills and 25% undergoing incineration, with only 20% being recycled [92]. Hence, plastic waste is a substantial contributor to solid waste. Key thermoplastics in this category, including LDPE, LLDPE, HDPE, PP, polystyrene (general and HIPS), PET and ABS constituted a significant portion. Notably, none of these plastics is biodegradable, leading to their accumulation in landfills and the natural environment [41,63,122]. Consequently, recent investigations have suggested using post-consumer materials through thermal recycling as secondary resources to formulate WPCs. This method efficiently captures carbon dioxide, providing an alternative resource to address the scarcity and price fluctuations of polyolefins with a minimal carbon footprint, thus improving the circularity of WPCs while significantly reducing potential plastic waste from the environment and extending their use in the product life cycle and enhancing their final degradability [3,11,63,123].

Table 2.3 summarizes key recent advances in WPCs made from recycled polymers and lignocellulosic materials, showing performance comparable to or exceeding that of conventional virgin polyolefin-based WPCs. Characteristic polymeric matrices and ingredients, such as degrees of crystallinity, purity, molecular mass distributions, and processing conditions, were excluded. The main findings were identified by comparing the composite properties with the corresponding unfilled polymeric matrix, particularly focusing on potential plastic waste, manufacturing methods, and compositions. The consistent trend observed in these studies shows that incorporating lignocellulosic fibers or particles into a plastic matrix result in a notable enhancement in flexural strength (FS), modulus of rupture (MR), tensile modulus of elasticity (TME), and stiffness. While the TS increased with the addition of coupling agents, the IS decreased compared with that of the base matrix except with the formulation where impact modifiers were included. Nevertheless, heat and oxidative deterioration, polymer chain scission, and the degree of polymer material degradation over several continuous cycles were not fully addressed and require further investigation for the long-term use of recycled plastics as an alternative material.

Table 2. 3 Potential WPCs formulated from recycled resources.

Recycled (r) Polymer matrix	*disperse-phase*	*Compounding &forming*	*Mixing ratio and additives in (Wt.%)*	*Main findings of the investigations*	**Ref.**
rPP	cotton stalk powder (CSP)	High-speed Intense mixer (HIM) and IM	CSP (0, 1, 3, 5, and 7%), granite (0, 3, 6, 9, and 12 %), KF/rPP (100-W_f)	-Exceptional Maximum FS, maximum IS, and high dynamic load resistance were found with unusual performance compared with unfilled polymer.	[124]
rLLDPE (consumer packaging materials)	Rice husk (RH) fibers	Melted mixed with a two-roll machine and consolidated by CM	MAPE (3%), Both NSMTVS and ONCNM at (2%, 4% and 6%), RH/rLLDPE:35/65%	-The highest increase in mechanical properties was attained at 6% loading of NSMTVS and 4% of ONCNM	[125]
rHDPE/PET: microfibrillar blends (MFBs) blend (from the bottle scraps)	Pine flour (PF)	Mixed, melt - blended, and extruded by CTS	PF to blend matrix (75/25%) with EGMA (2%), The polymer matrix/ PF: 40/60 with MAPE (1%.2%, 2.4%, 3.6%)	-Mechanical properties increased exceptionally at 2% EGMA and 2.4% MAPE in the composites -The blend of rHDPE/rPET (75/25) MFBs resulted in better PF crystallites	[126]
rABS, rPP, rPE (construction and demolition waste)	Spruce wood flour (SWF)	Compounded and consolidated with CTS	Fusabond E226 (3%), lubricant (3), (ABS, PP, PE)/SWF:30/64	-Comparatively rABS WPCs show better moisture and strength properties. But rPP-based WPC values were lowered.	[127]
rABS (Electronic waste)	Maple wood flour (MWF)		MWF (50%), ABS (100-W_f), (SAMA, SEBS-g-MA, SANMA) (2%, 4% and 10%), lubricant (5%)	-Essential Properties of WPC unchanged when the virgin ABS is replaced by rABS with SAMA except IS which showed better results with the SEBS-g-MA.	

Blend of rPET/rPA (waste textiles)	Wood Flour (WF)	TSE for WPC pellets, IM for the consolidation	rPET to rPA6 [60/40%, 50/50%, and 40/60%)]/ WF:70/30%, Epoxy resin (3%), POE-g-MA and MBS (3%), lubricant and antioxidant (0.03%)	- POE-g-MA based WPC was better than that of MBS. -WPC with rPET/rPA6:40/60% showed excellent mechanical performance both before and after aging compared with the existing commercial WPCs.	[128]
rHDPE (packaging waste)	Spruce fiber (SP)	IM and CM	Both HDPE/SP at 30% and 68%) alternatively, PEMA (3%)	-30% SP is feasible technically and economically for both WPC formulated from virgin materials and recycled HDPE matrix.	[129]
rHDPE (post-consumer extruded bags)	WF (pulverized saw dust)	IM and CM	HDPE (80%), NRL (5-20%), WF (5-25%),	-Both fillers synergistically improve the FS, IS and thermal degradation compared with the matrix at 80 %HDPE, 5%WF, and 15%NRF with excellent toughness.	[130]
The blend of rLDPE/HDPE/PP	Date palm fibers (DPF)	Granulation by TSE and pressed with hot CM	DPF (20%)/ [LDPE (10%) / HDPE (35%) /PP (35%) and MA] (1 and 2%	Mechanical and physical properties were comparatively better with 1% than 2%MA	[131]
rHDPE	Wood and bamboo fibers	blended in a DCB, granulated in TSE and CM	Wood and bamboo flour (10-40%), HDPE (90-60) MAPE and GMAPE (5%)	-Coupled WPCs by GMAPE and wood flour fillers showed best performance (TS and FS) at 30% than MAPE and bamboo flour.	[132]
rABS and rPS (from post-consumer WEEE)	Recycled Particle board (PB) and Norway Spruces fibers (NSF)	Compounded and granulated in TSE and formed by CM.	Fiber's content (30% and 60%) in both rABS and rPS, and SMA (3%)	-WPCs from ABS and PB achieved sufficient results of TS, FS, MOE with SMA than PS and increased with wood content than NSF. - PS was reinforced with PB due to better interfacial bonding with SMA.	[123]

rPP (nonwoven textile and food packaging	WF from residual waste	Dry blending and consolidated with CM	filler/matrix, (40 and 60%), No Coupling agents	-WPCs of PP fiber showed higher ductility achieving FS and MR comparable to High-Performance grades of boards MDF.	[133]
rPP (Post-industrial waste pipes)	Mahogany wood flour (WF) particle sizes	dry-mixed in a HIM, granulated with SSE, molded CM	WF/matrix:40/60%. MAPA (3%)	-Reduced particle size ranges resulted in better density, FS, MR, MOE, and IS regardless of MAPP and WPCs coupled with MAPP showed higher values at any size except lower EAB.	[134]
PS (from foam waste)	Flax fiber (Ff)	IME and CM	Ff/PS:40/60, DOP (2%)	-Better TS, FS and CS compared to any other WPCs based on PVC, HDPE, and PP matrices	[135]
HDPE	waste Pine fiber filler (PF)	IME microwave-assisted CM and	PF/HDPE:20-60%	-The composites reinforced with 20% showed the highest TS, FS, and IS	[136]
rHDPE (Municipal waste)	Wood Flour (WF)	IME and mini-IM	WF/HDPE/Nanographene/MAPE:30/70/ (1%,5%, 2%, 2.5%) / 3%	-Nanographene up to 5% has improved the FS, FM, and notched IS and thermal degradation of the composite	[137]
rPVC /virgin PVC (50/50% based mix)	WF (beech, poplar, oak, hornbeam, and maple)	SSE and IM	WF (40%), rPVC/ neat PVC (50%), MAPP (5%), Zink and calcium stearate (2%), NC (1.5%,3%,5%),	-NC improved all Physio-mechanical properties at 5% in all three PVC types of virgins, recycled, and mixed matrix.	[138]
rPP (consumer packaging plastics)	Mango wood flour (MWF)	micro conical CoTS and micro-IM	Both rPP and MWF at (70%,50%,40%) with the MAPP (3 and 5%)	-Tensile and flexural properties of WPCs formed from rPP matrix with and MAPP are higher than neat PP composites control of the same batch.	[139]

rPP (end-of-life PP products)	WF (saw dust and recycled poplar flour modified by phenolic resin).	Mixed in HIM, Compounded, and extruded in CoTS	WF (60–85%) in rPP and neat PP, MAPP (3%), Lubricant (2%)	-The ultrahigh filled WPCs of recycled poplar flour (80%) containing phenolic resin resulted in strong mechanical properties and reliable creep resistance compared with original WF composites.	[70]
rPP (Post-industrial waste from cotton swabs)	Sisal fibers (SF)	Melt mixing in batch Haake Rheomex (HR) and CM	SF (10-40%), PP (90-50%), MAPP (3%,5%,7%,)	-Increase in TS to 11%, 20%, and 31.36 % and IS to 78.72%, 77%, and 81% for silane, GMA and OBDC treated SF respectively for WPC of rPP/SF/MAPP at ratio (65/30/5) compared to rPP matrix.	[140]

Kevlar fiber (KF), Nanosilica modified by triethoxyvinylsilane (NSMTVS) and Organophilated nano clay of Sodium montmorillonite) (ONCNM), ethylene-glycidyl grafted maleic anhydride copolymer (EGMA), polyolefin elastomers maleic anhydride (POE-g-MA), methyl methacrylate-butadiene-styrene copolymer (MBS), polyamide 6 (PA6), Styrene maleic anhydride (SMA), Styrene ethylene butylene midblock grafted maleic anhydride (SEBS-g-MA), styrene acrylonitrile grafted maleic anhydride (SANMA), glycidyl methacrylate-grafted polyethylene (GMAPE), double-cone blender (DCB), waste of electrical and electronic equipment (WEEE), High Intense mixer (HIM), dioctylphthalate (DOP), Natural rubber latex (NRL), regenerated car tire rubber (RR), Nano clay (NC), Glycidyl Methacrylate (GMA), O-hydroxybenzene Diazonium Chloride (OBDC), elongation at break (EAB)

2.2.4 Comparative advantages and application of WPCs

WPC applications extend traditional wood composites, such as high-density fiberboard (HDF), plywood, and medium-density fiberboard (MDF) to a new generation of cost-effective structural components for building materials that possess better mechanical properties, hydrophobicity, and dimensional stability than MDF and HDF. The thermoplastic matrix facilitates flow during melt processes, encapsulates the fiber or filler surfaces, forms a barrier layer that retards moisture intrusion and water vapor permeability and reduces the number of accessible hydroxyl groups that typically interact with water molecules. Notably, the thermoplastic matrix releases negligible non-toxic emissions, unlike traditional adhesive-bonded wood-based products, and is easily molded. Compared with unfilled plastics, WPCs exhibit better thermal and creep performance, including a higher modulus and less tendency to sag, while being easily machinable. WPCs utilize renewable fibers acquired at a remarkably low cost compared to the most expensive and unstainable glass fibers, aramid fibers, and carbon fibers, even though these synthetic fibers are higher in tensile strength and stiffness. Similarly, considering their sustainability, functionality, and cost-effectiveness, bio-based resources are affordable, non-toxic, widely available, and have a high specific strength, low density per weight, and less machine wear during manufacturing [14,20,134].

WPCs are technically manufactured using well-established plastic fabrication methods with an impressive screw-holding capacity and excellent machinability, resulting in an improved surface finish, thus minimizing the need for multiple post-manufacturing steps, which usually add additional costs to the final products. Nevertheless, WPCs have certain drawbacks, such as lower strength and stiffness compared to synthetic fibers, as well as moisture sorption and swelling when compared to solid polymer matrices [88]. The limited interfacial adhesion results from the distinct chemistry of the hydrophilic lignocellulosic fibers and hydrophobic matrix requires coupling or crosslinking agents for effective compatibility at the interphase [141]. Currently, WPCs offer diverse applications as building materials. Internally, they are used in kitchen cabinets, wall and door panels, bathroom doors, window frames, decorative panels, office and household furniture, partitioning systems, roof tiles, and racks[14,93] Externally, WPCs serve as decking products, flooring, wall cladding, railings, decorative garden furniture, architectural

fencing, and sliding panels, as some of them are shown in **Figure 2.2**. Beyond construction, WPCs formulated from short fibers and manufactured via thermoforming [142] have been used in automotive parts such as door panels, noise insulation panels, headliner panels, wheel boxes, casing and cabinets of electronics, electrical appliance packaging of various goods, and other useful household products such as mailboxes, mirror casings, wastepaper baskets, floor parquets, flower vases, park benches and picnic tables [92,143].

Figure 2. 2 Applications of WPCs as building material

2.2.5 Factors influencing properties and performance of WPCs.

WPC properties are primarily influenced by three key components directly involved in their formulation. The first component involves the type, quality, and quantity of the three main constituents integrated during the manufacturing process: thermoplastic polymeric matrix and dispersed phase comprising either the filler or reinforcement [144]. Recent reviews by Nassar. et al [24], Khan. et al. [92], and Porebska, A. [145] discussed the properties of eco-composites such as WPC related to fiber or filler type, chemical modification of fillers, and the base polymer

matrix. They highlighted polymer properties, chemical additives, fabrication techniques, manufacturing processes, coupling agents, and additives. They also emphasized that the irregular shape of natural fibers typically diminishes the strength of WPC due to weak interfaces, poor compatibility, and inadequate wetting between polar plant fibers and non-polar polymers and recommended to explore the optimal filler content to attain desired properties, as an excessive amount can lead to fiber agglomeration and poor dispersion, resulting in excessive voids. Similarly, they highlighted the crucial role of coupling agents in addressing these issues by reducing gaps and enhancing filler encapsulation within the matrix, thereby enhancing the homogeneity and overall quality of the WPC. However, concise findings on the variations of mechanical properties, interphase modification, and their characterization method were mostly not discussed in depth.

Generally, factors influencing WPC properties and functional performance include the type of polymeric matrix, filler or reinforcement (species, particle size, and aspect ratio), processing parameters (temperature, pressure, mixing time, and screw rotation of the extruder), and interphase modification [21,24]. The nature of the matrix and dispersed phase, including their fractional composition, interphase compatibility, and processing parameters, are the most critical factors affecting the ultimate performance. Despite the complexity of the influencing parameters and the significance of all the factors, some parameters can be monitored before formulation. Sections 3 and 4 delve into the properties significantly affecting WPC performance, focusing on concise interphase modifications of WPC. It examines the effects of dispersed phase size and loading rate, shedding light on optimal formulation areas that have received limited attention in the literature. Additionally, it provides a comprehensive summary of characterization methods related to WPC, accompanied by appropriate case studies.

2.3 Interphase Surface Treatment and Modification

2.3.1 Lignocellulosic chemical composition and structures

The plant cell wall has four distinct layers of arrangement at the nanoscale [13] as shown in **Figure 2.3a**. These are the primary cell-wall layers that contain three sections, secondary layers, and a porous open channel called the middle lamella [96]. These cell wall layers are primarily composed of higher and more complex sugar molecules of cellulose (40–60%), hemicelluloses

(20–40%), and non-sugar molecules of lignin (20–25%) sharing 90% of the main structural components [96] and a smaller subsidiary component of organic and in organic matter [21,146]. Cellulose (**Figure 2.3d**) is a polymer of glucose made up of β-1,4-glycosidic linkages of D-glucopyranose units cemented within an amorphous matrix of hemicellulose and lignin via hydrogen bonds and other linkages. The cellulose content determines the strength and stiffness of the fibers [96,147] and its mechanical properties depend on the total cellulose content and degree of polymerization, including the microfibril angles. Hemicellulose (**Figure 2.3b**), which exhibits the highest degree of chain branching and is non-crystalline in nature, contains numerous monomeric sugar units of C_5 and C_6, such as glucose, mannose, xylose, and arabinose, collectively called xylan, and sugar acids such as methyl glucuronic and galacturonic acid.

The quantity of hemicellulose was used to monitor the moisture absorption, thermal degradation, and biodegradation properties of natural cellulosic fibers. However, lignin is an intricate hydrocarbon polymer composed of amorphous, hydrophobic, aliphatic, and aromatic components. It is more thermally stable than cellulose but extremely sensitive to UV radiation and responsible for UV fiber degradation from environmental exposure [96]. Conversely, the rigid structure enhances the properties of the natural fibers specifically the thermal properties [148]. Mostly it is an aromatic polymer with a rigid and complex three-dimensional network structure of active alcohol hydroxyl groups [149].

Lignin is commonly considered a phenolic polymer derived from 4-hydroxy-3-methoxy phenylpropane monomeric unit [150] and naturally exists in three forms, i.e., coniferyl alcohol, syringyl alcohol, and coumaryl alcohol (**Figure 2.3c**) tightly binding cellulose fibrils and hemicellulose [96,116,151]. The chemical constituents of lignocellulosic fibers, their variability, and modifications significantly affect the fundamental properties of WPCs. Moisture and UV radiation are the primary agents that cause lignocellulosic fibers degradation and its composites.

Lignin contains a significant UV-absorbing chromophore component and is the main cause of UV degradation. Other components, such as hemicellulose and non-crystalline cellulose, including crystalline cellulose, absorb some range of UV radiation and could result in the same degradation. Moisture absorption is predominantly attributed to the high hemicellulose content, followed by non-crystalline cellulose, lignin, and crystalline cellulose. Hence, altering the

inherent surface chemistry of these fibers without compromising their strength is essential for their effective use in WPCs [152].

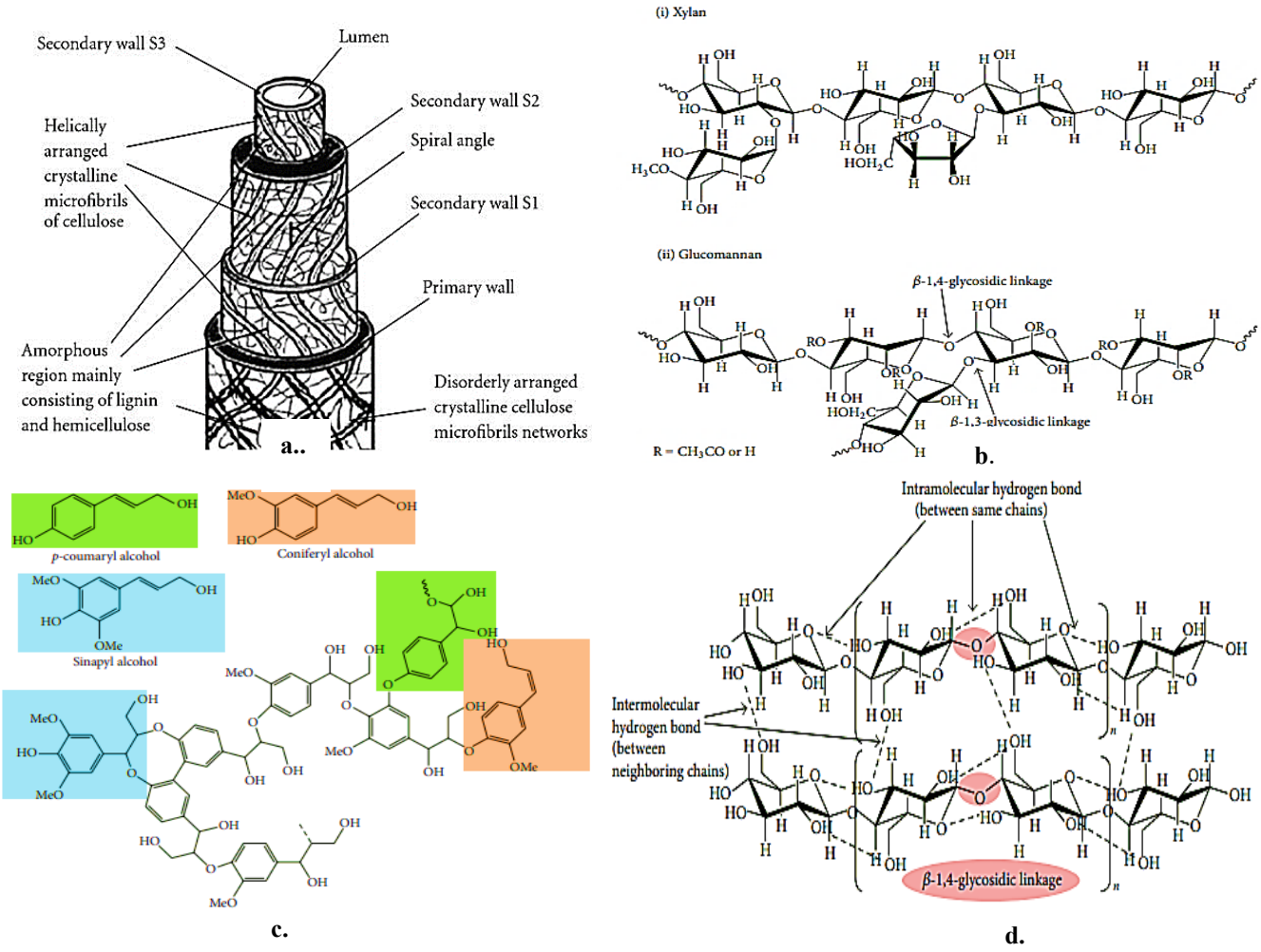

Figure 2. 3 a) Natural fibers cell wall [153], and molecular structures of b) hemicellulose, c) lignin, and d) cellulose [154].

2.3.2 Interphase surface modification and mechanisms

Blending hydrophilic lignocellulosic fibers with a non-polar hydrophobic matrix results in a weak interphase, which affects the overall properties of WPCs. Addressing this issue requires the initiation of strong bonds, primarily by modifying the surface chemistry and functional groups of these components. Enhancing the fiber and matrix interphase involves modifying the polar hydroxyl molecular networks of the cellulosic fiber surfaces before compounding and modifying the polymer matrix by incorporating compatibilizing agents or crosslinking agents before or during compounding [20]. The interphase in WPCs is not a separate phase with clear boundaries,

but a region between two layers of adjacent phases (bulk polymer fibrous or particle disperse phase), where chemical, physical, and mechanical properties, including microstructure, differ from the dispersed phase or matrix polymers [21]. The modification of the interphase involves tougher and more flexible boundary layers and the formation of strong interactions involving complex phenomena, as shown in **Figure 2.4.** These include (a) inter-diffusional elements, (b) electrostatic attraction, (c) chemical reaction leading to new bond, (d) mechanical interlocking, (e) chemical reaction forming of a new compound and (f) certain secondary bonds of like hydrogen bonding and van der Waals forces [84,90]. As a result, different interphase surface modifications comprising chemical, physical, processes, and nanotechnologies are summarized in **Figure 2.5**.

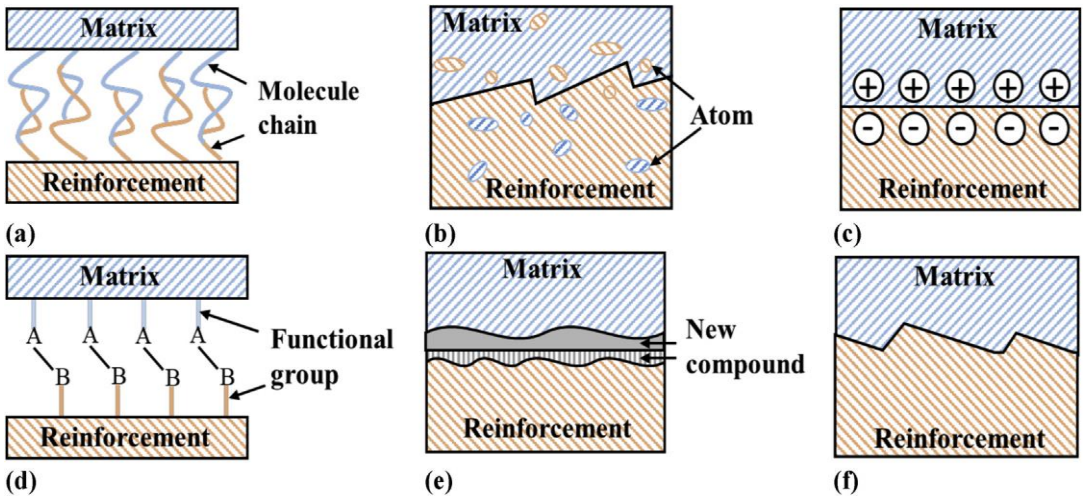

Figure 2. 4 Interfacial bonding mechanism redrawn from Ref. [90] with permission granted.

Surface modification using physical or chemical methods commonly leads to changes in the hydrophilicity of the fiber surfaces. Physical treatments include corona or plasma treatments, whereas chemical methods involve treatments with alkaline, silane, permanganate, acrylonitrile, acetylation, benzoylation, peroxide, isocyanate, zirconate, titanate, stearic acid, and coupling agents [147]. These methods can either add functional groups to the fiber surface or eliminate the weak components of natural fibers, thereby enhancing thermal stability and improving wettability. For example, alkaline treatment removes extractable materials and surface contaminants (waxes, lipids, pectin, hemicellulose, oils, and lignin), resulting in a cleaner and more uniform fiber surface with reduced crystallinity, while coupling agents enhance fiber compatibility with polymers [21] [102]. In contrast, plasma-based physical treatment utilizes

partially ionized gas of equal balance densities of negative and positive particles in macroscopic volumes and time, containing neutral particles like radicals, electrons, atoms, ions, and molecules [103]. The interaction of energetic ions with a material's surface leads to chemical and physical changes. Plasma treatment imparts surface oxidation in the presence of oxidizing agents like atomic oxides, oxygen-free radicals, and Ozone [104]. It cleans the surface natural fiber without altering the material's bulk characteristics which in turn enhances surface wettability by increasing the number of various functional groups depending on the nature of wood fiber, type of plasma gas, and process parameters.

In their recent study and review by Sanjay et al. [103] and Gupta et al. [104] into four common plasma treatments—Atmospheric, Dielectric Barrier Discharge Treatment, Corona, Atmospheric Pressure Glow Discharge, Atmospheric Pressure Plasma Jet, and Low-pressure Vacuum Treatment—they have demonstrated better performance in surface treatment of plant fibers. These treatments have shown enhanced copolymerization of certain monomers on various plant fibers such as jute, pine, banana fibers, and others, resulting in improved interface adhesion with matrix composites like HDPE and PLA attributed to mechanical interlocking derived from surface roughness, hydrophobicity, and imparted functionalities. Similarly, Hünnekens et al. [155] treated extruded and injection-molded WPC comprising HDPE and jute fibers for surface coating, leading to the formation of low-molecular-weight oxidized materials on the surface. These materials contribute adhesive forces, facilitating efficient surface coating.

Compared with the solvent-based treatment, plasma treatment is an effective, environment-friendly, and cost-efficient method for activating matrix polymers or fiber surfaces. However, adding new functional groups to the polymeric surfaces may lead to their degradation of the polymer surface and weaken the fiber surface which needs future work for determining the optimal gas dose, treatment temperature, and natural surface chemistry changes and their relation with the composites [155]. Heat treatment involves heating lignocellulosic fibers or particles below their degradation temperature. This process alters the water content, chemistry, cellulose crystallinity, and degree of polymerization, which enhances the wettability and adhesion with the polymer matrix if properly optimized. Moreover, grafting nanoparticles such as nano clay and nanocarbon tubes can make fiber surfaces rougher, promoting chemical reactivity and improving interfacial compatibility through reactions between the grafted nanoparticles and the matrix,

including the inclusion of intrinsic functional nanoparticles with good chemical reactivity [43]. Nanosized reinforcements, such as nanocellulose, have the potential to markedly increase stiffness and strength at low concentrations. However, the high costs associated with nanoparticles, including nanocellulose, pose a challenge for broad commercial applications. The extensive surface area of nano-based particles contributes to increased expenses, primarily because of the elevated costs of energy and chemicals involved in extraction, immobilization, and compatibilization before compounding [20].

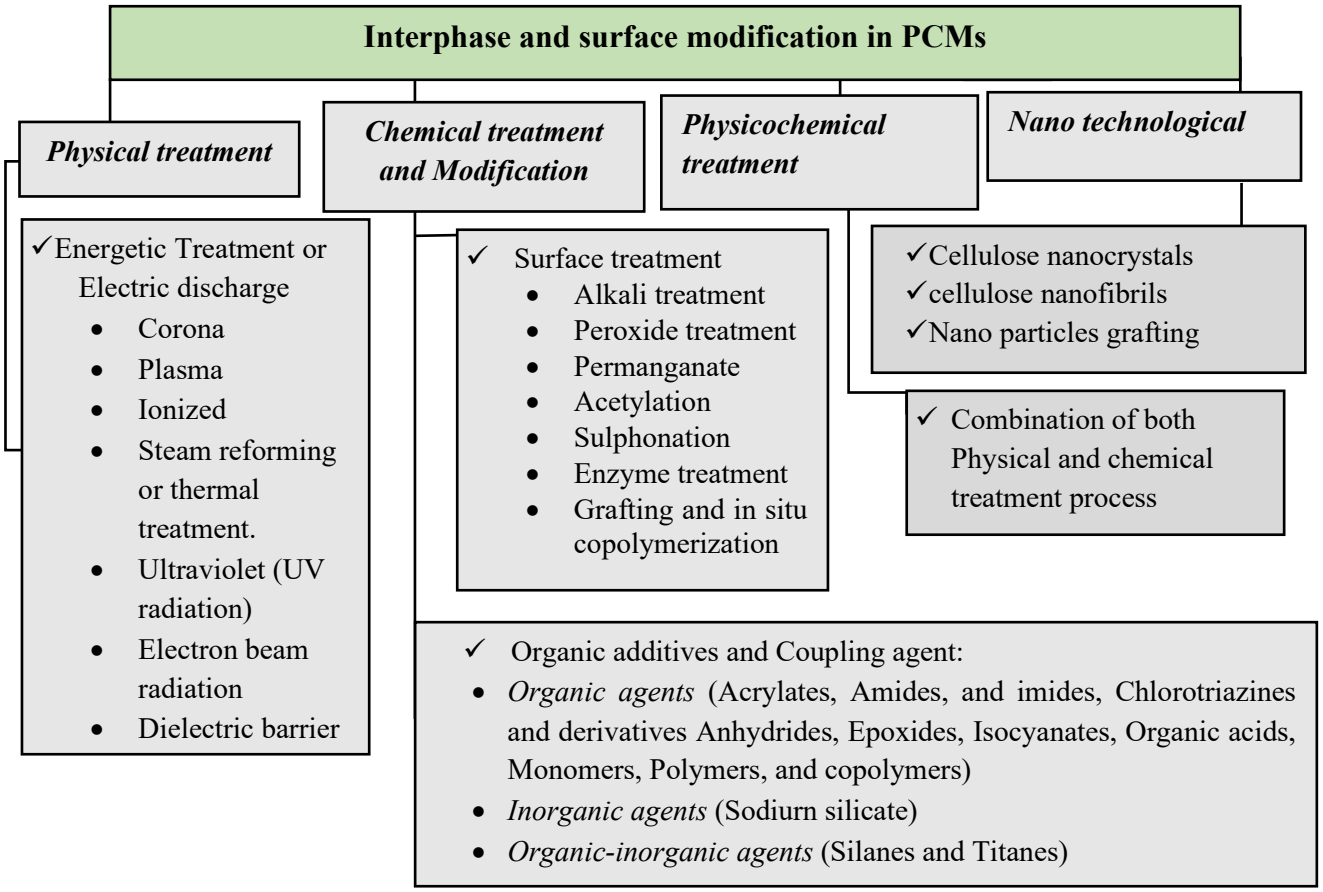

Figure 2. 5 Summary of the surface treatment and interphase modifications of WPC.

Chemical methods, specifically coupling agents (CAs), demonstrate superior effectiveness at the commercial scale compared to other methods reported in the literature [84]. CAs are added in small quantities to improve the miscibility at the interface of the polymer matrix and lignocellulosic fibers and minimize the interface energy. They exhibit dual functionality by reacting with the hydroxyl group of lignocellulosic fibers, while the others combine with the polymer matrix through an acid-base reaction resulting in covalent bonds, polymer chain entanglement, and strong interactions, such as hydrogen bonding. Additionally, CAs enable

uniform dispersion of fibers in a polymer matrix, forming new interfaces that stabilize the surface polarity of the fibers. The most efficient CAs in WPCs are MAPP, MAPE, and recently, SEBS-g-MA and SMA, including different forms of silane [144,156,157]. Generally, the performances of more than 40 CAs, comprising organic, inorganic, and organic-inorganic types, have been investigated. Organic agents typically bear two or more functionalities such as -N=C=O (isocyanates) and -$(CO)_2O$- (maleic anhydrides) in their molecular networks [158]. Through esterification and hydrogen bonding, they interacted with the polar hydroxyl groups (–OH) of cellulose to establish covalently coupled sites and combined with the polymer matrix through graft copolymerization. The following section briefly discusses common CAs, including a recent study in this area.

2.3.2.1 Maleic anhydrides coupling agents.

Most organic CAs belong to the maleic-anhydride (MA) family. These compounds feature an α, β-unsaturated double bond of carbonyl and two carboxylate groups (-COO-). They exhibit graft reactivity, in which the C=C on the heterocyclic ring engages in additional reactions with the polymer matrix. MA serves as a highly reactive monomer for grafting, allowing efficient utilization in smaller quantities because of its elevated reactivity, thermal stability, and less challenging homopolymerization [159]. Nevertheless, maintaining a low MA graft level in their CAs prevents undesired alterations to the polymer backbone. To enhance the efficiency of the shorter molecular chain of MA, radical initiators, typically organic peroxides such as dibutyl peroxide (DCP), benzoyl peroxide (BPO), tert-butylperoxybenzonate (TBPB), and ditert-butyl peroxide (DTBPO), are used at 0.5–1% by weight of the total WPCs. These initiator catalysts, particularly DCP, are commonly used with MAPP, silanes, and isocyanates of poly [methylene(polyphenyl isocyanate)] including amides of N,N-m-phenylenebismaleimide [90,156,158]. MA-modified thermoplastics such as MAPP and MAPE are the most effective compatibilizers for polyolefin matrices in WPCs. Malleated polyolefins differ from crosslinking silanes in that they are grafted onto the OH groups on the fiber surface. One end of the MA diffuses or enters the molecules in the polymer matrix, whereas the unreacted MA and OH groups of the fiber undergo acid-base interactions. To achieve effective entanglement or interdiffusion, a larger molecular chain length of MAPP is required; however, a lower anhydride content is necessary to prevent chain scission and a decrease in molecular weight, which requires an optimum amount of both molecular weight and anhydride content. Xiaolong Hao et al. [160]

performed a comparative investigation of the influence of MAPE both as the matrix by itself and as a compatibilizer for WPCs from HDPE and wood fiber contents ranging from 60% to 85% by weight. The results showed that the composites with 80 wt.% wood fiber employing MAPE as the matrix led to a significant increase of 187% and 186% in tensile and flexural strengths, respectively. Similarly, utilizing MAPE (3%) alone as the CA improved tensile strength by 224% and flexural strength by 189%. These findings suggest that the coupling efficiency of MAPE is more pronounced than that of the matrix polymer or an equal blend matrix with HDPE.

Leu et al. [161] optimized the amount of common CAs, such as MAPP, for WPCs based on PE and PP matrices, with 3 wt.% considered optimal for compositions with a fiber weight fraction below equal weight fraction of fibers and matrix polymer, whereas 5 wt.% was found to be optimal for compositions exceeding equal weight fractions. Yeh et al. [144] examined the synergistic effect of PPMA and SEBS-g-MA in PP-based WPCs with maple wood flour. The optimal MAPP loading level was identified as 2% for WPCs containing 50 wt.% maple flour. The blend of 1% SEBS-g-MA and 2% MAPP demonstrated a synergistic toughening effect, significantly enhancing reverse-notch IS without substantial reductions in TME and TS, including a notable reduction in water absorption. Similarly, adding 10 wt.% SEBS-g-MA in WPCs at 40 wt.%, along with 4 wt.% PP-g-MA, resulted in a remarkable 107% increase in notched IS and a slight reduction in the tensile modulus.

In another study, Yeh et al. [162] investigated the impact of SEBS-g-MA and SMA on various polymer matrices, including both original and recovered ABS and PS as the matrix polymers and 50% wood particles. These findings indicated enhanced miscibility and compatibility of ABS and PS, which was attributed to the shared chemical moieties. As shown in **Figure 2.6,** the composite system incorporating SMA exhibited superior properties compared to SEMA.g.MA, with enhanced stiffness when recovered ABS was used. Notably, CA amounts exceeding 5% did not lead to significant changes in SMA, whereas SEMA-g-MA adversely affected mechanical properties in all composite systems except percent elongation, possibly attributed to the poor interface compatibility or the inherent ductility of SEMA-g-MA. However, the results confirmed that the recovered ABS can be used in formulating WPCs without separating polymeric impurities and is likely stiffer and stronger than commercial WPCs with polyolefins as matrix polymers, except for the unpleasant odor of ABS, which needs to be masked with a thin layer of neat ABS.

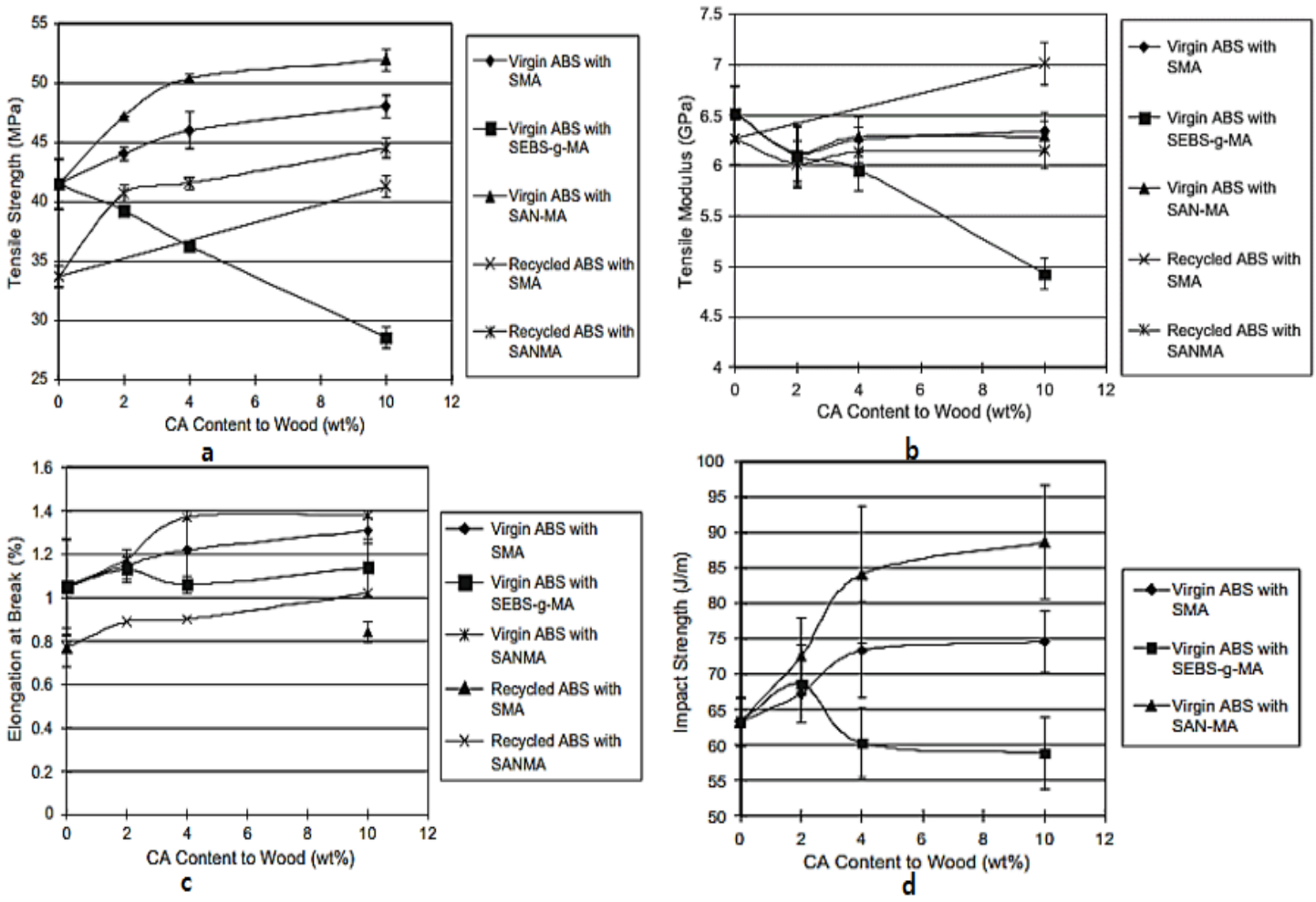

Figure 2. 6 (a, b, c, d) Variation of TS, TM, EAB and reversed Izod IS of ABS–WPCs containing 50 wt.% wood fibers with different CA content, respectively—compiled and redrawn from Ref. [162] (permission granted).

2.3.2.2 Silanes

Silanes are CAs with the general structure R'(4-n)-Si-(RX), where R' represents alkoxy and X denotes reactive organofunctionality (such as amino, mercapto, glycidoxy, vinyl, or methacryloxy groups), forming covalent bonds with fibers and/or particles in the WPCs, and R is a non-reactive alkyl, combining with non-polar matrices. Silanes primarily interact with natural fibers and polymeric matrix through four mechanisms. These include the hydrolysis of alkoxy groups from silane to form reactive silanol (Si-OH) groups, condensation of silanol groups into siloxane (Si-O-Si) oligomers, absorption of free silanol monomers and oligomers onto the hydroxyl groups of the fibers to create covalent bonds and grafting of the remaining alkyl part onto the matrix polymer via covalent bonding. Various types of organofunctional silanes are used in natural

WPCs [32]. From these silanes Wang et al. [163] carefully investigated the performance of well-known silane: n-propyl-tri-methoxysilane (PTS), γ-amino-propyltrimethoxy silane (APS), γ-methacryloxypropyltrimethoxy silane (MPS), and allyltrimethoxy silane (ATS) at 3% concentration in wood flour composites of both HDPE and PP matrix at a 60:40 ratio. Radical initiator DCP (0.15%) in MPS and ATS treatments were also included and variations in mechanical performance were evaluated considering formulations without treatment. Except for the PTS and APS treatments with a slight reduction in the FS and IS of PP-based WPCs, all organosilane treatments improved the properties of the WPCs. Incorporating DCP into the formulations of both PP- and PE-matrix-based specifically for wood flour treated with MPS and VTS resulted in a significant increase in all properties, attributed to the formation of covalent bonds between the methacryl/vinyl groups of the silanes and the C-C linkages of the matrix through radical reactions. Composites treated with MPS silane and ATS resulted in a 90%, 60%, and 50% increases in FS, TS, and IS, respectively. VTS treatment led to greater improvement than MPS treatment, which was attributed to less steric hindrance and enhanced matrix accessibility [163]

2.3.2.3 Isocyanates

Isocyanate-based organic CAs have been explored for applications in WPCs. They react with the fiber surface and polymer matrix carbon chains and fiber surfaces leading to the creation of a urethane structure or carbamate between the OH groups of the fibers [89]. In a previous study involving WPCs formulated with aspen fiber and polymer matrices of both PS and PVC, the coupling efficiency of common isocyanates—ethylisocyanate (EIC), hexamethylene diisocyanate (HMDIC), polyethylene(polyphenyl isocyanate) (PEPPIC), poly [methylene (polyphenyl isocyanate)] (PMPPC), and toluene 2,4 diisocyanate (TDIC)—at 0.5 wt.% of the polymer matrix revealed better interfacial adhesion with PMPPIC, followed by TDIC, attributed to their large accessible delocalized π-electrons [158]. Recently reported isocyanate with the best performance compared with MAPP was isopropenyl-α-α-dimethylbenzyle isocyanate (m-TMI)-grafted-polypropylene (m-TMI-g-PP) prepared from the graft polymerization of polypropylene/m-TMI/DCP at ratio of 100/10/10 (by wt.) with efficient grafting 5.6% m-TMI onto PP [164]. It resulted in substantial increase in 50%, 78%, and 270% increases in TS, FS, and TME at 50% filler loading compared to unfilled virgin PP matrix unlike MAPP coupled composites [165]. Despite their higher cost, isocyanates exhibit superior properties with increased strength and

ultimate failure compared with both silane and uncoupled systems. Moreover, unlike silanes, which require solvents to unleash their reactivity and coat fiber surfaces, natural fibers and isocyanates can react during compounding.

2.3.2.4 Common organic additives and polymers for interface adhesion

In previous studies, common organic additives belonging to the acrylic acid and methacrylate families, such as polymethyl methacrylate, epoxypropyl methacrylate, methacrylic acid, ethylene–acrylic acid copolymers, glycidyl methacrylate, and hydroxyethyl methacrylate, have demonstrated coupling efficiencies in polymer fiber composites. These additives are characterized by α, β-adjacent double bond unsaturation, and an active carbonyl structure, likely inducing crosslinking and improving interfacial adhesion [128]. Likewise, organic acids such as abietic acid and linoleic acid, featuring dienes, carboxylate groups, and reactive allylic groups (-CH_2-), have been grafted onto polymer matrices. Additionally, other organic polymers like N,N'-m-phenylenebismaleicimide-modified PP, polystyrene modified polymethacrylic acid, and polyvinyl acetate, dimethylolmelamine resin were studied for their interface compatibility [147,166]. Furthermore, non-reactive additives commonly known as dispersing agents like waxes and stearates of co-polymerized with olefin polymers, such as PE and PP were incorporated into the WPC formulations. They altered the surface energy of the fibers inducing thermodynamic segregation, which reduces the interactions between the fibers and enhances the interaction between the fibers and matrix [104].

In summary, MA-grafted polyolefins, such as PE, PP, SMA, SEBS-g-MA and recent discoveries of m-TMI-g-PP have proven to be effective as compatibilizers for lignocellulose-based fibers or particles in WPC formulations. However, the specific coupling mechanisms with both the matrix and plant-based fibers or particles and the optimal amount of CAs required for ideal properties considering the backbone polymer structure, chain length, and graft level for satisfactory material properties and cost-effectiveness in industrial production remain unclear. These areas require further investigation despite the significant progress in the exploration of interface compatibility.

2.3.3 Effect of particle size and loading rate on mechanical properties of WPCs

WPC performance relies on crucial mechanical properties such as the TS, TM, elongation at break, FS, modulus of rupture (FM), Hardness and IS. These properties were determined by

subjecting the samples to shear or impact forces and measuring the deformation or ultimate failure. Standardized method like ASTM D63 and ISO 527-2 for TS and its modulus, and ASTM D 790 and ASTM D 7264 for flexural properties were used on universal testing machine of Instron tester (Model: 4201), or Zwick/Rowell model Z010 with in the load cells of 10–20kN capacity. The IS was evaluated using ASTM D 256 or ISO 178. The composite strength is assessed before failure, which can result from factors such as fiber or particle failure, debonding, agglomerated fibers, or occasional plastic matrix failure [20,21,84] and is dependent on the component properties, composition, structure, fillers, and/or reinforcement (size and weight fraction), along with the particle-matrix interfacial adhesions. Hydrophobic matrices filled with natural fibers may experience a decrease in the interface strength without CAs or other interfacial modifications [58]. Conversely, the module of elasticity and rupture typically increase with fiber content, with minimal dependence on the interfacial strength. The composite strength often increases with a modified interface but may decrease at higher loadings owing to insufficient wetting, resulting in poor stress transfer between the particles and matrix [21,81,83]. In subsequent discussions, an effort was made to thoroughly explore the impact of particle sizes ranging from nano-to micro-sizes obtained through standard mesh screens, modified interphase, and loading rate, based on recent relevant data. This effort aimed to clarify the limited information from previous studies that have often presented diverse and contradictory results, making it challenging to grasp an overall understanding.

2.3.3.1 Variations in tensile and flexural strength and their modules

TS is the maximum stress that a material can sustain under uniaxial tensile loading. For micro- and nano-particulate composites, TS relies on the effectiveness of the stress transfer between the matrix and fillers. Similarly, flexural strength (FS), also known as bending strength, measures the ability of a material to withstand deformation under applied bending loads. Factors such as particle size, particle/matrix interfacial strength, and particle loading significantly affect composite strength. Most studies agree that a fiber must have a length greater than the critical length (Lc) to increase its load-bearing efficiency and aspect ratio [20,167]. WPC formulations from such fibers and particles are impossible because mixing results in poor fiber dispersion during compounding and a higher degree of agglomeration. Similarly, very fine particles can agglomerate and become a point of stress concentration that initiates local micromechanical

deformation processes and can potentially grow into macroscopic deformation. Although the aspect ratio of filler particles of 1–5 has been reported to improve the strength of WPCs sufficiently for various uses, the particle size and its loading rate have a profound effect on WPC properties; the following discussion investigates these variations.

Bahari et al. [168] study indicated that reducing bamboo particle sizes 0.25 to 0.12 mm resulted in a 17.8% increase in TM, a 13.8% increase in FS, and a 9.74% increase in TS, attributed to the larger surface area. Marek Kociszewski et al. [169] conducted a study on the impact of wood particle sizes in WPC formulation, comparing sieved mesh particle sizes: very small (0.25–0.5 mm), small (0.5–1 mm), large (1–2 mm), and very large (2–4 mm). The findings revealed a progressive increase in the TS and FS as the particle size increased from very small to large, followed by a decline at very large particle sizes.

Similarly, Akdogan et al. [170] explored the influence of three different mesh-sized beech particles (1200–800 µm, 800–400 µm, and <400 µm) on the mechanical properties of LDPE-based WPCs with MAPE, with the results indicating 1.23- and 1.56-times higher TS than that of neat LDPE for the first and second particle ranges, respectively. The study suggested that sieving below 400 µm may not be worthwhile due to less pronounced enhancement compared to the second type composite.

On the other hand, the study analyzed a composite of HDPE and wood flour with compositions ranging from 50% to 80% by weight, utilizing particle sizes of 40–60 mesh, 80–100 mesh, and 160–180 mesh incorporating MAPE at 0–3% of wood fiber weight, revealed a moderate FS increase from 160–180 mesh to 40–60 mesh size ranges, enhanced TM and TS across all particle sizes with a 3% MAPE addition. The study highlighted that CAs played a more substantial role in flexural properties than wood particle size and significantly affected the composite strength and toughness [167,171]. However, Ashura et al. [172] observed TS and TM for PP-based composites of wood particles for both larger (350–425 mm) and smaller (<250 mm) reinforcements compared with intermediate sizes (250–350 mm), showing a non-consistent trend with increasing wood fiber size [134]. In contrast, Vedat Çavuş et al. studied the effects of mahogany particle size ranges 0.074–0.149, 0.177–0.250, and 0.400–0.841 mm on the selected properties of neat and recycled PP-based WPCs with 3% MAPP and demonstrated that WPC

characteristics were significantly influenced by the particle size, PP type (neat or recycled), and presence of MAPP. Without MAPP, the density, FM, TM, and IS increased with decreasing particle size, and the FS values increased as the particle size decreased. Irrespective of the particle size, the addition of MAPP to the composites enhanced all mechanical properties while lowering their elongation at break. The authors attributed the deterioration of the mechanical properties of the recycled composite to the chain length and molecular weight reduction of the polymer during recycling. They also identified that the particle size, polymer time (recycled and non-recycled), particle size, and MAPP had statistically significant effects.

Similarly, Xu et al. [173] examined the influence of four different sizes of 65% Populus fibers and 4% additives (MAPE and lubricant) with mesh size ranges of 10–20, 20–40, 40–80, and 80–120, either individually or in combination, on the mechanical properties of coupled WPCs with an HDPE matrix. The formulations exhibited outstanding mechanical properties, with the finding that fiber size (80–120 mesh) resulted in the lowest FS and TS properties, but the highest contrasts with the three mesh sizes. The formulation incorporating a mix of 20–40 mesh and 40–80 mesh resulted in superior FS, FM, TS, TM, and IS. These studies affirmed the correlation between the mechanical strength and particle size of the fillers, considering their loading and coupling reactions.

We analyzed the data derived from HDPE-based WPCs (**Figure 2.7**) to better comprehend and clarify the previous discussions and explore the impact of lignocellulosic-based fiber size and loading ratios across the nanoscale to the microscale considering the size of different fibers varied in origin as the cellulose length. The fiber content ranged randomly from 20% to 60% including 1–10% for nanocellulose fibers (cellulose nanocrystals, nanofibrillated cellulose, and microcrystalline cellulose). The results indicated that formulations incorporating interphase surface modification using CAs from established treatments, such as MAPE and MAPP, consistently exhibited higher strength and superior performance compared to uncoupled formulations. Similarly, as depicted in **Figure 2.7i**, the influence of the particle size on the TS is generally small to moderate, with a weak positive relationship between the TS and cellulose-based particles. Notably, the studied particle size ranges from 100 μm to 1000 μm exhibit slight increases in TS. In contrast, the overall trend in Fig. 6ii indicates a positive correlation in TM with increasing particle size for both the coupled and uncoupled composites, implying that the

composite stiffness is easily enhanced by the loading rate at any of the particle sizes mentioned. Although the analysis lacks data for the smallest particles, such as CNC, a positive relationship is observed in FS and FM with the size of the particles and CAs across all data points **(Figure 2.7iii, iv).** Moreover, in polar-bearing thermoplastic matrices such as polyurethane, polyethylene oxide, PLA, PET, and PA, the incorporation of cellulose-based particles, ranging from nano to long fibers, fosters strong interactions and results in improved TS and FS, including TM and FM, compared to their respective PMCs. Similarly, high-aspect-ratio nanofibrillated cellulose is likely to contribute significantly to the strength of such composites compared to other microcellulose fibers. However, for hydrophobic thermoplastics, the trend observed in the graphs likely occurs in most composites [20,174].

Generally, the TS, TS, FS, and FM of WPCs depend on the particle size distribution, surface chemical nature, shape, impurities of the natural fibers, CAs type, content, conditions, and method of fabrication. Even if these factors may be complex, the big picture that can be drawn from the previous study shows particle sizes range of 100μm-1000μm can be used as reinforcement in thermoplastics matrices like LDPE, HDPE, PVC, and PP including engineering plastics ABS and PS with optimal interphase surface modification. However, the properties of the polymeric matrix (modulus and strength, crystallinity fraction, impurities, and molecular mass) require further study with dedicated experiments on well-characterized matrices and reinforcements to address these limitations.

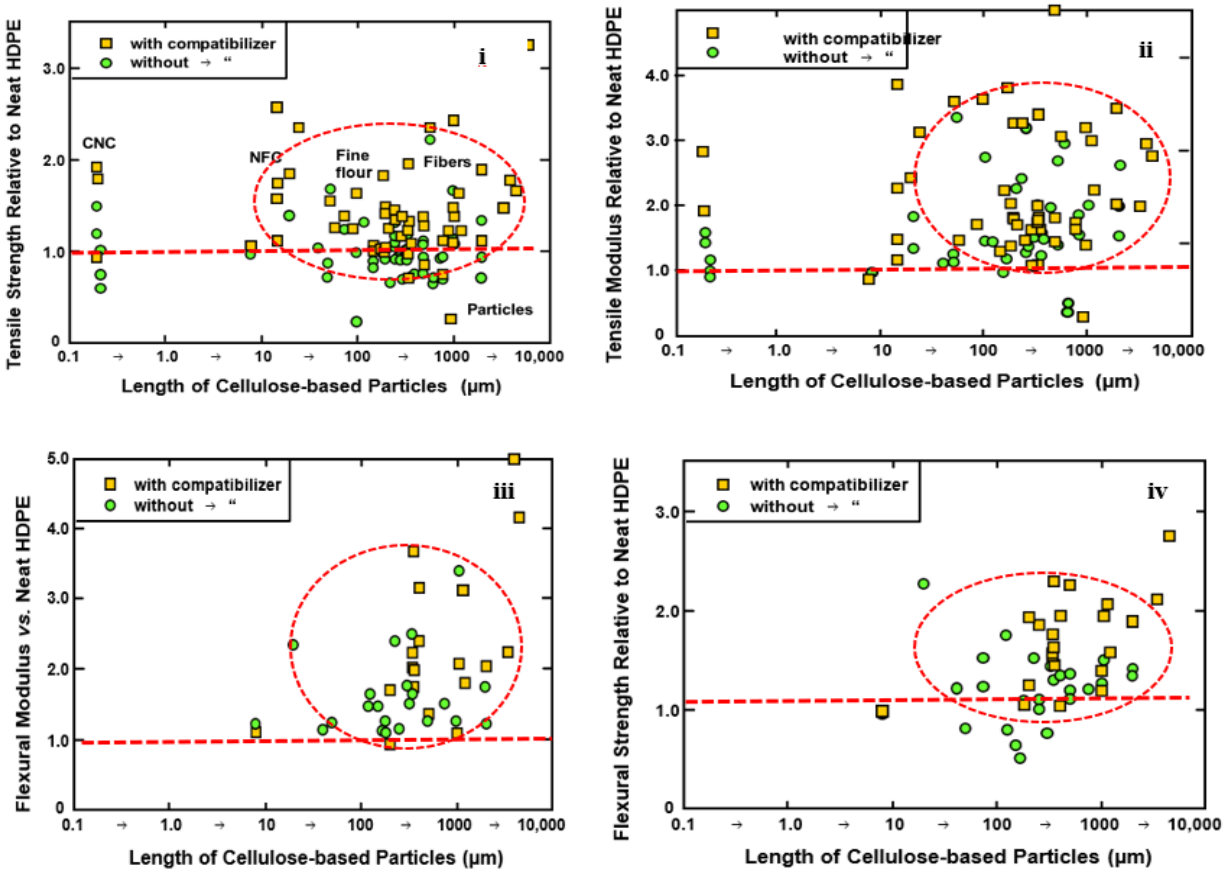

Figure 2. 7 Variations in the mechanical properties of HDPE natural fiber composites reproduced with some modifications from Ref. [20]

2.3.3.2 Impact strength

The IS measures the ability of a material to resist a sudden force or shock by exposing it to a sudden impact. The energy absorbed before breaking or distortion was assessed using Charpy or Izod impact tests. Previous studies on WPCs revealed two distinct scenarios for IS variations—involving increasing and decreasing trends with specific levels of dispersed phase constituents and an overall negative correlation observed with the composition of the dispersed phase in WPCs [175]. In a study examining a WPC formulated from a PP matrix, 30–50% short jute fibers, MAPP (1 and 2%), and three impact modifiers (Excellent VA 1803, Royal Tuf 465, and Excellor PO 1015) [176], both notched IS (NIS) and unnotched IS (UIS) exhibited increasing trends. The composite met minimum requirements for broader applications, especially at 40% fiber fraction, 2% PPMA, and 9% olefinic material-based impact modifiers (Excellor PO 1015). In a separate case, Jute fibers incorporated into PP at 10–40 wt.% showed increasing trends up to 30%, followed by a decreasing trend attributed to fiber agglomeration. Similarly, WPCs formulated

with (0–30%) fiber and (0–40 wt.%) PP and HDPE matrix, fabricated via CM, exhibited an initial increase in Izod NIS up to 30% fiber content. Earlier studies on abaca fibers and sisal fibers also reported increasing NIS trends up to 30% fiber fractions in different polymer matrices. The UIS of the fiber content (0–60 wt.%) in CM for short randomly distributed banana fiber PP composites showed an almost linear increase as the fiber content reached 50% and decreased with further additions due to non-uniform stress transfer. Similarly, Li et al. [175] studied the NIS of the Izod test and the UIS of the Charpy test in a PP-matrix-based WPC formulated from 0 to 40 wt.% sawdust fibers and 5% MAPP exhibited increased strength surpassing the neat matrix polymer when compounded by CoTS and consolidated by IM. In the absence of MAPP, IS decreased with increasing filler content, indicating a positive influence of the MAPP compatibilizer.

A similar positive correlation was observed for the IS of the WPC made from recycled plastics. The addition of ethylene–vinyl-acetate (EVA) and ethylene-propylene-diene monomer (EPDM) to wood flour and sawdust-recycled PP resulted in enhanced IS, with the most significant improvement at 9% EVA addition, although still lower than their respective virgin PP-based composites. This enhancement resulted in slight reductions in the FS and MR of the recycled PP composites. In a related study, IS was improved in composites containing wood flour and recycled PP through the incorporation of nano-clay, leading to significant enhancements in NIS, UIS, FS, TS, and TM while reducing water absorption and thickness swelling [177].

Generally, NIS of the WPC formulated from fibers increases up certain level, mostly 30%, and UIS will increase up to 40–50% for short fibers and particle-reinforced thermoplastic matrix whenever appropriate CAs and impact modifiers are incorporated in the formulations. In the second scenario, a clear inverse correlation was observed between fiber content and IS. In the case of PP-matrix-based WPC with 0–40% Aspen fiber content and a mix of polybutadiene isocyanate and MAPP manufactured by CM, the Charpy–Izod tests showed a decrease in IS as fiber content increased, attributed to the poor compatibility of the Aspen fibers with equally mixed-coupling agents. Similarly, the coupled WPC produced from PP and poplar fibers (10–40 wt.%) via CM, wood flour content (30 and 40 wt.%) with LLDPE manufactured by IM, and various other fiber-reinforced composites exhibited decreasing trends in both NIS and UIS as fiber content increased. Recycled injection-molded hemp-PP composites with 0–20 wt.% fiber content with MAPP and lignin inclusion also demonstrated a similar reduction in IS for both NIS

and UIS [82,178,179]. The reported decline in the observed trends was attributed to inadequate interfacial adhesion, fiber agglomeration leading to regions of insufficient wetting, the formation of fiber-fiber attractions creating new stress concentration points, and a shift in the fracture characteristics of the matrix from ductile to brittle [81]

In summary, despite the complex trends observed in the IS of WPCs with increasing reinforcement of fillers or fibers and the challenges posed by different forces and test methods, the IS of WPCs can be potentially enhanced further, achievable by incorporating suitable CAs and impact modifiers to strengthen the interphase while simultaneously optimizing other mechanical properties.

2.3.3.3 Dynamic mechanical thermal properties

Dynamic mechanical thermal analysis (DMTA) is a technique used to assess the mechanical and viscoelastic properties of materials by subjecting them to a dynamically varying sinusoidal stress and strain, measuring parameters such as storage modulus (E'), loss modulus (E''), and damping properties (Tan δ). E' reflects a material's elastic or energy storage capability, whereas E'' represents its viscous or energy dissipation capability, which is influenced by the molecular arrangements, heterogeneities, motions, and phase transition processes. The damping factor, which is the ratio of the loss modulus to the storage modulus, indicates the damping characteristics of a material. Unlike non-elastic or rigid materials, a large elastic material with a high damping factor cannot deform easily when subjected to external forces [180]. DMTA provides a comprehensive view of the glass transition temperature (Tg) in composite processes, considering three potential temperatures: the onset of storage modulus (E'), the maximum loss modulus (E''), or the highest point of tan δ (**Figure 2.8i**). A composite with improved interfacial bonding exhibits a lower energy loss owing to restricted internal molecular mobility structures [181–183].

DMTA has been extensively used to investigate the viscoelastic properties of WPCs. The influence of additives on the viscoelastic properties of extruded wood flour-PP including HDPE composites indicated that incorporating coupling agents exhibited lower tan α values, but superior retention of storage modulus (E') at specific temperatures. These findings further reveal that the addition of wood flour enhances both the storage and loss moduli. Zhou et al. [184] recently explored the application of DMTA to analyze rubberwood-plastic composites (RubWPCs).

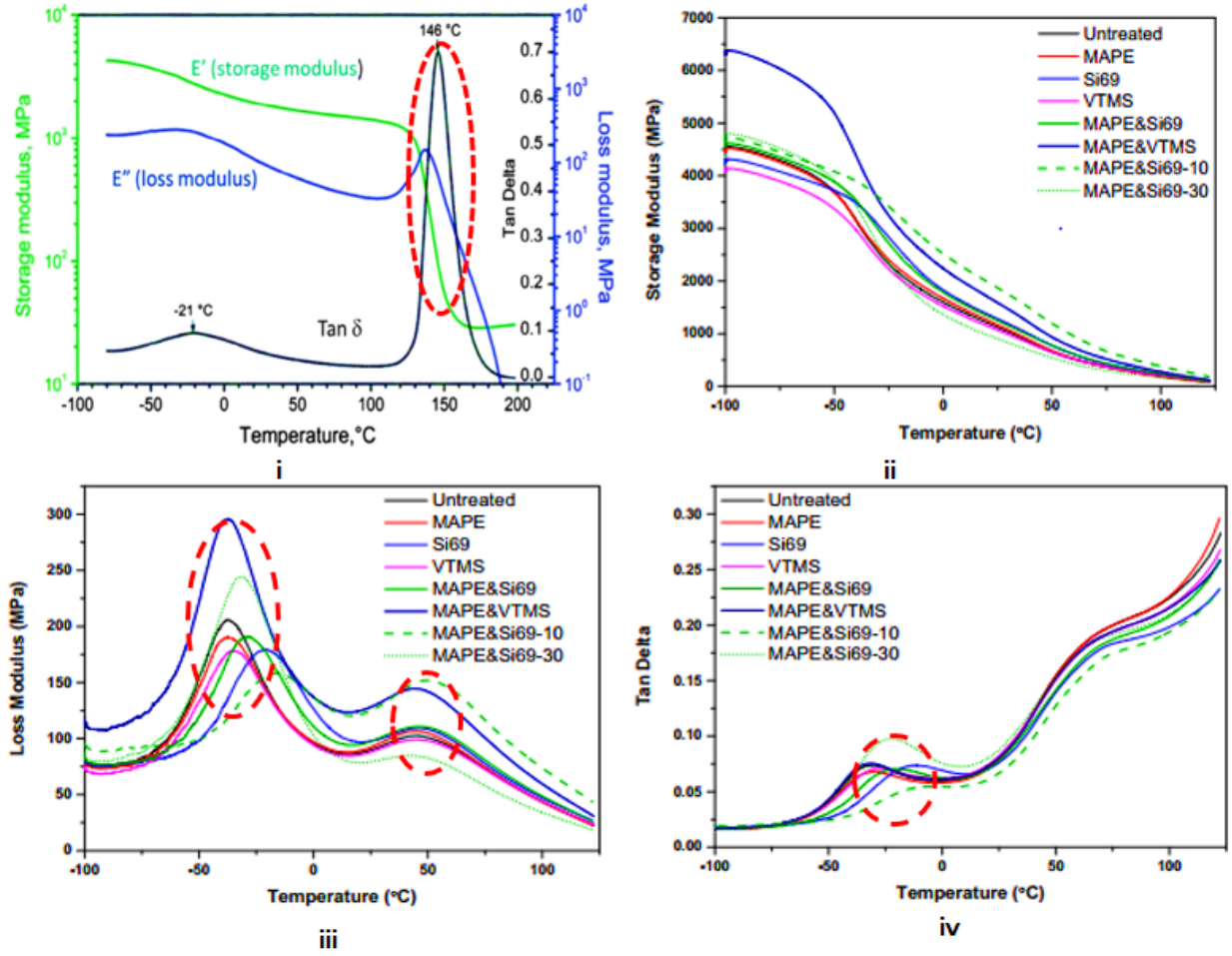

Figure 2. 8 (i) Determination of Tg reproduced from Ref. [186] with permission granted. ii) Storage modulus, (iii) loss modulus, and iv) tan δ of untreated and coupling-agent-treated RubWPC as a function of temperature—reproduced from [184].

These innovative composites were formulated using recycled tire rubber (rTR), wood fibers, and recycled HDPE as the polymer matrix, incorporating coupling agents (MAPE, bis(triethoxysilylpropyl)tetrasulfide (Si69), and vinyltrimethoxysilane (VTMS) and lubricants. During the formulations, the compositions of the wood fibers and HDPE matrix were held constant at 30% and 40%, respectively. The compositions of three CAs and their equal blend ratios were 3% and 1.5% respectively with 3% lubricant throughout the formulations. rTR compositions were fixed at 20%, except for the mixed ratios of MAPE, Si69-10, MAPE, and Si69-30, where their rubber contents were 10% and 30% respectively with 10% more addition for both the wood fibers and the polymer matrix. The results showed that the composites treated with multiple coupling agents (MAPE, VTMS, and a combination of MAPE and Si69) exhibited a

greater storage modulus than both the untreated and single CA-treated composites, owing to their superior interfacial bonding (**Figure 2.8ii–iv**). As shown in **Figure 2.8ii**, E′ decreases in all the composites with individual CAs, i.e., MAPE, Si69, or VTMS in the temperature range from -100 to -50 °C, compared with untreated ones, which did not have any CAs, except lubricants. However, at temperatures above -50 °C, Tg and E′ of MAPE- and Si69-treated composites mostly showed higher values compared with the untreated composites. Similarly, the composites formulated with combined MAPE and VTMS, resulted in greater E′ than both untreated and single CA-treated composites for both MAPE and Si69 or MAPE and VTMS maximizing the capability of interface refining and bonding strengthening of each CAs [185].

As seen in **Figure 2.8iii**, the relaxation peaks between -38 and -16 °C, linked with the molecular movements of the rubber phase related to its Tg, were minimized with less E″ values when the temperature was raised, thus confirming the improved adhesion between the rubber particles and other constituents of the CA-treated composites. Moreover, the relaxation peaks around 50 °C which is related to the α transition of HDPE matrix because of the chain segment mobility. The non-negligible E″ at this temperature increased after CA treatment owing to possibly the minimum flexible mobility of the macromolecules. Similarly, the Tg of the composites treated with CA shifted to higher temperatures owing to intermolecular crosslinking caused by groups of Si69 and the vinyl groups of VTMS and MAPE with rubber, HDPE, and wood fiber macromolecules. However, storage modulus (E') gradually decreased with further addition of rTR, even with MAPE and Si69 inclusions, and became evident with a 30% rTR attributed to challenges in achieving a uniform filler distribution and insufficient wetting rTR within the HDPE matrix system. Conversely, with a lower addition of rTR (10%), relaxation peaks were observed for the RubWPC at higher temperature regions, resulting in an elevated Tg, suggesting that stronger interactions between rTR-wood fibers and rTR-HDPE in the composites contributed to immobilizing polymer chains along the interfaces, leading to a decrease in the corresponding tan δ amplitude.

2.5 Interphase characterization method of WPCs

At the modeling scale, an interface is defined as the shared boundary between the dispersed phase (fibers or particles) and the polymer matrix, where the matrix ends, and the reinforcement (fiber or particle) begins. This interface encompasses a three-dimensional transition region known as the interphase, which is characterized by properties and microstructures that differ from both the dispersed phase and matrix polymer [90,91] Four methods are commonly used to characterize the morphology and chemical composition of the interphase, as shown in **Figure 2.9**. These methods include nano-and micromechanical techniques, spectroscopy, surface morphology analysis, and thermodynamic techniques. Nanoscale analysis involves the use of scanning probe microscopy (SPM) or atomic force microscopy (AFM) to directly measure the interfacial shear strength. Microscale mechanical measurements included fiber fragmentation, single fiber pull-out, and fiber push-out tests.

Scanning electron microscopy (SEM) and transmission electron microscopy (TEM) were employed for the microscale analysis of the interface morphology and phase distribution, while Energy-Dispersive X-ray Spectroscopy (EDS) was used to determine the composition. Macro-scale mechanical measurements assess the overall composite properties, and tests include 45 °in-plane shear, fracture toughness, tensile strength, impact, DMTA, thermal analysis with Differential Scanning Calorimetry (DSC) and Thermogravimetric Analysis (TGA). These tests adhered to ISO or ASTM standard test methods. Morphological and chemical analysis techniques can be categorized into direct and indirect observations of the interphase. Direct observations involve optical microscopy (OM), atomic force microscopy (AFM), scanning electron microscopy (SEM), transmission electron microscope (TEM), micro- or nano-X-ray computed tomography (CT), and nanoindentation, providing internal and external morphological patterns, compositions, fiber dimensions, surface properties, and in situ assessment of the fiber-matrix interface [187]. Nanoindentation provides direct measurements of the hardness and reduced elastic modulus at the sample surface, allowing quantification at the fiber-matrix interface.

In contrast, indirect interface analysis methods such as X-ray photoelectron spectroscopy (XPS), X-ray diffraction (XRD), Fourier-transform infrared spectroscopy (FTIR), energy-dispersive X-ray (EDX) spectroscopy, Raman spectroscopy (RS), and Solid-State Nuclear Magnetic

Resonance (NMR), and thermal analysis techniques such as TGA and DSC offer indirect information about the interphase. Thermal analysis (DSC and TGA) determined that the material weight loss during melting and crystalline shifted with increasing temperature and indirectly predicted the reaction products in the interphase. FTIR and RS detect chemical moieties or changes in functional groups on fibers, polymer matrices, and composites, indirectly predicting interfacial properties. Similarly, EDX coupled with TEM and XPS qualitatively identify and quantify combinations of various components at the interface depending on how the sample and X-ray excitation interact [15]. XPS provides detailed information on the chemical compositions and electronic states of elements in a specific sample, even in the parts per thousand range. Meanwhile, Nuclear Magnetic Resonance (NMR) leverages its sensitivity to chemical shifts, relaxation times, and dipolar couplings of polymers at the interface to predict the structure and dynamics through magnetization response from the surface of reinforcement [90].

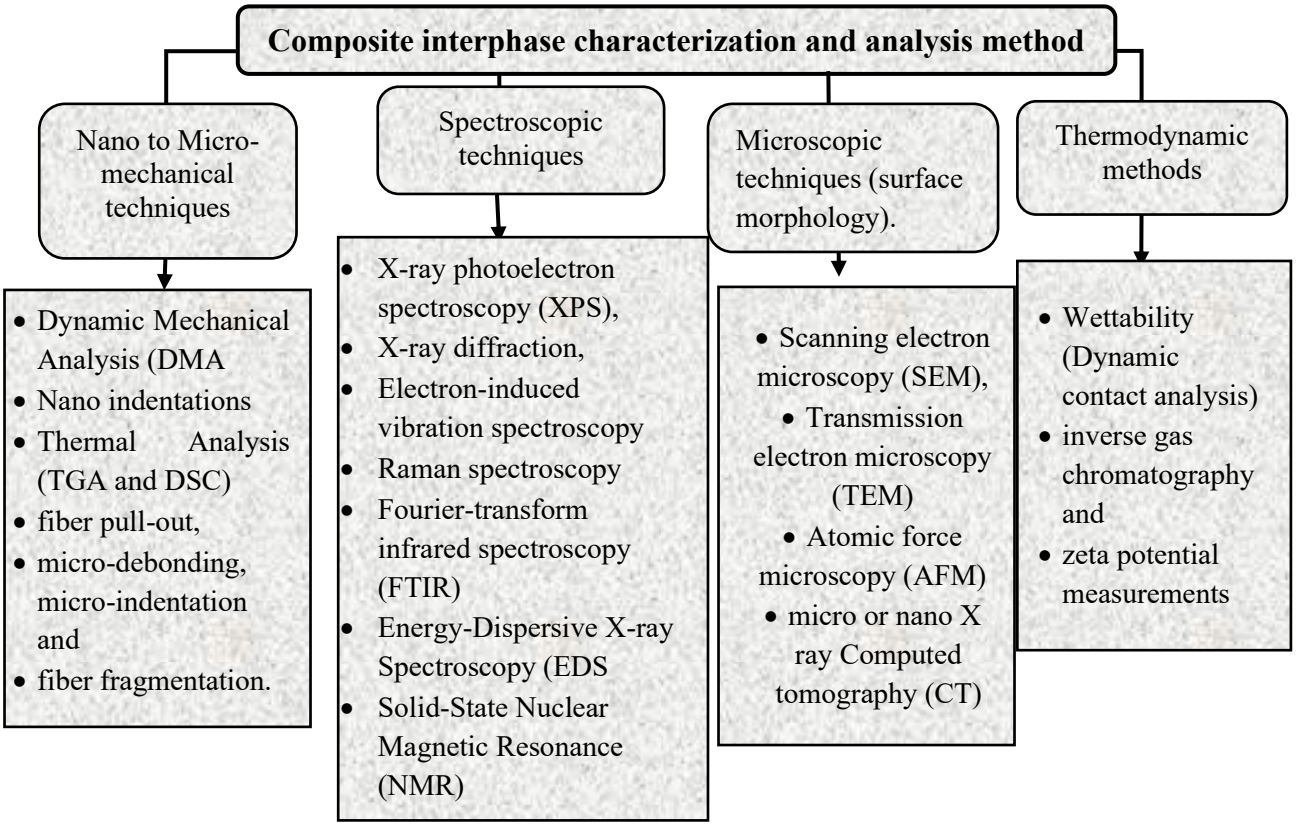

Figure 2. 9 Interphase surface characterization methods

The selection of the interphase characterization method relies on the specific material system and desired level of detail for evaluating the interphase compatibility. The following sections discuss

widely used techniques that aim to enhance our understanding of their role in interphase analysis, drawing insights from previous studies.

2.5.1 FTIR and XRD spectroscopy

FTIR is used to identify functional groups and chemical bonds by analyzing molecular vibrations in the infrared region. They utilize vibrational stretching (symmetrical and antisymmetric) and bending modes (scissoring, rocking, wagging, and twisting) to absorb specific infrared wavelengths [188]. These unique absorption patterns serve as fingerprints for different chemical groups, allowing the analysis of interfacial bonding and associated functional groups [26]. XRD, employed to determine the crystallographic structures of the materials, analyzes the diffraction patterns created when X-rays interact with a crystalline polymeric matrix or reinforced phases, with the degree of crystallinity in both the dispersed phases and polymer matrices and changes within composite systems assessed. Recently, Yu et al. [189] examined the FTIR and XRD spectra of WPCs made from poplar fiber (WF) and recyclable plastic wastes (ABS, PE, PVC, HDPE, and PP) in a polymer matrix with a WF ratio of 9:1 by weight. In the FTIR spectra (**Figure 2.10a**), the peak at 1035 cm^{-1} indicates the molecular fingerprint of C-O symmetric stretching in cellulose and hemicellulose. The absorption bending peak observed at 1456 cm^{-1} corresponds to C-H rocking in methyl (CH_3) and methylene (CH_2) respectively, similar to the stretching of C-H in CH_3 and CH_2 observed around 2924 cm^{-1} [32], with reduced broad O-H stretching of hydroxyl groups (-OH) lignocellulose peak at 3339 cm^{-1} implying potential compatibility [188]. Similarly, as illustrated in **Figure 2.10b**, two distinct peaks are observed in WPCs and poplar fibers around the 2θ values of 15.6° and 22.4°, corresponding to the crystal structures (101) and (002), respectively [70,190] Using these crystal peaks, the relative crystallinity indices (CrI) were determined, yielding values of 62.54%, 55.53%, 63.37%, 64.23%, and 58.41% for WF/PVC-9, WF/ABS-8, WF/HDPE-9, WF/PE-9, and WF/PP-9, respectively. These values are lower than the CrI of poplar fibers (68.31%). The authors attributed the changes in cellulose crystalline and surface functionality to enhanced compatibility.

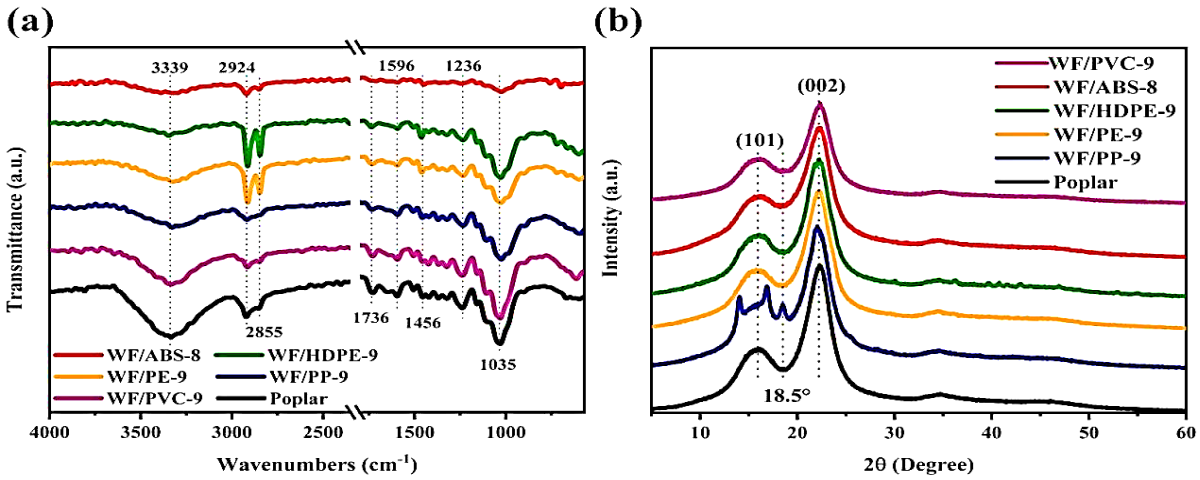

Figure 2. 10 (a) FTIR spectra of WPS and poplar (b) XRD spectra of WPCs and poplar—adopted from Ref. [189].

2.5.2 Energy-dispersive X-ray spectroscopy (EDX) coupled with both SEM and TEM

Using SEM-EDX and TEM-EDX, the interfacial properties of the reinforcement-matrix systems were explored by examining the electron sets generated when high-voltage beams were focused on the sample, interacting with atoms, and causing the emission of secondary electrons, backscattered electrons, and characteristic X-rays. Secondary electrons play a key role in producing microscale high-resolution topographies and in capturing unique signal components in composite systems. Backscattered electrons are sensitive to the atomic number of the elements within the sample. The intensity of the BSE signals facilitated the creation of compositional contrast images, with regions containing higher atomic number elements appearing brighter in the BSE image. Likewise, Characteristic X-rays are generated as the inner-shell electrons are ejected by the primary electron beam, and the outer-shell electrons move to lower energy levels to fill vacancies. The detection of the emitted X-rays allows the identification and quantification of the elements present in the sample. The analysis was integrated with SEM or TEM, utilizing signals from secondary electron images or electron scattering to reveal surface details. Simultaneously, the EDX spectra and elemental maps provided insights into the elemental composition and distribution within the sample. As shown in **Figure 2.11**, Meekum et al. [191] investigated a bonding state system for toughening WPCs with a PP matrix. In this study, 35 parts per hundred (Phr) wood flour, 8 Phr Silane (vinyltrimethoxy silane) as crosslinking agents, 0.3 Phr of DCP as a free radical initiator, 20 Phr talc, 2 Phr heat or process stabilizer, and varying

amounts of ultra-high molecular weight polyethylene (UHMWPE) (5, 10, 15, 20, 25 Phr) were used as a toughener. The results indicated improved IS of WPCs up to 10 Phr UHMWPE loading, with higher concentrations leading to UHMWPE agglomeration and subsequently inferior mechanical properties, as observed in the SEM morphology of specimens with UHMWPE contents of 0, 10, and 25 Phr. As shown in **Figure 2.11b**, the interfacial bonding formed at the interphase of the WPC system was relatively good because there was no interfacial incompatibility or recognizable split between the fiber and matrix phases and the macro elongated UHMWPE, which could have been induced by shearing during IM. However, a moderately weak dispersion of UHMWPE in the PP matrix phase was observed (circles), which grew larger with increasing UHMWPE content (**Figure 2.11c**) and resulted in phase separation, as observed at higher magnification (300x) (**Figure 2.11d**). They concluded that the addition of UHMWPE above 20 Phr reduced the toughness of the composite, mainly because of the agglomeration of the UHMWPE particles. Similarly, Yang et al. [191] investigated the main chemical substances in the non-metallic parts of waste printed circuit boards (NPCB) using SEM-EDS to reinforce the wood filler for excellent WPC formulations. The glass fibers in the NPCB recycled from waste printed circuit boards were milled using a novel approach called solid-state shear milling (S^3M) and further treated with 2% silane CAs. Before compounding in CoTS, the LLDPE/WF/NPCB-S^3M composites with filler contents of 10–50 wt.% and NPCB: WF of 1:1 was co-milled together in the S^3M at ambient temperature. As shown by the SEM-EDS results in **Figure 2.12a**, the significant amounts of silicon, aluminum, and calcium found in the NPCB could originate from the chemical constituents of SiO_2, Al_2O_3, and CaO, which were traced back to the major chemical constituents of the fiberglass and were determined to be nearly 70 wt.% in NPCB indicating valuable resource that needed to be cascaded for the composite's fabrications. Similarly, elemental analysis shows that NPCB has a significant fraction of carbon (32.4%), oxygen (34.7%), and bromine (4.9%) which came from epoxy resin and brominated flame retardants widely utilized in the printed circuit board as shown in **Figure 2.12b**. Carbon percentage decreased to 5.6% wt. with S^3M treatment, whereas the concentrations of silicon, aluminum, and calcium significantly increased, showing that S^3M potentially removed the epoxy resin from the fiberglass surface and facilitated compatibility, as observed in the better mechanical properties than commercial polyolefin WPCs.

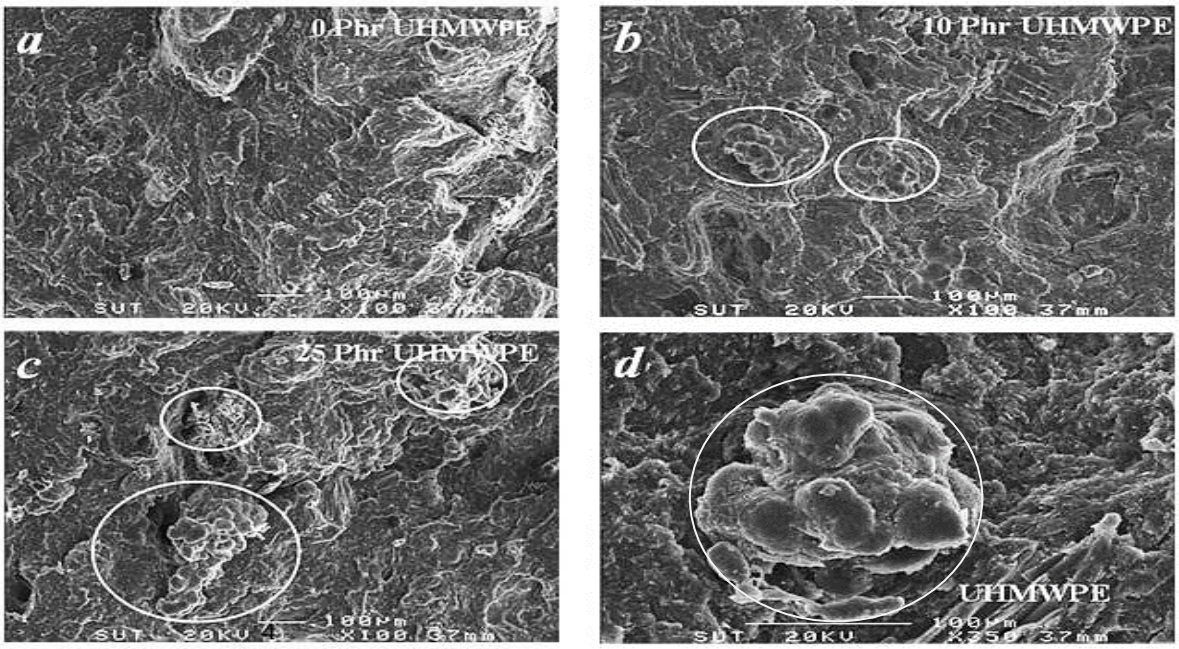

Figure 2. 11 SEM morphology of NIS specimens with UHMWPE content of 0 Phr (a), 10 Phr (b), and 25 (c, d). Phr adopted from Ref. [191] with permission granted.

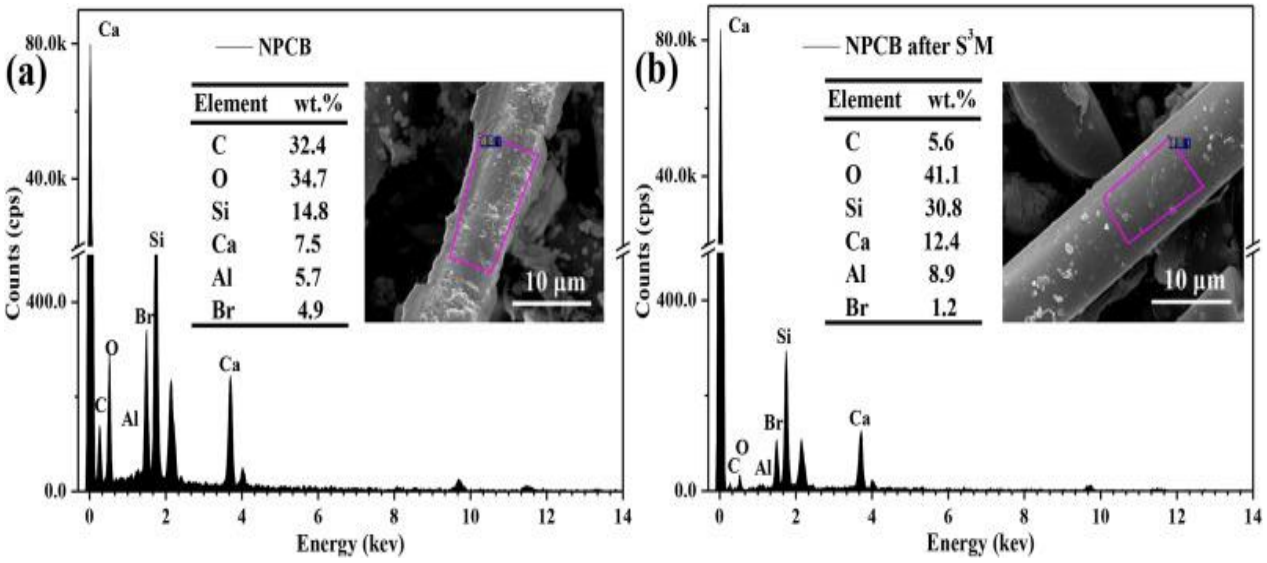

Figure 2. 12. SEM-EDS for (a) untreated NPCB and (b) NPCB treated with S^3M—redrawn from Ref. [74] with permission granted.

2.5.3 X-micro ray computed tomography (XµCT) and atomic force morphology (AFM)

XCT is a non-destructive method employed to scan two-dimensional (2D) cross-sectional images, which are then processed into three-dimensional (3D) representations based on X-ray attenuation.

The varied levels of X-ray attenuation passing through the materials lead to distinct phases based on density variations, offering detailed insights into the internal structures through high-resolution imaging, in contrast to the overall 2D morphology provided by SEM or TEM. Krause et al. [192] employed XμCT to visualize the particle size distribution and internal structure of WPCs, analyzing size, morphology, and spatial alignment to understand phase fractions and determine the potential reutilization of recycled particles compared to virgin wood particles in WPCs. The color coding in the analysis represents the air fraction, wood particles, PP matrix, and high-absorbing particles as black, light grey, dark grey, and bright white, respectively. WPC formulations included recycled thermoset composite particles (RCPs) from particle boards (PB) and MDF, virgin wood particles (VWP) from both Spruce (S) and Beech (B), and reprocessed WPC particles (RWPs) originally made from Spruce and Beech. Visualizations highlighted the spatial structure of the largest 10% of wood particles/fibres in red (RWPs) and blue (RCPs) within an isolated 3D volume. As illustrated in **Figure 2.13**, XμCT morphology revealed diverse sizes, morphologies, and spatial alignments of wood particles in all composites along the melting flow. The particles displayed uniform dispersion and were enriched with a polymer layer on all surfaces. In the core layer, elements such as fiber fragments, single fibers, and wood fiber bundles, including small particle agglomerations, were aligned perpendicular to the melt flow.

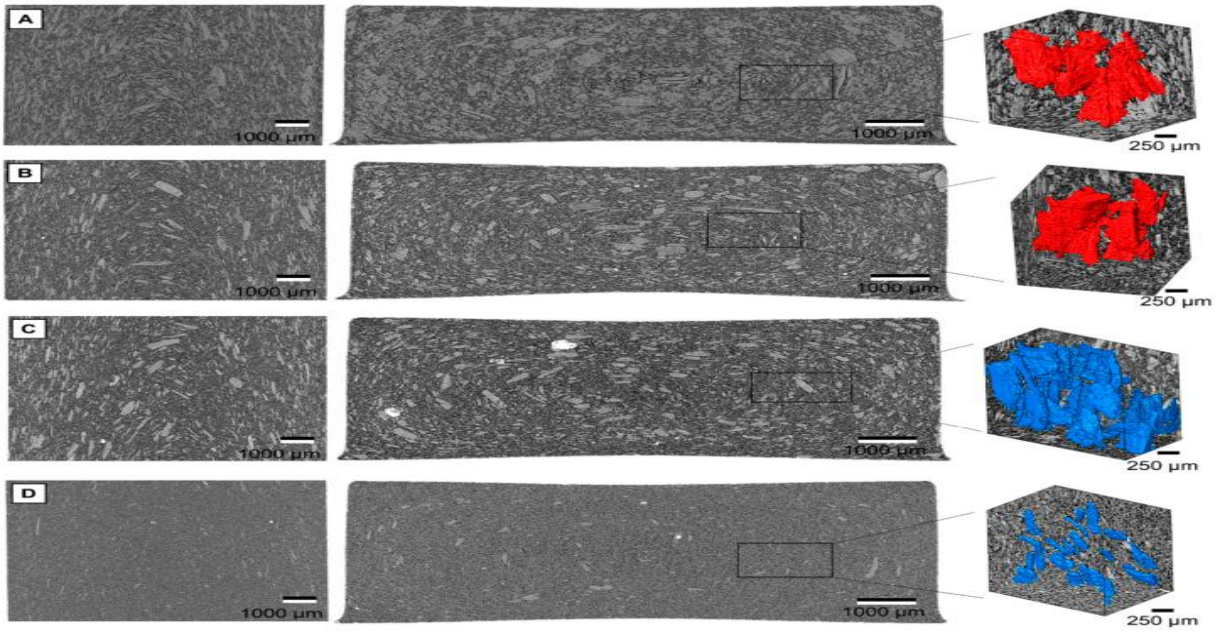

Figure 2. 13(Left) XμCT images RWPs [A: RWPC (B); B: RWPC (S)] and RCPs [C: WPC (PB), D: WPC (MDF)], (Middle) Orthogonal view, (Right) 3D volume of wood tissue (blue) and wood fiber/particle agglomerations (red). Redrawn from [192].

Unlike other composites, MDF-based WPCs have many thin particles/fibers and fewer fiber bundles. The phase fractions per unit volume (polymer, wood, and void space), length, and aspect ratios of WPCs are listed in **Table 2.4**. Compared with the original particle size (11296 µm) of MDF the particles that remain in their WPCs were largely reduced in size but retained their high aspect ratio compared with other composites, which were nearly reduced by half. Similarly average void fractions found in the core layers surrounded by polymers were between 0.16% (WPC (MDF)) and 0.62% (WPC(B)) with average volume fractions of wood components ranging between 56.4% and 58.9%. Furthermore, highly absorbing particles were partially observed in both RCP composites (**Figure 2.13 C and B**). Comparatively, fibers from MDF remained in their composites with reduced fiber degradation during the injection molding process, resulting in a smaller void fraction compared to WPCs formulated with virgin fibers, implying enhanced adhesion, possibly facilitated by residual adhesives.

Table 2. 4 Quantification of different phases of WPCs with standard deviation in parenthesis of two-dimensionally considered phase fractions—determined based on their volume fraction of tomographic (voxel). Reproduced from with modification from Ref. [192]

Sample		**Phase fractions**			**Wood particles**	
SID	Particle type	Wood/v%	Polymer /v%	Voids/V%	Length/ µm	Aspect ratio
WPC(B)	VWPs	57.34(2.2)	42.04(2.2)	0.62(0.11)	362(143)	2.7(1.2)
WPC)	VWPs	57.57(1.6)	41.89(1.5)	0.54(0.08)	410(180)	3.1(1.3
R-WPC(B)	RWPS	56.58(2.3)	42.86(2.3)	0.56(0.09)	366(194)	2.6(1.1)
R-WPC(S)	RWPS	57.38(1.3)	42.2(1.4)	0.42(0.08)	404(164)	3.2(1.2)
R-WPC(PB)	RCPS	56.39(2.2)	43.24(2.1)	0.37(0.08)	401(140)	3.8(1.6)
WPC (MDF)	RCPS	58.91(2.2)	40.93(2.2)	0.16(0.07)	395(138)	7.5(2.8)
Initial particles dimensions before compounding						
SID label			Particles type		Length (µm)	Aspect Ratio
Beech wood			VWPC		839	5.2
Spruce Wood			RWPS		879	5.3
Particle board			RCPS		1052	6.4
MDF			RCPS		1126	8.7

SID: sample identification; VWPs: virgin wood particles; RWPs: reprocessed WPC particles; RCPs: recycled composite.

AFM is performed by scanning a sharp tip over the sample surface and evaluating the interaction forces between the tip and the sample. The tip connected to a flexible cantilever records the deflection of the cantilever to generate a topographical map of the sample surface. In contrast to X-ray computed tomography (CT), which emphasizes detailed internal structure information, AFM excels in high-resolution imaging and characterization of surface features at the nanoscale. AFM operates in non-contact, semi-contact (tapping), and contact modes. Cantilever deflection is determined by the contact force, with the tip periodically touching the sample surface at a larger amplitude when crossing a concave area and at a lower amplitude when crossing a convex zone. Therefore, the variation in the oscillation amplitude was utilized to evaluate the topographic variations on the sample surface. Ephah et al. [187] conducted an interesting review on the application of AFM to characterize the interfacial adhesion components of WPCs; this review is recommended for detailed insights. In addition, recent studies have used AFM to characterize composite surface properties, particularly surface roughness, to investigate the interface surface adhesion required for a strong interphase. Hünnekens et al. [155] used AFM to investigate the atomic-scale features of the WPC surface roughness required for coating to impart a wide range of fiber surface insulation. Similarly, Royan et al. [193] characterized the changes in the surface topography and morphology of a surface subjected to modification of rice husk fibers treated with alkali, acid, and ultraviolet-ozonolysis (UV/O3) to enhance compatibility with the recycled HDPE matrix.

2.5.4 X-ray photoelectron spectroscopy (XPS) and X-ray fluorescence (XRF)

XPS analyzes the X-ray photoelectrons generated by low-energy X-rays by measuring the intensity spectrum as a function of the electron binding energy. The kinetic energy and ejected electron data offer insights into the elemental composition and chemical state of the sample surface, which is typically a few nanometers to micrometers deep. In contrast, XRF excites inner-shell electrons using high-energy X-rays, resulting in characteristic X-ray fluorescence. While both methods use X-rays to examine the elemental composition, XPS is surface-sensitive, focusing on the outermost layers and providing details on the composition and chemical state but not detailed bonding information. On the other hand, XRF is a bulk technique offering comprehensive insights into the overall chemical state, composition, and bonding of elements [91,194]. Hao et al. [195] recently enhanced the dimensional stability of WF/HDPE composites

by incorporating a nanoscale carbon black (CB) network. They oxidized CB with concentrated nitric acid to obtain oxidized carbon black (OCB), which was further modified with vinyltrimethoxysilane (VTS) to create VTS-modified OCB (VTS-OCB). This modified OCB was then integrated into the WPC pellets to form a CB-network-distributed WPC through mechanical mixing and hot pressing. The resulting WPC exhibited improved thermal, tensile, and impact properties, creep resistance, lower water absorption, reduced thermal expansion, and enhanced dimensional stability compared with the carbon black-free control. XPS analysis confirmed the efficacy of carbon black (CB) oxidation, as indicated by the higher O/C ratio in the oxidized CB (OCB) than in the original CB. Furthermore, VTS modifications alter the O/C ratio in the VTS-modified OCB (VTS-OCB) because of the simultaneous inclusion of oxygen and carbon. High-resolution XPS of C1s spectra was conducted to identify changes in various oxygen-bearing groups, focusing on the peaks around 285.0 eV, 287.6 eV, and 289.2 eV, with their breakdown into five parts (**Figure 2.14**): C_1(C, H), C_2(C–O), C_3(C=O), C_4(O=C–O), and C_5(π-π) [196]. As shown in **Figure 2.14a**, the built-in inset at the upper left corner of the C_2-C_4 values for the untreated CB is extremely low. However, as shown in **Figure 2. 14b**, the amounts of C_2, C_3, and C_4 increased considerably with oxidation and after the VTS treatment. Both C_2 and C_4 were reduced compared to the OCB (**Figure 2.14c**), implying that the hydrolyzed VTS probably reacted with the hydroxyl and carboxyl groups present in the oxidized CB. Similarly, Si-O was found on VTS-OCB (**Figure 2.14d**), demonstrating a further reaction between VTS and OCB. Additional investigation of the TEM morphology revealed that the untreated CB existed in a spherical shape with particle sizes ranging from 10–40 to nm (**Figure 2.15a**). The anchoring sites of these primary CB particles were observed with larger aggregate collections on the surface of the composite due to van der Waals forces, and the VTS modification also did not change the size of the CB (**Figure 2.15b**), thus confirming the dimensional stability and better mechanical performance of WPCs owing to significantly stronger interfacial bonding matrix via nano carbon black network embedding, especially for the formulation based 2% (VTS-OCB), 48% (wood flour), 45% (HDPE), 3% (MAPE), and 2% (stearic acid lubricant).

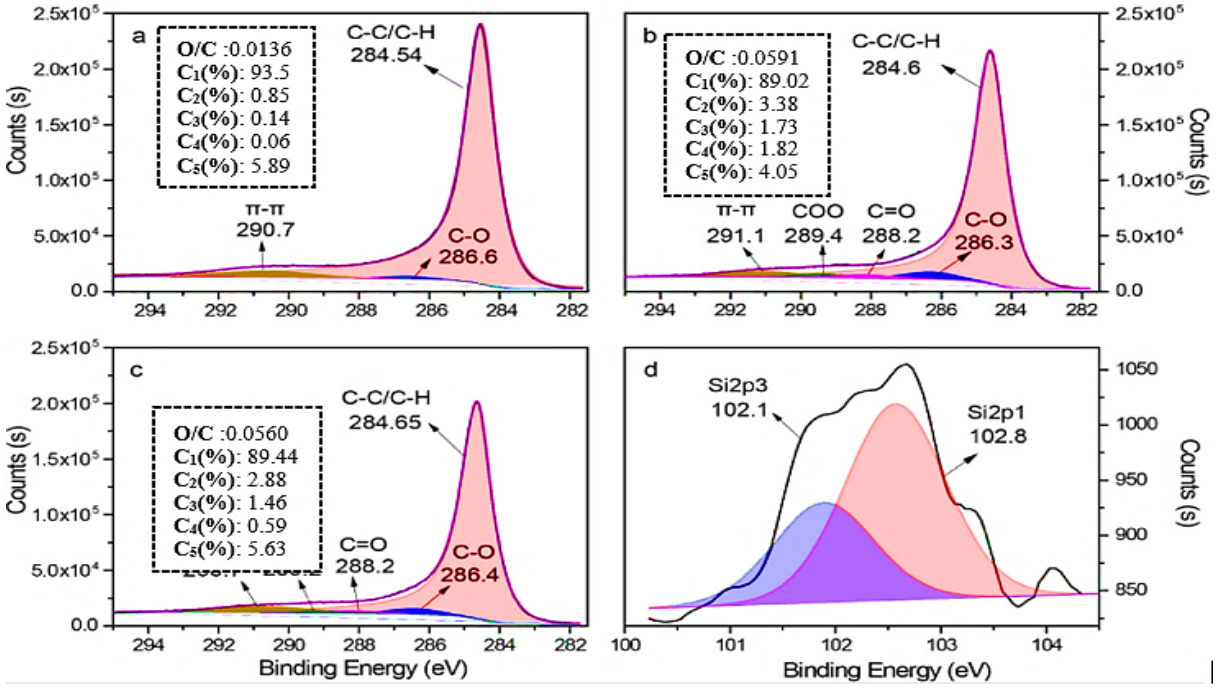

Figure 2. 14 C1s spectra of the CB (a), oxidized CB (b), improved oxidized CB with VTS (c), and Si2p spectra of oxidized CB improved with VTS (d). Redrawn Ref. [195] with some modifications with permission granted.

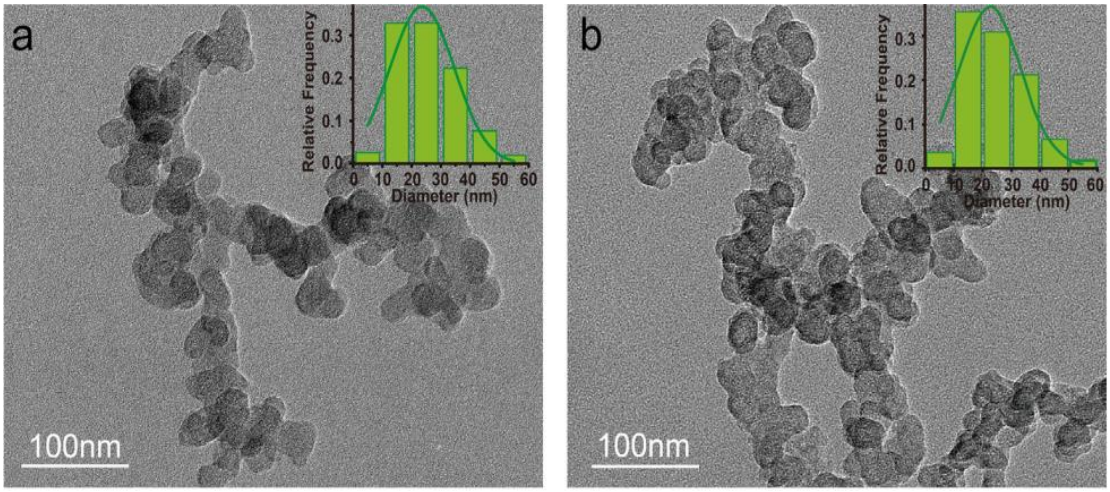

Figure 2. 15 TEM of the original CB (a), VTS modified OCB (b), and the size distribution of the corresponding CB (upper right corner). Redrawn from Ref. [195] with permission granted.

2.5.5 Thermogravimetric analysis (TGA) and Differential Scanning calorimetry (DSC)

DSC and TGA, along with its DTG, are effective thermal analysis techniques for studying material thermal properties. TGA measures the weight change with temperature, offering

insights into the decomposition temperature, volatilization, oxidation, and thermal stability, including the interface compositions where unique decomposition temperatures of the reaction products exist [24,130,197]. DSC measures the heat flow related to physical and chemical changes as a function of temperature and provides information on phase transitions (melting, crystallization, and glass transition temperatures), reaction kinetics, and enthalpy changes associated with chemical reactions.

Recently, Rathish Rajan et al. [197] explored the impact of incorporating graphene carbon plates (GNP) on the thermal degradation properties of WPCs with loadings of 5%, 10%, and 15% wt. TGA and DTG results for various compositions including PP-neat, PP/GNP (PP-G15), PP/wood flour (PP-W20), and PP/wood flour/GNP (PP-W20-G5, PP-W20-G10, and PP-W20-G15) were investigated. Adding GNP, especially at a 15% loading rate (PP-GNP), markedly raised the PP matrix's initial degradation temperature (2% mass loss) by 78 °C, attributed to the barrier effect caused by the dispersed GNPs, which prevented the diffusion of the condensed phase and breakdown products. In addition, the GNPs absorbed free radicals generated during the breakdown process. In contrast, the initial degradation temperature of PP-W20 was 288 °C, 52 °C lower than the neat PP matrix, like the single-stage thermal decomposition pattern observed in PP-G15. Early decomposition temperature of PP-W20-G10 and PP-W20-G15 increased to 294 °C and 293 °C, respectively, compared to PP-W20 (288 °C) of free of GNPs. They concluded that the inclusion of GNP interrupted the thermal decomposition by impeding the diffusion of oxygen and volatiles. The lignin phenylpropanoid units in wood flour, in conjunction with the GNPs, were found to contribute to thermal stability, particularly at higher temperatures. However, increased GNP content led to diminished effects on stability owing to agglomeration, a challenge that could be addressed with a dispersing agent and optimized formulations of strong interphases.

2.5.6 Surface thermodynamics of interphase characterization techniques

The investigation of interphase thermodynamics involves analyzing the surface free energy of both the matrix and reinforcement, considering the contributions from the polar and dispersion components. The interface energy was calculated based on the surface energy of the reinforcement, the surface energy of the matrix, and the adhesion energy between them. The total

surface free energy, which encompasses various contributions from different bond types, particularly the matrix, is typically adequate for assessing the interface interactions and stability [198]. The detailed relationships and their influence on each other, particularly on the interface energy of the interphase, were carefully and precisely reviewed recently by Huang et al. [90]. These investigations commonly utilize sessile probe liquids with a young approach for flat surfaces or dynamic contact angle analysis employing the Wilhelmy Plate method, which involves attaching the fiber or sample to a sensitive microbalance and evaluating the force as the sample is withdrawn from the liquid. The use of various probe liquids with known surface free energies, considering the sample geometry (perimeter) and contact angles, enables the precise measurement of a sample's surface free energy, especially for fiber reinforcements [91,160]. Compacted powder pellets or inverse gas chromatography (IGC) can be used to analyze the particulate dispersed phase. IGC has a specific algorithm for calculating the free surface energy, and its application in this context was reviewed by Jesson et al. [91]. This method uses a column (stationary phase) as the specimen of interest and gas-phase probes with known characteristics. Unlike wetting experiments, which probe average surface sites, IGC selectively probes high-energy sites, leading to larger surface free energy values than contact angle measurements. Recent investigations utilized contact angle methods to identify the surface properties of composites, specifically for understanding WPC properties, with deeper insights provided in [199–201]

2.5.7 Nanoindentation

Nanoindentation is a technique for measuring in-situ mechanical properties, focusing on the elastic modulus and hardness at the nanometer scale. It uses a sharp indenter to penetrate the surface of a material while controlling the applied force based on the indentation depth. Integration with AFM or SEM allows real-time imaging, which is commonly used to assess thin films and small material volumes. However, this technique has limitations in evaluating WPCs owing to the complex hierarchical structure of the lignocellulosic cell wall-dispersed phase, which makes it challenging to distinguish changes in hardness and reduced elastic modulus from the matrix/fiber interface or the hierarchical structure of plant fibers. Changes likely occur at both the matrix/fiber interface and the interface between the cell walls (i.e., the middle lamella) [184,202]. Crešnar et al. [202] recently utilized nanoindentation as an innovative approach to assess the mechanical properties (nanoindentation modulus and hardness) of WPCs. These WPCs were

formulated from wood fibers (WFs) comprising spruce (20%) and pine (80%) along with both recycled and virgin PP. WF composition varied between 10%, 20%, 30%, and 40% for both neat PP (WF-PP) and recycled PP (WF-R-PP) fabricated using CTS and IM. As shown in **Figure 2. 16a, b,** a positive correlation between the hardness and modulus across all indentation depths was observed, suggesting improved interfacial properties. The authors also explained the decreasing trends of the hardness at lower WF compositions because the thickness of the polymer matrix layer decreases with the addition of stiffer wood fibers. Additionally, they observed characteristic differences between PP- and R-PP-based WPCs, with the latter exhibiting reduced modulus values by 0.25–0.30 GPa with depth, attributed to the recycling process and the exposure of the recycled polymer to severe conditions and impurities from the origin (**Figure 2.16 c, d**).

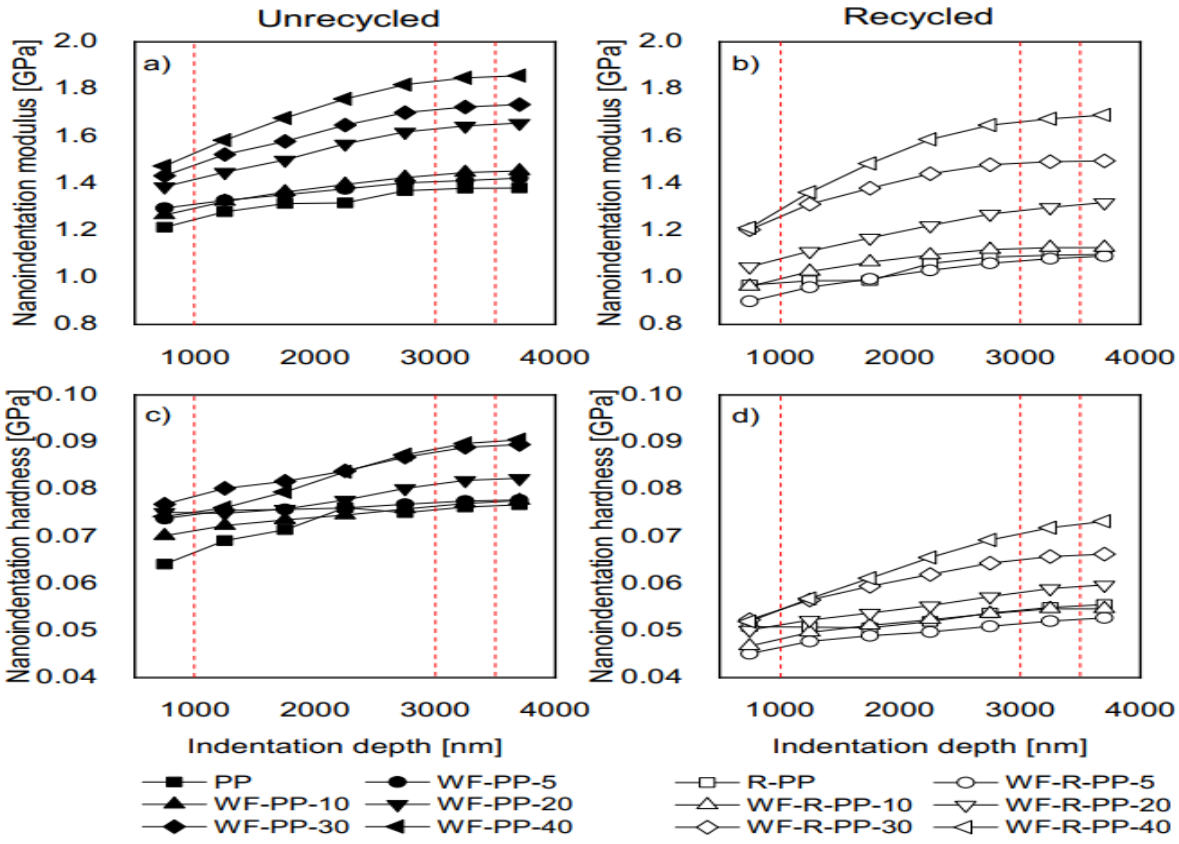

Figure 2. 16 Nanoindentation modulus (a, b) and hardness (c, d) as a function of indentation depth for unrecycled (a, c) and (b, d) recycled polymeric materials. Redrawn from Ref. [202] .

2.6 Conclusion and Future Remarks

This review comprehensively examined the key aspects of wood plastic composites (WPCs), including matrix and filler composition, interphase functionalization, characterization methods, and the modification of hydrophilic fibers within hydrophobic polymer matrices. It also explored recent advancements using recycled plastics and natural fibers, providing insights into the mechanical performance, processing methods, and existing challenges in WPC development. Among manufacturing techniques, extrusion systems such as SSE, CoSE, and CSR, followed by injection (IM) or compression molding (CM), were found most effective for homogeneous mixing and enhanced interfacial bonding. Reactive extrusion with coupling or crosslinking agents proved more efficient than solvent-based treatments, with factors like initiator type, functionalization state, temperature, pressure, and time significantly influencing performance. Eco-friendly surface modifications—such as plasma, steam reforming, and thermal treatments—also show potential, though care must be taken to avoid fiber degradation from excessive functionalization.

Chemical interphase strengthening using MA-grafted polymers (e.g., MAPE, MAPP, SMA, SEBS-g-MA), silanes, and isocyanates improve WPC performance, especially when fibers are properly treated to remove surface impurities. The overall composite properties depend on filler size, shape, content, interfacial adhesion, and processing parameters. Optimal mechanical performance has been observed with surface-treated lignocellulosic fibers below 50 wt.% and particle sizes of 100–1000 μm. Impact strength is best achieved with 30–50 wt.% fibers and suitable impact modifiers. Functional elastomers like thermoplastic elatomers could further enhance toughness but require more research for compatibility and performance optimization.

WPCs made from recycled thermoplastics show promising mechanical and thermal properties comparable to those using virgin polymers. In summary, WPCs present strong potential for sustainable materials development by utilizing recycled plastics and underexploited lignocellulosic fibers, supporting the circular economy. To unlock their full capabilities, future research must focus on improving dispersion, interfacial adhesion, and durability under environmental stressors. Additionally, greener chemical treatments, deeper investigation into interfacial mechanisms, and improved long-term stability under biological, thermal, and UV degradation are needed. Addressing concerns around treatment costs, long-term mechanical integrity, and toxic degradation byproducts will be crucial to expanding WPC applications in advanced, sustainable materials.

CHAPTER THREE

Wood polymer composites based on the recycled polyethylene blends from municipal waste and Ethiopian indigenous bamboo (*Oxytenanthera abyssinica*) fibrous particles through chemical coupling crosslinking

Abstract

Valorization of potential thermoplastic waste are effective strategies to address resource scarcity and reduce valuable thermoplastic waste. In this study, new ecofriendly biomass-derived wood polymer composites (WPCs) were produced from three types of recycled polyethylene (PE) municipal waste, namely, linear low-density polyethylene (LLDPE), medium-density polyethylene (MDPE), and high-density polyethylene (HDPE). Bamboo particle reinforcements derived from indigenous Ethiopian lowland bamboo (LLB), which had never been utilized before in WPC formulation were used as the dispersed phase. Before utilization, recycled LLDPE, MDPE, and HDPE were carefully characterized to determine their chemical compositions, residual metals, polycyclic aromatic hydrocarbons, and thermal properties. Similarly, the fundamental mechanical properties of the WPCs, such as tensile strength, modulus of elasticity, flexural strength, modulus of rupture, and unnotched impact strength, were evaluated. Finally, the thermal stability and interphase coupling efficiency of maleic anhydride grafted polypropylene (MAPP) were carefully investigated. WPCs formulated from melt blending potential PE wastes at equal ratio and bamboo-particle reinforcement significantly improved because the MAPP improved interfacial adhesion and thermally induced crosslinking, regardless of the inherent immiscibility. These results were confirmed using FTIR, SEM, and TGA analysis. The formulated WPCs may promote PE waste valorization, offering sustainable alternatives and maximizing LLB utilization. Furthermore, comparison with well-known standards for polyolefin-based WPCs indicated that the prepared WPCs can be used as alternative sustainable building materials.

Keywords: Wood plastic composite, Interfacial compatibility, Mechanical properties, Bamboo fibrous particles, Cascading thermoplastic waste.

3.1 Introduction

The growing demand for resources and environmental sustainability have emerged as a paramount concern to search for sustainable materials and efficient utilization of resources [3]. In particular, the use of fossil-fuel-based nonbiodegradable plastics has steadily increased, contributing to solid plastic waste (SPW), primarily consisting of six major commercial polymers. These include low-density polyethylene (LDPE), high-density polyethylene (HDPE), polypropylene (PP), polystyrene, polyethylene terephthalate, and polyvinyl chloride (PVC). Currently, the generation of these materials is assumed to exceed 150 million tons annually, of which with only 20% is recycled [2-4].

Polyethylene (PE) is utilized extensively in various applications, such as packaging, construction, and consumer goods, because of its versatility, cost-effectiveness, and low production cost [204,205]. Consequently, they are highly accumulated as SPW (50%–70%) with infiltration in different parts of the environment [5]. Such difficult situations and resource wastage demand sustainable utilization to minimize the PE waste fractions [129]. Among these methods, thermomechanical recycling is commonly applied because it relatively retains most of the material properties [206]. Meanwhile, other processes, such as incineration and common landfills release secondary pollutants to the an environment [26] and the pyrolysis of multipolymer systems and depolymerization techniques are not well developed [207]. Consequently, theses have led to alternatives for valorizing thermoplastic waste with eco-friendly biomass materials and reintegrating them into the product life cycle before incineration or landfilling [208].

Wood polymer composites (WPCs) have emerged as one promising materials for post-consumer PE plastic waste valorizations with sustainable natural fibers [120]. Moreover, unlike mineral fibers, plant fibers used in wood-plastic composites (WPCs) are eco-friendly, widely available, and significantly cheaper than synthetic fibers like carbon, glass, and aramid. While mineral fiber-based composites undeniably offer superior mechanical properties, they are costly, environmentally unfriendly, and unsustainable [3]. Furthermore, WPCs produced from secondary resources and sustainable bio-based fibrous particles offer a promising route for the intermediate cascading utilization of lignocellulosic biomass and thermoplastic waste valorization [106,123]. Moreover, it can address issues of energy-intensive conventional building materials, such as cement, which releases one ton of CO_2 per ton of production owing to energy-intensive

calcination reactions [209]. Similarly, structural materials, such as Fe and steel, also contribute to approximately 11% of industrial CO_2 emissions [4]. Although these construction materials cannot be easily replaced, WPCs can be used in various diverse applications, from buildings and construction (e.g., decking and cladding) to infrastructure and transportation (e.g., automotive parts), and various outdoor products [143,210]. This combines the desirable properties of wood with the processability of thermoplastic polymers, making it suitable for high-volume production using standard plastic manufacturing techniques [211].

Lignocellulose fibers contain complex molecules, such as cellulose, hemicelluloses, lignin, and pectin [4], which are physiochemically different from thermoplastic polymers. These natural-fiber molecules are rich in polar hydroxyl (–OH) and carbonyl groups and weakly combine with nonpolar hydrophobic matrix polymers, resulting in a weak interphase [39,210]. Hence, improving the interfacial compatibility between the two distinct WPC phases is a critical aspect of WPC formulations. These techniques mostly include the use of coupling agents, silanization, controlled free-radical grafting, and grafting polymerization [19][20-22]. Chemical coupling and crosslinking agents offer a strong commercial advantage over traditional solution-based treatments [33]. They efficiently form bonds through various mechanisms, such as diffusion, electrostatic attraction, chemical reactions, and secondary bonds, such as hydrogen bonds and van der Waals forces [90]. In WPC formulations chemical coupling and crosslinking agents can be applied through in situ reactive compatibilization and multimonomer graft copolymerization [27,29] without generating secondary waste, unlike solution-based processes, which make it difficult to maintain optimal levels [156].

Recently, various studies have been performed using polymeric thermoplastic matrices and different lignocellulosic fibers for WPC production. Polyolefins, such as linear low-density PE (LLDPE) [34], HDPE [63,64], PP [18, 30-32], and PVC [40,41] have been used as matrix polymers for WPCs [4,18]. Despite these advances, several areas remain uninvestigated. First, no prior studies have thoroughly characterized WPCs formulated from three potential recycled polyethylene (PE) waste fractions—specifically polyblends composed of rLLDPE, rMDPE, and rHDPE— either individually or in blended ratios as the polymer matrices. Moreover, the reinforcement potential of short, fibrous LLB particles with a wide size distribution has not been fully explored. Its integration into WPCs, particularly when compatibilized with commercially

available coupling agents such as MAPP, could yield improved interfacial bonding, thermally induced crosslinking, and enhanced immiscibility balance in polyblend matrices. Furthermore, the influence of blending highly contaminated rLLDPE with rMDPE and rHDPE on composite properties has not been adequately investigated, nor has the retention of key performance properties in such blends. Thus, the main objective of this study is to explore the combined use of three potential recycled PE waste fractions, namely recycled LLDPE (rLLDPE), recycled MDPE (rMDPE), and recycled HDPE (rHDPE) as polymeric matrices, along with the untapped potential of Ethiopian native Oxytenanthera abyssinica as reinforcement particles utilized without fiber extraction, which is energy-consuming and leaves almost no carbon footprint. Additionally, we explore how immiscibility between phases can be improved with MAPP which has wider commercial footprint. The WPC formulations consist of individual and equal blends of three recycled polyethylene types (rLLDPE, MDPE, rHDPE) as the matrix and short fibrous LLB particles of wider distribution ranging from 200 to 600 μm as the dispersed phase to investigate its wide range reinforcement. The comprehensive mechanical performances of the composites, including the coupling efficiency of the MAPP compatibilizer, were carefully investigated. Finally, the WPCs that satisfy the minimum WPC standards were further evaluated for thermal degradation and stability and further characterized with FTIR and SEM for interphase compatibility. The formulations involved mixing and compounding various compositions of the polymer matrix and LLB particles using a pilot-scale Haake mixer configured with twin-screw extruders, followed by hot-press consolidation to create a WPC board prototype.

3.2 Materials and Methods

3.2.1 Post-consumer thermoplastic and low-land bamboo fibrous particles

Waste fractionated from recycled post-consumer PE-related materials was collected from bulky urban waste streams in Addis Ababa and classified as rLLDPE, rMDPE, and rHDPE, based on their resin codes. They were further treated to obtain plastic grades of higher quality, involving size reduction, washing, regrinding, and pelletization using a counter-rotating extruder. The densities of recycled polymers and coupling agents were determined according to ASTM D792-20 and Melt flow index (MFI) were evaluated using ISO 1133 are shown in **Table 3.1**. PP grafted with 8%–10% MAPP (Mw ~9100, GPC) from Sigma Aldrich (USA) used as the coupling agent. Matured EHB culms of four to five years of age were collected from ages were harvested from

Arjo Gudatu (9° 4' 52" N, 36° 37' 30" E) district of the Oromia regional provinces in Ethiopia. After removing the topmost part, the sample was cut into small strips, air-dried, and pulverized using a micronized cross-beater mill (Retsch type SM 2000, Germany). Subsequently, the LLB particles were sieved to target size of 200–600 µm with wide distribution ranges. Finally, it was dried in a vacuum oven at 90°C until the moisture content dropped below 2% and was used directly for the WPC formulations.

Table 3. 1 Properties of the recycled PE polymers and MAPP

Polymers	MFI (g/10min)	Density (g/cm3)
rLLDPE	1.98	0.92
rMDPE	1.25	0.93
rHDPE	0.2	0.96
MAPP	21	0.934

3.2.2 Free sugar content, cellulose, hemicellulose and lignin analysis of LLB

The chemical characterization of the LLB was performed according to Lorenz et al. [213], using two-stage acid hydrolysis and high-performance anion exchange chromatography coupled with ultraviolet–visible spectrophotometry (HPAEC-UV/VIS). The entire process is summarized as follows. The milled and dried biomass was hydrolyzed by adding 100 mg of each sample to 1 mL 72% H_2SO_4. The suspensions were conditioned to 30 °C for exactly 60 min before being hydrolyzed. After further dilution to 2.5% H_2SO_4, the samples were treated in an autoclave for 30 min at 120 °C and the hydrolysis residue was filtered, washed, dried, and weighed. The filtered solutions were analyzed using the chromatographic borate HPAEC analysis using Dionex Ultimate 3000, anion exchange resin MCL GelCA08F (Mitsubishi Chemical), and a 5 mm × 120 mm column (Omnifit) packed at 65 °C for chromatographic separation. The mobile phase of two potassium tetraborate/boric acid-buffers in water with 0.3 M solution of pH 8.6 (C) and 0.9 M solution of pH 9.5 (D) were used. Separation was performed at 65 °C with a flow rate of 0.7 mL/min, and the elution program was started with 90% C and 10% D solutions, which were changed to 10% C and 90% D solutions after 35 min. This rate was kept constant for 8 min and changed back to 90% C and 10% D in 7 min. Before detection, post-column derivatization by Cu-bicinchoninate (0.35 mL/min) was applied at 105 °C in a Teflon® coil of 30 m length and 0.3 mm

diameter. Absorbance was measured at 560 nm using UV–vis detection. Finally, characterization was performed with following conditions: equal fraction of cellulose from glucose, total sum of xylose, mannose, galactose, arabinose, arabinose, and rhamnose for hemicellulose, and total sum of the hydrolysis residue and acid-soluble lignin for lignin.

3.2.3 Chemical structure and thermal properties of WPCs and Polymeric matrix

The chemical structures, melting characteristics, and thermal properties of post-consumer rLLDPE, rMDPE, and rHDPE were analyzed. FTIR analysis of the polymeric matrix films initially prepared by hot-pressing and WPC samples was performed using KBr matrix-bound pellets under hydraulic pressure (60 N/m²). An Agilent (Model Cary 640, USA) FTIR spectrometer was used to scan the samples from 4000–400 cm^{-1} at 64 scanning resolution with an optical resolution of 4 cm^{-1}. The reference neat LDPE spectra were used for comparison. For the thermogravimetric analysis (TGA), 10 mg samples of both recycled plastics matrices and WPCs were analyzed using a Q50 TGA instrument (New Castle, DE, USA) in a nitrogen atmosphere (flow rate: 60 mL/min) with scanning from 30 to 700 °C at 10 °C/min. First-derivative thermogravimetric analysis (DTGA) was used to analyze the temperature-dependent transition peaks. DSC was performed using 6 mg recycled PE on a TGA instrument (STA Q600, New Castle, DE, USA) in an inert nitrogen environment (flow rate: 60 mL/min). The heating and cooling cycles were implemented at rates of 10 °C/min in the range of 25–350 °C to determine the crystallization temperature (T_c), melting temperature (T_m), melting enthalpy (ΔH_m), and crystallization enthalpy of the recycled polymeric matrices. Finally, the degree of crystallinity (X_C) of the recycled PE was calculated based on the ratio of the absorbed enthalpy during the heating process to that of the highly crystallized pure PE (293 J/g) [214].

2.5 Residual elements, metal ions and polycyclic aromatic hydrocarbons (PAHs) analysis

The PAHs were determined following the test procedures and guidelines used in a previous work [215] which can be summarized as follows. Approximately 500 mg rLLDPE, rMDPE, and rHDPE samples were extracted with 20 mL toluene for 1 h at 60 °C in a 200 W ultrasonic bath of surface area of 706 W/cm^2. An aliquot of the extract was cooled to room temperature (25°C) and purified by column chromatography. The PAHs were determined using gas chromatography coupled with mass spectrometry, employing the selective-ion monitoring method. Samples (1 µL) were

injected using pulse splitless with the separation involved in the HT8 column (25 m long, 0.22 mm internal diameter, 0.25 μm film thickness). The injector temperature was 280 °C, and the transfer-line temperature was 260 °C. The initial and final temperatures were 50 and 320 °C, with the initial and final times of 2 and 8 min, respectively, at a heating rate of 11 °C/min [46]. Similarly, the use of recovered thermoplastic waste should follow a specific threshold for residual heavy metals impurities to ensure end-user safety. Furthermore, large residual metal ions can catalyze the thermo-oxidation or photo-oxidation of matrix polymers, leading to unwanted polymerization and emission of volatile organic compounds, resulting in uncontrolled porosity in WPC materials and affecting their durability [17]. The residual elements specifically heavy metals impurities in rLLDPE, rMDPE, and rHDPE were assessed by obtaining the analytical parameters adhering to TOXEL standards developed by DSM Resolve and PANalytical which includes certified standards for regulated elements, such as Cr, Cd, Hg, Pb, As, Ni, Cu, Zn, Ba, and Br [216,217].

3.2.4 Formulation of WPCs

WPC preparation involved the compounding and consolidation of two compositions of LLB particle reinforcements (40 and 60 wt.%). Formulations involving a total of 20 samples, including unreinforced polymer matrices of rLLDPE, rMDPE, and rHDPE, and equal-mixed blend ratios (EM), are shown in **Table 3.2**. The first letter of the polymer matrix is used with the subscript number to indicate their compositions in the matrix composites, and LB represents the LLB particle reinforcement. During compounding, polymeric matrix was added to the preheated mixing chamber (HAAKE Reomix) and melted for approximately 5 min at 150, 160, 170, and 165 °C for rLLDPE, rMDPE, rHDPE, and rEM, respectively. Subsequently, the dried LLB particles and MAPP were added and homogeneously compounded for an additional 10 min until constant torque and viscosity were achieved. Finally, the dried WPC granules were further reduced using a cutting mill (Retsch type SM 2000, Germany) with a mesh size of 8 mm. The consolidation of the WPC boards was performed in a computer-controlled hot-compression press with a steel mold frame with dimensions of 180 mm × 200 mm × 4 mm. This process involved cycles of low-pressure melting for 1 min, compression at 20 bar for approximately 8 min, continuous pressing by increasing the pressure to 60 bar for the next 1 min, and pressing at 100 bar for an additional 1 min. While maintaining a constant pressure, cooling was performed with

an external water coolant flow until the temperature decreased to less than 80 °C. Finally, the WPC board prototype was removed from the frame.

Table 3. 2 Formulations of WPCs samples

Polmer matrix type	Polymer matrix (%)	LLB reinforcement (%)	Coupling agents (MAPP)	Sample ID
rLLDPE	100	-		L_{100}
	60	40	-	L_6-LBU
	58.5	38.5	3	L_6-LBC
	40	60	-	L_4-LBU
	38.5	58.5	3	L_4-LBC
rMDPE	100	-		M_{100}
	60	40	-	M_6-LBU
	58.5	38.5	3	M_6-LBC
	40	60	-	M_4-LBU
	38.5	58.5	3	M_4-LBC
rHDPE	100	-		H_{100}
	60	40	-	H_6-LBU
	58.5	38.5	3	H_6-LBC
	40	60	-	H_4-LBU
	38.5	58.5	3	H_4-LBC
rEM	100	-		EM_{100}
	60	40	-	EM_6-LBU
	58.5	38.5	3	EM_6-LBC
	40	60	-	EM_4-LBU
	38.5	58.5	3	EM_4-LBC

3.2.5 Sample preparation and mechanical tests.

The tensile strength (TS) was evaluated using 10 dumbbell-shaped test specimens with dimensions of (170 mm × 10 mm × 4 mm) from the two replicates, following ISO 527-1 requirements. A universal testing machine (ZWICK videoXtens, Germany) was used to test the mechanical properties. The load cell and crosshead speeds were 20 kN and 1 mm/min, respectively. The flexural strength (FS) and modulus of rupture (FM) were measured for specimens with dimensions of 80 mm × 10 mm × 4 mm according to the test compliance of ISO 178-1 with a span length of 60 mm and crosshead speed of 1 mm/min. Unnotched impact strength (UIS) was measured following ISO 179-2 set at 80 mm using a Charpy impact tester (Zwick-

Roell HIT5.5P, Germany) for approximately 12 samples from the two replicates with similar dimensions as those of the FS (**Figure 3.1**).

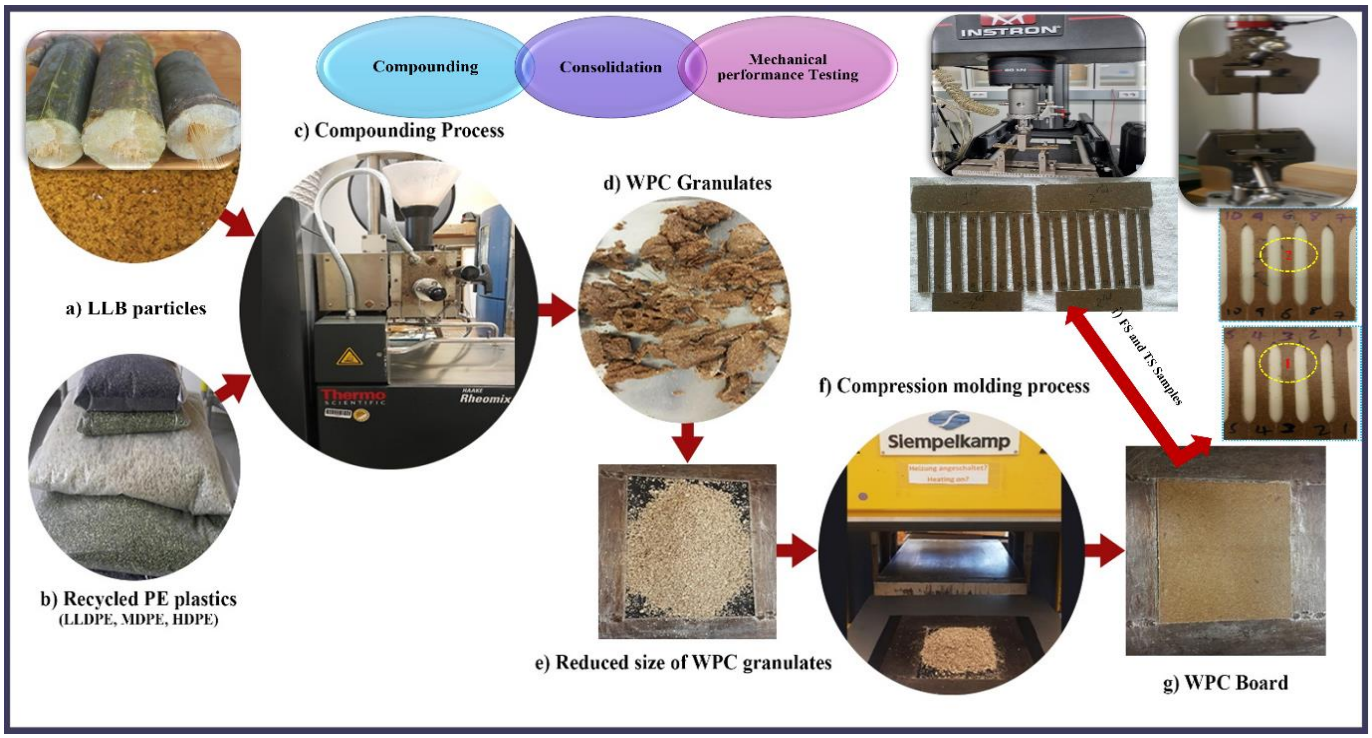

Figure 3. 1 Compounding, consolidation and mechanical testing of the WPCs

3.2.6 Scanning electron microscope (SEM) observation.

SEM micrographs of the fractured surfaces of representative WPC samples from the IS tests (1 cm × 1 cm × 1 cm) were examined using a QUANTA 200 scanning electron microscope (FEI, USA) to obtain the indirect information on the interfacial adhesion between the matrix and particles. The surfaces were sputter-coated with a 2 nm Pt layer to enhance conductivity, and observations were conducted at an accelerated electron beam voltage of 10.0 kV.

3.3 Results and discussion

3.3.1 Characterization of Ethiopian low land bamboo (*O. abyssinica*)

The amounts of free sugar and corresponding polysaccharides of xylose, glucose mannose, galactose, arabinose, and rhamnose in indigenous Ethiopian LLB were 12.05%, 57.16%, 0.62%, 0.39%, 1.16%, and 0.07%, respectively. Accordingly, the cellulose, hemicellulose, and lignin contents were 57.16%, 14.29%, and 25.94%, respectively. LLB contains a higher cellulose content than other bamboo fibers of different species, with lower hemicellulose content and similar lignin content [46, 47] This implies that cellulose plays an important role in bond formation, the higher content of cellulose a higher potential for wood-polymer bond formation coupling agents. Additionally, the amounts are comparable to widely utilized lignocellulosic fibers, such as hemp, jute, oak, and pine fibers, which is potential to replace conventional fibrous fillers and/or reinforcements [18].

3.3.2 FTIR and DSC analysis

Figure 3.2(a–c) show the spectra of the three recycled PE polymeric plastics with characteristic regions separated into three parts of 750–720 cm^{-1} (a), 1485–1445 cm^{-1} (b), and 2845–2865 cm^{-1} (c), representing methylene (CH_2-) rocking deformation, C–H bending deformation of CH_2-, and C–H asymmetric and symmetric stretching of CH_2-, respectively [188]. As shown in Figure 2, all three recycled PE plastics exhibited similar strong C–H asymmetric and symmetric stretching vibrations at 2914 and 2846 cm^{-1}, respectively (c). Moreover, they depicted similar FTIR band regions at 745–690 cm^{-1} for methylene C–H rocking deformation in $(CH_2)_n$ (a) and 1350–1550 cm^{-1} for methylene C–H bending deformation (b) compared with LDPE as a reference. The CH_2 rocking peak in rHDPE split the peak near its shoulder at 718 and 728 cm^{-1} (a), whereas the split is not clear for rMDPE, indicating its lower crystallinity than rHDPE. However, rLLDPE displayed a broad peak in the medium-absorption region of 700 cm^{-1}, which can be ascribed to the characteristic band region of the C–H plane bending in 1-hexene copolymerized with ethene [218]. The PE of higher crystallinity resulted in a higher splitting after a larger absorption, implying that the recycled polymeric plastic was properly sorted without other contaminants. Although the intensity and extent of splitting compared with LDPE reference are different, this can be ascribed to the thermal reprocessing, which can reduce the regularity of the polymeric

chains and affect the crystal structure [218]. Additionally, the absence of a carbonyl peak at 1725 cm^{-1} indicates the absence of oxidation of the recycled matrix during composite formulation and/or degradation [188], except for residual impurities.

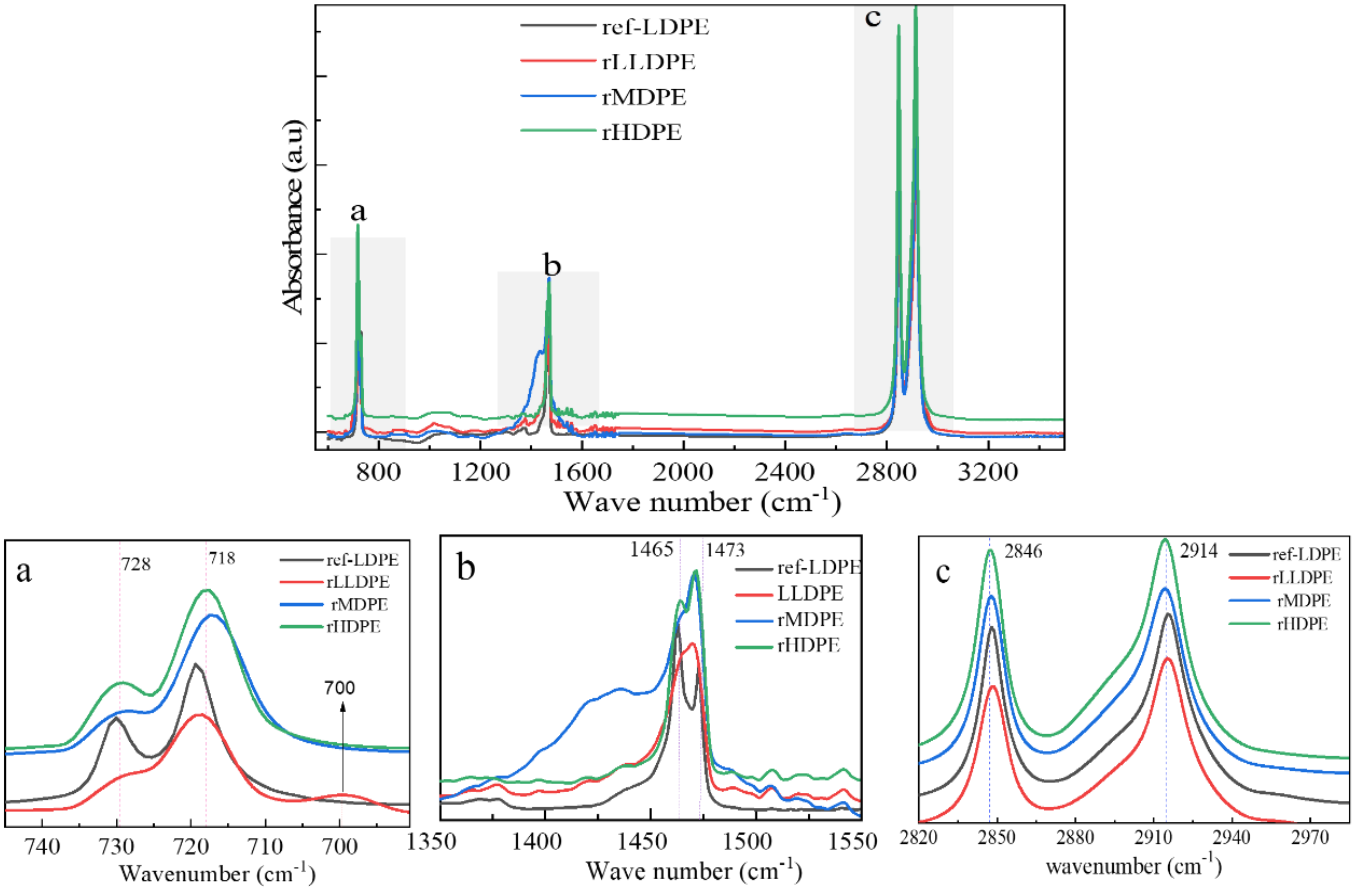

Figure 3. 2 FTIR spectra of recycled PE waste plastics: methylene C–H rocking deformation in $(CH_2)_n$ (a), methylene C–H bending deformation (b)and C–H asymmetric and symmetric stretching vibrations (c).

Figure 3.3a and **b** present the DSC data for rLLDPE, rMDPE, and rHDPE, including their Xc and ΔHm. As shown in **Figure 3.3b**, the Tm and Xc vary among the recycled PE types. Notably, rLLDPE exhibits the lowest Xc (**Figure 3.3a**) and a broad, small, and less defined melting peak (**Figure 3.3b**), reflecting its relatively high amorphous content. In contrast, both rMDPE and rHDPE maintained sharp crystallinity and melting properties, with rHDPE having a larger Xc value than rMDPE, which is consistent with the reported literature values for virgin PE with minor differences. For instance, rLLDPE was reported to have a weak crystallization peak at approximately 95 °C, followed by a sharp T_c at 109 °C, and a sharp T_m at approximately 123 °C.

Similarly, virgin HDPE and MDPE were reported to have ΔH_m values of 152.89.7 and 144.3 J/g, respectively [219]. Furthermore, a recent study on the DSC characteristics of four neat PE polymers reported Xc values of 36.65%, 39.52%, 48.35%, and 51.28% for LDPE, LLDPE, MDPE, and HDPE, respectively [48, 49]. These values are comparable to the crystallinity measured in the present study, which were 39.54%, 46.64%, and 51.08% for rLLDPE, rMDPE, and rHDPE, respectively. The slight variations are attributed to the thermal processability affecting the crystallization of the polymer, with similar retained properties as their virgin counterparts. These results imply that thermomechanical recycling can retain properties like those of the respective virgin polymers and can be used as a secondary resource.

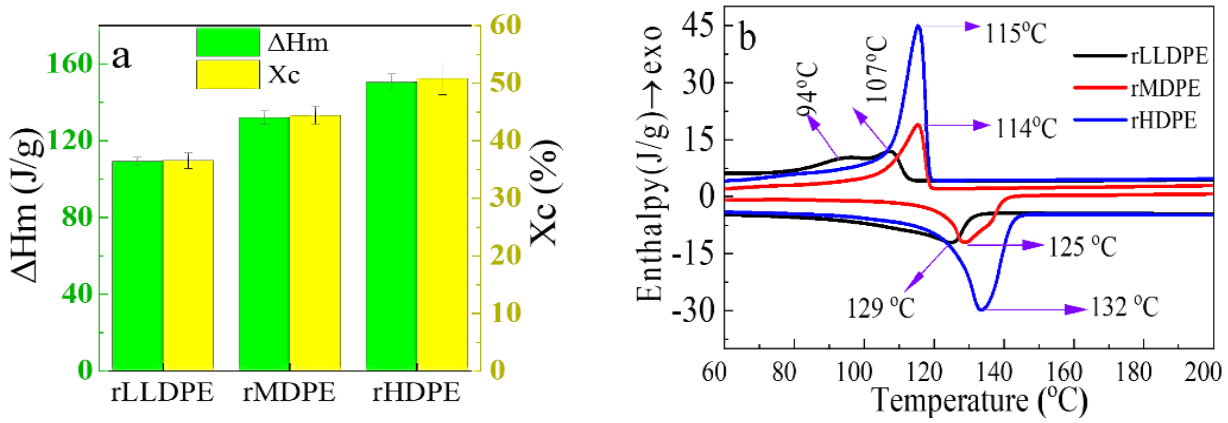

Figure 3. 3X_c and enthalpy of melting (a) and DSC thermograph of endothermic and exothermic heating cycle (b).

3.3.3 Elemental composition and polycyclic aromatic hydrocarbons of PEs

As shown in **Table 3.3,** the highest Ti, Ba, Cl, Zn, Ca, and Fe contents were detected in rLLDPE and rHDPE. However, in rMDPE, only Ba and Fe were detected in relatively large amounts. Such residual impurities can be attributed to the prehistoric production of their respective neat polymers, including residual catalysts of Neiglar Natta or metallocenes, inorganic pigments (TiO_2, ZnO, and Fe_2O_3), flame retardants (Sb_2O_3 and brominated organics), and stabilizers of Ba, Sn, and Zn [12, 44]. However, rMDPE was less contaminated owing to its white opaque color. The content of heavy metals, such as Cd, should be less than 100 ppm (mg/kg) and that of Pd, Hg, and Cr (VI) should be less than 1000 ppm (mg/kg) [216]. The detected amounts below these thresholds indicate that the recovered PE can be used as a secondary resource for WPC

formulations when properly sorted from the waste fractions. Nevertheless, improved sorting and representative sampling should be performed continuously over an extended period.

Table 3. 3 Main elemental composition of recycled PE (rLLDPE, rHDPE and rHDPE)

Element	rLLDPE (ppm)	rMDPE (ppm)	rHDPE (ppm)	Threshold (ppm)
Ti	314.8 (2.7)	26.9 (4.60	805.9 (9.3)	n.a.
Cl	735.8 (7.4)	36.4 (2.91)	305.2 (7.87)	n. a
Fe	626.8 (2.4)	137.1(5.8)	315.6 (2.4)	n.a
Ca	128.6 (9.58)	78 (0.23)	1056.3 (12.6)	n. a
Ba	1226.5 (56.27)	133.9 (2.17)	225.7 (9.2)	n.a
Sn	12.2 (0.5)	12.1(0.33)	7.5 (0.1)	n. a
Cr	8.2 (0.68)	18.6 (0.72)	22.7(0.78)	10^3
Cd	4.4 (0.3)	3.8 (0.26)	6.3 (0.3)	10^2
Pd	2.3 (0.1)	1.3 (0.8)	177.6 (0.2)	10^3
Hg	2.3 (0.3)	3.8 (0.45)	1.8 (0.4)	10^3
Zn	81.8 (4.5)	3.2 (0.1)	282.1 (3.5)	n. a
Cu	5.1(0.7)	4.3 (0.4)	14.9 (0.8)	n.a
Mn	51.5 (2.3)	2.4 (0.79)	19.1(1.2)	n. a

*The numbers in brackets indicate the standard deviations the measurements done from three replicates

PAHs are hydrocarbons composed of multiple aromatic rings, which are recognized for their toxicity, carcinogenicity, and mutagenicity. Common PAHs and their detected amounts, including their threshold quantities, are shown in **Figure 3.4**. The combined total amounts of naphthalene, acenaphthylene, acenaphthene, and fluorene should be below 10 mg/kg. Similarly, the amounts of residual phenanthrene, anthracene, fluoranthene, and pyrene molecules must remain below 50 mg/kg (ppm), according to well-established standards for protection of the PAHs [215].Benzo(a)anthracene, chrysene, benzo(b)fluoranthene, benzo(k)fluoranthene, benzo(a)pyrene, indeno(1,2,3-cd) pyrene, dibenzo(a,h)anthracene, and benzo(ghi)perylene concentrations did not exceed 1 mg/kg. The rMDPE has relatively high concentrations of polycyclic arenes compared with both rHDPE and rMDPE. The sources of these PAHs could be residual impurities trace back to their corresponding monomer and/or polymer productions, catalyst residuals and different impurities associated with additives during the productions.

However, the PAHs levels detected in rLLDPE, rMDPE, and rHDPE complied with these requirements, making them suitable for valorization as secondary resources for the WPC core-matrix polymers. However, the evaluation requires continuous testing.

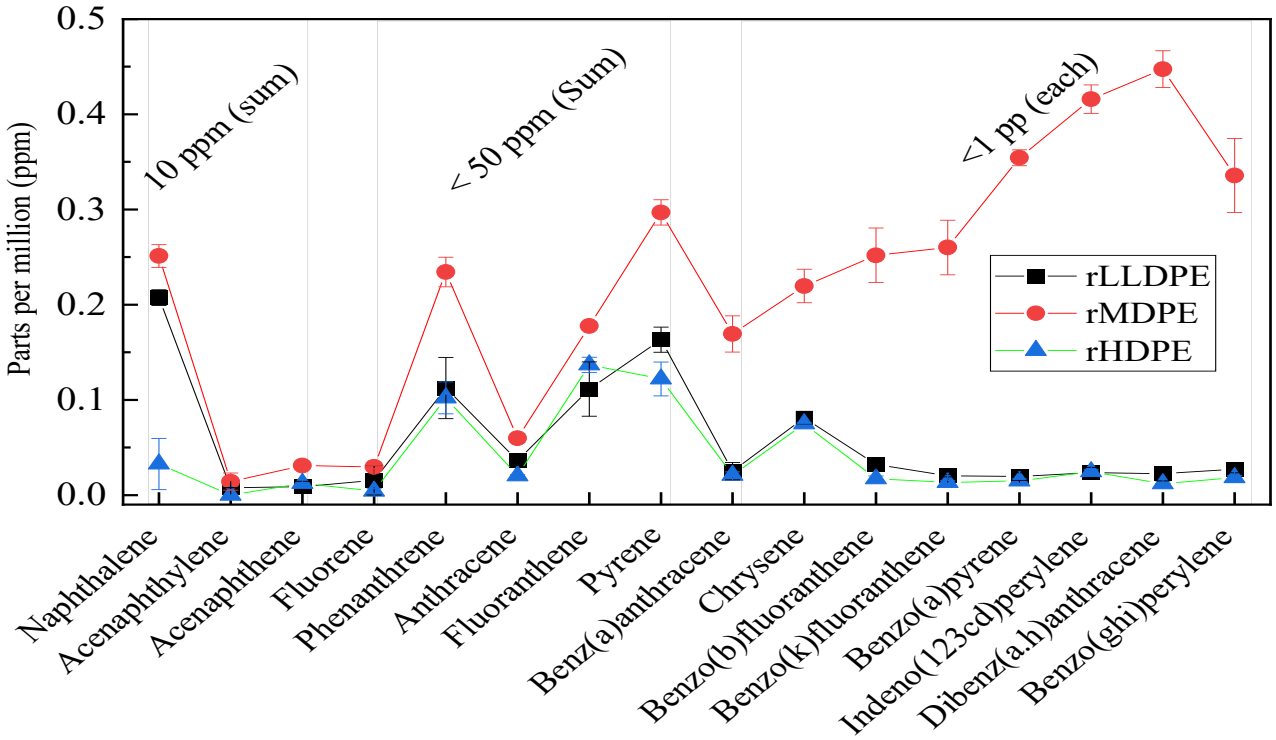

Figure 3. 4 PAHS contents of the recycled rLLDPE, rMDPE and rHDPE

3.4 Mechanical properties of the WPCs

The mechanical properties of the formulated WPCs, including the TS, TM, FS, FM, and UIS, are listed in Table 3.4. It shows the properties of the corresponding unfilled polymer matrix as a baseline for comparison. The subsequent discussion covers each of these key property variations with bamboo fibrous filler loading varied from 40% to 60%, complemented by the graphs for quick interpretation. The numbers in brackets represent the standard deviation of the ten specimens tested from two duplicates for all formulations. In the UIS column, the letters "ub," "pb," and "b" were used to indicate unbroken, partially broken, and broken specimens, respectively.

Table 3. 4 Mechanical properties of formulated WPCs

Matrix	SID	TS (MPa)	TM (MPa)	FS(MPa)	FM (MPa)	UIS (KJ/m^2)
LLDPE	L_{100}	9.93(1.73)	398.98(53)	7.63(0.45)	230.57(88)	ub
	L_6-LBU	7.85(0.87)	866.60(48)	13.45(1.23)	1123.67(37)	12.97(1.3) (pb)
	L_6-LBC	12.73(0.2)	909.85(52)	18.82(1.18)	1324.65(21)	18.21(2.1) (pb)
	L_4-LBU	5.84(0.1)	1284.38(63)	12.08(0.41)	1634.68(48.5)	10.01(2.1)
	L_4-LBC	9.86 (0.6)	1382.26(77)	14.53(0.87)	1835.6(63.6)	11.95(0.2)
MDPE	M_{100}	14.72(1.3)	530.75(57)	13.58 (0.84)	428.94(66)	38.56(1.5) (pb)
	M_6-LBU	13.67(0.5)	1891.8(32)	28.316(0.55)	2263.4(11.5)	9.49(0.7)
	M_6-LBC	19.51(0.2)	2014.5(50)	32.1(1.86)	2467.2(14.78)	12.86(0.9)
	M_4-LBU	10.27(0.1)	2113.8(38)	19.93(2.12)	2745.8(57.56)	8.41 (0.4)
	M_4-LBC	15.33(0.8)	2218.7(30)	23.23(0.16)	2804.8(104.14)	10.57 (0.3)
HDPE	H_{100}	22.15(1.5)	892.85(58)	18.6(0.76)	693.58 (76)	26.56(0.8)
	H_6-LBU	19.57(0.5)	2010.46(50)	31.89(1.2)	2634.6(68.67)	8.59(1.9)
	H_6-LBC	29.37(0.1)	2317.7(30)	39.54(2.32)	3019.5(165.32)	12.35(0.9)
	H_4-LBU	15.75(0.2)	2565.7(22)	21.308(2.12)	3433.2(73.52)	7.34(0.44)
	H_4-LBC	22.35(0.1)	2756.8(55)	28.58(3.15)	3628.6(28.2)	10.89(0.47)
EM	EM_{100}	17.5(0.5)	650.67(68)	14.561.05)	530.87(87)	31.56 (1.2) (pb)
	EM_6-LBU	14.03(0.7)	1778.85(47)	25.52(1.6)	1847.9(69)	11.68(1.4)
	EM_6-LBC	21.23(0.9)	1806.84(27)	31.85(1.3)	2191.5(87)	15.24(2.14)
	EM_4-LBU	12.63(0.6)	2099.36(37)	18.45(1.48)	2527.8 (20.6)	10.58(0.25)
	EM_4-LBC	18.45(0.4)	2280.88(90)	24.23(1.44)	2798.5(111.4)	13.60(0.36)

*The numbers in brackets represent the standard deviations of ten specimens measured in two independent duplicates.

3.4.1 Tensile strength and tensile modulus

As shown in **Figure 2.5**, WPCs with 40% bamboo particles exhibited higher tensile strength (TS) than those with 60%, indicating that TS decreases with increasing particle loading, while tensile modulus (TM, stiffness) rises. Incorporating bamboo particles substantially enhanced the stiffness of both coupled and uncoupled composites. For 40% particle content, TM increased 2.2–3.8 times compared with unreinforced rLLDPE, rMDPE, rHDPE, and rEM. Raising the reinforcement to

60% further increased stiffness, with TM increasing 2.8–8.0 times across the composite series (L4-LBU, L_4-LBC, M_4-LBU, M_4-LBC, H_4-LBU, H_4-LBC, EM_4-LBU, EM_4-LBC) relative to their respective unreinforced matrices. This demonstrates that bamboo particles have a stronger influence on stiffness than coupling agents, which contributed only ~15% TM improvement in coupled versus uncoupled composites. Unlike TM, TS did not rise proportionally with bamboo content in uncoupled composites due to fiber agglomeration and weak adhesion. However, at 40% bamboo loading, coupled WPCs (L_6-LBC, M_6-LBC, H_6-LBC, EM_6-LBC) showed TS gains of 21.31–32.5% over unreinforced rLLDPE, rMDPE, rHDPE, and EM, and 34.0–62.0% over their uncoupled counterparts. At 60% bamboo, coupled WPCs further improved TS by 41.9–68.0% compared with uncoupled composites. This demonstrates that Fusabond MAPP (8–10% MA) effectively enhances interfacial bonding, while composites without coupling agents suffer from poor compatibility and reduced TS. This work achieved better results than WPCs produced from smaller particles and flour dispersed phase. In particular, the reported TS was 9.5–23.2 MPa for 30%–50% dispersed phase, 3% MAPP (Epolene G-3015), and maleic anhydride grafted PE (MAPE). This improvement can be attributed to the wider distribution of LLB particle reinforcement, higher cellulose content, or probably residual impurities that may enhance interactions, and higher grafted portions of MA in MAPP [65,221,222].

WPCs produced by melt-blending equal amounts of rLLDPE, rHDPE, and rMDPE (EM composites) showed superior TS compared with both coupled and uncoupled rMDPE composites. Specifically, EM-based composites (EM_6-LBU, EM_6-LBC, EM_4-LBU, EM_4-LBC) achieved ~70–116% higher TS than their rLLDPE counterparts (L_6-LBU, L_6-LBC, L_4-LBU, L_4-LBC). These improvements exceeded the reductions observed in both TS and TM of rMDPE- and rHDPE-based composites relative to EM-based systems, though in some cases rMDPE composites showed comparable values. Overall, blending weak and highly polluting rLLDPE with stronger rMDPE and rHDPE produced composites with unique performance despite their intrinsic immiscibility. The improved interfacial bonding is further promoted by MAPP, whose hydrophobic backbone interacts with nonpolar EM chains, while the MA end groups bond with hydrophilic bamboo fibers through hydrogen or ester linkages [92]. These phenomena were indicated by significant changes in the FTIR spectra of both the LLB-reinforced EM-based coupled and uncoupled composites. Furthermore, the mechanical interlocking of a wider particle distribution and molecular entanglement in mixed PE poly blends are considered to inhibit the

mechanical failure at the weakest point of rLLDPE. Similarly, high-temperature compounding and high-pressure compaction can also reduce the viscosity and enhance the matrix flow to encapsulate bamboo reinforcement.

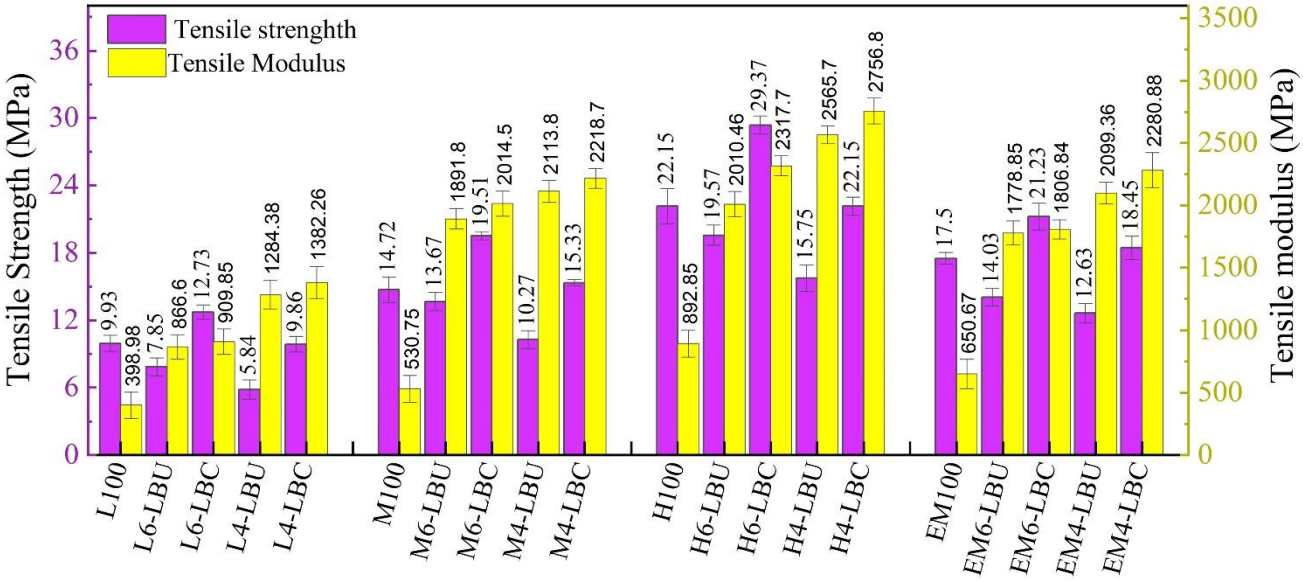

Figure 3. 5 Tensile strength and tensile modulus of WPCs based on recycled PE matrices.

3.4.2 Bending strength (FS) and modulus of rupture (FM)

The FS and FM results are shown in **Figure 3.6.** The FS of the formulated composites increased for both coupled and uncoupled composites compared with that of the core polymer, unlike the TS. Bamboo-particle reinforcement improved the low FS of all unreinforced matrices. However, the FS decreased slightly with increasing bamboo particle contents. On the other hand, the FM of the composites increased substantially compared with the unreinforced matrices, showing a positive correlation with LLB particle content. At 40% loading (60% matrices compositions), both coupled and uncoupled composites exhibited FM enhancements by ratio factors of 3.8–5.8 times relative to unreinforced matrices. At 60% LLB loading, the FM improvements were even greater, with corresponding factors of 4.7–7.9 times. In contrast, the inclusion of MAPP had only a marginal effect on FM at both 40% and 60% filler contents. Moreover, FS of both uncoupled and coupled WPCs incorporating 40% LLB particles showed notable improvements compared to their respective unreinforced polymer matrices (rLLDPE, rMDPE, rHDPE, and rEM-based formulations) ranging in the increase's ratio factors from 1.7–3.4. Similarly, for composites with 60% LLB particle loading the FS was enhanced by factors of 1.2–1.9, relative to the corresponding unreinforced matrices. These results demonstrate that bamboo particle

reinforcement contributes significantly to flexural performance, with greater enhancements generally observed at 40% filler content. Additionally, the FS of coupled WPCs with the same LLB particle content (40% and 60%) demonstrated significantly increasing trends with MAPP inclusion compared with uncoupled samples. Furthermore, the FS of EM-based composites (EM6-LBU, EM6-LBC, EM4-LBU, and EM4-LBC) improved by 52.7–89.7% compared with their respective rLLDPE-based formulations. Similarly, the FM of EM-based composites increased by 52.4–65.4% relative to the corresponding rLLDPE-based composites, highlighting the enhanced mechanical performance achieved through the EM blend.

For conventional WPC applications in decking and wall cladding with 40%–60% wood fiber or polymer content, the minimum recommended FS and FM are 20 MPa and 1200 MPa, respectively. For non-structural applications, such as ceilings, sidings, and modular kitchen interiors, the minimum TS and FS are 10 MPa and 15 MPa, respectively, in accordance with ISO 178, ASTM D6109, and ASTM D7032 standards [88]. The formulated coupled EM-based WPCs satisfied these requirements. Although most PE-based composites use MAPE as the coupling agent, our results are consistent with those of other studies using various coupling agents. These include functionalized polyolefins, maleic-anhydride-grafted LLDPE (LLDPE-*g*-MA), acrylic-acid-grafted HDPE (HDPE-g-AA), MAPP, and maleic-anhydride-grafted styrene-ethylene-butylene-styrene, as extensively reviewed by Kaseem et al. [211]. They found that WPCs containing MAPP and HDPE-AA exhibited better properties, except that the maximum impact strength was achieved when LLDPE-g-MA was used as a coupling agent, which can be ascribed to the intrinsically high IS of its main block polymer, LLDPE.

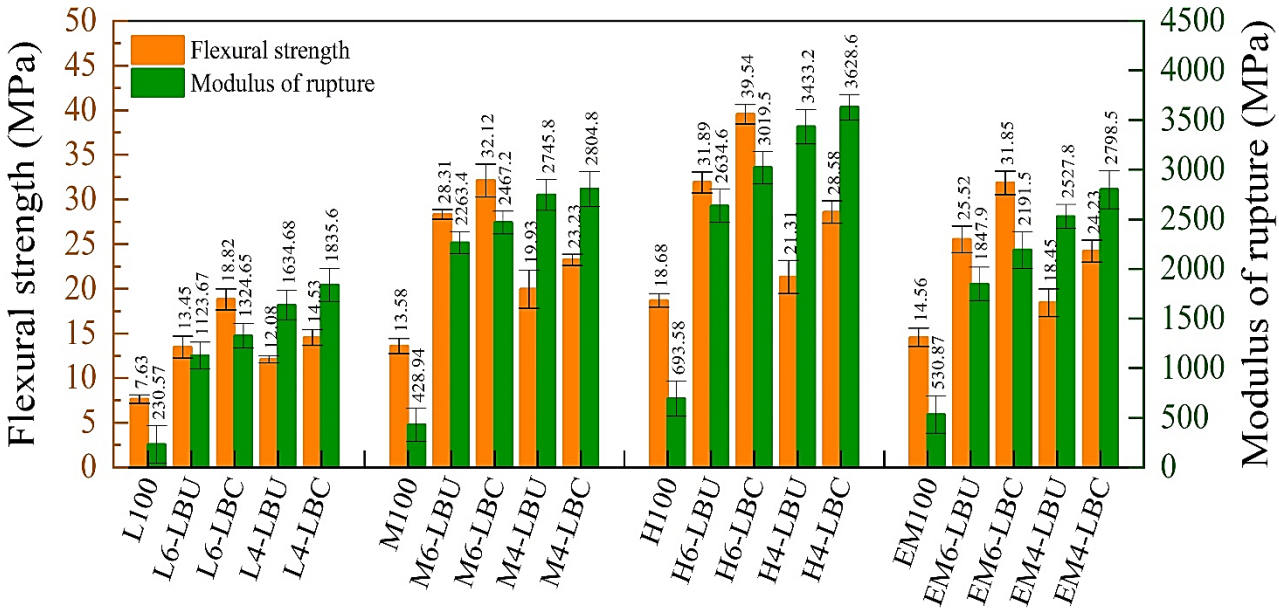

Figure 3. 6 The flexural strength and modulus of rupture of WPCs based on recycled PE matrices.

3.4.3 Impact strength (IS)

In the IS evaluation, the rLLDPE matrix remained unbroken with the ISO pendulum, whereas rMDPE and rEM were partially broken, and rHDPE was fully broken. As indicated in **Figure 3.7**, the rLLDPE results were not included in the graph, and the IS was evaluated based on the other WPCs. Accordingly, the IS of the WPCs was in the range of 7.34 kJ/m² (H_4-LBU) to 18.2 kJ/m² (L_6-LBC) without considering the polymeric matrix. Increasing the LLB content from 40% to 60% reduced the IS. Additionally, formulations without MAPP exhibited a low IS, which is likely attributable to the weak interfacial compatibility. However, the IS of both rMDPE- and rHDPE-based WPCs improved when melt-blended with MAPP and rLLDPE owing to their increased ductility and compatibility with the blend matrix. The IS of the WPCs with short fibrous fillers was significantly affected by the rigidity of the natural fibers, restricting the polymer chain mobility, reducing the energy absorption during fracture, and breaking the composite [55, 56]. Except for H_4-LBU, the WPCs satisfied the minimum requirements for a wide range of practical applications [88]. According to ISO 179-1 test compliance, an impact strength (IS) greater than 8 kJ/m² is recommended for structural WPCs intended for outdoor decking applications. In contrast, non-load-bearing applications have less stringent requirements, favoring WPCs that are sufficiently stiff and resistant to rupture, meeting minimum standards comparable to plastic lumber, with flexural strength (FS) and flexural modulus (FM) values of 6.9 MPa and 340 MPa,

respectively [101]. MAPP inclusion improved the IS of the WPCs by enhancing the LLB particle dispersion and interphase bonding, increasing the energy absorption and resistance to breakage [28].

The impact strength (IS) of EM-based composites (EM_6-LBU, EM_6-LBC, EM_4-LBU, and EM_4-LBC) increased by 23.4–44.2% compared with rHDPE-based matrices (H_6-LBU, H_6-LBC, H_4-LBU, H_4-LBC) and by 18.5–28.6% relative to rMDPE-based composites (M_6-LBU, M_6-LBC, M_4-LBU, M_4-LBC). These improvements indicate a consistent enhancement in toughness due to the EM matrix, reflecting the synergistic effect of incorporating flexible rLLDPE components.

The improved IS in all coupled WPCs compared with that in the uncoupled WPCs indicates the improved chemical interactions and the physical interlocking. In WPCs without coupling agents, the IS decreased owing to the weak interfacial bonding between the filler and polymer matrix, facilitating microcrack initiation and reducing the energy required for crack propagation. The coupling agents improved IS by reducing the viscosity, enhancing the matrix flow, ensuring uniform particles distribution, and improving the interfacial adhesion between the LLB particles and matrix through chemical reactions [129]. The results and trends align with those of Sommerhuber et al. [7], showing that the addition of wood fibers to the WPCs formulated from neat and recycled HDPE with 3% MAPE and Norway spruce fibers leads to decreasing IS. Specifically, the IS values were in the range of 7.6–8.4 kJ/m² at 30% wood-fiber content and 5.4–8.0 kJ/m² at 60% wood-fiber content, indicating improvement in IS with MAPE inclusion. Similarly, Migneault et al. [224], Poletto et al. [225] and Khamtree et al. [93] noted that using MAPP, PEMA, and styrene-maleic anhydride significantly improved the IS. Compared with these studies, enhanced toughness was observed in the EM-based WPCs formulated in this study, which could be attributed to both the coupling efficiency of MAPP and intrinsic toughness of rLLDPE.

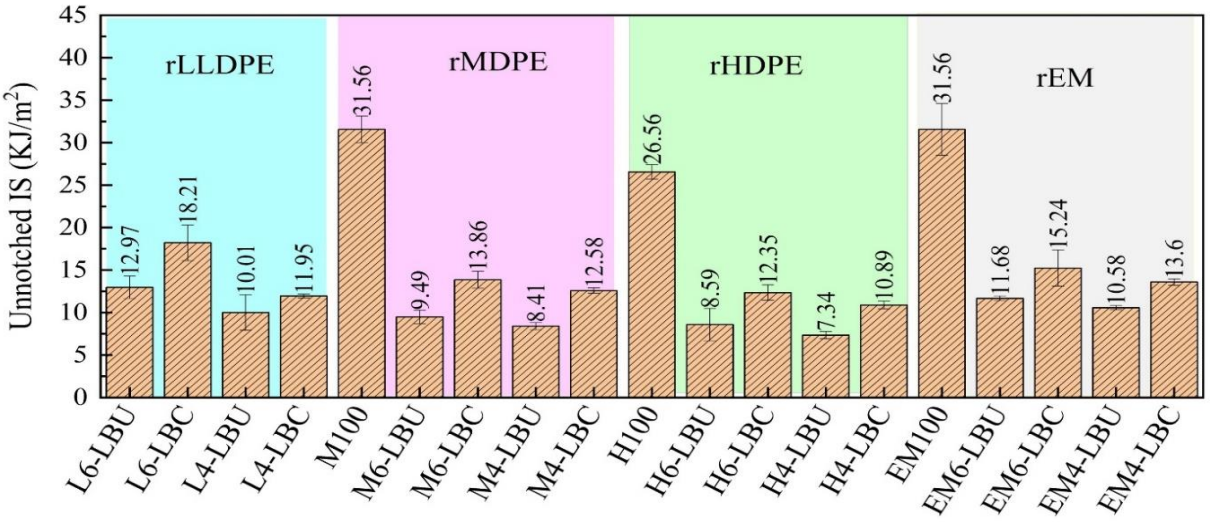

Figure 3. 7 The Impact strength properties of WPCs based on recycled PE matrices.

3.5 SEM-microscopic characterization

The SEM morphologies of the WPC surfaces formulated from equal compositions of the representative polymer blends (EM) obtained by the fractured IS test are shown in **Figure 2.8**. The analysis included uncoupled WPCs (EM_6-LBU) (**Figure 3.8 a and b**) and coupled WPCs (EM_6-SLBC) (**Figure 3.8 c and d**), which were each examined twice from two replicates of the same formulation. As shown in **Figure 3.8a, b**, several smaller particles were removed from the matrix during the IS testing, leaving large particles pulled out from the areas, smaller holes, and loosely embedded particles. This can be ascribed to incompatibility, resulting in weak interactions and reduced mechanical properties of the composite. Conversely, coupled EM_5-LBC (**Figure 2.8 c, d**) demonstrated good dispersion of the bamboo fibrous particles in the polymer matrix without visible agglomerates and fiber pull-out areas. Furthermore, several particles were homogeneously embedded within the matrix (**Figure 2.8c**). Similarly, the morphology was uniformly distributed across the matrix composites, covering well-oriented surface layers without particle-matrix deformation (**Figure 2.8d**). The absence of clear voids or particle agglomerates indicates the reduced fiber pull-out areas and improved interfacial bonding between the particles and polymer matrix by the compatibilizer. This leads to improved mechanical properties compared with their uncoupled counterparts. The absence of large voids and gaps, including fractured fiber surfaces, has also been reported to confirm the presence of a strong fiber–polymer interphase and coupling efficiency[123,129,226].

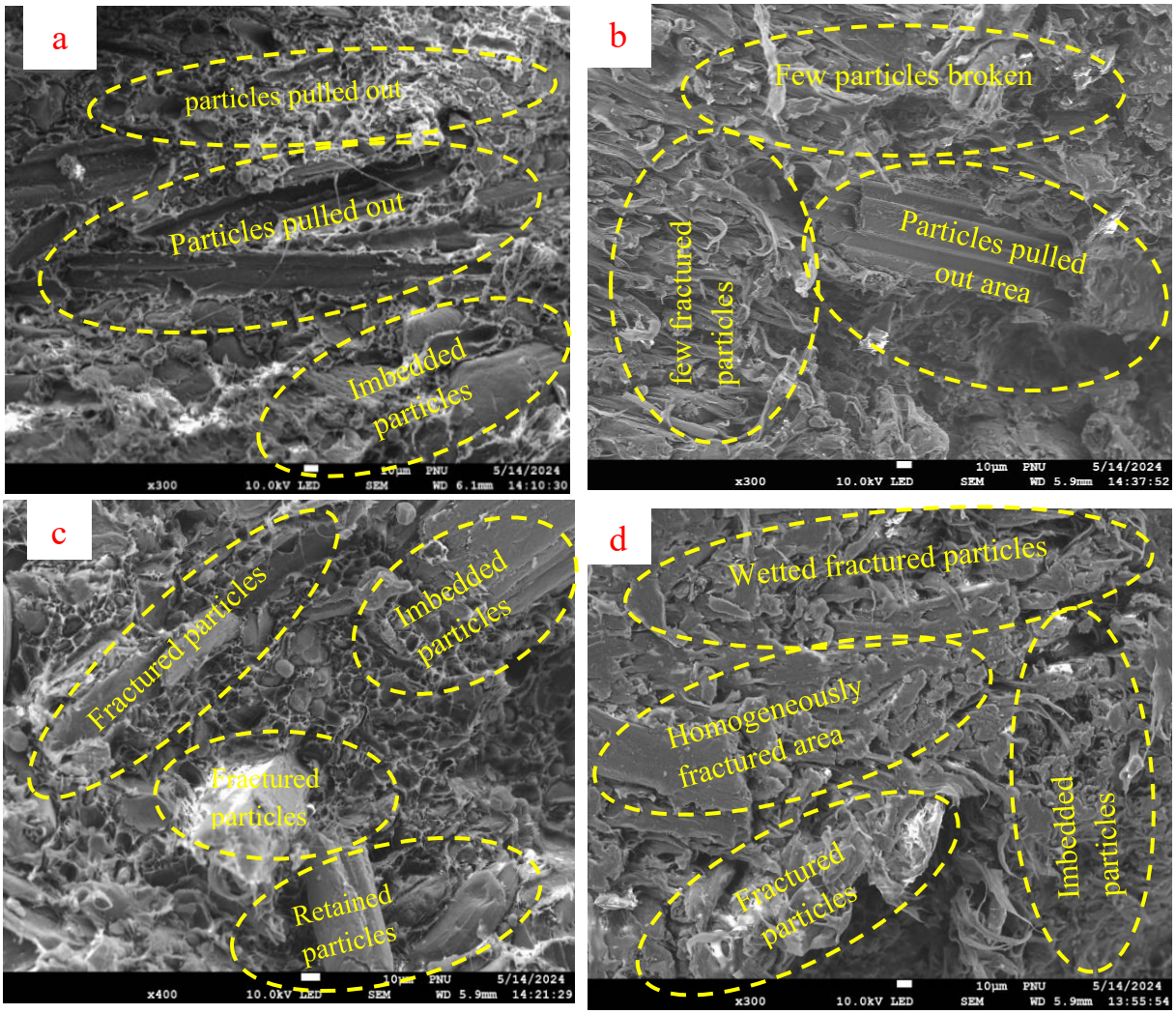

Figure 3. 8 SEM morphology of EM-based WPCs of both uncoupled (EM-LBU) at two site points (a, b) and coupled (EM-LBC) at two different site points (c, d)

3.6 FTIR characterization of WPCs

The representative FTIR spectra of the coupled and uncoupled EM-based WPCs and LLB particles are shown in **Figure 3.9**, with the spectra shifted vertically for clarity. The fingerprint regions of most lignocellulosic fibers at 600–1600 cm^{-1} represent major constituents, such as cellulose, hemicelluloses, and lignin molecular vibrations [62]. Similarly, the broad spectral region within 3500-3250 cm^{-1} represents the hydroxyl (-OH) stretching vibration of mostly cellulose and hemicellulose. The other important regions from 1060–1030 cm^{-1} were assigned to C-O stretching of mostly cellulose, and the region from 1750–1700 cm^{-1} represents carbonyl region carboxylic acid and ester groups [29]. As shown in Figure 3.9, MAPP reduces the –OH

functionalities of the LLB particles, as depicted by the weakening of the OH stretching at approximately 3430 cm^{-1} and C–O lignin stretching at approximately 1050 cm^{-1} [29] with changes in the peak intensity length, denoting chemical changes [63]. Additionally, several typical vibration peaks of cellulose, hemicellulose, and lignin biomass in the complex regions of 1152–1755 cm^{-1} were affected compared with those of the coupled composites. These included OH– in-plane bending and lignin C–H bending in CH_3 at 1454 cm^{-1}, lignin aromatic skeleton vibrations at 1508 cm^{-1}, and C–H bending at 1462 cm^{-1}. Moreover, hemicellulose COO stretching, lignin C–O stretching, hemicellulose (C–O stretching in carboxylic acid), and lignin (C–C, C–O, C=O) stretching are noted at 1380, 1264, 1240, and 1226 cm^{-1}, respectively [62, 63]. Compared with LLB, some of these absorption peaks disappeared and/or shifted to lower or weaker intensities in the coupled WPCs. The anhydride carbonyl group of MA in PP (1180 cm^{-1}) was detected in the coupled composites. Although the LLB particles have an ester band region at approximately 1728 cm^{-1} [63], compared with the EM_6-LBC composites, this band region was clearly observed in EM_6-LBC. Similarly, the CH_2 stretching vibration peaks at 2920 and 2852 cm^{-1} and CH_2 bending vibrations were more intense in the EM_6-LBC systems than in EM_6-LBCU, implying improved interactions with the hydrophobic blend chains. These phenomena indicate synergetic interphase modification with MAPP and polymer blending, resulting in improved mechanical properties, as observed during mechanical property characterization.

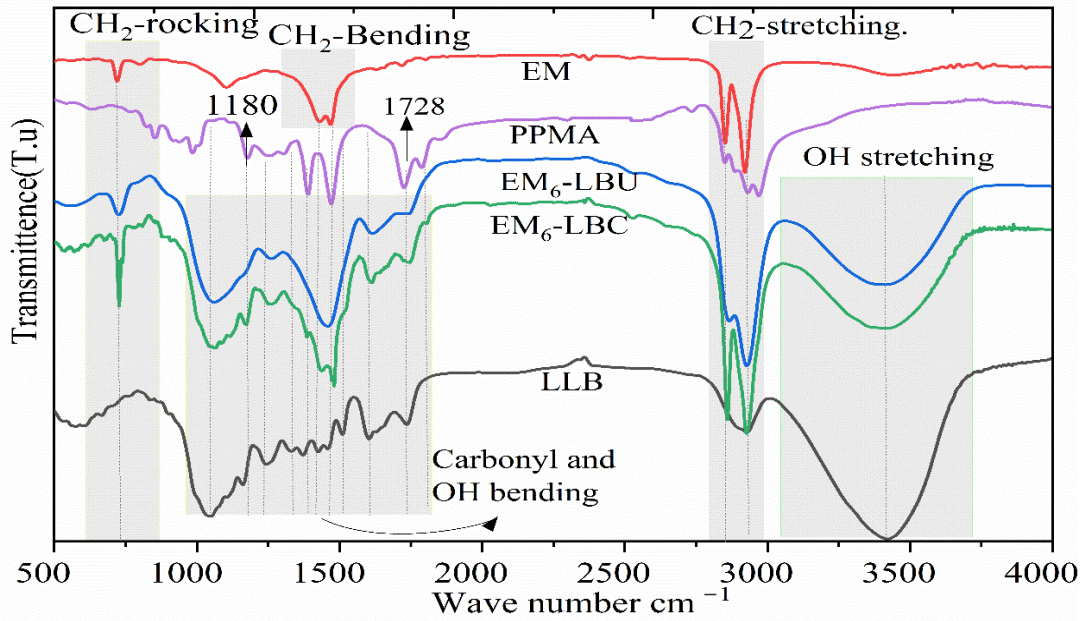

Figure 3. 9 FTIR spectra of WPCs based on the EM of (LLDPE, MDPE and HDPE)

3.7 Thermogravimetric analysis of WPCs

As shown in **Figure 3.10**, the temperature at 5% mass loss ($T_{5\%}$) for LLB is 225.8°C, which is higher than previously reported values for other bamboo fibers [65]. This could be attributed to the high concentrations of cellulose and stable lignin, as inferred from the chemical bamboo characterizations. The first shoulder peak (P_0) appeared in region II (206–236 °C) with a weight loss of 9.65%. At 236–372 °C (including P_1 and P_2), a weight loss of 68.5% was noted owing to cellulose and lignin decomposition, especially at P_2 at approximately 365 °C. In stage III (365–600 °C), complete LLB decomposition occurred with a mass loss of 18.54% due to the oxidative decomposition of carbonized residue and volatilization of anhydrous sugars, leaving a residual char of 13.07%. Similarly, Guo et al. [65] observed two major decomposition peaks (P_1 and P_2), with P_2 being the most prominent. In our case, the overlap of hemicellulose and cellulose at high temperatures for P_1 (315 °C) and a larger mass loss rate at P_2 are likely attributable to the low hemicellulose and high cellulose contents of the LLBs.

Incorporating LLB fibrous particles into WPCs changed the thermal degradation into multiple stages, decreasing it below that of the unreinforced matrix polymers, particularly up to region II. In region I, the degradation below 200 °C includes volatilization of residual water and extractives and degradation of amorphous hemicellulose of LLB incorporated into the WPC matrix. The major degradation between regions II and III is ascribed to the decomposition of the cellulose, hemicellulose, and lignin fibrous bamboo particles, which mostly occurred below the decomposition of the polymeric matrix. Hemicellulose that degraded earlier continued to degrade in the temperature range of 270–360 °C in region II, along with the active pyrolysis of the remaining cellulose (α-cellulose). Lignin is a thermally stable and highly networked phenolic molecule that decomposes over a wide range and contributes to char formation at 510 °C and higher [65]. Similarly, the peak intensity in region III was greater than that in region II because of the significant degradation of the WPC polymer matrix in region III. Region IV is likely ascribed to the complete decomposition and evolution of the pyrolysis gas products and their final decomposition to ash.

The WPC composites containing MAPP exhibited higher thermal stability than the uncoupled composites because of the improved interfacial force and encapsulation of the fibers within the polymeric matrix. Similarly, it shifted $T_{5\%}$ and T_{max} at the end of region III to higher values.

Specifically, in region III between $T_{50\%}$ and $T_{25\%}$, the T_{max} of the WPCs of EM and rHDPE with MAPP exceeded the degradation temperature of their corresponding matrix with increased residue [227]. It was reported that MAPP improved the interphase and catalytically carbonized [228] and promoted the release of high-carbon char from lignin, which acted as a thermal barrier during its wide thermal degradation range because of its stable aromatic phenyl groups [229]. This phenomenon enhanced the thermal stability of the coupled melt-blended WPCs of the polymers in region III compared with the unreinforced polymeric matrix and coupled and uncoupled WPCs based on rLLDPE and MDPE. Additionally, EM-based composites benefit from the high thermal stability of the rHDPE matrix, improved fiber encapsulation, and efficient dispersion due to MAPP. The T_{max} of the EM matrix (477.9 °C) in region III shifted to 486.8 °C in EM6-LBC, realizing complete oxidation at temperatures above 500 °C. However, beyond 500 °C at the end of region III, the carbonization effects of the LLB decreased, leading to complete WPC degradation. Free radicals from coupling agents and polymer matrix degradation catalyzed composite pyrolysis and increased reactivity, resulting in minimal differences in the remaining mass at 650 °C compared with LLB [228,230]. However, with the rising temperature the detectable decomposition ranges are revealed around 600 °C with 6.24% mass loss. This second phase could originate from the slow pyrolysis of inorganic mineral fillers such as $CaCO_3$ as high amounts of Ca were found in our previous determination of metal additives.

WPCs with neat and recycled HDPE using pine and bagasse fibers, coupled with PEMA and carboxylated polyethylene, have T_{max} values of approximately 470 °C. A slight increase in T_{max} of over 19 °C in our study is likely attributable to the residual mineral fillers and improved MAPP compatibility. Similarly, WPCs from rHDPE and commercial wood fibers (poplar, Douglas fir, black locust, white oak, and ponderosa pine) started to degrade at comparative temperature ranges with little variations [21]. All PE-based recycled WPCs (both coupled and uncoupled), including the EM-based composites, performed well, except for the rLLDPE-based composites. In particular, the obtained thermogravimetric degradation characteristics are similar to those previously reported, depicting improved performances than commercial WPCs made from neat PE [17, 52].

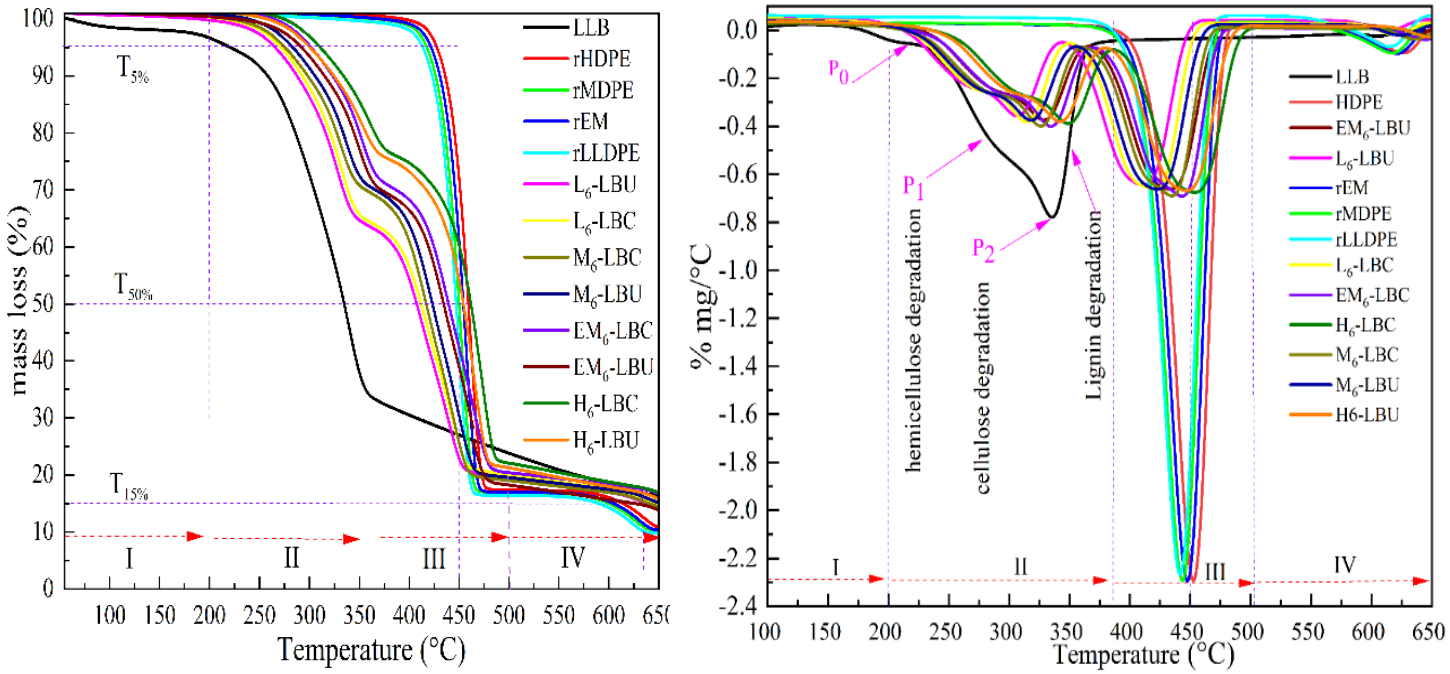

Figure 3. 10 TGA (left) and DTGA (right) curves of the WPCs and its polymer matrices

Table 3. 5 Thermographic data of polymer matrix and its WPCs.

Sample ID	$T_{5\%}$ (°C)	$T_{50\%}$ (°C)	$T_{25\%}$ (°C)	T_{max} (II) (°C)	Remaining mass (%) at T_{max} (II)	T_{max} (III) (°C)	Remaining mass (%) at T_{max} (II)	Remaining mass at 650°C
LLB	225.8	335.6	460.2	361	33. 10	-	23.13	16.7
rHDPE	427.9	458.9	469.76	-	-	480.9	17.8	10.8
rMDPE	417.2	451.6	459.3	-	-	474.8	17.4	10.2
rEM	421.6	453.6	464.6	-	-	477.9	17.6	10.9
rLLDPE	412.5	447.4	455.4	-	-	470.5	16.8	10.0
L_6-LBU	265.5	408.5	442.6	341.8	65.1	456.7	20.8	13.7
L_6-LBC	274.8	412.7	439.5	352.1	65.4	462.2	20.6	14.7
EM_6-LBC	298.4	440.8	468.2	377.5	72.1	486.8	21.48	16.1
EM_6-LBU	292.1	434.3	464.8	369.7	71.4	475.5	20.9	14.5
M_6-LBC	283.8	423.5	464.8	363.1	70.4	473.8	21.2	15.1
M_6-LBU	276.8	417.8	456.8	357.7	69.6	468.1	20.8	14.2
H_6-LBC	309.8	462.9	485.8	387.5	75.6	496.9	21.9	15.1
H_6-LBU	300.6	455.5	471.0	379.1	76.3	481.6	22.6	16.2

Conclusions

This study developed new WPCs by combining rPE waste fractions (rLLDPE, rMDPE, rHDPE) with indigenous Ethiopian bamboo particles (Oxytenanthera abyssinica) as reinforcements with key findings outlined below.

Indigenous Ethiopian bamboo fibrous particle, contains high levels of cellulose, lignin, and hemicellulose, making it a potential substitute to conventional wood fibers in WPC formulations. The residual elements (Ti, Ba, Cl, Zn, Pd, Hg, Br, and Cr VI) in the PE waste fractions and PAHs were below the threshold limits and remained intact during recycling, as confirmed by FTIR, DSC, and TGA, ensuring their suitability as a secondary resource for WPC formulation instead of waste.

In situ reactive compounding with MAPP greatly enhanced the interfacial strength compared with the unfilled polymer matrices through thermally induced chemical coupling and effective dispersion of bamboo particles for mechanical interlocking.

The ultimate tensile strength and flexural strength decreased as the LLB loading increased from 40% to 60%. Enhanced mechanical performance was achieved at 40% loading, primarily due to improved melt flow and better matrix encapsulation of the bamboo particles. However, even at 60% loading, significant mechanical strength was retained with the addition of MAPP. Notably, the bending strength and flexural modulus of all reinforced composites increased markedly compared to the unreinforced matrix across all formulations. The TM and FM increased with the LLB loading, with minor variations observed with the coupling agents. Moreover, WPCs formulated form coupled mixed blends of rLLDPE, rMDPE, and rHDPE showed improved mechanical properties by MAPP compatibilization and melt blending of rLLDPE with rMDPE and rHDPE. Similarly, the thermal stability of the WPCs produced from EM-based composites with the coupling agent's inclusion benefit from the high thermal stability of the rHDPE matrix, compared with the unreinforced polymeric matrix and WPCs based on both rLDPE and rMDPE matrix. The MAPP improved fiber encapsulation, and efficient dispersion within the matrix polymers which highly improved the thermal degradation of the LLB particles.

These WPCs offer practical alternatives to traditional wood and plastic products, including polyolefin-based composites with wood fiber or polymer contents of 40%–60%, satisfying the

ISO 178, ASTM D6109, and ASTM D7032 standards for FS, FM, and TS, respectively. Formulated WPCs could be suitable for furniture, wall cladding, ceiling boards, interior designs, decking, and construction applications, such as insulation, with low biodegradation risk and deformation, with properties comparable to commercial products.

Future studies should focus on enhancing the IS of the composites using dual-functional coupling agents with multiple monomers for broader property improvements. Exploring alternative production methods, such as extrusion and injection molding, is crucial for achieving better particle distribution within the polymer matrix. Moreover, benchmarking the PE waste fractions and identifying target applications can unlock the full potential of WPCs. Further research is also needed to understand the impact of recycled thermoplastics on the durability of WPCs and optimize the product properties.

CHAPTER FOUR

Wood Polymer Composite (WPC) Formulation from Ethiopian Indigenous Lowland Bamboo Particles and Post-consumer Plastic Blends: Synergetic and Dual Effects of Both Coupling Agent and Organic Crosslinking Catalyst

Abstract:

Currently, the rapid increase of potential thermoplastic waste, which does not circulate back into ecosystem through biodegradation, has led to valuable resource waste and environmental pollution. To utilize the economic value and reduce environmental impact, ecofriendly biomass-based wood polymer composites (WPCs) were produced from potential thermoplastic waste blends. Both recycled polystyrene (rPS) from electronic waste and recycled high-density polyethylene (rHDPE) from post-consumer waste were used as polymeric matrices. Ethiopian indigenous lowland bamboo particles *(Oxytenanthera abyssinica*), which had never been used in WPC, was utilized as the dispersed phase reinforcement. The formulation involves in situ reactive melt blending and chemical crosslinking using maleic anhydride grafted polypropylene (MAPP) and dicumyl peroxide (DCP) as an organic catalyst initiator, without preliminary solvent-based bamboo particles treatment. The properties of WPCs formulated from varying sizes of LLB particles and compositions of rHDPE, rPS, and their equal melt blends were thoroughly investigated using established standards. Similarly, the chemical composition, structure, crystallinity, thermal degradation, and contaminants of the recycled plastics were carefully evaluated and characterized before use. In situ melt blending and reaction induced crosslinking interfaced with MAPP compatibilizer and DCP crosslinking synergistically enhanced the composite properties, which were not achieved with separate polymer matrices. The result shows a very significant increase in fundamental static and dynamic mechanical properties, including thermal stability of the composites compared with uncoupled composites. Formulated WPCs can provide low-cost and sustainable building materials which can replace energy intensive and non-sustainable conventional building materials.

Keywords: *Wood polymer composite, interfacial adhesion, Mechanical properties, Postconsumer plastic utilization, polymer blending*

4.1 Introduction

Wood polymer composites (WPCs) are polymer matrix-based composites primarily consisting of thermoplastic matrix and plant based dispersed phase in the form of short fibers, particles, and flour [3]. The polymer matrices in WPCs are thermoplastic polymers that flow easily when heated below the thermal degradation of lignocellulose fibers (200–220°C) and regain their properties upon cooling. Common examples include polyethylene (PE), polypropylene (PP), ultrahigh-molecular-weight polyethylene (UHMWPE), and polyvinyl chloride (PVC) [182]. Currently, the rapid increase of postconsumer thermoplastic waste, which does not circulate back into the ecosystem, has resulted in resource wastage and pollution infiltrating various parts of the environment. These critical problems demand sustainable solutions to reduce or valorize their waste, offering alternatives to conventional incineration and landfilling, which releases secondary pollutants and wastage of valuable resources. Similarly, specific chemical recycling techniques involving pyrolysis of multi-polymer systems, and depolymerization techniques are not well developed as optimal environmental solutions due to substantial investment requirements [3]. These have prompted exploring alternatives like thermomechanical recycling and valorizing them to more sustainable, eco-friendly materials and/or chemicals, which can reduce post-consumer waste before considering incineration or landfilling [4]. WPC has emerged as promising materials for cascading post-consumer thermoplastic waste with ecofriendly sustainable lignocellulosic fibers. This simultaneously enhances the recycling economy prior to energy recovery, reduces the environmental carbon footprint, and linear economy of single use thermoplastics [3, 4]. Unlike mineral fibers, fibrous plants used in WPCs are not only eco-friendly and widely available [42], but the cost of obtaining them is also a small fraction of that associated with synthetic fibers such as carbon, glass, and aramid fibers [30]. Similarly, their corresponding fiber-based composites are very expensive, environmentally unfriendly and unsustainable though they exhibit better mechanical properties [79]. However, WPCs combine the aesthetic properties of woody like natural fibers with the high molding capability, thermal processability, and moisture resistance of plastics [4]. It demonstrate superior specific strength, specific modulus, and low density, making them suitable for various applications [231].

Furthermore, WPC formulations from post-consumer plastic blends will have reduced environmental impact throughout their service life and have a potential for multiple recyclability and biodegradation to the end of service life [6]. As a result, WPCs has gained popularity across sectors such a building materials, transportation, interior house decoration, furniture, and automotive interiors, marking a significant step towards large-scale industrialization [108]. However, the primary limitation of WPCs is their incompatibility between hydrophobic thermoplastics and polar hydrophilic natural fibrous particles. This is mainly due to the high density of hydroxyl and carbonyl groups in cellulose, hemicellulose, and less hydrophobicity of lignin [4]. Addressing this challenge through chemical and physical modifications, such as altering surface properties and modifying polar hydroxyl networks with coupling or crosslinking agents, is a major focus of current research. These modifications aim to enhance the interphase in WPCs as well as the durability of WPCs. Various methods have been explored to achieve this interphase compatibility, including physical treatments like plasma and UV radiation, and chemical treatments such as alkaline, silane, permanganate, acrylonitrile, acetylation and isocyanate [30,212]. Additionally, polymer grafting and copolymerization on fiber surfaces, including free-radical grafting, Ziegler-Natta grafting, and polycondensation grafting, have been investigated [226]. These techniques aim to reduce surface hydrophilicity, eliminate weak components in natural fibers (especially hemicellulose), improve wettability, and minimize photodegradation during the service life [8, 11].

Chemical coupling agents (CAs) have shown better performance and gained commercial footprint compared to conventional solution-based treatment methods, which involves challenging and expensive solvents difficult to be separated and maintain a constant optimal levels [4]. Small quantities of coupling agents and graft copolymers can create strong interfacial chemical bonds by interacting with the polymeric matrix and reinforcing natural dispersed phase [83]. This approach has resulted excellent results through in situ reactive compatibilization, , and multimonomer graft copolymers [3, 13, 14]. Noteworthy, examples of effective coupling agents include maleic anhydride grafted polypropylene (MAPP), maleic anhydride grafted polyethylene (MAPE), styrene-ethylene/butylene-styrene-maleic anhydride-graft (SEBS-g-MAH), and styrene maleic anhydride (SMA) grafted ethylene-vinyl acetate (MA-EVA) [21,29]. They enhance compatibility through radical melt grafting in reactive extrusion compatibilization, esterification

and hydrogen bonding interactions between maleic anhydride and the hydroxyl groups of natural reinforcements. Interfaced crosslinking radical initiators such as DCP, benzoyl peroxide (BPO), tert-butylperoxybenzonate (TBPB), and ditert-butyl peroxide (DTBPO) are commonly used to improve the efficiency of the shorter molecular chain of MA [27,232].

The most utilized lignocellulosic fibers in WPCs include conventional fibers such as kenaf, pine, oil palm, spruce, flax, beech, poplar, hemp, sisal, maple, oak, coir, and jute, and agricultural residue biomass like rice husk and coconut fibers [4]. However, untapped potential of indigenous Ethiopian bamboo, which is rich in fibers, remains underexplored. In Ethiopia, two indigenous bamboo species—Oxytenanthera abyssinica (Lowland bamboo - LLB) and Yushania Alpina (Highland bamboo - HLB)—cover more than 1.47 million hectares, accounting for about 67% of the total bamboo coverage on the African continent and 7% of the global coverage [50]. LLB, which has no hollow cross-section, covers 85% of the total national bamboo coverage, while the remaining 15% is shared by HLB (containing hollow cross section) [26,52]. We firmly believe that using indigenous LLB fibrous particles, which have never been utilized as fibrous particles in WPC formulations, alongside recycled polymers as the core matrix, not only enhances the market value chain for local indigenous bamboo resources but also promotes their industrial use. It offers a dual benefit by supporting recycling efforts and potentially providing affordable building materials, which are highly demanded because of fast growing population, specifically in Sub-Saharan region countries. Similarly, the utilization of recycled valuable thermoplastic plastics from e-waste is rare. However, they can be used in circular cascading use for sustainable and environmentally friendly WPCs, which can be recycled or decomposed before energy recovery [3]. Few studies investigated recovered high impact polystyrene (HIPS), acrylonitrile butadiene styrene (ABS) and pulverized waste printed circuit boards (PCB), including difunctional epoxy resins like bisphenol A, multifunctional epoxy resins, and bismaleimide triazine epoxy blends [74,75]. To the best of our knowledge, there is no prior research exploring the potential use of Ethiopian indigenous LLB, known for its abundant fiber content, in combination with rPS from computer parts and printer toner, and recycled rHDPE from post-consumer packaging as the polymeric matrix blends for WPC formulations. As a result, this work investigated these gaps through in situ compatibilization of MAPP and crosslinking of organic peroxide DCP catalysts during WPC formulations. It comprehensively evaluated the effects of LLB particle loading and size, and the synergistic influence of MAPP and DCP on mechanical

properties. Similarly, dynamic thermomechanical properties, thermal stability including melting characteristics were further characterized with the representative WPCs of equal contents of polymeric matrix and LLB particles reinforcement. The formulations involved a two-step process, homogenous compounding and chemical cross linking in the pilot-scale HAAKE Reomix configured with a tangential counter-rotating twin screw followed by consolidation with a hot press compression to produce a WPC board protype.

4.2 Materials and Methods

4.2.1 Preparation of Post-consumer Plastic Blends

Recycled HDPE from post-consumer packaging materials and rPS from e-waste (including computer keyboards, monitors, and printer toner materials) were sorted, cut into small pieces, cleaned, vacuum dried, and pelletized into granulates using a counter-rotating extruder. The measured melt flow rate (MFR, ISO 1133) of the rHDPE and rPS were 0.2g/10 min (230°C/2.16 kg) and 0.9g/10 min (230°C/2.16 kg), with corresponding densities of 0.96 g/cm³ and 1.043 g/cm³, respectively. Polypropylene grafted with 8-10% maleic anhydride (MAPP) (Sigma Aldrich, USA), with an MFI of 21g/10 min (230°C/5.0 kg), a density of 0.9341 g/cm³, molecular weight ~ 9100 (GPC) was also used as an interfacial compatibilizer. Analytical grade dicumyl peroxide (Sigma Aldrich, USA) with a density of 1.56 g/cm³ was used as the crosslinking agent.

4.2.2 Lowland Bamboo Collection and Preparation.

Matured LLB culms were collected from the Arjo Gudatu (9° 4' 52" N, 36° 37' 30" E) district of the Oromia region provinces located in Ethiopia. It was cut into small strips, air-dried, and ground using a hammer mill (Retsch SR 200 Grauβ, Haan, Germany). Two wide side ranges, large size (L) (1 mm-0.5 mm) and small size (S) (<0.5 mm) of the particles were selected by sieve mesh size with a vibrating sieve without eliminating particles in the powder. A wide particle size distribution was chosen to enhance the wider use of resources and investigate their reinforcement performance at multiscale distribution. Finally, it was dried at 105°C in vacuum oven for 24 hours until the moisture content fell below 2% and immediately used for WPC formulation **(Figure 4.1)**.

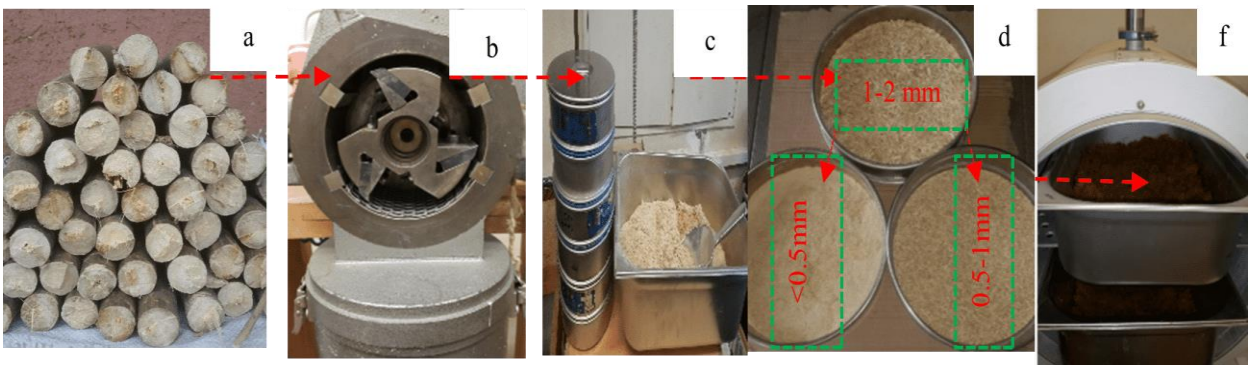

Figure 4. 1a) LLB biomass b) grinding c) sieving to targeted particle size d) sieved particle size f) Vacuum drying.

4.2.3 Chemical Structure Thermal Properties of the Recycled Polymeric Matrix and Its WPCs.

Fourier transform infrared (FTIR) analysis was performed using KBr matrix-bound pellets and analysed in transmittance mode using an Agilent Spectrum Two Model spectrometer. Spectra were recorded in the range of 4000–400 cm^{-1} with a scan rate of 64 per sample and an optical resolution of 4 cm^{-1}. For thermal degradation, about 10 mg samples of both matrix polymers and WPCs were used in a TGA (Q50 New Castle, DE, USA) with nitrogen a flow rate of 60 ml/min. It was performed from 30°C to 700°C at an isothermal heating rate of 10°C/min and first-derivative thermogravimetric curves (DTGA) were used to analyze the transition peak. Similarly, about 6 mg samples of recycled films and WPCs samples were used for differential scanning calorimetry (DSC) analysis using a TA instrument (STA, Q600, New Castle, DE, USA) in a nitrogen atmosphere at a flow rate of 60 ml/min. Both heating and cooling cycles were conducted at a rate of 10ºC/m from 25ºC to 350ºC to obtain both melting and the crystallization curve. Finally, the degree of crystallinity (X_C) was determined using equation (1).

$$X_c = \left[\frac{\Delta H_m}{\Delta H_m^{\circ}(1-\varphi)}\right].100\% \qquad (1)$$

where ΔH_m (J/g) represents for the melting enthalpy, ΔH_m° (J/g) stands for the theoretical melting enthalpy of a fully crystalline HDPE (293 J/g) [220] and φ corresponds to the weight fraction of LLB particles.

4. 2.4 Scanning Electron Microscope (SEM) Observation.

The SEM morphologies of the fractured surfaces from the impact strength tests of WPCs samples were examined using a QUANTA200 scanning electron microscope (FEI, USA) to obtain indirect information regarding interfacial adhesion between the matrix and particles. The surfaces were sputter-coated with a 2 nm layer of platinum to enhance conductivity. The observations were conducted at an accelerated electron beam voltage of 10.0 kV.

4.2.5 Metal Additives and Halogens Analysis in Recycled Polymers

The metal additives and elemental composition of rHDPE and rPS were assessed in accordance with the European Union directives on e-wastes [123]. The evaluation process also adhered to the Reduction of hazardous heavy method for polyethylene (PE) [233] using an Epsilon 5 XRF spectrometer. Analytical parameters were determined based on certified standards from TOXEL prepared by DSM Resolve and PANalytical collaboratively. Each TOXEL set comprised five standards containing regulated elements: chromium (Cr), cadmium (Cd), mercury (Hg), lead (Pb), arsenic (As), nickel (Ni), copper (Cu), zinc (Zn), barium (Ba), and bromine (Br).

4.2.6 Composites Formulation

The experimental design included 16 batches of WPCs and 2 additional batches of unfilled recycled rHDPE and rPS matrices, designated as rHD_0 and rPS_0, respectively as shown in **Table 4.1.** For sample ID (SID) designations, a composition of 100 wt. % based was used as the subscript, while MAPP and DCP were subtracted from both phases. The subscript in the SID represents the proportion of the polymer matrix. Samples containing the coupling system were labelled with a 'C,' while those without were labelled with a 'U' at the end of the sample ID. Contents of MAPP and DCP, were fixed at 3 wt.% and 1 wt.%. Vacuum oven dried LLB particle reinforcement of two size ranges—large (L) (1-0.5 mm) and small (S) (<0.5 mm) were used. Homogenization was performed by adding uniformly distributed dry-mixed polymer matrix granulates and a compatibilizing agent (rHDPE, rPS, MAPP, and DCP) to the pre-heated mixing chamber (Thermo Scientific HAAKE Reomix 3000 OS) of counter rotating screw configurations. They were compounded and melted for approximately five minutes, followed by LLB particles addition and continued for another 10 min until a constant torque and viscosity were reached for the total mixing of 15 min. This process was conducted at 180°C for unblended rHDPE-based composites and 190°C for the rest of both rPS and EM at a screw rotation speed of 50 rpm. Finally

compounded WPC granules were dried and stored in plastic bags at a relative humidity of 65 % and a temperature of 23 ± 2°C.

Table 4. 1 Experimental design of WPC formulation

SID	Matrix Polymer (wt.%)	LLB (wt.%)	MAPP (wt.%)	DCP (wt.%)
rHD_0	100	0	0	0
rPSo	100	0	0	0
HD_5-SLBC	48	48	3	1
PS_5-SLBC	48	48	3	1
EM_4-SLBU	40	60	0	0
EM_5-SLBU	50	50	0	0
EM_6-SLBU	60	60	0	0
EM_4-SLBC	38	58	3	1
EM_5-SLBC	48	48	3	1
EM_6-SLBC	58	38	3	1
HD_5-LLBC	48	48	3	1
PS_5-LLBC	48	48	3	1
EM_4-LLBU	40	60	0	0
EM_5-LLBU	50	50	0	0
EM_6-LLBU	60	40	0	0
EM_4-LLBC	38	58	3	1
EM_5-LLBC	48	48	3	1
EM_6-LLBC	58	38	3	1

4.2.7 Preparation of WPC by Compression Hot Molding

The dried WPC granules were reduced in size using an 8 mm sieve and placed in a carbon steel die frame (180 mm × 200 mm × 4 mm), covered with the Teflon sheets and then inserted into a computerized preheated lab-scale hydraulic hot-press. WPCs were fabricated using isothermal hot compression molding at 190 °C for rHDPE and 200 °C for both rPS and EM, corresponding to the typical processing temperatures of their respective polymer matrices [4]. Optimized

processes of better cyclic pressing pressure involving different steps were applied. These include low-pressure melting with a slight plate opening for 1 min at 20 bars, pressing at 50 bar for 8 minutes, pressing at 70 bars for 1 min, increasing to 100 bar for 2 minutes, and holding at 100 bars during slow cooling for 1.5 minutes until the temperature dropped below 40°C. Finally, the press was opened, and WPCs board protypes were removed from the frame and cooled at room temperature (**Figure 4.2**).

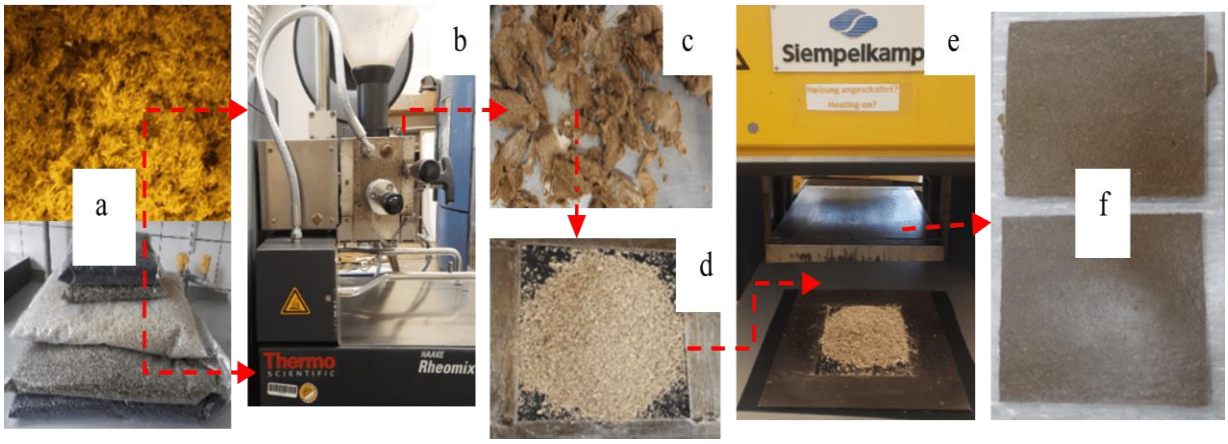

Figure 4. 2 a) LLB particles, rPS, rHDPE and MAPP b) compounding process c) WPC granulates d) reduced WPC granules e) compression molding f) WPC protype (2 replicates)

4.2.8 Measurements of Static and Dynamic Mechanical Properties

Flexural strength (FS) and its modulus (FM), and Charpy unnotched impact strength (UIS) were determined according to ISO178 and ISO 179, respectively, using dimensions of 80 mm × 10 mm × 4 mm. Tensile strength (TS) and tensile modulus (TM) were measured according to p and 65% relative humidity. Values were determined from ten independent measurements conducted on two duplicates of each formulation, considering their dimensions during successive measurements. A universal testing machine (Model 3369, Instron, USA) with a 50 kN load cell and a crosshead speed of 5 mm/min was used to measure both the FS and TS at a strain rate between 0.05% and 0.25%. Representative samples, consisting of an equal mix of coupled and uncoupled wood-plastic composites (WPCs) with dimensions of 55 mm × 12 mm × 4 mm, were prepared in accordance with ASTM D 7028-07. These samples were evaluated for dynamic mechanical thermal properties (DMTA) using a dynamic mechanical analyzer (DMA Q 800, TSA, USA)

operating in dual cantilever mode. The analysis involved a dynamic temperature ramp from 20°C to 130°C, with a heating rate of 3°C/min, a frequency of 1 Hz, and an amplitude of 20 μm.

4.3 Results and discussion

4.3.1 Metal and Nonmetal Additives Analysis Results in the Recycled Plastics

The utilization of recycled thermoplastics requires adherence to specific threshold levels of heavy metals. Table 2 presents the residual metal additives in recycled rHDPE and rPS, based on triplicate measurements with standard deviations indicated in brackets. As shown in **Table 4.2**, relatively high concentrations of Ca, Ti, Ba, Cl, Zn, and Fe were found in rHDPE and Sb, Ca, and Br were found in rPS. These residual elements may originate from various sources, such as mineral fillers such as $CaCO_3$, residual catalysts such as Ziegler-Natta, and metallocenes used in the production of HDPE, as well as inorganic admixtures such as pigments (e.g., TiO_2, ZnO, and Fe_2O_3), flame retardants (e.g., Sb_2O_3 and brominated organics), and stabilizers (for example, Ba, Sn, and Zn). Although trace amounts of heavy metals and toxic contaminants were detected, the threshold values for toxic elements, particularly Cd, Br, Cr, and Hg, did not exceed 0.1% or fall below the equivalent of 1000 ppm [123,233]. The other components are less toxic, and some of the elements are below the limit of detection (LOD), which suggests that rPE and rPS remain below these levels and can be utilized as secondary resources for WPC formulation, followed by continuous monitoring over an extended period.

Table 4. 2 Results of residual metal additives in recycled rHDPE and rPS

Element	rPS (ppm)	rHDPE (ppm)	Element	rPS (ppm)	rHDPE (ppm)
Cr	5.63 (0.72)	23.7 (0.8)	Se	<LOD	<LOD
Ba	123.9 (2.17)	231 (9.2)	As	0.30 (0.10)	1.1 (0.3)
Ti	<LOD	816 (9.3)	Hg	<LOD	1.8(0.4)
Cl	<LOD	312.9 (7.87)	Zn	46.85 (0.23)	291.4 (3.5)
Sb	235.23 (8.98)	9.38 (0.4)	Cu	10.69 (1.47)	14.9 (0.8)
Sn	13.1 (0.33)	7.51 (0.1)	Ni	6.78 (0.37)	16.4 (0.4)
Cd	9.58 (0.26)	6.35 (0.3)	Co	7.98 (0.62)	5.0 (0.7)
Sr	<LOD	37.9 (0.1)	Fe	137.1 (5.8)	321.9 (2.4)

Bi	<LOD	<LOD	Mon	2.4(0.79)	19.1(1.2)
Pd	1.5 (0.01)	177.6 (0.2	V	<LOD	15.5 (0.6)
Ca	167.85 (5.85)	4356 (13.58)	Pb	7.45(0.87)	<LOD
Br	512.85 (12.5)	0.6 (0.1)	Ag	<LOD	< LOD

*The numbers in brackets indicate the standard deviations the measurements done from three replicates

4.3.2 Mechanical Properties of the WPCs

Variations of key mechanical properties WPCs are discussed as follows in comparison within each unreinforced matrix, coupled, uncoupled including the blend and unblended formulations. The vertical regions in the graphs are labeled as M, S, and L, to separate the unreinforced polymer matrix (M), WPCs with smaller (S) and larger (L) LLB particle size fractions facilitate quick intuition.

4.3.2.1 Tensile Strength and Modulus of Elasticity

As shown in **Figure 4.3**, TM of the polymer matrix improved in all formulations. Within the smaller LLB particle fractions (S), Modulus of elasticity (MOE) ranges from 2.32GPa (HD_5-SLBC) to 3.42GPa (EM_4-SLBC), representing the smallest and largest extreme values of MOE, respectively. In the larger fractions (L), it ranges from 2.22 GPa (EM_6-LLBU) to 2.97 GPa (EM_4-LLBC). The inclusion of LLB particles resulted in a linear increase of MOE larger than both core polymer matrices (M), making the WPCs stiffer regardless of the size fractions. All coupled WPCs with both S and L particle sizes showed significant increases in MOE compared to their uncoupled counterparts and unreinforced matrices. Specifically, TM of EM_4-SLBC, EM_5-SLBC, and EM_6-SLBC increases of 13%, 22%, and 23% compared with EM_4-SLBU, EM_5-SLBU, and EM_6-SLBU, respectively, and 15%, 30%, and 29% compared with EM_4-LLBC, EM_5-LLBC, and EM_6-LLBC, respectively. This highlights the dominant effect of particle size on MOE, with only some influence from coupling agents (MAPP, DCP) as well. Similarly, when the same equal-mix blend of these coupled S fractions was compared with coupled HD_5-SLBC, significant variations were observed, increasing by 47%, 41%, and 31%, respectively. However, only EM_4-SLBC and EM_5-SLBC showed 10% and 6% increases, respectively, compared to PS_5-SLBC. Additionally, the TM of the coupled WPC sets of S fractions containing an equal blend compared to the control matrices of rHDPE and rPS showed an increase by factor rations of 4, 3.7, 3.4, 2.8, 2.7, and 2.5,

respectively. Compared even though related trends were observed for the WPCs set of coupled WPCs with larger fractions (L) compared with their respective TM of the control matrix, the increasing amounts were smaller compared with the coupled WPC sets of S fractions of LLB particles.

Coupled WPCs exhibited higher TS than their uncoupled counterparts and polymer matrices. Within the S particle fractions of LLB, TS ranges from 22.18 MPa (EM_4-SLBU) to 32.98 MPa (EM_6-SLBC), while within L fractions, it ranges from 19.34 MPa (EM_4-LLBU) to 28.187 MPa (EM_6-LLBC). The TS of EM_4-SLBC, EM_5-SLBC, and EM_6-SLBC increased by 27.6%, 28.5%, and 22.9%, respectively, compared to their uncoupled counterparts and by 8.9%, 15%, and 14.2%, respectively, compared to their respective coupled large fractions L. Similar comparison with unblended HD_5-SLBC showed significant increases of 12.17%, 19.5%, and 27%. Composites from the larger L fractions, EM_4-LLBC, EM_5-LLBC, and EM_6-LLBC, showed TS increases of 27.7%, 17.34%, and 14%, respectively, compared with uncoupled WPCs in the L region; 11%, 12.7%, and 21.4%, respectively, compared with unblended coupled HD_5-LLBC; and 16%, 12.7%, and 24.5%, respectively, compared with unblended coupled PS_5-LLB. Similarly, compared with unreinforced rHDPE, TS of EM_4-SLBC, EM_5-SLBC, and EM_6-SLBC significantly increased by 25%, 33.5%, 42%, respectively and increased by 12%, 17.7%, and 25% compared with rPS, which was greater than the increases for their respective unblended matrices, HD_5-SLC and PS_5-SLBC. Generally, increasing LLB particle content reduced TS performance, especially for larger particles, due to agglomeration and voids causing stress concentration. However, coupled WPCs with smaller particles showed better performance most probably due to higher specific surface area, uniform dispersion, improved matrix flowability, and enhanced stress transfer [171]. Additionally, this phenomenon likely results in the preferential localization of both MAPP and DCP near the fiber-matrix interface, thereby increasing homolytic or heterolytic breakdown, leading to crosslinking with other polymer chains [172]. This simultaneously increases the chance of better compatibility which leads to improved TS as observed in the FTIR spectrum (section 3.2). The findings of this work align with WPCs made from fine wood flour (53-105μm), 2% SMA, and recycled PS, showing a maximum TS of 34.23 MPa and TM of 2.14 GPa involving formulated using a contour rotating commercial extruder [234]. Similar findings by Hwang et al. [235] for WPC composites using spray-dried cellulose nanofibrils with a neat PP matrix and MAPP (27.84-33.03 MPa) fall within the same range. Furthermore, Porebska et al. [145] reported

TS values of 26.3 MPa, 35 MPa, 27.3 MPa, and 14.4 MPa for WPCs made from commercial neat PS, ABS, PLA, and polyester resin with cellulose fibers, and MOE values of 6.8 MPa, 4.6 MPa, 3.9 MPa, and 1.8 MPa, respectively. These are comparable to WPCs with S fractions, indicating that similar TS similar with the neat polymers can be achieved without fully extracting cellulosic fibers which is a relatively expensive process.

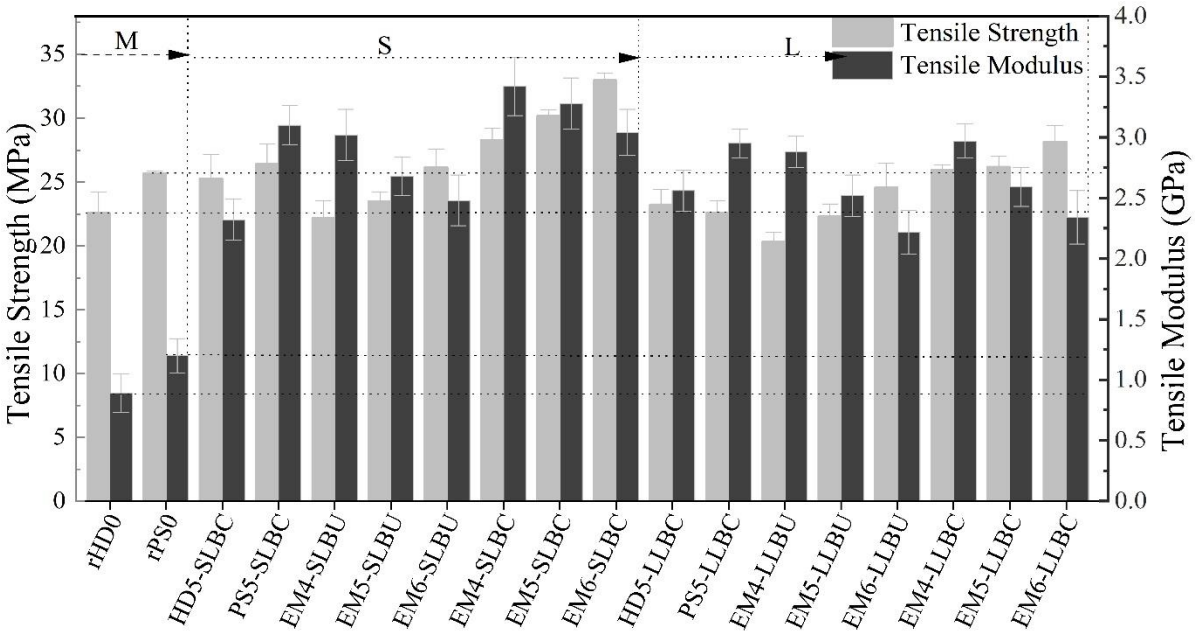

Figure 4. 3 Tensile strength and Tensile modulus of WPCs Samples

4.3.2.2 Flexural Strength and Flexural Modulus (Modulus of Rupture)

FS of the formulated WPCs varied from 42.18 MPa (EM_6-SLBC) to 22.57 MPa (EM_4-LLBU) as the largest and smallest values as shown in **Figure 4.4**. Like the MOE, FM increased with increasing LLB particle loading regardless of particle size ranging between 2.31GPa and 3.67GPa for WPCs HD_5-LLBC and EM_4-SLBC, respectively. Comparison with the extreme FS and FM values of WPCs with those of the unreinforced rHDPE matrix shows large improvements by ratio ranging from 1.22 to 2.3 for FS and 3.3 to 5.3 for FM. Similarly, FS of S regions of WPCs of EM_4-SLBC, EM_5-SLBC, and EM_6-SLBC increases by 28.4%, 18.6%, and 24.6%, respectively, compared with their respective uncoupled EM_4-SLBU, EM_5-SLBU, and EM_6-SLBU, respectively. However, compared to rPS, composites of EM_6-SLBC, EM_5-SLBC and unblended rPS_5-SLLBC exhibited improvements of 25.8%, 14.6%, and 8%, respectively. FS of equally blended composites of the L regions EM_4-LLBC, EM_5-LLBC, and EM_6-LLBC showed an

increase in percentage changes of 25.1%, 22.7%, and 20.2%, respectively, compared with their respective uncoupled WPC composites EM_4-SLBU, EM_5-SLBU, and EM_6-SLBU. This suggests that improvements in rPS matrix-based composites likely come primarily from the inclusion of coupling agents in the S regions of the WPCs. This implies that all the WPCs from the smaller particles and the modified interphase result in better FS than the WPCs of L fractions because of a similar mechanism explained by the TS of the composites.

FS trends show significant dependence on coupling agents and are influenced by the polymer matrix, with minor variations as LLB content increases. However, FM is highly dependent on LLB particle content, with treated WPCs showing higher FM than those without coupling agents similar to previous investigations [93]. The notable increase in FS and TS with coupling systems is probably due to interfacial adhesion facilitated by MAPP's polar anhydride groups and DCP-interfaced chemical reactions facilitated by thermal crosslinking, which strengthens adhesion and improves shear stress transfer. In unmodified composites, bamboo particles bonded to the thermoplastic matrix only through mechanical interlocking. Under stress, weak interfaces hinder stress transfer, causing stress concentration sites leading to rupture.

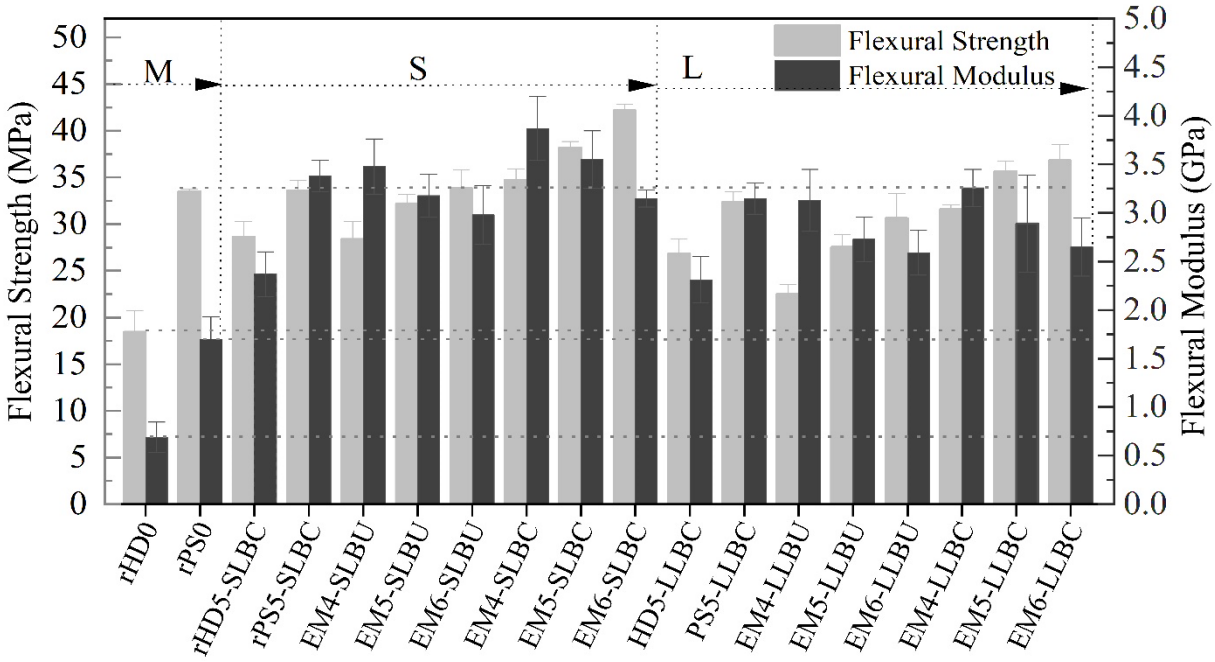

Figure 4. 4 Flexural strength and Modulus of rupture (FM) of WPCs Samples.

4.3.2.3 Tensile Fractural Energy and Elongations Strain at Break

Figure 5a shows typical stress-strain curves for representative WPCs to display the effects of particle size and coupling efficiency in comparison with unreinforced matrices. Figure 5b indicates fracture energy of WPCs, calculated from the integrated areas of tensile stress versus elongation, considering both elastic and plastic deformation areas to assess tensile toughness of WPCs. As seen in Figure 5a, the elongation at break decreased with the addition of reinforcing LLBs, especially in composites formulated from large particle (L) fractions lacking coupling agents, specifically at a higher loading rate of LLB particles, which correspondingly reduced fracture energy. However, the EM_6-SLBC showed the highest fracture energy among the WPCs, demonstrating the robustness and integrity of the formulation. This was supported by high tensile strength and the formation of stiffer composites with increased fracture strength, though this improvement reduced elongation at break compared to unreinforced matrices, which are more ductile and tough, exhibiting higher fracture energy but lower fracture and tensile strength. In general, coupled WPCs with smaller particle size and fractions showed enhanced fracture energy by preventing crack propagation and premature failure avoiding particle agglomerations in composites with weak interfacial zones which act as points for the crack initiations. Among all studied formulations, EM_6-SLBC displayed the best overall properties, as shown by its higher elongation and fractured energy, which made it more resistant to cracking and better able to absorb energy before failure. Similarly, the blended composite EM_5-SLBC showed considerable fractured energy, with better tensile and fractured strength compared to unblended HD5-SLBC, despite the latter's larger fracture energy. Interface modifications using MAPP and DCP significantly improved the fracture energy of lightweight developed WPCs, suggesting their potential use in applications like non-load-bearing structural materials, like recent work by Chen et al. [6].

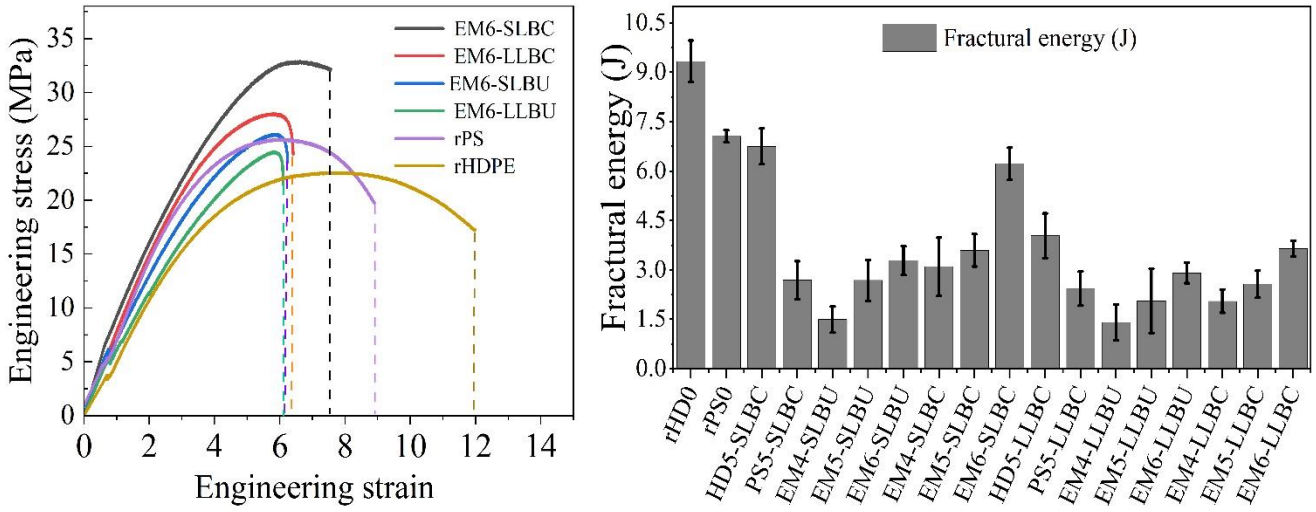

Figure 4. 5 Representative Engineering stress–strain curves of WPCs with 40 wt.% of LLB reinforcements (a) and tensile fractural energy (b).

4.3.2.4 Impact Strength Resistance

WPCs have lower UIS than rHDPE as shown by **Figure 4.6.** Natural particle reinforcements are more rigid than the polymer matrix, which increase WPC stiffness and reduce polymer chain mobility and decreases energy absorption as common in WPCs [34, 35]. An UIS greater than 8 kJ/m² is recommended for structural applications such as decking, as per ISO 179-1, but non-structural applications have less stringent requirements as long as the WPCs are not ruptured [28], 37]. IS ranging from 3.23 kJ/m² for EM_4-LLBU to 12.6 kJ/m² for HD_5-SLBC were observed in the sets of formulated WPCs, which was improved significantly with coupled WPCs. WPCs without coupling agents result in poor interfacial bonding and larger particles easily agglomerate as potential sites for microcrack initiation, which can be propagated with less energy [41]. However, smaller LLB particles improve IS and reducing stress concentration areas needed for crack initiation [223]. Adding a small amount of DCP enhances the grafting of MAH part of MAPP onto the bamboo fibrous particles and improves the IS. The IS variation in the S regions i.e., EM_4-SLBC, EM_5-SLBC, and EM_6-SLBC showed percentage increases of 87.4%, 174.6%, and 60.4%, respectively, compared with the uncoupled regions EM_4-SLBU, EM_5-SLBU, and EM_6-SLBU respectively. Similarly, IS of S WPCs increased by 14.7%, 31%, and 40%, compared with unreinforced rPS matrix. Furthermore, IS of coupled S regions i.e., EM_4-SLBC, EM_5-SLBC, and EM_6-SLBC indicate percentage increases by 84%, 60%, and 33.5% compared with the equally blended composites of the L regions EM_4-LLBC, EM_5-LLBC, and EM_6-LLBC,

respectively. This improvement was attributed to the ductile part of rHDPE, including the synergistic effects of MAPP and DCP like the previous studies. Song et al. [12] found that adding SEBS-g-MA and mixtures of DCP and MAH to recycled PP/HDPE/PS and wood flour blends increased unnotched IS due to a strong elastomeric interphase around the wood flour. Khamtree et al. [93] used MAPP as a coupling agent with recycled PP and various wood wastes, achieving the highest IS at 40% wood content, significantly enhanced by MAPP. Similarly, Kiaeifar et al. [224] and Poletto et al. [225] observed improved IS when formulating WPCs from expanded PS with wood flour (10-40%) and SMA as a coupling agent.

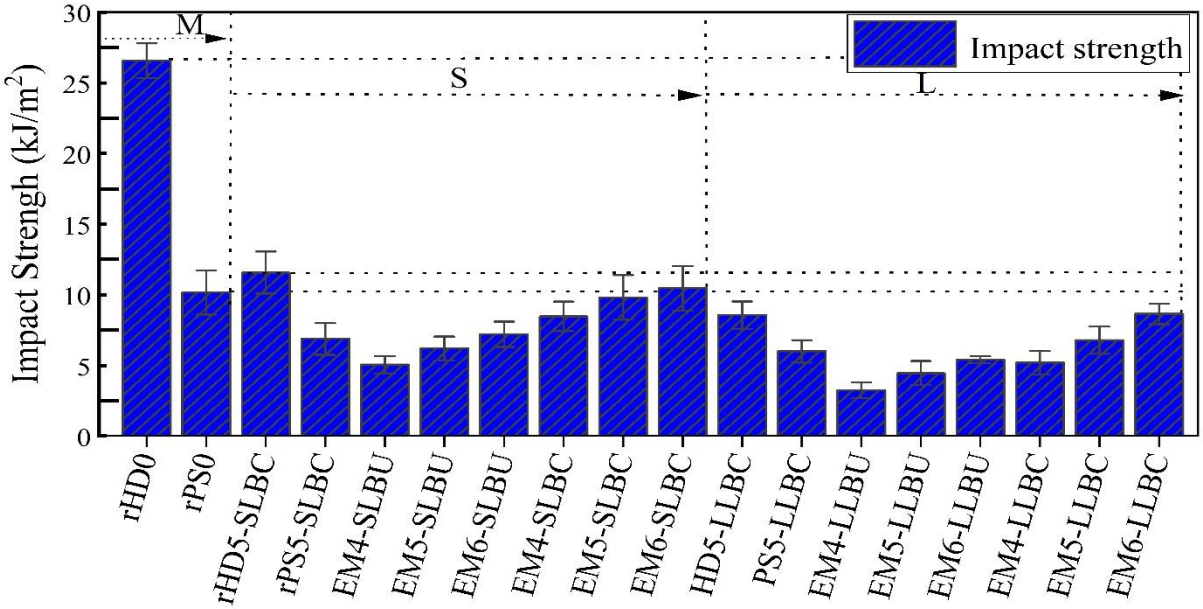

Figure 4. 6 Impact Strength of WPCs samples.

4.3.4 Dynamic Mechanical Properties of WPCs

Figure 4.7 presents two key dynamic mechanical properties of the WPCs: storage modulus (E′) and glass transition temperature (Tg) derived from damping (tanδ). These properties were utilized to analyze the dynamic changes in the viscoelastic behavior of WPCs composed of equal amounts of polymer matrix and LLB particles. E′ corresponds to the stored energy during the dynamic cycle of viscoelastic materials [236]. As illustrated in Figure 6a, the storage modulus of the composites generally exceeds that of the unreinforced matrix, except in the rubbery phase. This increase in E′ is attributed to the stiffer bamboo particles, which restrict macromolecular mobility during deformation. Furthermore, the modified interface with MAPP and DCP enhances E′ for the same particle reinforcement composition. The presence of LLB particles (L and S) and coupling agents (MAPP and DCP) directly influences the E′ of the WPCs, following the

decreasing order: EM_5-SLBC > EM_5-LLBC ≥ EM_5-SLMU > EM_5-LLBU > HD_5-SLBC > HD_5-LLBC. Composites with larger LLB particles (L) tend to have lower E′ values due to weaker interfaces, whereas those with smaller S fractions and interfacial compatibilizers exhibit improved bonding, leading to stiffer composites with higher E′ values in the glassy regions. These are likely because of in situ chemical bond aided crosslinked fiber–matrix interface, which resulted in distinct variations between coupled WPCs of EM_5-SLBC and EM_5-LLBC and their uncoupled composites EM_5-SLBU and EM_5-LLBU. Additionally, the equal melt blending of rHDPE and rPS increases stiffness in these regions compared to unblended counterparts, maintaining higher E′ values due to better compatibility and reduced interlaminar crystalline shearing from bamboo particle reinforcements.

Figure 4.7b shows the plot of Tan δ versus temperature for WPCs, with peak maxima in damping profiles occurring between 80°C and 110°C. The shift in peak positions for tan δ and Tg in the WPCs is linked to changes in the amorphous (non-crystalline) component of the rPS within the composites. Unfilled rPS displays its highest damping peak at a Tg of 98.5°C, but this peak decreases with the incorporation of LLB fibrous particles, reaching minimal values for both EM_5-SLBC and EM_5-LLBC in the viscous regions, indicating lower energy dissipation due to a stronger interface. A slight increase in tan δ around Tg for both EM_5-SLBC and EM_5-LLBC suggests increased toughness and the plasticizing effect of MAPP. As a result, the T_g of coupled composites EM_5-SLBC (105.98°C) and EM_5-LLBC (101.9°C) is higher than that of uncoupled composites EM5-SLBU (97.5°C) and EM5-LLBU (95.87°C), indicating that improved interfaces enhance interchain chemical heterogeneity, further improved by the higher specific surface area of smaller fractions. This leads to low tanα and minimal energy dissipation of composite's stored energy. These trends were further supported by previous studies of Zhou et al [184] and Geethamma et al [237]. The higher E′ followed by a decrease in tanδ in their respective viscous regions indicate a stronger particle-matrix interphase, suggesting reduced mobility of molecular chains, which leads to enhanced stiffness and strength [45, 44].

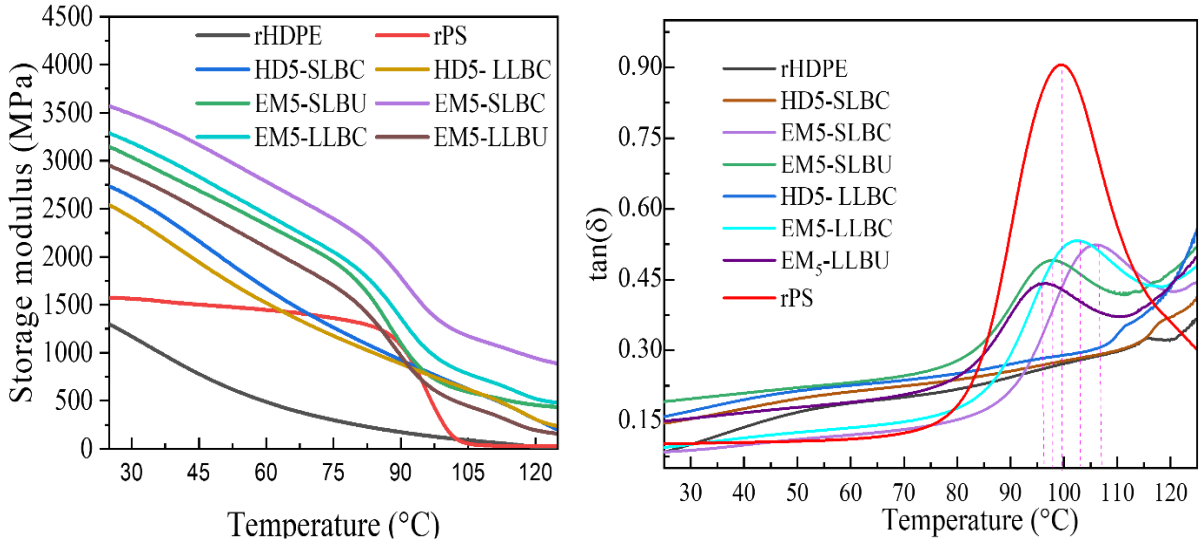

Figure 4. 7 E′(a) and tan δ (b) as a function of temperature

4.3.5 FTIR Analyses of the Recycled Plastics and Its WPCS Systems

As shown in **Figure 4.8**, rHDPE strong C-H stretching of methylene (-CH_2-) at 2920 and 2852 cm^{-1},– CH_2 bending doublets at 1424 and 1460 cm^{-1}, bending vibrations around 720 or 730 cm^{-1} and C-C stretching at 1103 cm^{-1} were observed [74]. In the FTIR spectra region of rPS, aromatic C–H stretching around 3060-3025 cm^{-1}, C–H stretching of both CH_3 and CH_2 around 2920–2860 cm^{-1}, C–C aromatic stretching around 1603 cm^{-1} were detected. Similarly, C–H bending in the region 900–675 cm^{-1} being intense at 697 cm^{-1} and 757 cm^{-1}, and CH_2 deformation of C=C aromatic ring at 1452 cm^{-1} and 1492 cm^{-1} [238] show the existence of the benzene ring. Specific peak region of 748-695 cm^{-1} is the characteristic monosubstituted benzene ring, indicating evidence of rPS, including in their respective WPCs [188]. The absence of the carbonyl peak at 1725 cm^{-1} indicates no oxidation of rPS during composite formulation and/or degradation. In the spectra of LLB, the region from 600 to 1600 cm^{-1} represents the fingerprint regions of cellulose, hemicelluloses, and lignin [239]. Similarly, the broad spectral region within 3500-3250 cm^{-1} particularly (3430 cm^{-1}) represents the hydroxyl (-OH) stretching vibration, the region from 1060 to 1030 cm^{-1} was assigned to C-O stretching mostly of cellulose and region from 1750–1700 cm^{-1} represents the carbonyl regions. Additionally the peak of 1730 cm^{-1} corresponds to carboxylic acid and ester groups [64]. In Figure 4.7, the changing intensity of vibration characteristics of the-OH band regions are observed. Similarly, a moderately strong spectrum region at 880 cm^{-1}, representing stretching vibrations of peroxides linkage, most likely indicates potential grafting

and crosslinked network of DCP molecules [188]. Likewise, the molecular structures of rHDPE and rPS within the WPCs appeared stable and significantly intensified with the stretching vibration peaks of $–CH_2$ at 2920 cm^{-1} and 2852 cm^{-1} [28]. This indicates the addition of DCP did not cause chain scission of the polymer matrix or weaken the composite. Furthermore, MAPP reduces the-OH functionalities of LLB particles, as evidenced by the weakening at 3430 cm^{-1} of OH stretching and at 1050 cm^{-1} implying interface compatibility [64]. In addition, many typical cellulose, hemicellulose, and lignin absorption peaks of the biomass occurred within 1152 cm^{-1}-1562 cm^{-1} [239]. Compared with LLB, some of these absorption peaks disappeared and others shifted to lower or weaker values in the coupled WPCs. Specifically, moderately well-defined C–O stretching of acetyl groups lignin at 1247 cm^{-1} and aromatic C-H deformation in methoxy groups of lignin at peak region 1457 cm^{-1} [239,240] in both LLB and uncoupled composites (EM_5-SLBU) disappeared in the coupled composites (EM_5-SLBC). Slightly intensified and overlapped band regions around 1593 cm^{-1} corresponds to the presence of a crosslinking mono-substituted benzene ring of rPS [241]. Additionally, overlapped weak methyl group (CH_3) symmetric bending vibration from the MAPP blockchain is observed around 1375 cm^{-1} [28,242]. These phenomena are likely to indicate synergetic interphase modification with MAPP and DCP inclusions even though many overlapping spectrum regions of the lignocellulosic fibers are inherently difficult to clearly understand.

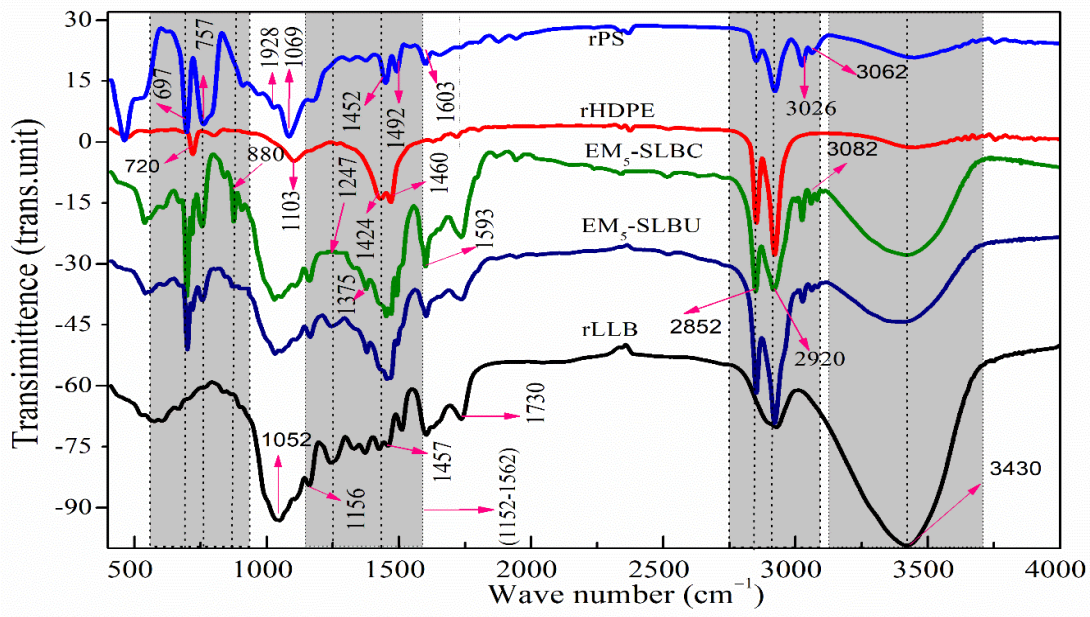

Figure 4. 8 FTIR spectra of LLB fibrous fillers, coupled and uncoupled WPCs and its matrix

4.3.6 Thermal Degradation of Recycled Plastic Matrix and Its WPCs

TGA and DTGA thermograms of rHDPE, rPS, LLB including their representatives WPCs are shown **Figure 4.9a** and **4.9b**, respectively. Thermal decomposition of rPS is initiated at around 250–300°C and ends before reaching 500 °C through three stages. The first onset started at 250°C and ended at 285°C with a 3% mass percent loss which could be attributed to residual impurities during production and recycling. The second degradation occurred from 300°C to 375°C with a 15.4% mass loss, mostly attributed to the degradation of brominated flame-retardant additives [243] as detected in the residual element analysis. The third degradation stage continues from 375°C to 470°C, with a maximum mass loss reaching 79.5%, leaving ash products of 3.1% of a weak charring ability. The major degradation pattern is similar with the previously reported trends [231,244] with some variations on the first stages and final degradation temperature probably because of the residual impurities. However, the onset or end degradation of this rPS did not affect its applicability because it occurred far above its T_g. rHDPE degraded on the first stage around 450°C and ended at 500°C with a maximum mass loss of 84.5%. With the rising temperature the degradation becomes stable until the second decomposition is revealed around 600 °C with 6.24% mass loss. This second phase could originate from the slow pyrolysis of inorganic mineral fillers such as $CaCO_3$ as high amounts of Ca were found in our previous determination of metal additives. Similarly, the degradation of LLB and WPCs with equal compositions of LLB particle reinforcement (S and L) and matrices but differing in the coupling and crosslinking agent inclusion were shown in **Figure 4.9**.

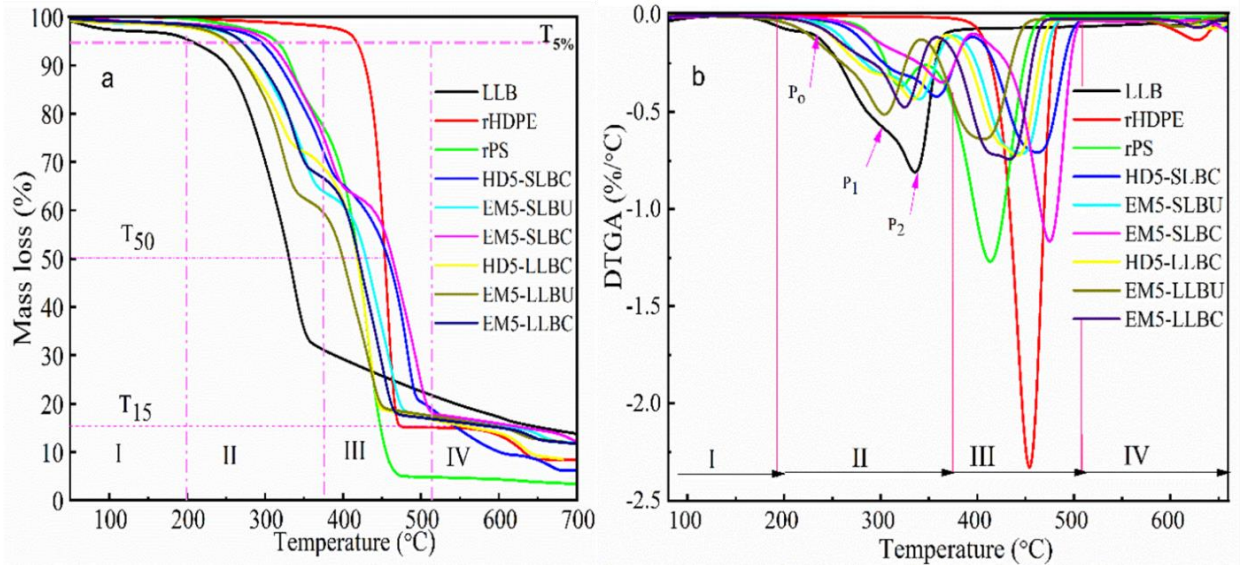

Figure 4. 9 TGA (a) and DTGA (b) curves of the recycled rHDPE, rPS, LLB and their WPCs.

The addition of LLB significantly altered the thermal stability of the WPCs, leading to a multistage degradation process compared with LLB degradation patterns. It is divided into four regions (I-IV), with the starting of the degradation temperature at 5 wt.% mass ($T_{5\%}$). Furthermore, onset degradation temperature (T_o), peak temperature (T_p), final maximum temperature (T_{max}) within each transition peak is tabulated in **Table 4.3**. Characteristic patterns of the WPCs degradation showed two clear peaks in the regions of II and III (Figure 9b). The first degradation of WPCs and LLB particles (I) mainly involved the thermal decomposition of moisture, volatile compounds, and weak bonds in the amorphous part of hemicellulose. In region II (200°C-380°C), hemicellulose and cellulose degrade and active pyrolysis of cellulose, lignin, and the polymer matrix occurs in the region III (380°C-515°C) [42]. $T_{5\%}$ for LLB occurs at 225.8°C higher than the previously reported values [55, 56]. Similarly, the first shoulder peak (P_0) appears in region II (206°C-236°C) with a weight loss of 9.65%. From 236°C to 365°C, extending to 372°C (including P_1 and P_2) a maximum weight loss of 68.5% occurred due to significant decomposition of cellulose and lignin, particularly at P_2 around 365°C with the emerging carbonization effect. Furthermore, in region III (365°C-600°C) and above, complete LLB decomposition of carbonized residue occurred with a 18.54% mass loss [244] leaving residual chars of 13.07%.

Table 4. 3 TGA analysis data of formulated WPCs and their polymer matrix.

Sample ID	The transition peaks	Degradation temperature of the peak			Residue at 700°C
		T_0	T_p	T_m	
LLB	2	$T_{5\%}$	-	236	13.73
	2	236	-	365	
	3	365	-	700	
rHDPE	3	$T_{5\%}$	454	480	8.77
	4	480	-	700	
rPS	2	$T_{5\%}$	320	350	4.77
	3	350	470	471	
	4	471	-	700	
HD_5-SLBC	2	$T_{5\%}$	367	395	8.68
	3	395	461	506	
	4	506	-	700	
EM_5-SLBC	2	$T_{5\%}$	366	400	13.66
	3	400	479	512	
	4	512	-	700	
EM_5-SLBU	2	$T_{5\%}$	344	375	11.97
	3	375	445	485	
	4	485		700	
HD_5-LLBC	2	$T_{5\%}$	334	368	6.87
	3	368	422	486	
	4	486	-	700	
EM_5-LLBU	2	$T_{5\%}$	304	343	9.23
	3	343	404	464	
	4	464	-	700	
EM_5- LLBC	2	$T_{5\%}$	324	358	12.46
	3	358	422	473	
	4	473	-	700	

Thermal analysis revealed two distinct diffused peaks of WPCs with transition zones II-III, positioning between the curves of LLB and rHDPE up to $T_{50\%}$. However, as the degradation progressed to stage III, the remaining $T_{50\%}$ -$T_{15\%}$ of all coupled WPCs (S) exceeded those of rPS, and both HD_5-SLBC and EM_5-SLBC surpassing the degradation of rHDPE in region III (below $T_{50\%}$). Similarly, $T_{5\%}$ of the WPCs significantly improved compared to that of the lignocellulosic fibers, after encapsulation within the polymer matrix. However, it remained lower than that of both rPS and rHDPE, owing to the degradation of cellulose, hemicellulose, and lignin in stage II (Figure 8b). Consequently, this resulted in a lower $T_{5\%}$ in stage II than in the matrix [227]. The

T_{max} (step III) of the WPCs exceeded that of the polymer matrices, with an overall increase in residue. This is due to the carbonization effect of lignocellulosic fibers, transforming rPS pyrolytic species into solid char, primarily from lignin. WPCs coupled with MAPP and DCP further increased residual char compared to unblended and untreated composites, due to the catalytic carbonization effect of MAPP and DCP [228]. Blending the matrices enhanced rPS maximum thermal degradation region (III) shifting the T_{max} of WPCs to higher temperatures, though the pattern rarely changes with large bamboo particle reinforcement. Additionally, the lager surface area from the S particle fractions and combined effects of the MAPP and DCP significantly affected stage III degradation. This improvement is due to the release of high carbon char from wide thermal degradation range lignin, which acts as a protective char barriers and high thermal conductivity of MAPP [229]. The T_{max} degradation of unfilled polymeric matrix and WPCs in the regions III before entering region IV are 471°C, 480°C, 506°C, 512°C, 485°C, 486°C, 464°C, and 473°C for rPS, rHDPE, HD_5-SLBC, EM_5-SLBC, EM_5-SLBU, HD_5-LLBC, EM_5-LLBU, and EM_5-LLBC, respectively. Notably, the combination of S factions of LLB particle reinforcement and a strong interface leads to better thermal stability, retaining more than 50% degradation of rHDPE and shifting T_{max} from 480°C to around 506°C in HD_5-SLBC and 512°C in EM_5-SLBC. Similarly, the rate of weight loss for the coupled S fractions improved significantly with a better final char residue.

4.3.7 Differential Analysis of Characteristics Recycled Plastic Matrix and Its WPCs.

DSC thermogram data for WPCs formulated from equal contents of the polymer matrix and bamboo particles are shown in **Figure 4.10**, with refined data presented in Table 4.4. rHDPE and WPCs exhibited clear endothermic and exothermic peaks. However, rPS polymer matrix lacks a typical melting and crystallizing point due to its amorphous nature except T_g around 98.5 °C as detected by DMTA. From **Figure 4.10b**, the peak melting temperature (T_m), crystallization temperature (T_c), crystallization enthalpy (ΔHc) and X_C of rHDPE are comparable to the reported values [246]. This implies both unreinforced rHDPE and rPS maintained its characteristics melting and crystallization with no significant alterations in their molecular structures. As seen from **Figure 4.10 (a)** and table 5, T_C of WPCs of L fractions shifted to slightly lower temperatures, with significant differences in the crystallization enthalpy. Larger LLB particles have a lower surface area, restricting polymer flow and slowing down the crystallization process. In untreated WPC systems, crystallization is reduced because untreated fibrous fillers increase the chain

mobility and free volume of the matrix chains through the weak packing of fibers within the matrix [10]. However, the coupled WPCs S fractions showed higher crystallinity than their respective untreated and coupled L fractions including rHDPE-based WPC samples. This suggests that interface modifications led to a new fiber-matrix interfacial crystal layer, and smaller particles assisted nucleation during cooling stages as they can easily dispersed in the WPC system providing more accessible nucleating sites. Similarly, both endothermic melting T_m (Figure 4.10b) and melting enthalpy (ΔH_m) (**Table 4.4**) of WPC of S and L fractions coupled with PPMA and DCP show increasing compared with uncoupled composites. Furthermore, the corresponding degree of crystallinity (Xc) for the WPC sets of HD_5-SLBC, EM_5-SLBC, EM_5-SLBU, HD_5-LLBC, EM_5-LLBU, EM_5-LLBC, and HDPE were 51.5%, 54.5%, 40.2%, 38.6%, 37.8%, 53.2%, and 46.9%, respectively. These significant changes in X_C and melting temperatures are most likely attributed to the existence of interaction forces at the chemical bonds. This enhanced the release of the overall melting enthalpy of the composites even for the approximately 25% of rHDPE in the WPC system compared to the unreinforced rHDPE. Similar findings have been reported for the crystallization and melting behavior of isotactic PP-red pine wood flour composites and compatibilized PP composites with hemp fibers [93,247] which showed inclusion of short fibers and/or particles in WPCs induces a heterogeneous nucleating effect on the crystallization WPCs. This effect reduces the free energy of nucleation and significantly enhances the overall crystallization rate and nucleation density on the fiber surface. Similarly carbonyl groups of MAPP act as active heterogeneous nucleation sites, promoting diffusion and orderly chain arrangement toward crystal nuclei [248]. These mechanisms probably contribute to a relatively higher crystallinity of WPCs containing polar MAPP, and crosslinking DCP, which leads to increased melting temperature and enthalpy of melting [249].

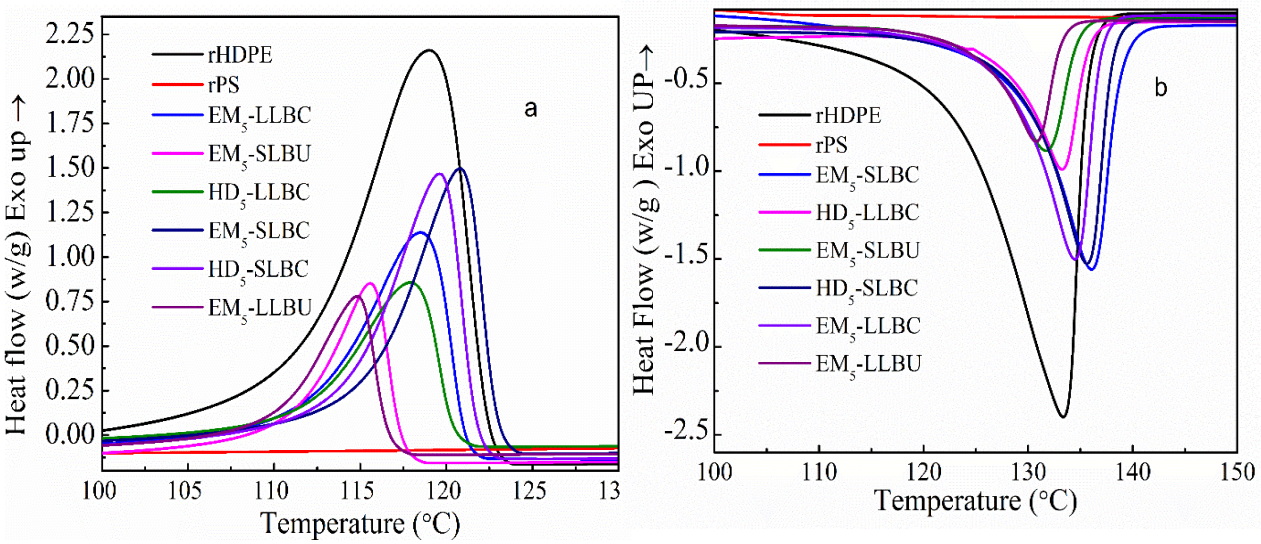

Figure 4. 10 DSC thermograms of a) exothermic process, b) endothermic process

Table 4. 4. DSC Analysis of data formulated WPCs and their polymer matrix

WPCs	T_c(°C)	T_m (°C)	ΔHc (J/g)	ΔHm (J/g)	Xc (%)
rHDPE	118.9	133.4	123.1	138.2	46.4
HD5-SLBC	119.6	134.5	56.2	76.8	51.5
EM5-SLBC	120.8	136.5	68.2	81.4	54.6
EM5-SLBU	115.1	131.8	52.2	59.9	40.2
HD5-LLBC	117.2	133.4	51.2	57.5	38.6
EM5-LLBU	114.8	130.9	45.8	56.3	37.8
EM5-LLBC	118.2	135.6	64.1	79.3	53.2

4.3.8 SEM-Microscopic Characterization

The SEM morphologies of the representatives fractured surfaces of the WPCs of equal compositions of the polymer blends (rPS and rHDPE) are shown in **Figure 4.11**. Morphologies of EM_5-SLBU (**Figure 4.11a**) have many small particles removed from the matrix during IS testing, leaving smaller holes and loosely embedded particles due to weak interactions and incompatibility with the hydrophobic polymer matrix. This results in reduced mechanical properties. Conversely, EM_5-SLBC (**Figure 4.11b and e**) shows good dispersion of bamboo particles without agglomerates i.e., all particles are well embedded, resulting in a uniform cracked surface morphology. Furthermore, there was no clear gap between the bamboo particles and polymer matrix, indicating better interfacial bonding and enhanced mechanical properties. The

absence of large voids, gaps, and smaller fiber pull-out areas further evidences a strong fiber-polymer interphase and coupling efficiency [250]. Similarly, the uncoupled composites made from large LLB particles (EM_5-LLBU) (**Figure 4.11c**) composite exhibited areas where large particle agglomerates were removed, leaving large holes and gaps on the fractured surface. The clear interface between the wood fibers and the matrix indicates poor interfacial adhesion owing to weak interactions, with a significant portion of the particle surface insufficiently bonded and unprotected by the matrix. This resulted in reduced mechanical performance. Conversely, composites with coupled large fractions (EM_5-LLBC) (**Figure 4.11d and f**) showed a more uniform coverage of large particles by the melted plastic matrix, with many well-oriented large surfaces and fractured surface particles left in the matrix. Although some voids and defects remain, the incorporation of a compatibilizer enhances the adhesion quality, reduces the fiber pull-out areas, and confirms better interfacial bonding between the particles and the polymer matrix. This likely resulted in improved mechanical properties compared to those of the untreated counterparts.

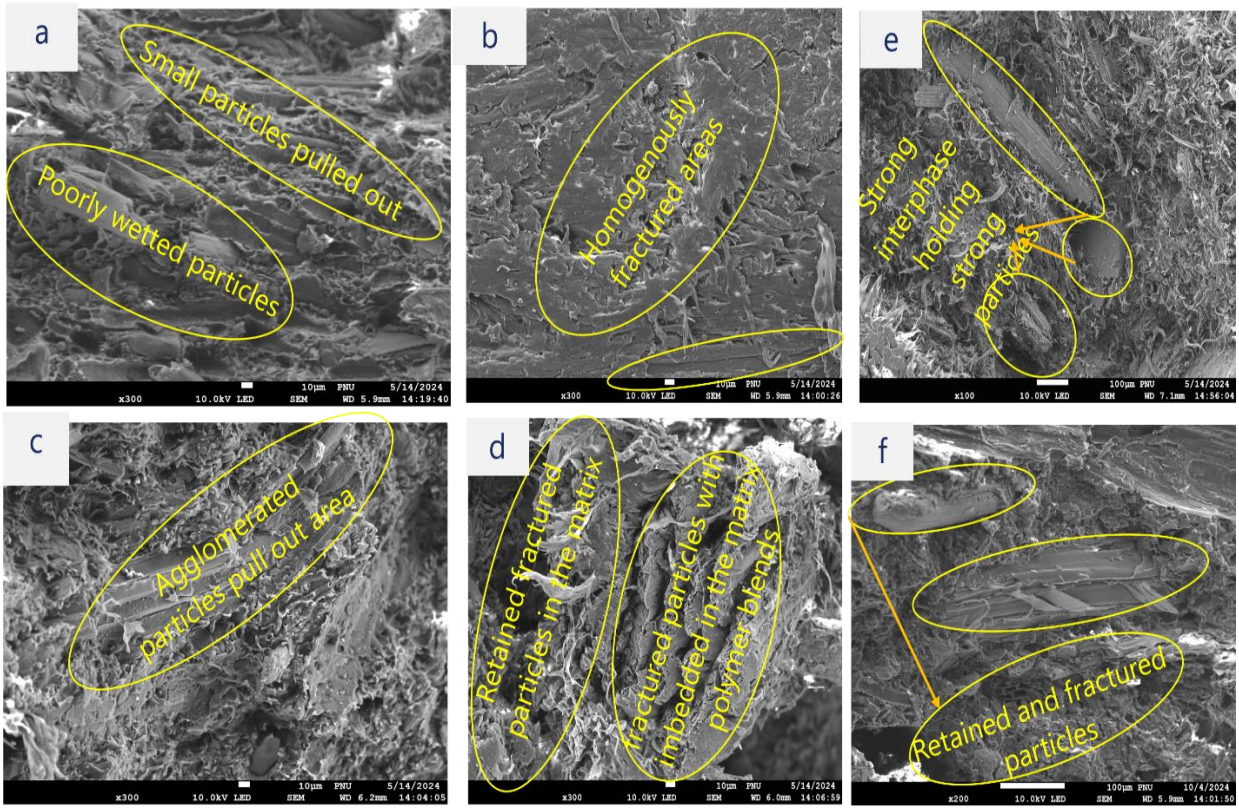

Figure 4. 11 SEM morphology of WPCs from equal mix polymer blends; EM5-SLBU (a), EM5-SLBC(b, e), EM5-LLBU(c), and EM5-LLBC(d, f)

4.4 Conclusions

WPCs was successfully formulated using Ethiopian indigenous lowland bamboo (Oxytenanthera abyssinica) particles, rHDPE, rPS, and their blends as secondary resources. This work focused on utilizing recycled thermoplastics and LLB fibrous particles as affordable and sustainable building materials and related applications. The recycled polymeric matrix contained residual Ti, Ba, Cl, Zn, Pd, Hg, Br, and Cr (VI), all below their maximum threshold limits for utilization. FTIR, DSC, and TGA analysis of the recycled plastics (both rPS and rHDPE) show their chemical structure, crystallinity, melting temperature, and thermal stability are similar with their respective neat counterparts. This implies there is no significant thermal degradation or oxidation during recycling that could affect their performance.

In-situ reactive compounding of WPC formulations using MAPP and DCP significantly enhances interfacial strength, surpassing unfilled polymer matrices. This method improves interphase integrity through thermal and chemical crosslinking, resulting in chemical bonds and mechanical interlocking of fibrous particles. Enhanced mechanical properties, including tensile and flexural strength, impact strength, melting characteristics, dynamic viscoelasticity, and fractional crystallinity, substantiate interfacial modifications. FTIR analysis and morphological studies confirm improved interfacial adhesion and polymer blend compatibility with LLB particles. FTIR showed reductions in hydroxyl bands and changes in carbonyl regions, while SEM revealed that coupled composites have better fiber embedding and fewer voids compared to uncoupled composites.

The ultimate tensile and flexural strengths decreased with increasing bamboo particle loading across in both LLB particle fractions (below 0.5 mm and 0.5-1 mm), regardless of coupling agents and crosslinking additives. Despite this, notable mechanical properties were maintained due to the broader particle size distributions reinforcing multiple scales. Conversely, tensile and flexural moduli increased. Coupled composites such as EM_4-SLBC, EM_5-SLBC, EM_6-SLBC, and EM_6-LLBC showed better properties than those with their respective uncoupled composites and unblended composites, due to improved interfacial bonding and meet practical WPC requirements. Similarly, the impact strength (IS) of WPCs significantly improved compared to unreinforced unfilled rPS and synergistically with DCP and MAPP additions in the Equal mixed WPCs.

Dynamic mechanical analysis shows that coupled equal melt blending of rPS/rHDPE with particle sizes below 0.5 mm improved the dynamic storage modulus, and damping properties compared to larger fractions (0.5-1 mm). The tanδ peak shifted to higher temperatures, and significant storage modulus was retained below the glass transition. Thermal stability, as indicated by TGA, and fractional crystallinity were also maintained, with an increased DSC melting point likely due to better dispersion of smaller LLB particles and a strong interphase acting as nucleating sites.

These WPCs can substitute conventional wood flour or fiber-based composites, avoiding energy-intensive fiber extraction and lowering carbon footprints. Retained lignin improves thermal stability via high-temperature carbonation, while the formulations provide practical alternatives to traditional PE-, PP-, and PVC-based WPCs with 40–60% fiber or polymer content.

CHAPTER FIVE

Optimization of effects of cross-linked coupling agent and initiator catalyst on the properties of wood polymer composites (WPC) formulated from recycled thermoplastic polyblends and bamboo particles

Abstract

In this work, eco-friendly WPCs were produced using a 50/50% weight-based blend of recycled rHDPE and recycled rPS as the polymer matrix, compounded with indigenous Ethiopian lowland bamboo (LLB) particles. Reactive melt compatibilization was evaluated using MAPP and SEBS-g-MA, each synergistically cross-linked with 1% DCP. The coupling agents were varied at 3%, 5%, 7%, and 10% to optimize fundamental WPC properties. Compatibility was characterized using Fourier transform-infrared spectroscopy (FTIR), thermogravimetric analysis (TGA), and scanning electron microscopy (SEM). Results showed that SEBS-g-MA significantly improved impact strength of the formulated WPCs due to its flexible ethylene-butylene molecular blocks and its compatibility with both polymer matrix and LLB particles. In contrast, MAPP and DCP synergistically enhanced tensile, flexural, and storage modules, with 5% MAPP and 1% DCP achieving optimal performance, followed by a decline at higher concentrations. Similarly, 3% SEBS-g-MA and 1% DCP provided better tensile, flexural, and storage modules of WPCs, while dimensional stability, water absorption, and thermal stability improved with further increases in SEBS-g-MA content. These findings demonstrate the potential for valorizing thermoplastic waste into sustainable building materials, highlighting reactive melt-compatibilization as a viable approach for producing high-performance WPCs.

***Key words**:* In-situ melt compatibilization, Interface compatibility, Wood plastic composite, recycled thermoplastic, lignocellulosic reinforcements, sustainable materials, ecofriendly composites

5.1 Introduction

Currently, thermoplastic waste is being utilized in wood polymer composite (WPC) as valuable secondary resources, combined with the untapped potential of lignocellulosic fibers. This contributes to cascading utilization, increasing the potential for multiple recyclability and the production of low-cost composites [3]. WPC is an innovative group of materials comprising sustainable lignocellulosic fibers and/or particles as reinforcements and thermoplastic matrices, primarily polyolefins[4,12] Recently, polyamides or acrylonitrile-styrene-butadiene terpolymer (ABS) reinforced with bio-based reinforcements, have become competitive with conventional synthetic fiber-based composites for structural, non-load-bearing building materials [8,28]. Advanced synthetic fibers, such as carbon, aramids, and glass-based composites, are currently designed to prioritize high strength, high stiffness, and long-term durability. However, their unsustainability and non-recyclability, including the use of polymeric resins such as epoxies, esters, and polyurethane, along with solvent-based toxic chemicals like formaldehyde, phenolics, and isocyanates, are major drawbacks [251]. As result, alternatives renewable materials origins like WPCs are inevitably needed in search for new paradigm of environmentally friendly composites products.

WPCs are widely used in buildings and construction in applications such as decking, fencing, furniture, interior parts including automotive panels, truck floors and, etc. [4]. This is due to their environmentally friendly nature, recyclability, lightweight characteristics, reasonable strength and stiffness, and ease of production [3,252]. However, natural reinforcements are hydrophilic and poorly compatible with nonpolar, hydrophobic plastics due to their complex molecules, like cellulose, hemicellulose, and extractives, containing hydroxyl and other polar groups [8]. This incompatibility results in weak interfacial bonding and poor stress transfer from the matrix to the fibrous particles, leading to poor mechanical properties. Consequently, improving interphase compatibility of WPCs through modifications of fiber and/or polymer surface chemistry, enhancing wettability, eliminating weak boundary layers, and forming tougher and stiffer boundary layers via chemical bonding are key areas of current research. These advancements involve two distinct approaches: modifying the surface of natural reinforcements at an initial stage and/or altering the polymer matrix by incorporating compatibilizers and crosslinking agents [4]. Some of these methods are acetylation, alkali treatments, organosilane treatments, energetic monomer grafting under UV radiation or plasma discharge, and chemical coupling

compatibilizers [8]. The use of compatibilizing agents and graft copolymerization were effective in enhancing WPC's interphase compatibility among these methods.

Coupling agents are bifunctional group molecules that establish molecular interactions with polymer matrix chains and fibrous particles through in situ reactive compatibilization [27] and/or reactive polyfunctional monomers (graft copolymerization), commonly maleic anhydride (MA) and its isostructural analogues [253]. They create strong interfacial interactions via chemical esterification between the maleic anhydride and the hydroxyl groups of natural fibers, along with physical interactions such as interdiffusion, adsorption wettability, and molecular entanglement [4]. Various types of coupling agents, including silanes, titanates, zirconium aluminates, and maleic anhydride graft copolymers, have been employed in existing research [4,28]. Among these, maleated polyethylene (MAPE) and maleated polypropylene (MAPP) were found effective in forming covalent linkages and hydrogen bonds [29] in polyolefin-based WPCs, resulting in a uniform microstructure, improved dimensional stability, and enhanced mechanical properties [17]. Similarly, urethane linkages are formed between the isocyanate functionality and the hydroxyl groups of natural fibers. Additionally, silanes hydrolyze into active silanol groups capable of reacting with hydroxyl groups [30].

Different graft copolymers have also been successfully utilized in WPCs. Cecilia Zárate-Pérez et al.[28] evaluated the mechanical and thermal properties of PP-wood flour composites using poly(styrene-co-methyl methacrylate-co-glycidyl methacrylate) graft copolymers via a melt-blending process, achieving improved intermolecular performance, which enhanced strength, thermal properties, and deformation rates. Furthermore, ethylene-glycidyl maleic anhydride copolymer (EGMA), polyolefin elastomers grafted with maleic anhydride (POE-g-MA), and methyl methacrylate-butadiene-styrene copolymer (MBS) have been effectively applied for multipurpose WPC formulations [4].

The use of recycled rHDPE from different waste fractions instead of the corresponding neat HDPE in the WPCs demonstrates similar and practically comparable composite mechanical properties, dimensional stability, interfacial bonding, and durability, which are statistically comparable to corresponding neat HDPE-based WPCs [8,65–68] Similarly, recovered PS, especially high-impact polystyrene (HIPS) (rPS), ABS, and pulverized waste printed circuit boards (PCB), including difunctional and multifunctional epoxy resins and bismaleimide triazine

epoxy blends [74,75], from E-waste used in the WPCs showed promising results. Likewise, Kiaeifar et al. [224] and Poletto et al. [225] observed improved IS when formulating WPCs from expanded PS with wood flour (10–40%) and styrene-maleic anhydride copolymer (SMA) as a coupling agent.

The current research area is also in strong momentum to expand the use of recycled plastics as a secondary resource for circular use in WPCs, with multifunctional polymeric coupling agents imparting additional improvements while simultaneously capable of melt compounding, thermal processability and enhancing toughness of WPCs which sacrificed due to rigid and stiffer natural particle reinforcement[4]. Poly(styrene-b-butadiene-b-styrene), poly(styrene-b-ethylene-butylene-b-styrene), methacrylate-butadiene-styrene terpolymer, poly(styrene-b-isoprene-b-styrene), poly(styrene-co-methyl methacrylate-co-glycidyl methacrylate) [26], and polystyrene-block-poly(ethylene-random-butylene)-block-polystyrene-graft-maleic anhydride (SEBS-g-MA) represent the largest category [3]. In SEBS-g-MA, SEBS is known for its good UV and heat resistance, better toughness, and improved molecular entanglements with the polyolefin polymeric matrix [59]. Moreover, the acid groups of MA impart compatibility with natural fibers, and the styrene-rich hard phase enhances the mechanical strength when compounded with similar chemical moieties [60].

Most of the research on WPCs using rHDPE and rPS has focused on single types of waste streams with constant compositions of coupling agents, lacking investigations into optimum compositions and combined blends of rHDPE from post-consumer waste and rPS from electronic waste. Specifically, the effects of optimum amounts of multipurpose coupling agents on fundamental mechanical properties, thermal degradation and stability, dynamic thermal properties, dimensional stability, and water absorption have not been extensively investigated. As a result, the focus of this work is to comparatively investigate the effects of two widely used commercial compatibilizers, MAPP and SEBS-g-MA, on WPCs formulated from a blend matrix of rHDPE and rPS, with synergistic compatibilization of immiscible polymers facilitated by the crosslinking organic radical initiator, DCP. This investigation centers on key fundamental properties of WPCs by varying the coupling agent content to identify their optimum amounts. Natural fibrous particles derived from the untapped potential of Ethiopian indigenous lowland bamboo, which covers nearly one million hectares in Ethiopia but whose advanced use in WPCs has not been fully

explored, were used as the dispersed phase. Bamboo particles were applied without pre-existing chemical treatments, which require multiple steps, additional costs, and complexity. The formulations included evaluating potential compatibilizers during reactive blending via grafting mechanisms and functionalization in a HAAKE Rheomix OS batch kneader, followed by compression molding, preferably considering their low cost through reactive melt compounding. Finally, the best formulation combinations and their targeted applications were identified.

5.2 Material and Method

5.2.1 Materials

Recycled HDPE from post-consumer packaging materials and rPS from e-waste (computer keyboards, monitors, and printer toner materials) were sorted, cut into small pieces, cleaned, vacuum dried, and pelletized into granulates using a counter-rotating extruder. The melt flow rates (MFR, ISO 1133) of rHDPE and rPS were measured at 0.2g/10 min (230°C/2.16 kg) and 0.9g/10 min (230°C/2.16 kg), respectively, with corresponding densities of 0.96 g/cm³ and 1.043 g/cm³, determined according to ASTM D792-20. Commercial MAPP (Sigma Aldrich, USA), containing 8-10% maleic anhydride, had an MFR of 21g/10 min (230°C/5.0 kg), a density of 0.9341 g/cm³, and a molecular weight of approximately 9100 (GPC). SEBS-g-MA (Sigma Aldrich, USA) with a melt index of 21 g/10 min (230°C/5.0 kg) was used as the coupling agent. The SEBS-g-MA was grafted with 1.84 wt.% MA, containing 70 wt.% ethylene-butylene block and 30 wt.% styrene blocks. DCP (Sigma Aldrich, USA), a crosslinking agent with a density of 1.56 g/cm³, was used in its analytical grade form.

Mature LLB culms were collected from the Arjo Gudatu district (9° 4' 52" N, 36° 37' 30" E) in the Oromia region of Ethiopia. The bamboo was cut into small strips, air-dried, ground using a hammer mill (Retsch SR 200 Grauβ, Haan, Germany), and sieved using a vibrating shaker to obtain particle reinforcements between 200-600µm. Finally, it was dried in a vacuum oven at 105°C for 24 hours until the moisture content dropped below 2%, and then immediately used for WPC formulation.

5.2.2 Processing of Composites

The experimental design comprised 11 independent run formulations, including 8 batches of WPC samples with equal blend ratios containing coupling agents, 2 batches of unreinforced

rHDPE and rPS matrices, and 1 batch of WPC without any coupling additives, as shown in **Table 5.1**. The first four experiments were conducted to evaluate the synergistic effects of both MAPP and DCP, while the second four focused on formulations containing SEBS-g-MA and DCP. The compositions of the coupling agent were varied at 3%, 5%, 7%, and 10%, with a constant DCP composition of 1%, based on the oven-dry total mass of the WPCs. DCP was kept constant, referring to the optimum level recommended in previous studies [4]. The LLB particles and matrix polymers were compounded at a 50/50% weight-based ratio, as suggested in prior research works. Reinforcement smaller particles (50% or less) compositions resulted in better mechanical properties, whereas higher particle content led to reduced physical and mechanical properties in WPCs [161].

According to **Table 5.1**, in situ melt compounding was first carried out by uniformly mixing dry-mixed rHDPE, rPS, DCP, and coupling agents in the pre-heated mixing chamber of a HAAKE Rheomix OS batch kneader (Thermo Fisher Scientific) with counter-rotating screw configurations. LLB particles were added in three equal portions over a 5-minute interval, with compounding continuing for an additional 10 minutes until a constant torque and viscosity were achieved, totaling 15 minutes. The compounding was conducted at 190°C, with a rotational speed of 50 rpm. Finally, the compounded WPC granules were removed from the kneader, dried, and stored in plastic bags at a relative humidity of 65 ± 2% and a temperature of 23 ± 2°C.

Table 5. 1. Experimental design and formulation compositions of WPCs

SID	Matrix Polymer (%)	LLB (%)	MAPP (%)	SEBS-g-MA (%)	DCP (%)
rHD	100	-	-	-	-
rPS	100	-	-	-	-
Co	50	50	-	-	-
CP_3	48	48	3	-	1
CP_5	47	47	5	-	1
CP_7	46	46	7	-	1
CP_{10}	44.5	44.5	10	-	1
CS_3	48	48	-	3	1

CS_5	47	47	-	5	1
CS_7	46	46	-	7	1
CS_{10}	44.5	44.5	-	10	1

5.2.3 Hot Press Compression Molding Process

The dried WPC granules were further ground and size-reduced using an 8 mm sieve, then placed in a carbon steel die frame (180 mm × 200 mm × 4 mm), which was covered with Teflon sheets. The frame was then inserted into a computerized, preheated lab-scale hydraulic hot press (Carver Press, Inc., Wabash, IN, USA). WPCs were formed using isothermal hot compression molding at 200°C. An optimized process involving cyclic pressing pressures was applied through several stages. This included low-pressure melting with a slight plate opening for 1 minute at 20 bars, pressing at 50 bars for 8 minutes, followed by pressing at 70 bars for 2 minutes, increasing to 100 bars for 2 minutes, and holding at 100 bars during slow cooling for 1.5 minutes until the temperature dropped below 40°C. Finally, the press was opened, and the WPC board prototypes were removed from the frame and allowed to cool to room temperature.

5.2.4 Characterization of molecular structure and thermal properties analysis.

The molecular structure was analyzed using an FTIR spectroscopy (Nicolet 6700, Thermo Scientific, USA) by preparing sample films. 2 mg of the samples were ground with 200 mg of KBr and pressed to the form of KBr matrix-bound pellets using a steel pellet die under hydraulic pressure for 1 min at 60 N/m^2. The scan was performed at a rate of 64 repetitions and an optical resolution of 4 cm^{-1} in transmittance mode within the range of 4000-400 cm^{-1}. For thermogravimetric analysis (TGA), 10 mg samples of both recycled plastic matrices and WPCs were analyzed using a Q50 TGA instrument (New Castle, DE, USA) in a nitrogen atmosphere (flow rate: 60 mL/min) from 30 to 700 °C at a heating rate of 10 °C/min. First-derivative thermogravimetric analysis (DTGA) was employed to evaluate the temperature-dependent transition peaks.

5.2.5 Static and Dynamic Mechanical Properties

Flexural strength (FS) and modulus (FM), as well as Charpy unnotched impact strength (IS), were determined according to ISO 178 and ISO 179, respectively, using samples with dimensions of

80 mm × 10 mm × 4 mm cut and machined from the hot-pressed composite panels. Tensile strength (TS) and tensile modulus (TM) were measured according to ISO 527-2 using dumbbell-shaped samples with dimensions of 170 mm × 10 mm × 4 mm at 20°C and 65% relative humidity. Values were calculated from five independent replicates of each composite formulation, with their dimensions measured during successive tests. A universal testing machine (Model 3369, Instron, USA) equipped with a 50 kN load cell and a crosshead speed of 5 mm/min was used for both FS and TS measurements. For the flexural tests, a three-point bending test was performed with a support span length of 60 mm. The impact test was conducted on unnotched specimens with an impact speed of 3.46 m/s and an impact angle of 150° using a pendulum impact tester (Zwick/Roell, model HIT5.5P; Germany). Dynamic mechanical thermal analysis (DMTA) was performed using a dynamic mechanical analyzer (DMA Q 800, TSA, USA) according to ASTM D 7028-07 in the stress generated in dual cantilever mode. Samples with dimensions of 55 mm × 12 mm × 4 mm (length × width × thickness), equilibrated at room temperature, were cut from compression-molded WPC prototypes. A dynamic temperature ramp from 25°C to 130°C, with a constant heating rate of 3°C/min, a frequency of 1 Hz, and a constant amplitude of 20 μm, was applied to characterize the samples' storage modulus (E′) and damping characteristics (tan δ).

5.2.6 Water Absorption and Dimensional Stability

The percentages of water absorption (%WA) and thickness swelling (Ts) of the composite samples were determined according to ASTM D570-98. WPC specimens measuring 25 mm × 25 mm × 4 mm (length × width × thickness) were vacuum oven-dried at 80°C for 24 hours until a constant weight (Wi) was achieved. The specimens were then immersed in an ultra-pure beaker filled with distilled water at 23 ± 1°C and monitored for 30 days. Weights were measured at time t in days (Wt.) continuously for the first five days, with subsequent measurements taken at 7, 10, 15, 25, and 30 days. Excess water was removed from the surface before each measurement. The percentages of WA and TS for each formulation were calculated based on equations 5.1 and 5.2, respectively, from at least two replicates.

$$\%\mathrm{WA} = \left(\frac{\mathrm{W_t} - \mathrm{W_i}}{\mathrm{W_i}}\right) \mathrm{x}100 \qquad (5.1) \qquad Ts = \left(\frac{T_t - T_i}{T_i}\right) x100 \qquad (5.1)$$

Where Wt. and Wi represent the specimen weights at a specific time after water absorption and the initial weight of the sample, respectively. Ts (%) is the thickness swelling at time t, where Tt

(mm) and Ti (mm) are the thicknesses of the specimens after immersion for a given time and the constant original oven-dried thickness, respectively.

Another important parameter that evaluates the extent to which water molecules have penetrated the bulk material is the diffusion coefficient (D), which is determined using Fick's second law (Equation 3) for one-dimensional diffusion, considering time and constant diffusion as expressed in Equation 4.[195][254].

$$\frac{\partial C}{\partial T} = -D\frac{\partial C^2}{\partial X^2} \qquad (3) \qquad D = \pi\left(\frac{h}{4Mm}\right)^2\left(\frac{M_2-M_1}{\sqrt{t_2}-\sqrt{t_1}}\right)^2 \qquad (5.2)$$

where C is the concentration of the diffusion, X is the space coordinate measured normal to the section and D is diffusion coefficient, M_m is the maximum water uptake of the samples, h is the sample thickness, M_1 and M_2 are the water absorptions at corresponding times t_1 and t_2, respectively.

5.2.7 SEM morphology

The SEM morphologies of the fractured surfaces from the impact strength tests of WPC samples were captured using a QUANTA200 scanning electron microscope (Thermo Fisher Scientific, Hillsboro, OR, USA). The surfaces were sputter-coated with a 2 nm layer of platinum to improve conductivity. Observations were made at an accelerated electron beam voltage of 10.0 kV.

5.3 Results and discussion

5.3.1 Mechanical properties of the WPCs

A summary of the mechanical properties of the formulated WPCs is presented in **Table 5.2** and **Figure 5** for quick reference, followed by the discussion

Table 5. 2. Summary of Mechanical properties of WPCs

WPCs	Tensile Stress (MPa)	Tensile Modulus (GPa)	Flexural Strength (MPa)	Flexural Modulus (GPa)	Impact strength (kJ/m^2)
rHD	22.15 (1.58)	0.89 (0.6)	18.56 (1.96)	0.69 (0.11)	26.56 (1.78)
rPS	25.68 (1.68)	1.21 (0.35)	33.37 (1.23)	1.73 (0.18)	8.25 (1.35)
Co	23.58 (1.76)	2.68 (0.23)	32.23 (1.54)	3.05 (0.7)	6.19 (1.58)
CP_3	30.56 (1.69)	3.28 (0.24)	38.21(1.74)	3.55 (0.63)	10.81 (1.74)
CP_5	31.87 (1.26)	3.38 (0.32)	43.34 (1.52)	3.68 (0.92)	11.42 (1.21)
CP_7	29.28 (1.73)	3.03 (0.28)	38.63 (1.38)	3.23 (0.17)	12.46 (1.32)
CP_{10}	27.29 (1.78)	2.93 (0.13)	34.85 (1.63)	3.17 (0.17)	13.53 (1.38)
CS_3	29.25 (1.82)	2.88 (0.16)	37.56 (1.56)	3.15 (0.26)	13.87 (1.16)
CS_5	27.04 (1.98)	2.86 (0.21)	34.83 (1.51)	2.98 (0.28)	14.73 (1.23)
CS_7	23.82 (1.77)	2.76 (0.26)	30.78 (1.32)	2.86 (0.25)	15.59 (1.22)
CS_{10}	22.38 (1.86)	2.24 (0.16)	28.52 (1.5)	2.74 (0.19)	17.76 (1.68)

* The number in brackets indicates the standard error ranges of measurements, showing the maxima and minima values of measurements.

5.3.3.1 Tensile strength and Modulus of elasticity

Figure 5.1 shows the TS and TM of WPC_S. Compared to the unreinforced polymer matrix, increasing the compatibilizer content of MAPP resulted in higher TS and TM over all compositions. This trend can be attributed to the rigid and stiffer nature of the natural fibrous particles, which restricted the movement of polymer matrix chains, reducing elastic deformation and enhancing the stiffness and rigidity of the composites. Additionally, improved interfacial bonding further contributed to these enhancements. For MAPP-based WPCs, the TM increased by a factor of 3.3–3.8 compared with unreinforced rHDPE and 2.4–2.8 compared with unreinforced rPS, with CP10 and CP5 representing the lowest and highest values, respectively.

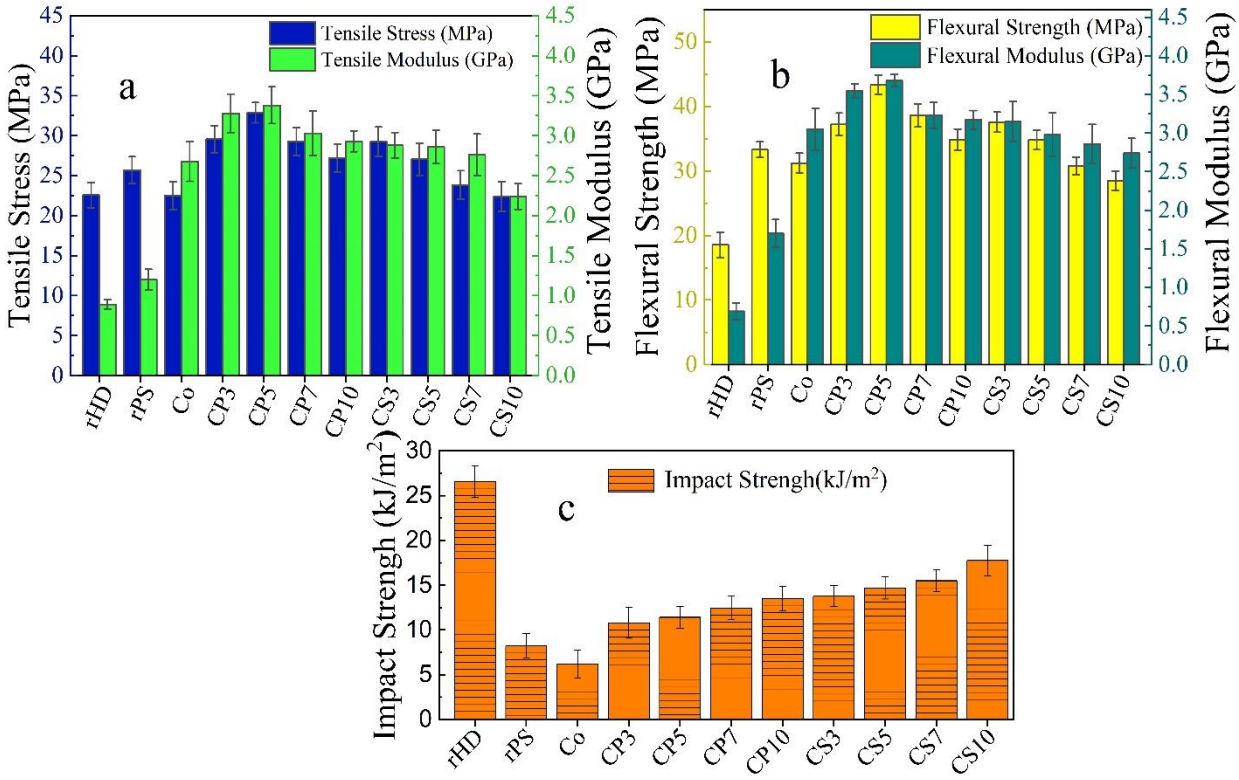

Figure 5. 1 Mechanical properties of the WPCs: (a) TS and TM, (b) FS and FM, and (c) IS

These extreme TM values in coupled composites showed only slight differences from those of uncompatibilized WPCs (C_0). In contrast, SEBS-g-MA reinforced composites exhibited TM increases of 2.5–3.2 relative to rHDPE and 1.8–2.4 relative to rPS, with CS10 and CS3 marking the lowest and highest values. Unlike the MAPP system, however, TM declined when SEBS-g-MA content exceeded 5%, with CS_3 showing only a 7.46% improvement over CO. This reduction is attributed to the higher proportion of rubber-like ethylene–butylene blocks, which offset the benefits of SEBS-g-MA in enhancing wettability, interfacial interaction, and toughness [144]. This variation indicates that the modulus of elasticity depends more strongly on particle reinforcement, whereas TS is primarily influenced by the type and content of coupling agents, which enhance interphase compatibility and amplify the reinforcing effect of LLB particles. Composites with 5% MAPP and DCP achieved the highest TS, surpassing rPS, rHD, and CO by 24.1%, 43.7%, and 35.1%, respectively. In comparison, 3% SEBS-g-MA increased TS by 14%, 29.5%, and 24.4% over the same references. These improvements are attributed to DCP-induced molecular entanglement within the rHDPE/rPS matrix and strong coupling interactions—particularly ester and hydrogen bonding between MA groups and the hydroxyl groups of LLB

particles. By contrast, non-coupled composites lacked effective interfacial bonding, resulting in weak stress transfer, lower mechanical strength, and earlier failure. Compared to Panaitescu et al. [255], who studied PP modified with 15% SEBS and 5% MAPP containing 30 wt.% short hemp fibers, our results show similar trends despite using lower amounts of MAPP and SEBS-g-MA. This is likely due to effective interactions from the grafted MA in the SEBS blend and the stiffness of rPS, further enhanced by DCP crosslinking through peroxide free radicals generated at high temperatures, which strengthened interphase bonding between adjacent polymer chains.

5.3.3.2 Flexural strength and Modulus of Rupture

Figure 5.1b illustrates the variation of FS and FM in the formulated WPCs. For MAPP-reinforced composites, FM increased by a factor of 4.59–5.33 compared with unreinforced rHDPE and 1.8–2.1 compared with unreinforced rPS, with CP_{10} and CP_5 representing the lowest and highest values, respectively, paralleling the trends observed in TM. However, these extreme FM values showed only slight increases (3.9–20.7%) over the uncoupled composite (C_0), indicating minimal effect of MAPP on FM beyond 5%. In SEBS-g-MA incorporated composites an increasing FM trends were also shown, ranging from 3.97 to 4.56 compared with rHDPE and 1.6–1.8 times relative to rPS, with CS_{10} and CS_3 marking the extremes. Unlike MAPP composites, only CS_3 showed a modest 3.27% improvement over uncoupled C_0. Further addition of SEBS-g-MA caused FM to decline, likely due to the higher elastomeric content weakening stress transfer and causing premature yielding. Overall, MAPP-based composites significantly outperformed SEBS-g-MA composites in flexural strength and modulus of rupture.

WPCs containing 5% MAPP crosslinked with DCP exhibited the highest FS of 43.34 ± 1.52 MPa, surpassing unreinforced rPS, uncoupled C0, and unreinforced rHDPE by 30%, 34%, and 133%, respectively. In comparison, 3% SEBS-g-MA achieved a maximum FS of 37.56 ± 1.56 MPa, corresponding to increases of 102%, 12%, and 16% relative to unreinforced rHDPE, rPS, and the uncoupled control (C0), respectively. Increasing SEBS-g-MA above 3% reduced composite stiffness, likely due to the low-modulus elastomeric nature of SEBS, making the composites more prone to rupture. These trends are consistent with previous studies on recycled polymer blend WPCs, where SEBS-g-MA below 5% improved blend compatibility and miscibility but reduced modulus. For example, in PP-based WPCs with 40 wt.% pine flour, 10 wt.% SEBS-g-MA, and 4 wt.% PP-g-MA, notched IS increased by 107%, while the modulus decreased by 35% [144].

5.3.3.3 Impact strength

Figure 5.1c presents the Charpy unnotched impact test results for the WPCs. The trends indicate that impact IS improved as the loading of both coupling agents increased. SEBS-g-MA consistently demonstrated better IS performance over all loading levels compared to MAPP. However, all values were lower than that of unreinforced rHDPE (26.56 KJ/m²), which exhibits high ductility and greater molecular flexibility. This reduction is attributed to the rigid natural fibrous fillers, which inherently increase composite stiffness, reduce polymer chain mobility, and consequently decrease energy absorption. The result is a common characteristic in WPCs [93,223]. However, IS significantly improved compared to the stiffer unreinforced rPS and the uncompatibilized WPC sample C_0 . It ranged from 10.81 KJ/m² (CP_3) to 13.5 KJ/m² (CP_{10}) in MAPP-based WPCs and from 13.8 KJ/m² (CS_3) to 17.76 KJ/m² (CS_{10}) in SEBS-g-MA-based WPCs, representing the observed extreme IS values. These results showed significant IS improvements of 31%–63 % for MAPP based composites and 67%–115% for SEBS-g-MA based composites compared to unreinforced rPS. Similarly, it increased by 74%–118% for MAPP based WPCs and 122%–186% for SEBS-g-MA WPCs compared to C_O.

Uncompatibilized WPCs exhibited poor interfacial bonding and reinforcement agglomeration, leading to microcrack initiation and propagation with lower energy absorption [41]. In contrast, coupled composites demonstrated improved interfacial compatibility and a more homogeneous distribution of fibrous fillers, which likely contributed to the increased IS. According to ISO 179-1, an unnotched IS above 8 kJ/m² is required for structural applications like decking [28], [160]. Improving composite toughness can be achieved by increasing the coupling agent content, particularly SEBS-g-MA. However, due to the high cost of coupling agents and the reduction in modulus at higher SEBS-g-MA concentrations, range of 3–5% appears to provide a balanced combination of TS, stiffness, and strength needed for most WPC building applications. Similar studies have shown that SEBS-g-MAH significantly enhances the impact strength of both neat and recycled wood floor-based WPCs [12].

5.3.4 Dynamic Mechanical properties of WPCs

The results of storage modulus (E′) and damping factor (tan δ) are shown in Figure **5.2**. The storage modulus (E′) represents the viscoelastic stored energy of the materials, which is related to the stiffness of the composites. All the composites show increasing trends in E′, compared to the unreinforced polymer matrix over the entire range of tested temperatures. As shown in Figure **5.2a**, E′ of WPCs coupled with MAPP exhibit better E′, with CP_5, showing the highest E′ in both viscous and rubbery regions due to its stiffness and improved interphase. However, as MAPP loading increases, E′ decreases, aligning with the modulus of elasticity measured during tensile strength evaluation, although they are not identical. The incorporation of SEBS-g-MA caused a reduction in E′ over the temperature range, despite the stiffer interphase and better compatibility. This is due to the elastomeric phase of SEBS, which has a low transition temperature for ethylene and butadiene segments, enhancing toughness but slightly reducing stiffness. As a result, composites with 10% SEBS-g-MA are the least stiff compared to all WPC samples. Despite this, a substantial E′ is maintained as the temperature increases, until a rubbery plateau is reached around 98.5°C, corresponding to the glass transition relaxation of macromolecular chains. It is also worth noting that CP_5 showed lower tan δ values than the unreinforced matrix in the glassy regions over the tested temperature range, indicating its better ability to maintain its stored energy and dissipate less energy. It was notable to observe the sharpest drop in E′ and corresponding damping factor (**Figure 5.2b**) around the glass transition temperature (Tg) for all samples between 90 and 110°C, indicating that the composites maintained greater flexibility and higher damping peak intensities. In the case of rPS, more chains are available for mobility, and the collective movement of chains generates internal friction leading to energy dissipation and a higher magnitude of the tan delta (tan δ) at Tg. Composites interfaced with coupling agents exhibited lower energy dissipation and a shift in T_g to higher temperatures, particularly in CP_3 and CP_5. This shift indicates restricted chain mobility and reduced free volume at T_g due to stronger interfacial adhesion, resulting in overlapping immobile chains, enhancing reinforcement [30]. Additionally, the increasing damping peak near T_g with higher coupling agent content, while maintaining tanδ values lower than rPS, signifies effective interfacial bonding, improved reinforcement and toughness as reflected in IS tests. In contrast, uncoupled WPCs showed lower T_g due to weak interfacial bonding, where rigid bamboo particles restricted chain mobility and impaired stress transfer. Nonetheless, at Tg, the lignin and crystalline cellulose structure of LLB

particles remained stable, contributing to higher stiffness compared to unreinforced rHDPE and rPS, aligning with previous findings.

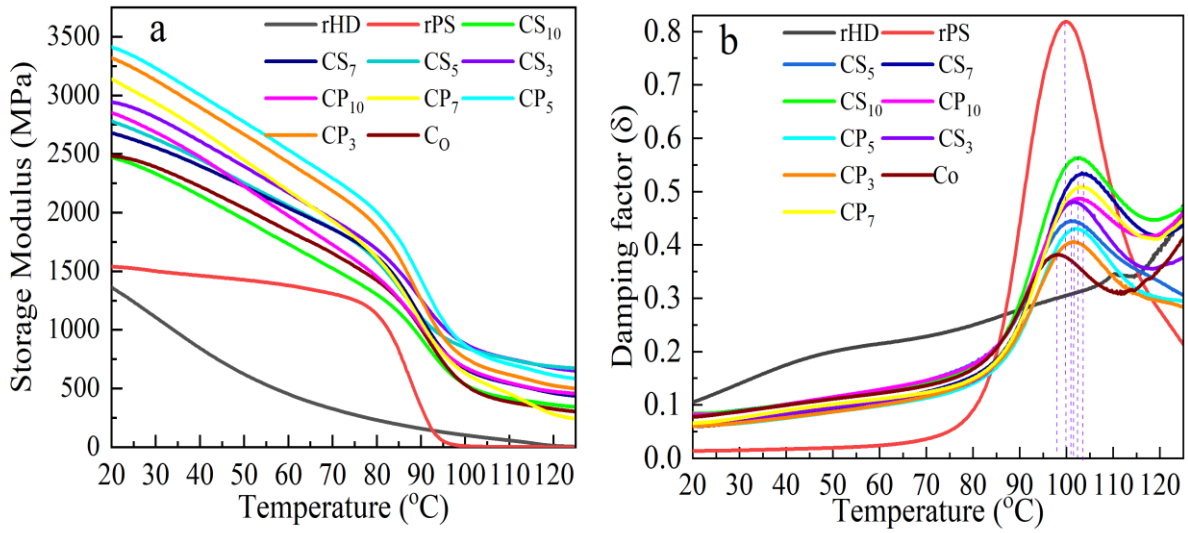

Figure 5. 2The storage modulus (a) and damping factor (b) of the WPCs.

5.3.6 Thermal Stability and Degradation of WPCs

Figure 5.3 and **Table 5.3** show the TGA curves of the WPCs, and the peak transmission evaluated using the DTG at two extreme values of both PPMA and SEBS-g-MA including the rHDPE, rPS, LLB and their WPCs, respectively. Thermal decomposition of rPS involves three stages ends before reaching 500 °C. The major degradation in the third steps from 375°C to 470°C, with a maximum mass loss reaching 79.5% similar to the reported trends [231,244] with some variations on the first stages and probably due to the residual impurities. rHDPE degraded on the first stage around 450°C and ended at 500°C with a maximum mass loss of 84.5%. After the stable degradations the next short-range degradations occurred around 600 °C with 6.24% mass loss, which could be the slow pyrolysis of inorganic mineral residuals in the prehistoric productions [8]. In the case of LLB reinforcements, the shoulder peak in the TGA curves, represented by P_0 (206–236°C) and both P_1 and P_2 (236–372°C), is mostly related to the decompositions of hemicellulose and cellulose, respectively, as previously investigated by Guo et al. [65]. They reported a slightly different results of low mass rate at shoulder peak P_1 and a larger mass loss rate at P_2, likely due to high cellulose contents than hemicellulose [8]. These decompositions nearly completed within the ranges of 365–600 °C of the region III as it interred the oxidative decomposition of carbonized residue and volatilization of anhydrous sugars.

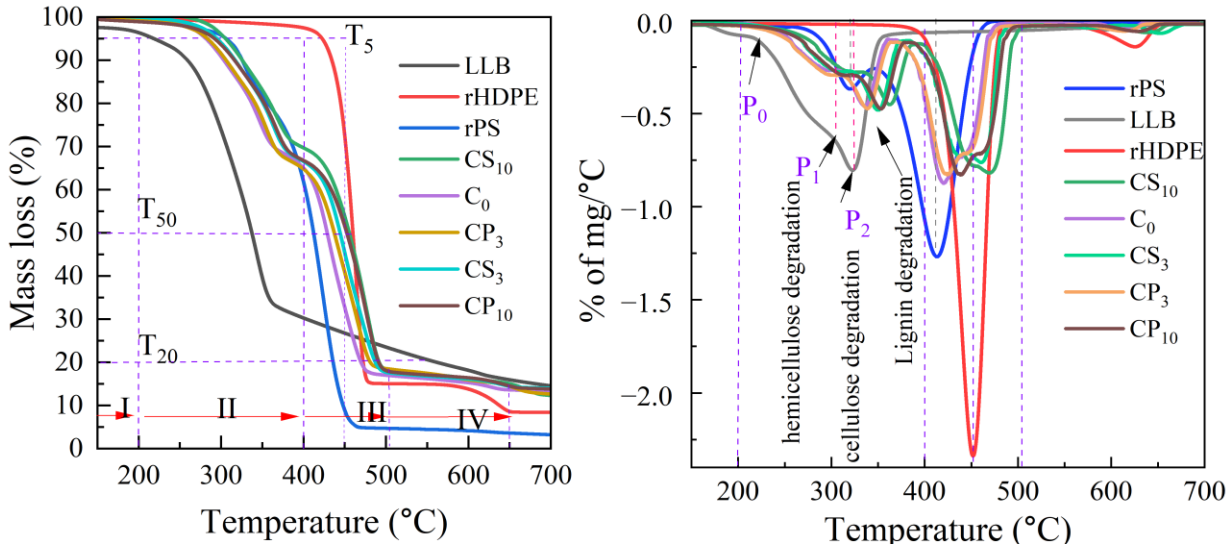

Figure 5. 3 TGA (a) and DTGA (b) of WPCs

However, the thermal degradation of WPCs involves multiple phases from region I to IV consisting of two major transition peaks as shown in Figure 5b. The degradation below 200°C (region I) were due to losing moisture and some low molecular weight compounds like extractives and amorphous hemicellulose in the WPCs. From 270–360°C (region II), the remaining hemicellulose, cellulose and lignin will degrade into volatiles decomposition and active pyrolysis. The peaks around 325 ◦C mark the end of cellulose degradation [30] and lignin decomposition occurred over a wide range because of its highly networked phenolic molecule contributing to char carbonizations [65] in the Stage III and largest peak intensity in the region III. The last region IV is likely representing the complete decomposition to ash and evolution of the pyrolysis gas products. The trends of TGA curves show better thermal stability increasing with both coupling agents loading increases. Furthermore, better stability is observed with SEBS-G-MA inclusions compared with the MAPP based WPCs because of the good thermal stability of triblock copolymer (SEBS) and the improved compatibility with LLB particles by grafted MA [256]. These two leads to shifting its TGA profiles to higher temperatures compared with their respective MAPP based WPCs and C_O. It is worth remarking that both CS_{10} (463.7°C) and CP_{10} (452.4°C) displayed higher T_{50} (the temperature at 50% weight loss) in more than 40.2°C and 128.2°C; 23.9°C,117.4°C, respectively, when both compared with the C_0 (428.5°C) and pristine LLB particles (335.5°C). LLB particles have intrinsically high carbonization effects of high charring ability which leads to stable T_{20} (the temperature at 20% remaining) in region IV and above. However, T_{20} obtained for SEBS-g-MA compared to MAPP shows an increase of 25.97°C and

18.47°C of T_{20} at 10wt.%, respectively, compared with rHDPE matrix (473.23°C); 29.2°C and 22.4°C increases, respectively, compared to uncoupled C_0. This suggests lower weight loss and improves thermal stability with increasing SEBS-g-MA content, attributed to enhanced cross-linking within the composite system, particularly in regions II and III. The influence of matrix blending is evident, as the lower thermal stability of rPS is enhanced, while SEBS-g-MA-based composites show improved maximum weight loss rates of LLB particles in region III through effective matrix encapsulation compared to pristine LLB particles. While the role of coupling agents in enhancing the thermal stability of WPCs has been previously reported, the cumulative effects of multicomponent coupling agents like SEBS-g-MA, compared with commercial MAPP, remain largely unexplored. Nonetheless, none of the WPCs exhibit the thermal stability of pure rHDPE above T_{50} or T_5 due to the limited thermal stability of LLB reinforcements. However, in-situ melt blending and compounding offer a promising method for preparing bio-composite WPCs, where coupling agents and crosslinking agents like DCP enhance interfacial compatibility, leading to improved thermal stability.

Table 5. 3 Refined thermographic values of the WPCs

Sample ID	$T_{5\%}$ (°C)	$T_{max(II)}$ (°C)	$T_{50\%}$ (°C)	$T_{20\%}$ (°C)	Remaining mass at 650°C
LLB	225.8	361.8	335.6	544.3	16.7
rHD	427.9	-	458.9	473.2	10.8
rPS	306.3	350.6	416.5	435.7	4.80
C_0	279.1	360.8	428.5	469.3	13.4
CP_3	283.5	365.7	438.8	481.3	14.1
CP_{10}	296.2	378	452.4	491.7	14.5
CS_3	298.7	375.5	445.4	487.6	14.8
CS_{10}	307.4	385.9	463.7	499.2	15.2

5.3.7 FTIR spectroscopic characterizations

Representative FTIR spectra of the uncoupled sample (C_O), coupled WPC samples (CS_5 and CP_5), and their components (unreinforced matrix, LLB, and MAPP) are shown in **Figure 5.4.** Variations in peak intensities were observed in the unreinforced polymeric matrix, particularly in key regions: aliphatic C-H asymmetric and symmetric stretching in CH_2 at 2920 cm^{-1} and 2852 cm^{-1}

(2960–2830 cm^{-1}), aromatic C-H stretching at 3026 cm^{-1} and 3062 cm^{-1} (3060–3025 cm^{-1}), C–C aromatic stretching at 1603 cm^{-1}, CH_2 deformation of the aromatic C=C ring at 1452 cm^{-1} and 1492 cm^{-1}, and C–H bending in CH_2 at 697 cm^{-1} and 757 cm^{-1} (900–675 cm^{-1}) [238]. These changes were more pronounced in the coupled WPC samples, particularly those with SEBS-g-MA. These variations are most probably due to interactions with the coupling agents in the composite systems through their hydrophobic chains which are significantly detected in the CS_5. Similarly, strong hydroxyl (-OH) stretching vibration of LLB around 3340 cm^{-1} decreases extremely, in the corresponding couples' composites. This implies eliminated number of original -OH groups most probably involved in the formation of new forms of bond and/or interactions like hydrogen bonds expected from the nucleophilic substitution reaction between -OH of cell wall matrix of LLB and the carbonyl group of the MA of the coupling agents [27]. This can be further evidenced by the reduced carbonyl peak intensity of MA at 1733 cm^{-1} in comparison to the coupled composites and appearing of C-C bonds weak band vibration present in MA at 822 cm^{-1}. Furthermore, one important band of C-O stretching intensity around 1736 cm^{-1} is decreased, which originates from the carbonyl groups of hemicellulose. Similarly, the bands related to C-O of aromatic skeletal vibration of lignin at 1506 cm^{-1} [28] almost disappeared in the coupled composites compared with the LLB.

Equally, even though the bands below 1460 cm^{-1} originates from the various vibrations of carbohydrate and lignin, [31] the band in between 1030-1050 cm^{-1}, which is related to both cellulose and lignin, has a narrow band region compared with LLB and has less intensified in the composites particularly in CS_5 [64]. Moreover, many typical absorption peaks of C-O, COOH and -OH bending frequencies in the cellulose, hemicellulose, and lignin occurred within 1152 - 1562 cm^{-1} [239].Compared with LLB, some of these absorption peaks shifted to lower or weaker values intensities in the coupled WPCs. Specifically, distinct C–O stretching of acetyl groups lignin at 1247 cm^{-1} [239,240] in both LLB and uncoupled composites (C_O) disappeared in the CP_5. These chemical bond vibration frequencies most possibly demonstrate the interactions of coupling agents aided by the crosslinking DCP in the composite systems, which result in better interphase compatibility and better mechanical properties as discussed above.

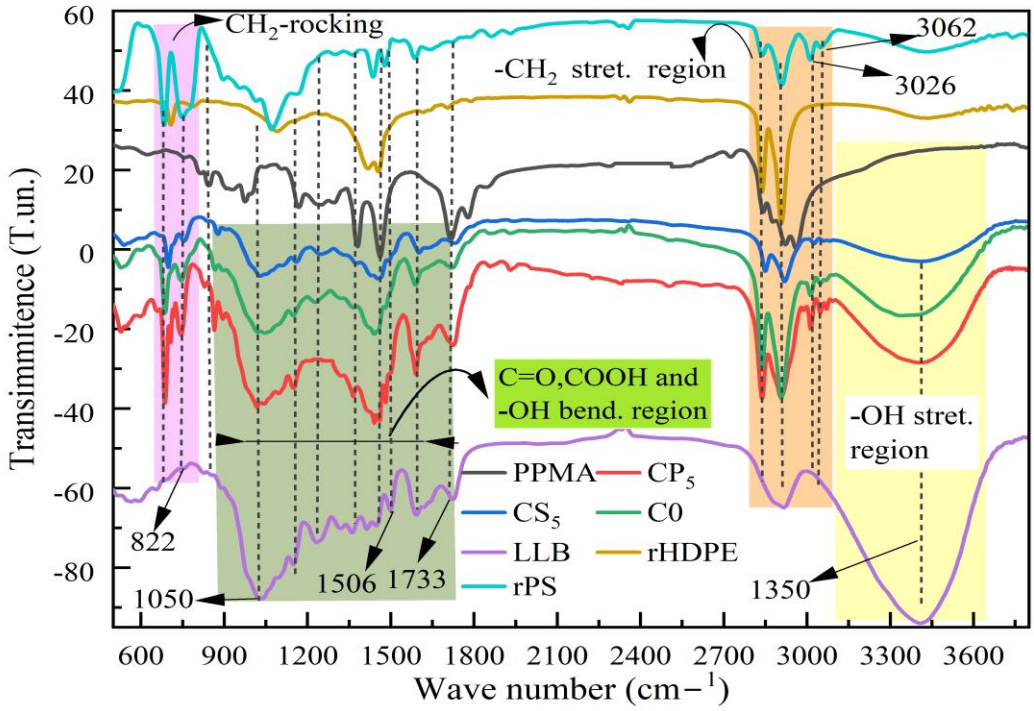

Figure 5. 4 The FTIR spectra of the representative WPCs, its unreinforced polymeric matrix, and LLB particles.

5.3.7 Water Absorption and Dimensional Stability

Water absorption primarily occurs at the outer layers of WPCs, decreasing progressively toward the bulk due to the hydrophilic and porous nature of lignocellulosic fibers. This process only contributes to the total weight increase of WPCs and does not affect water distribution within the material [88]. %WA (water absorption) and TS (thickness swelling) are key parameters used to assess the WPCs' resistance to environmental conditions. As shown in **Figure 5.5**, slight variations in %WA and TS were observed in the coupled composites compared to uncoupled WPCs (C_o) during the first five days, where Co exhibited %WA of 6.53% ± 0.32. Over 30 days of water immersion, %WA increased to 7.72% ± 0.38 for CP_{10} and decreased to 4.25% ± 0.13 for CS_{10}, representing a 27.59% to 131.76% reduction compared to C_O (9.85%). These results indicate that coupled composites have greater resistance to moisture uptake. However, MAPP-based composites showed slightly higher water uptake with increasing loading amounts compared to SEBS-g-MA-based composites, though both remained substantially lower than the uncoupled sample. For example, CS_{10} exhibited a 4.25% water uptake, less than half that of C_o (9.85%), while CP_{10} showed 7.72%, only 2.13% lower than Co. Similarly, TS followed a similar trend to

%WA, with greater values in uncoupled WPCs. TS ranged from 1.31% ± 0.59 to 1.63% ± 0.56 for MAPP-based composites and from 1.03% ± 0.12 to 0.635% ± 0.83 for SEBS-g-MA-based composites. Over both short-term (5 days) and long-term (30 days) measurements, SEBS-g-MA coupled with DCP demonstrated the lowest water uptake and TS. This performance is likely due to the water-repelling elastomeric rubber phase in SEBS-g-MA and the high maleic anhydride content in MAPP [257], which interacts with water molecules despite providing reactive sites for hydroxyl groups in natural fibers.

The polymeric matrix itself is inherently hydrophobic, resulting in negligible %WA compared to the hydrophilic reinforcements, which are intrinsically prone to water absorption due to their poor compatibility with the matrix. The reduction in %WA observed in WPCs, compared to natural fibers alone, can be attributed to hydrophobic matrix encapsulation and changes in polarity, which significantly improve interphase compatibility as similar findings have been reported in prior studies [30]. Maleic anhydride interacts with the hydrophilic hydroxyl groups, reducing free hydroxyl sites on LLB particles. Additionally, the hydrophobic polymer matrix, crosslinked with DCP, likely interacts with the hydrophobic regions of the coupling agents, further enhancing moisture resistance.

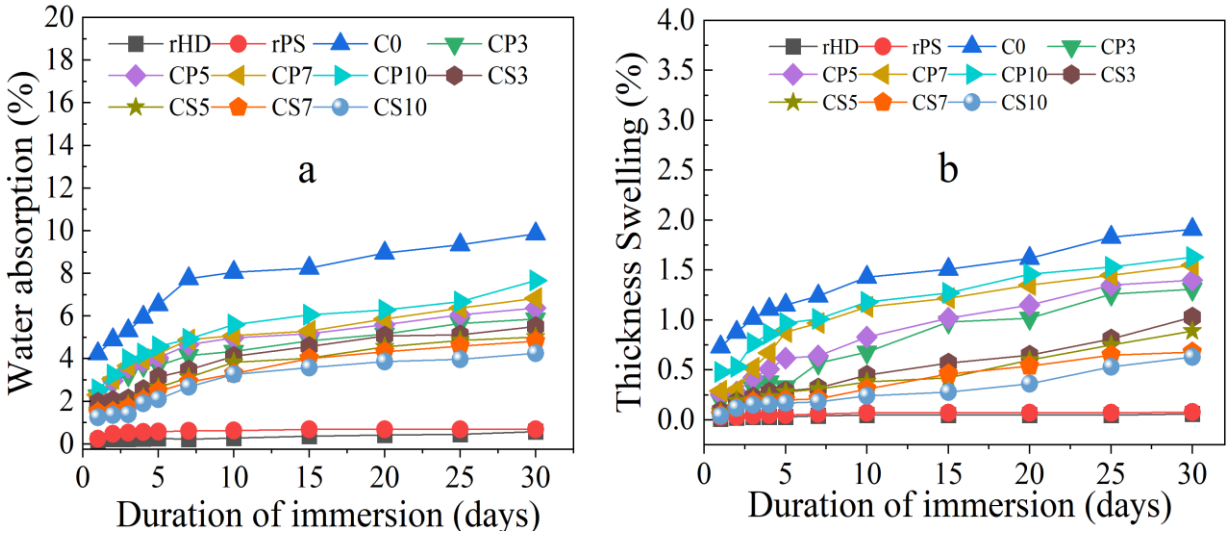

Figure 5. 5 Water absorption of WPCs (a) thickness swelling rate of WPCs (b)

Like %WA, the absorption kinetics determined by the diffusion coefficient (D) showed that water diffused relatively faster during the first 15 days, while the diffusion rate slowed in the following

15 days (**Table 5.4**). Coupled composites likely formed a barrier through the networked interphase created by the coupling agents, with D values for SEBS-g-MA being lower than those of the uncoupled and MAPP counterparts in both the first and second 15-day periods, exhibiting lower marginal values after prolonged submersion. Like %WA and TS, this suggests that the LLB particles in the WPCs are likely to reach a saturation point. Additionally, the coupling agents reduced the porosity of the cell wall by improving LLB particle dispersion and enhancing interfacial strength, resulting in better dimensional stability.

Table 5. 4 Diffusion coefficient of the WPCs samples

Samples	**Diffusion coefficient (x 10^{-15} m^2 s^{-1})**	
	1-15 days	15-30 days
rHD	Negligible	negligible
rPS	Negligible	negligible
C_O (control)	0.073	0.038
CP_3	0.030	0.015
CP_5	0.037	0.018
CP_7	0.041	0.034
CP_{10}	0.056	0.037
CS_3	0.031	0.012
CS_5	0.028	0.014
CS_7	0.027	0.010
CS_{10}	0.024	0.008

From a performance standards perspective, the water absorption and thickness swelling results were compared against relevant benchmarks established by EN 15534-1:2018 and ASTM D7031/D7032 for wood–plastic composites. For decking applications, where dimensional stability and moisture durability are critical, acceptable limits are ≤7% WA and ≤3–4% TS after 28 days of water immersion. For cladding and facade applications, slightly higher limits of up to 10% WA and 5% TS are tolerated, assuming structural integrity is maintained. Load-bearing applications impose stricter requirements, generally requiring WA ≤5–7% and TS ≤3% to ensure long-term durability. These standards simulate real-life exposure using ISO-aligned immersion conditions over 28 days. Most of the composites developed in this study met these performance

thresholds with better results interestingly, compared with prior studies [30,258,259] .Water saturation and TS generally plateaued after 20–30 days, suggesting that equilibrium had been reached. The favorable moisture performance is attributed to the combined effects of matrix encapsulation, improved interfacial compatibility, and limited permeability of the modified hybrid systems. Overall, these findings support the suitability of the formulated composites for semi-structural and outdoor applications. Further evaluation of their long-term mechanical performance under variable environmental conditions is recommended to validate service life reliability

5.3.8 SEM morphology

The SEM morphologies of the WPC samples, obtained from the fractured surfaces during impact strength (IS) testing, are shown in **Figure 5.6** (labeled a to h) to analyze particle dispersion and interfacial reactions. Images of uncoupled WPCs (Co) were taken at four points: the first replicate (a and b) and the second replicate (e and f). Coupled WPCs, formulated with CP_5 and CS_5, were represented by images (c, d) and (g, h), respectively. The uncoupled composites (Co) exhibited significant LLB particle debonding and removal during IS testing, leaving behind large pull-out holes, voids, and poor interphase homogeneity. This poor interfacial compatibility resulted in weak particle-matrix interactions, reduced mechanical properties, increased water absorption in voids, and decreased dimensional stability. In contrast, the coupled composites (CP_5 and CS_5) showed significantly improved morphology. Images (c, d, g, h) demonstrate better dispersion of bamboo particles in the polymer matrix, with no visible agglomerates and minimal particle pull-outs, voids, or gaps. The enhanced interphase homogeneity facilitated effective stress transfer to the particles, leading to particle breakage rather than pull-out. The fracture surfaces appeared solid, with tightly bonded particles and uniformly distributed tearing ridges. Furthermore, the coupled composites showed homogeneously embedded particles with strong adhesion and polymer coating, remaining intact after impact (e.g., **Figure 5.6. h**). Well-oriented, deformation-free surface layers were attributed to polymer chain adhesion to LLB particles, facilitated by coupling agents and DCP crosslinking. This process created an immobile layer on the particle surfaces (e.g., **Figure 5.6b**). The absence of voids and particle agglomerates indicates reduced particles pull-out areas and enhanced interfacial bonding, consistent with findings from previous studies [83][79].

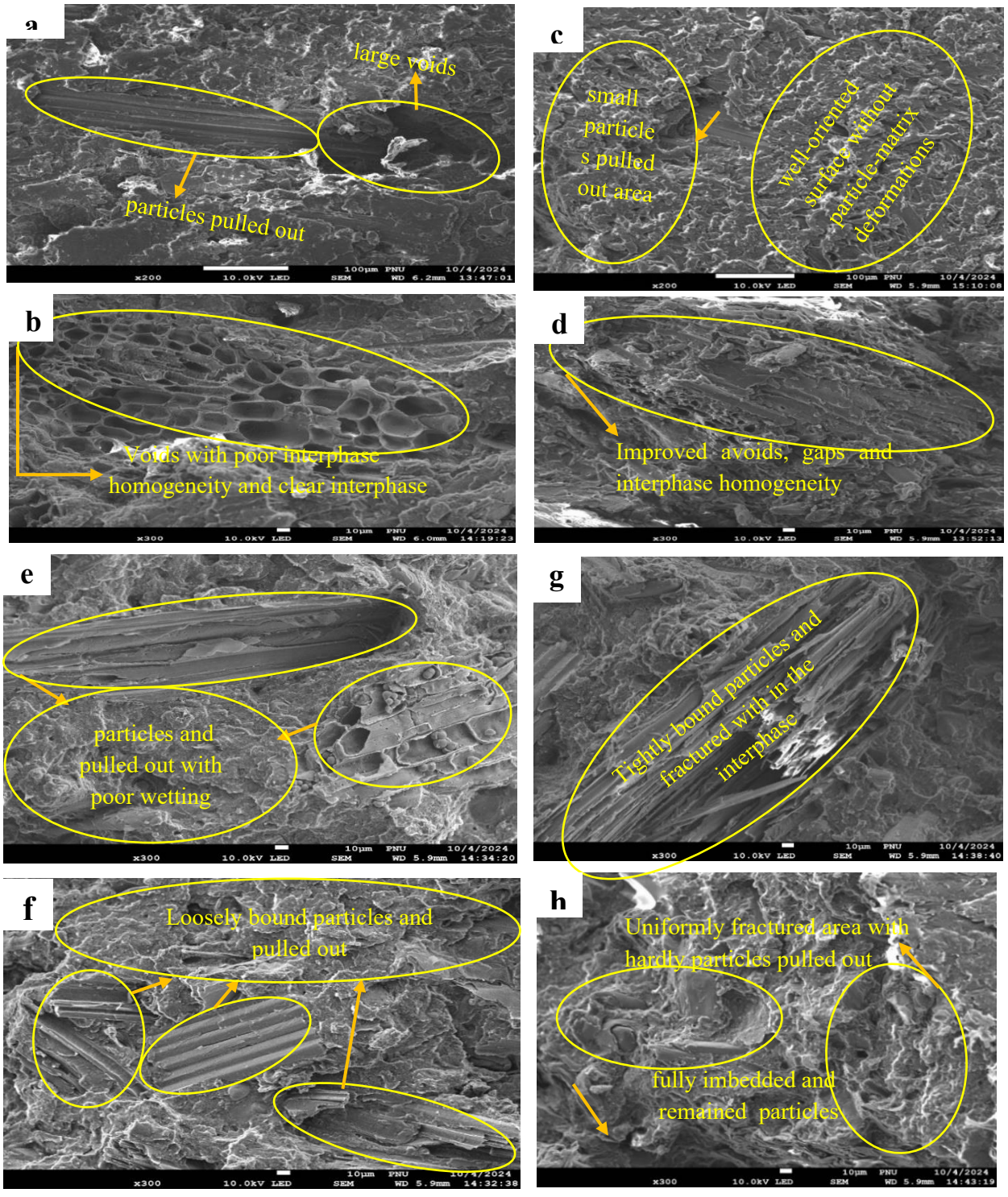

Figure 5. 6 SEM Morphology of WPCs uncoupled WPCs (a, b, e, f) and coupled WPCs (c, d, g, h)

Conclusion

Eco-friendly WPCs were produced using an equal blend of rHDPE and rPS as the polymer matrix, combined with Ethiopian LLB particles as reinforcements at a 50/50 wt.%. The materials were compounded via reactive melt compatibilization using a HAAKE Rheomix OS batch kneader and compression molded, focusing on cost-effectiveness. The effects of SEBS-g-MA and MAPP coupling agents, crosslinked with DCP at concentrations of 3%, 5%, 7%, and 10%, were evaluated to optimize mechanical performance, thermal behavior, dimensional stability, water uptake, and degradation resistance.

Generally, both coupling agents crosslinked with DCP significantly improved system compatibility, ensuring homogeneous dispersion of LLB particles within the matrix. This enhanced dispersion of rigid LLB reinforcements (50%) promoted mechanical interlocking, resulting in improved thermomechanical storage modulus and composite stiffness. FTIR spectral analysis confirmed improved mechanical properties through reduced −OH band intensities, changes in carbonyl regions, and removal of certain LLB characteristic bands. SEM images further demonstrated better dispersion of bamboo fibers within the polymer matrix, with minimal particle pull-outs, reduced voids and gaps, and improved interphase homogeneity. The coupled composites showed strong adhesion between LLB particles and the matrix, evidenced by particle breakage rather than pull-outs.

The results show that the toughness of the composites, evaluated through impact strength tests, improved significantly with SEBS-g-MA, driven by the flexible ethylene-butylene molecular blocks in its chain. This improvement increased as the content of both compatibilizers rose. In contrast, storage modulus, tensile strength, and flexural properties were notably enhanced with MAPP and DCP compared to uncoupled WPCs. These properties showed a slight increase from 3% to 5% MAPP, followed by a decline with further additions, indicating that 5% MAPP and 1% DCP provided the best results. For SEBS-g-MA, 3% combined with 1% DCP produced better tensile, flexural, and storage modulus values. Mechanical tests highlighted MAPP's strong potential to improve tensile and flexural properties, while SEBS-g-MA effectively synergized to enhance both impact strength and interphase compatibility in the equal blend ratio rPS/rHDPE-based WPCs. While many bio-composites suffer from high water absorption and dimensional stability, lower water uptake and improved thermal stability including dimensional stability

significantly increased with higher SEBS-g-MA content. Conversely, these properties decreased with increasing MAPP content.

For applications requiring better dimensional stability, water resistance, and the ability to withstand sudden impact forces, SEBS-g-MA-based composites are preferred. Meanwhile, MAPP-based composites are better suited for applications demanding higher strength, stiffness, and lower moisture exposure.

These findings support the advancement of thermoplastic waste valorization into sustainable building materials. In-situ reactive melt-compatibilization proved to be a viable method for manufacturing WPCs, with coupling agents and crosslinking enhancing interface compatibility and thermal stability. These WPCs probably can be a practical alternative to polyolefin-based composites, meeting standards for FS, FM, and TS with wood fiber or polymer contents of 40–60%. They could be suitable for applications such as construction materials, wall cladding, ceiling boards, interior design, and decking, offering low biodegradation risks, minimal deformation, and performance comparable to commercial products.

CHAPTER SIX.

Valorization of High-Value Thermoplastic Waste from Electronic Waste for the Development of High-Performance Bamboo Fiber-Reinforced Composites through Chemical Compatibilization and Toughening Agents.

Abstract

High-performance wood polymer composites (WPCs) were developed using recycled acrylonitrile butadiene styrene (rABS) and high-impact polystyrene (rHIPS) matrices reinforced with 50% Ethiopian indigenous lowland bamboo (LLB) particles reinforcements. Ethylene propylene diene monomer (EPDM) and methyl methacrylate-butadiene-styrene (MMBS) were applied synergistically with maleic anhydride (MA) and dicumyl peroxide (DCP) via in situ reactive melt blending and compatibilizations to enhance multipurpose toughening and synergistic influence on interfacial adhesion. EPDM and MMBS contents varied at 5%,10% and 15% were varied to optimize mechanical performance, while MA and DCP were fixed at 1% and 0.5%, respectively. Comprehensive evaluations of mechanical properties showed that MMBS-modified rABS and rHIPS composites (10% MMBS, 1% MA, 0.5% DCP) achieved superior strength (flexural strength 74.5 MPa), modulus of rupture (6.09 GPa), and dimensional stability (+65.65%) compared to uncoupled and unmodified composites. EPDM improved thermal stability and reduced water uptake in both systems, though excessive amounts slightly reduced stiffness and strength, yet still outperformed unmodified matrices. Dynamic mechanical (DMTA), morphological (SEM), chemical (FTIR), and thermal (TGA, DSC) analyses confirm enhanced interphase compatibility and thermal degradation stability. These findings show that formulated WPCs resulted superior performance compared to commercial polyolefin WPCs, serving as lightweight, cost-effective building materials while supporting circular resource use and eco-friendly innovation.

Key words: *Polymer-matrix composites, recycling, coupling compatibilizations, interface modifications, wood polymer composites, valorization of e-waste*

6.1 Introduction

The mounting global sustainability challenges have driven increased demand for products and processes that emphasize circular resource flows and efficient use of renewable materials. One of such critical concerns is the exponential increase in polymeric plastic waste, now nearing 150 million tons annually. Despite this, plastics remain indispensable across household, industrial, automotive, and aerospace sectors, serving as a globally significant commodity that permeates nearly every aspect of daily life due to their versatility and cost-effectiveness [3]. However, the inherent stability of their long-chain polymeric structures renders them highly resistant to natural degradation, leading to persistent global pollution [4]. Recycling has emerged as a more sustainable alternative to traditional landfilling, with approaches classified into primary, secondary, tertiary, and quaternary processes. Primary recycling involves repurposing uncontaminated, clean, or semi-clean plastic scrap, yet it is unsuitable for municipal solid waste due to contamination challenges. Secondary recycling employs mechanical processes, including heating and extrusion, to transform plastic waste into new products, while tertiary (chemical) recycling utilizes catalytic depolymerization and extensive thermal breakdown to revert plastics into their original monomers and valuable byproducts for feedstock applications.

Despite the promise of these methods, significant barriers—including high operational costs, technological complexity, and potential environmental hazards—impede their large-scale implementation. The final recycling stage (quaternary recycling) involves energy recovery through incineration which often generates hazardous secondary pollutants, further exacerbating environmental contamination [4,47]. However, plastic waste recovery though thermo-mechanical recycling almost retains both physical and mechanical properties of recycled thermoplastics and have proven to be among the most effective strategies in the circular use of resources. A particularly promising alternative in this domain is wood polymer composites (WPCs), a class of polymer-reinforced materials synthesized from thermoplastic matrices and lignocellulosic fibers as the dispersed phase reinforcements and/or fillers . WPCs are increasingly being developed as functional materials for diverse engineering applications. By integrating secondary plastic waste with bio-based natural fibers, they provide a sustainable, bioinspired solution that improves resource efficiency. WPCs utilize underexploited sustainable lignocellulosic fibers, which require far less energy than mineral alternatives, while simultaneously valorizing thermoplastic waste

before final disposal and retains in the product life cycle. This approach supports circular economy principles and reduces dependence on landfilling, incineration, or inefficient chemical recycling [260].

Thermoplastic waste from electrical and electronic equipment (EEE) plastics typically comprises approximately 10%–30% of total municipal waste [43]. HIPS and ABS are the most representative polymers in this market, and are derived largely from engineering thermoplastics, bridging commodity plastics, and high-performance engineering thermoplastics. This market continues to grow, driven by global industrialization and modernization, specifically in areas such as electrical/electronic and automotive/transportation applications, and urban construction [75].

Some experimental studies have investigated the formulation of WPCs using rABS and rHIPS derived from electronic waste, with some focusing specifically on their pristine properties. Yeh et al. [162] focused on the twin-screw extrusion of WPCs with 50 wt.% wood four and reported improvements in mechanical properties when using compatibilizers such as Styrene grafted maleic anhydride (SMA) and Styrene-Acrylonitrile grafted maleic anhydride (SANMA) with low impact strength performance and water absorption and dimensional stability. Similarly Sommerhuber et al. [123] extended this work to injection-molded WPCs using recycled rABS and rHIPS, with wood fiber contents of 30% and 60%. Their findings showed enhanced stiffness and strength, particularly when Norway spruce was used as the reinforcing fiber yet weak impact toughness performance. Similarly, Yu et al.[189] investigated rABS-poplar composite (80:20 wt.%) exhibited slightly better tensile strength (36.9MPa) and flexural strength (44.7MPa) lacking overall performance investigations and low fibrous fillers in the composite's formulations. Another studies on the corresponding virgin counterparts by Arslan and Dogan [261] examined the effects of different silane coupling agents which inherently involves the use of solvents adding additional costs on the mechanical properties of chopped basalt fiber (BF)-reinforced virgin ABS composites. They evaluated three silane agents: (3-aminopropyl) triethoxysilane (AP), 3-(trimethoxysilyl) propylmethacrylate (MA), and (3-glycidyloxypropyl) trimethoxysilane (GP). Composites treated with AP and MA showed increased tensile strength, while GP treatment led to a reduction. All three treatments improved flexural strength and modulus, with AP yielding the most significant gains. However, none of the silane treatments significantly affected the impact properties and the formulation involves low filling rates below 20% and dimensional stabilities

and the extents to which polar bearing silanes-based composites were not considered. In a related study, Kusić et al. [262] evaluated the incorporation of alkali-treated short banana fibers (10%, 20%, and 30%) into neat ABS, HIPS, and HDPE for injection molding consolidated WPCs. Thermal analysis showed that the composites retained thermal behavior, but stiffness increased with higher fiber content deteriorating the impact resistance while Flexural strength improved in the HIPS and HDPE at the expense of tensile strength. Likewise, Hui He et al. [263] a studied the effect of alkali treatment (4% NaOH) on the structure and mechanical performance of ABS/bamboo fiber (30%) composites. The fibers were functionalized with 7% styrene maleic anhydride (SMA). The alkali treatment effectively removed surface impurities (e.g., hemicellulose, lignin, wax). However, alkali treatment alone did not improve mechanical properties; significant enhancements in tensile, flexural, were observed only when SMA was used while low impact strength was reported. Furthermore, Ozenc et al. [264] investigated the addition of hemp fiber particles treated with 10% NaOH to neat ABS at low loading levels (1%, 5%, and 10% by weight). Compression and three-point bending tests showed that both compressive and flexural moduli increased with fiber content. However, compressive post-yield and flexural strengths decreased as fiber content rose. The added stiffness from hemp fibers negatively impacted the notch-impact resistance of the composites.

Previously mentioned recent studies focused on the WPCs from virgin or recycled ABS and HIPS have largely employed solvent-based surface treatments (e.g., alkaline or silane methods), typically at low biofiller loadings. These approaches not only involve toxic solvents but also yield limited improvements in key properties such as impact strength, toughness, and dimensional stability. To overcome these limitations, advanced solvent-free strategies are needed. In this regard, in situ reactive melt compatibilization using versatile thermoplastic elastomers offers a promising route to enhance interfacial adhesion and overall performance. Common TPEs used in WPCs include ethylene/propylene/diene terpolymer (EPDM), styrene-ethylene/butylene-styrene (SEBS), acrylonitrile/butadiene rubber (NBR), chlorinated polyethylene (CPE), ethylene vinyl acetate (EVA), polyisobutylene (PIB), maleic anhydride-grafted EPDM, maleic anhydride-grafted SEBS, and MMBS , Poly(styrene-co-methyl methacrylate-co-glycidyl methacrylate) (PS-MMA-GA), were effectively used via melt-blending compatibilization process. Moreover, EPDM, either alone or grafted with MA, is particularly attractive for its ability to improve toughness via cavitation and shear yielding, while also providing resistance to chemicals, oxygen,

ozone, heat, and harsh environments [30,61,253,265]. Likewise, MMBS copolymer—with its soft core and PMMA hard shell—presents additional potential through thermo-elastomeric crosslinking, combining toughness, stiffness, and polymer miscibility [19,57]. However, the systematic development of well-balanced WPCs through in situ solid-state reactive melt compatibilization of rABS and rHIPS—using MA and DCP synergistically with versatile impact modifiers (EPDM and MMBS)—remains largely unexplored and constitutes the core novelty of this work. Reinforcement with indigenous Ethiopian lowland bamboo particles, characterized by broad size distribution, is expected to impart superior strength and sustainability compared to conventional wood flour, with potential to replace scarce wood particles in commercial virgin polyolefin-based WPCs. To broaden the application potential of WPCs as sustainable alternatives to MDF, HDF, and related building materials, this study systematically investigates composites formulated from rABS and rHIPS, reinforced with LLB particles and incorporating common multipurpose impact modifiers, EPDM and MMBS, through in situ melt compatibilization. The effects of varying impact modifier contents (5 wt.%, 10 wt.%, and 15 wt.%) and coupling agents (1 wt.% MA and 0.5 wt.% DCP) on the mechanical properties, dimensional stability, and thermal resistance of the composites were examined. Composites exhibiting superior strength and dimensional stability were further characterized to elucidate interfacial interactions and comparatively evaluated for their potential application in building materials.

6.2 Materials Methods

6.2.1 Material

Samples of post-consumer white recycled ABS (PCS-ABS, commercial grade: MRC380L5) and HIPS were obtained from LG Chem, a globally recognized company known for recycling and modifying engineering plastics into a white opaque color. The MMBS copolymer (commercial grade: EM538) was also sourced from LG Chem, while EPDM (KEPA 1130) was supplied by LG Co. (Daesan Petrochemical, South Korea). Maleic anhydride (MA, analytical grade: 89529) and the crosslinking agent DCP (2-(2-phenylpropan-2-ylperoxy) propan-2-ylbenzene) with a density of 1.56 g/cm³ (analytical grade: 329541) were purchased from Sigma Aldrich, U.S.A. Matured LLB culms were collected from the Arjo Gudatu district (9° 4' 52" N, 36° 37' 30" E) in the Oromia region of Ethiopia and chopped into approximately 3-mm fibers, air-dried, and ground using a hammer mill (Retsch SR 200 Grauβ, Haan, Germany). Small fractions (<500 μm) were

obtained using a 0.5-mm vibrating sieve mesh and used without further particle elimination to ensure a wide particle size distribution. This approach aims to optimize resource utilization and evaluate reinforcement performance across multiple scales. Finally, the material was dried in a vacuum oven at 105°C for 24 hours until the moisture content was below 2%, then immediately used for WPC formulation.

6.2.2 Composites formulation and processing

The experimental design consisted of 18 independent formulation runs, as shown in **Table 6.1** based on the total weight of the composites. LLB particles, DCP, MMBS, and EPDM were dried separately in a vacuum oven at 80°C for 24 hours, except for DCP, which was sealed and stored in a refrigerator. The first four series of experiments aimed to evaluate the synergistic effects of MA and DCP, as well as MMBS and EPDM in rABS-based WPCs. The next nine formulations were based on rHIPS based WPCs. Formulations without LLB reinforcement, coupling agents, or impact modifiers served as the baseline compositions. The compositions of the coupling agents (MA and DCP) were kept constant, following recommendations from previous studies [3]. Generally, maintaining lignocellulosic fibrous fillers or reinforcements at 50% or less resulted in optimal mechanical properties, whereas exceeding 50% led to reductions in both physical and mechanical performance of WPCs [266]. Accordingly, LLB particles smaller than 500 µm were compounded at a relatively high and constant ratio of 50 wt.% to enhance their woody structure and texture. Similarly, the compositions of DCP and MA were adjusted in relation to the LLB reinforcement, as this combination and particle size contributed to improved mechanical properties. In contrast, larger particle sizes and higher contents led to diminished physical and mechanical properties, as observed in previous studies [73]. WPCs granulates were produced using a batch extrusion mixer (HAAKE Rheomix 3000, Thermo-Fisher Scientific Inc.). The in situ solid-state melting compatibilization process began with the premixing and melting of polymer matrices (HIPS and ABS) at varying at compositions as **Table 6.1**. Impact modifiers (MMBS and EPDM) were introduced at concentrations of 5, 10, and 15 wt.% according, and blending continued until a constant torque was reached at 190°C. The mixture was homogenized at a rotor speed of 50 rpm for 3 minutes. Subsequently, MA and DCP (1/0.5 wt.%) were added and mixed for approximately 2 minutes, followed by the gradual incorporation of LLB particle reinforcement (50 wt.%) in three separate sequences. This approach minimized excessive shear force and viscosity buildup, ensuring homogeneous compounding. The process continued until

constant torque and viscosity stabilization were achieved, typically within 12–15 minutes. The uniformly compounded WPCs were then removed, air-dried at room temperature, and ground using a circular cutter (model SM 2000, Retsch GmbH, Haan, Germany) with an 8-mm mesh size to obtain uniform granules. These granules were stored in plastic bags at a relative humidity of 65 ± 2% and a temperature of 23 ± 2°C in preparation for hot compression molding (**Figure 6.1**).

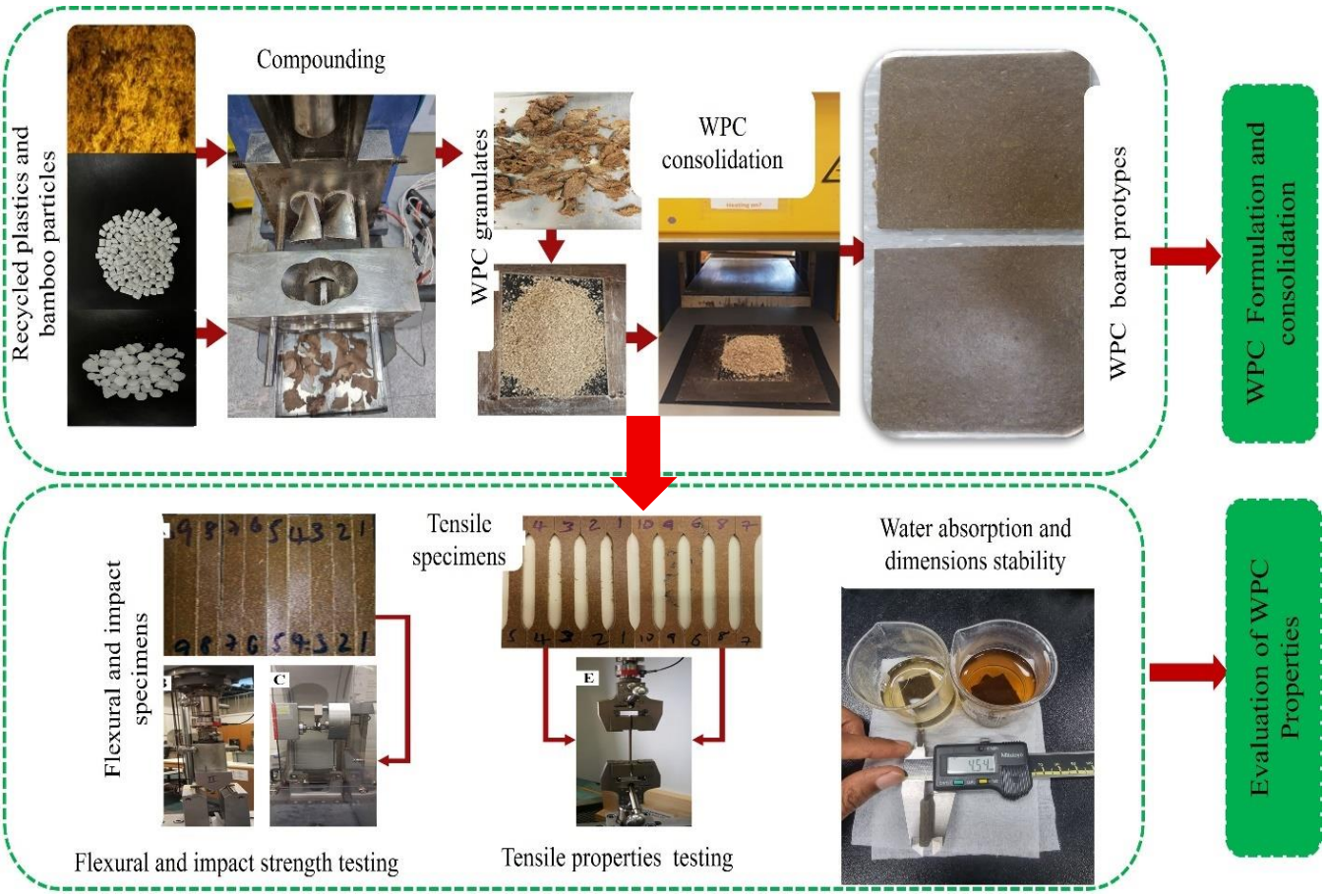

Figure 6. 1 WPCs based on the rABS and rHIPS formulation and properties evaluations

Table 6. 1 WPC formulations were developed using rHIPS and rABS matrices, reinforced with 50 wt.% LLB particles and modified with impact modifiers EPDM and MMBS

Polymers base matrix	**Matrix compositions (wt.%)**	**MMBS (wt.%)**	**EPDM (wt.%)**	**MA/ DCP (wt.%)**	LLB Particles **(wt.%)**	Sample ID
rABS	100	0	0	0	0	rABS
	50	0	0	0	50	CA_0
	50	0	0	1/0.5	48.5	C_AMa
	45	5	0			C_AM_5
	40	10	0			C_AM_{10}
	35	15	0			C_AM_{15}
	45	0	5			C_AE_5
	40	0	10			C_AE_{10}
	35	0	15			C_AE_{15}
rHIPS	100	0	0	0	0	rHIPS
	50	0	0	0	50	CH_O
	50	0	0	1/0.5	48.5	C_HMa
	45	5	0			C_HM_5
	40	10	0			C_HM_{10}
	35	15	0			C_HM_{15}
	45	0	5			C_HE_5
	40	0	10			C_HE_{10}
	35	0	15			C_HE_{15}

6.2.3 WPC board panel protype preparation

The dried and grinded WPC granule was placed within a carbon steel die frame (180 mm × 200 mm × 4 mm). The frame was lined with Teflon sheets before being inserted into a computerized, preheated laboratory-scale Carver hydraulic hot press. The uniform WPC granules were then consolidated into WPC board panel prototypes under controlled isothermal conditions at 200°C through a multi-stage pressing cycle. An optimized cyclic pressing procedure was employed to achieve enhanced compaction and mechanical properties. The process commenced with a pre-heating stage at low pressure, involving a slight plate opening for 1 minute at 20 bars. This was followed by pressing at 50 bars for 8 minutes. Subsequently, the pressure increased to 70 bars for full press-heating over 2 minutes, then further elevated to a maximum of 100 bars for an additional

2 minutes to ensure complete compaction. The final stage involved maintaining 100 bars during a slow cooling phase for 1.5 minutes, allowing the temperature to gradually decrease below 40°C. Upon completion of the pressing cycle, the press was opened, and the WPC board prototypes were removed from the metal frame. The boards were then cooled to room temperature before further processing and characterization.

6.2.4 Water absorption

The dimensional stability of the composite samples was evaluated through water absorption (WA) measurements in accordance with ASTM D570-98. WPC specimens with dimensions of 25 mm × 25 mm × 4 mm (length × width × thickness) were dried in a vacuum oven at 80°C for 24 hours until a constant initial weight (Wi) was obtained. The dried specimens were then submerged in ultra-pure beakers filled with distilled water at 23 ± 1°C and monitored for 30 days. Weight measurements (Wt.) were recorded continuously for the first five days, followed by subsequent measurements at 7, 10, 15, 25, and 30 days. Excess surface water was carefully removed before each measurement to ensure accuracy. The percentages of WA for each formulation were calculated using Equations 6.1 based on at least two duplicates per sample where W_t and W_i are the respective specimen weights at the specific time after water absorption and the initial weight of the sample, respectively.

$$WA = \frac{W_t - W_i}{W_i} x100 \ldots\ldots\ldots (6.1)$$

6.2.5 Characterization of Static and Dynamic Mechanical Properties.

The tensile and flexural properties of hybrid WPCs were evaluated using a universal testing machine (UTM) with a 50 kN capacity (Model 3365, Instron, Massachusetts, USA). The initial load was set at 0.09 MPa, and the crosshead speed was maintained at 5 mm/min under controlled conditions of 23 ± 2°C. Three-point bending flexural strength (FS) and flexural modulus (FM) were determined following ISO 178, while Charpy unnotched impact strength (UIS) was assessed according to ISO 179. Specimens with dimensions of 80 mm × 10 mm × 4 mm were machined from the hot-pressed composite panels for these tests. Tensile strength (TS) and tensile modulus (TM) were measured according to ISO 527-2 using dumbbell-shaped specimens with dimensions of 170 mm × 10 mm × 4 mm, under standard conditions of 20°C and 65% relative humidity. For

flexural testing, a support span of 60 mm was utilized. Unnotched impact tests were conducted at an impact speed of 3.46 m/s and an impact angle of 150° using a pendulum impact tester. All mechanical property measurements were obtained from at least five replicates per sample, ensuring consistency across successive dimensions. The dynamic mechanical thermal properties (DMTA) of the WPCs were analyzed using a dynamic mechanical analyzer (DMA Q800, TSA, USA) in accordance with ASTM D7028-07. Samples measuring 55 mm × 12 mm × 4 mm (length × width × thickness) were cut from compression-molded WPC prototypes and equilibrated at room temperature before testing. Dynamic temperature ramping was conducted from 25°C to 130°C at a constant heating rate of 3°C/min, with a frequency of 1 Hz and a constant amplitude of 20 μm to evaluate the storage modulus (E′) and damping characteristics (tan δ).

6.2.6 Characterization of thermal properties analysis.

The thermal properties and degradation behavior of the hybrid composite samples and their individual constituents were assessed using a Thermogravimetric Analyzer (TGA 55, TA Instruments, New Castle, DE, USA) following the ASTM E1131-20 standard. Approximately 10 ± 0.2 mg of each sample was analyzed within a temperature range of 40°C –700°C at a heating rate of 10°C/min under a nitrogen atmosphere, with a flow rate of 60 mL/min. Calorimetric analysis was conducted using Differential Scanning Calorimetry (DSC) in accordance with ASTM D3418, employing the TGA 55 Analyzer (TA Instruments, New Castle, DE, USA) in an inert nitrogen environment (flow rate: 60 mL/min). Samples (6 mg) were hermetically sealed in aluminum pans. The analysis involved an initial heating cycle (10°C/min) up to 250°C, followed by controlled cooling from 250°C to 40°C at the same rate to eliminate thermal history. A second heating cycle (40°C–250°C at 10°C/min) was then performed, with both heating and cooling phases held isothermally at 1°C. The glass transition temperature (Tg) was determined from the second heating cycle, as this process removes stress relief and enthalpic relaxation effects, thereby refining thermal transitions and improving data interpretation.

6.2.7 SEM morphology characterizations

The morphology of the composites was examined after sputter-coating with a 2 nm layer of platinum to enhance conductivity on the fractured surface created during the impact strength tests.

Image acquisition was conducted using a QUANTA 200 scanning electron microscope (FEI, USA) operated at an accelerated electron beam voltage of 10.0 kV.

6.3 Results and discussions

6.3.1 Mechanical properties of the WPCs

The fundamental mechanical properties of formulated WPCs, including tensile strength, impact strength, and flexural properties (modulus of elasticity and rupture), were analyzed in the following section. Unreinforced matrices and uncoupled composite samples serve as baselines to assess the effects the influence of coupling (MA, DCP) and multipurpose impact modifiers (MMBS, EPDM).

6.3.1.1 Tensile strength and Modulus of elasticity

TS and TM of the formulated WPCs are presented in Figure 6.2. The TS values measured for the uncoupled WPC samples—prepared without coupling or crosslinking agents and without the incorporation of impact modifiers—based on rABS and rHIPS matrices were 30.8 MPa (CA0) and 24.6 MPa (CH0), respectively. These comparatively lower values can be attributed to weak interfacial adhesion between the polymer matrix and bamboo particles in the absence of compatibilization, resulting in inefficient stress transfer across the composite interface. Further analysis indicates that rABS-based composites demonstrate superior performance when modified with MMBS compared to EPDM. The addition of 5 wt.% EPDM (CAE_5) results in a 12.27% increase in TS, while further increasing the EPDM content to 10 wt.% (CAE_{10}) yields a marginal increase of 6.3% relative to the uncoupled rABS-based composite (CA0). Notably, the inclusion of MMBS, DCP and MA enhances TS of rABS- based composites, increasing by 46.5% and 39% for 10 wt.% (CAM_{10}) and 15 wt.% (42.83 MPa, C_AM_{15}) MMBS content, respectively, compared to the uncoupled composite (CA_0). These results highlight the reinforcing and interphase-enhancing effects of LLB particles, as TS increases by 23.8% and 17.34% at the same 10% MMBS loading level relative to unreinforced rABS.

In rHIPS-based composites, TS values of 33.6 MPa (CHM_5), 36.6 MPa (CHM_{10}), and 35.5 MPa (CHM15) were recorded, reflecting increases of 36.8%, 49%, and 44.5%, respectively, compared to the uncoupled WPC (CH_0, 24.56 MPa). These values also correspond to increases of 19%,

29.6%, and 25.75%, respectively, relative to the unreinforced rHIPS matrix (28.23 MPa). These findings highlight the synergistic role of MMBS in modifying the interphase in conjunction with coupling and crosslinking agents, surpassing the TS improvements in comparable composites containing only MA and DCP, such as C_AM_a (28.81 MPa). Similarly, TS is also influenced by the addition EPDM as is incorporated at 5 wt.%, 10 wt.%, and 15 wt.% in WPCs, decreasing the TS values decrease to 28.4 MPa, 26.4 MPa, and 22.52 MPa, respectively. The 5 wt.% EPDM composite (C_HE_5) exhibits a 15.6% increase in TS compared to the uncompatibilized rHIPS-based sample (CH_0), but its increase relative to the rHIPS matrix at the same composition (5%) is marginal. Further increases in EPDM content led to reductions in TS. In contrast, rABS-based WPCs achieve a TS of 45.19 MPa with 10 wt.% MMBS combined with DCP and MA, likely due to enhanced interfacial adhesion between LLB reinforcements and the polymer blend. This improvement arises from the interaction of MA with cellulose hydroxyl groups and the compatibility of MMBS with the butadiene–styrene–acrylonitrile phase in rABS and the butadiene–styrene phase in rHIPS. The synergistic effect of MMBS, DCP, and MA is most effective at 10 wt.% MMBS in both matrices, yielding substantial TS improvements. Although TS continues to increase at 15 wt.%, the gains are less pronounced. By comparison, EPDM at 5 wt.% shows relatively better performance in balancing strength, impact toughness, and surface smoothness. In the presence of MA and DCP, limited interactions occur, as confirmed by SEM observations of improved interphase homogeneity and the formation of a dispersed rubbery phase within the matrix.

A key advantage of using a higher loading (50 wt.%) of well-distributed LLB reinforcements is the retention of composite stiffness. The modulus of elasticity remains higher than that of unreinforced rABS and rHIPS across all WPC formulations containing MMBS and EPDM. Both TS and TM exhibit concurrent increases when MMBS loading rises from 5 wt.% to 10 wt.%, followed by a marginal reduction at 15 wt.% MBS. This trend suggests that MMBS is highly compatible with ABS, owing to the shared chemical components (styrene and butadiene), which facilitate effective mixing and improved mechanical properties. MMBS functions as a compatibilizer as well, enhancing impact strength and processability by promoting a dispersed rubbery phase within the ABS matrix. Conversely, a slight reduction in stiffness is observed in EPDM-containing composites as EPDM content increases at the same loading rate in both matrices. This effect is attributed to the elastomeric and ductile nature of EPDM, whose modulus

is significantly lower than that of rABS or rigid LLB particles. Nevertheless, the improved impact strength and thermal stability offset this reduction in stiffness, as discussed in later sections. Comparatively, ABS-matrix WPCs containing 50 wt.% LLB particles exhibit a higher tensile modulus than rHIPS-based WPCs. By comparison, the tensile modulus of ABS-matrix WPCs containing 50 wt.% LLB particles has a better advantage in terms of the tensile modulus over similar rHIPS based WPCs. Tensile properties of this findings demonstrates comparable and shows better balance with the previously reported values of WPCs formulated with virgin and recycled ABS [162,267] and better performance compared with the other neat conventional polyolefins results incorporating the conventional wood fibers [129,160].

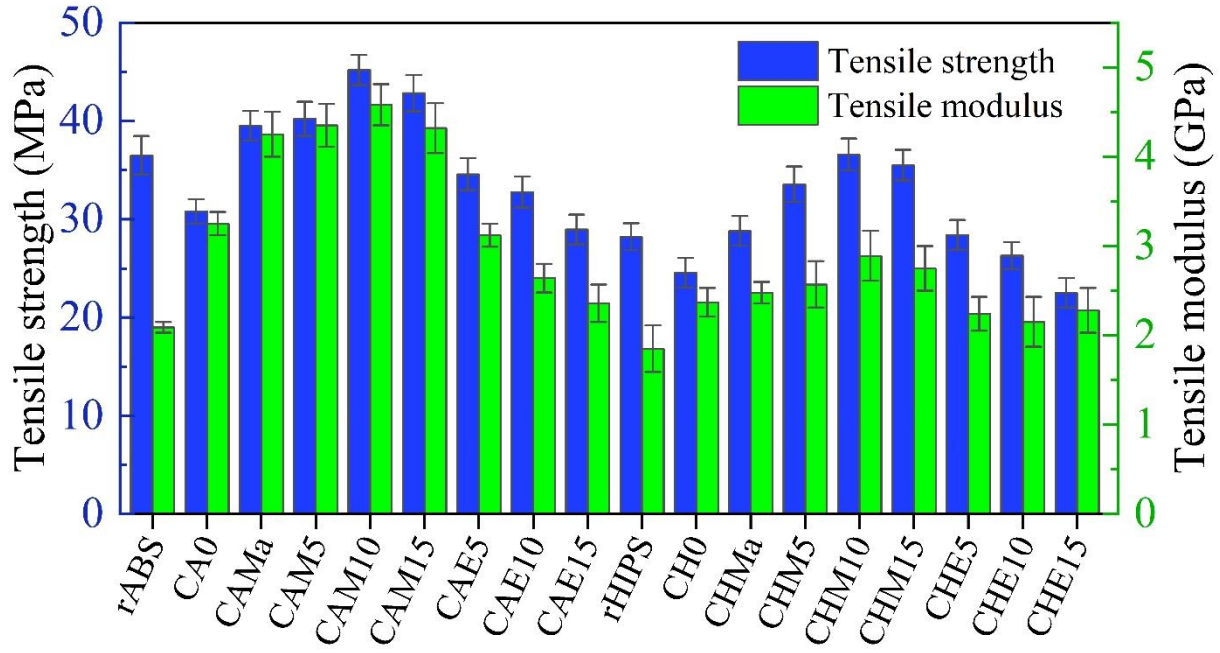

Figure 6. 2 Tensile strength and Modulus of elasticity of WPCs based on the rABS and rHIPS

6.3.1.2 Flexural strength and Modulus of Rupture

The trend in flexural properties of the tested WPCs follows a similar pattern to that of their tensile properties, as shown in **Figure 6.3**. The flexural strength of WPCs demonstrated superior performance compared to their tensile strength, exhibiting excellent modulus of rupture, particularly when compared with uncoupled and unreinforced composites. These enhancements are crucial for broadening the application potential of WPCs [98]. Significant improvements in flexural strength were observed in rABS composites reinforced with modified MMBS. The

flexural strength of C_AM_{15}, C_AM_{10}, and C_AM_5 composites reached 70.5 MPa, 74.5 MPa, and 68.28 MPa, respectively, representing increases of 31.7%, 39.2%, and 27.6% relative to the unreinforced matrix (53.5MPa). Similarly, the flexural strength of rHIPS composites incorporating MMBS was significantly enhanced. C_HM_{15}, C_HM_{10}, and C_HM_5 composites exhibited flexural strengths of 48.7 MPa, 47.5 MPa, and 42.5 MPa, marking increases of 45.4%, 41.8%, and 26.8.1%, respectively, compared with the unreinforced rHIPS matrix (33.5 MPa). These improvements indicate that MMBS effectively enhances flexural strength by forming a strong interface in synergy with MA and DCP. The combination of MA and DCP facilitates crosslinking and ensures uniform distribution of LLB reinforcements promoting an improved interfacial adhesion that enhances stress transfer under flexural loading. For rABS composites containing EPDM, only a marginal 4% increase in flexural strength was recorded. Further addition to EPDM, beyond 5% led to a decline in flexural strength compared with uncoupled composites, despite improvements in impact resistance and thermal stability, as discussed in Section 3.7. This reduction can be attributed to the dominant ductility of EPDM as its content increases. In contrast, while the flexural strength of rHIPS-based composites decreased with increasing EPDM content, improvements were observed at 5% (C_HE_5) and 10% (C_HE_{10}) loadings, with flexural strengths of 39.45 MPa (17.76% increase) compared with unreinforced rHIPS. Notably, the inclusion of MA and DCP still resulted in a slight 12% increase in flexural strength. This suggests that while EPDM increases the presence of soft segments at higher loading rates, the composites retain a relatively strong interface and reinforcement efficiency of LLB, particularly with the interfacial adhesion improvements enabled by MA and DCP.

An interesting trend in the MOR of the formulated WPCs indicates a significant enhancement in rupture resistance across all observed composites. The MOR consistently exceeded that of the unreinforced matrix, particularly in MMBS-modified systems. Recycled ABS-based composites incorporating MMBS exhibited comparable flexural modulus of WPCs formulated with virgin ABS and styrene-maleic anhydride coupling agents, as well as polypropylene-based composites [162]. Similarly, Both rABS and rHIPS-based WPCs demonstrate flexural strength comparable to commercial scale virgin PP-based WPCs formulated from Commercial wood fibrous fillers carefully incorporating the commercial coupling agents at relatively rate [156]. Using rABS as the matrix resulted in a flexural modulus of 6.09 GPa at an LLB content of 50 wt.%, which is significantly higher than the unreinforced modulus of both rABS and rHIPS. By comparison, the

flexural modulus of WPCs produced with commercial virgin polypropylene was reported to be 3.6 GPa [162]. This substantial increase in MOR is noteworthy, as WPC structural design is typically constrained by modulus of rupture rather than strength [268]. These findings demonstrate the potential of recycled polymers in high-performance WPC applications, positioning them as viable alternatives to leading polyolefin-based WPCs, which can offset the relatively higher cost of virgin rABS and rHIPS compared to conventional neat polyolefin composites. It also shows the better performance with the recent investigation done on with five recyclable plastic wastes including the rABS, MDF and HDF boards even at low compositions of commercial Poplar fibers [189]. Although impact modification with EPDM reduced the stiffness of the composites compared to other formulations, the modulus of EPDM-containing composites remained substantially higher than that of unfilled rigid rHIPS due to the reinforcing effect of LLB fibers. This variation is a common trade-off, wherein matrix stiffness is enhanced by the incorporation of LLB particles into the WPC structure. Changes in flexural strength in blends containing impact modifiers and coupling agents are closely linked to interfacial adhesion. The reduced flexural strength in uncompatibilized systems indicates weak interfacial bonding, while the polybutadiene and poly(styrene-co-methyl methacrylate) segments in MMBS promote excellent miscibility and adhesion with both rABS and rHIPS. Likewise, EPDM enhances flexural strength through rubber coating and improved stress transfer. However, when the impact modifier content exceeds 15 wt.%, it dominates the blend, increasing flexibility and softness but consequently reducing flexural strength and rigidity—consistent with previous findings [57].

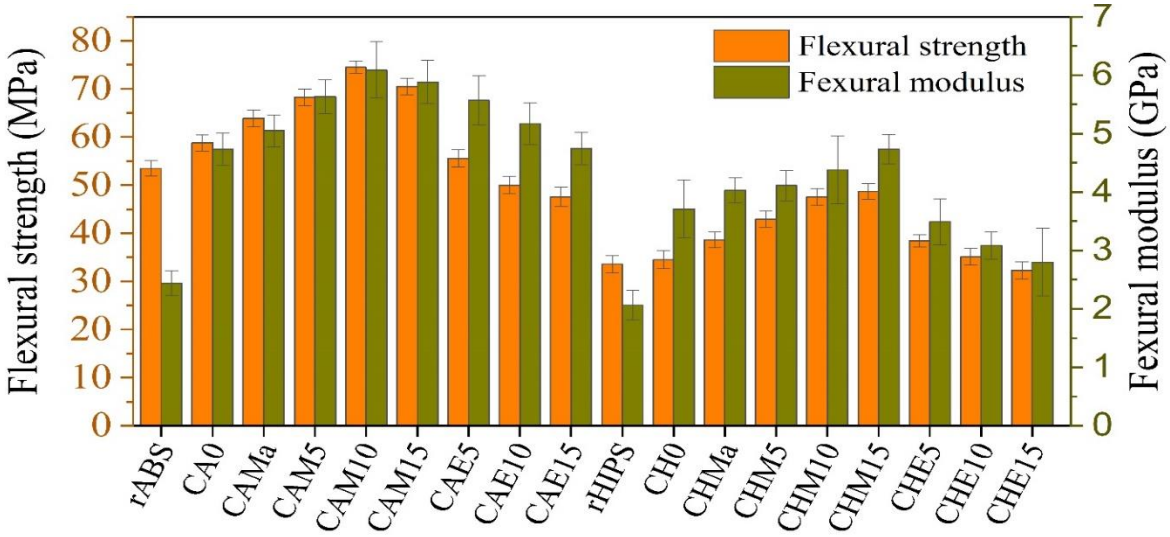

Figure 6. 3 Flexural strength and Modulus of rupture of WPCs based on the rABS and rHIPS

6.3.1.3 Impact strength

The unnotched impact strength of the formulated WPCs, as a function of EPDM and MMBS incorporation into rABS and rHIPS, is presented in **Figure 6. 4**. It is evident that the impact strength of composites lacking impact modifiers and coupling agents is significantly lower than that of unfilled polymeric composites. This reduction in impact performance is primarily attributed to the increase in WPC stiffness due to rigid lignocellulosic LLB particle reinforcements, which restrict polymer chain mobility and diminish the ability of WPCs to absorb impact energy. These effects are further exacerbated by poor interfacial bonding and the tendency of larger filler particles to agglomerate, thereby creating potential sites for microcrack initiation and propagation with minimal energy input. Consequently, the inhibition of ductile deformation in the matrix results in a greater proportion of fracture energy being dissipated through fiber debonding and frictional pull-out losses as fiber concentration increases. The impact strength of all formulated WPCs was observed to be lower than that of the unreinforced matrices, with rHIPS at 25.56 KJ/m² and rABS at 31.96 KJ/m². However, the incorporation of both MMBS and EPDM significantly enhanced impact strength, demonstrating a linear increase with loading amounts ranging from 5% to 15%, compared with the respective uncoupled composites, CA_0 (7.65 KJ/m²) and CH_0 (6.05 KJ/m²), as well as composites containing only DCP and MA, C_AM_A (8.56 KJ/m²) and C_HMa (5.02 KJ/m²).

In rABS-based composites, the impact strength varied from 11.65 KJ/m² (C_AE_5) to 18.25 KJ/m² (CAM_{15}), reflecting an increase of 52% to 138% compared to CA_0 (7.65 KJ/m²) and similar relative improvements compared to CAMA (8.56 KJ/m²). Likewise, EPDM-based rHIPS composites exhibited impact strength values ranging from 10.6 KJ/m² (C_HH_5) to 14.56 KJ/m² (CHE_{15}), corresponding to improvements of 75.2% to 140% relative to CH_0 (6.05 KJ/m²). These findings indicate that impact strength increases proportionally with impact modifier content in both matrices due to the synergistic enhancement of interphase bonding by DCP and MA and the toughening effect of impact modifiers. The highest performance was recorded at 15 wt.% MMBS C_AM_{15} (18.25 kJ/m²), followed by C_HM_{15} (15.5 kJ/m²), and finally C_HE_{15} (14.56 kJ/m²). However, beyond this threshold, the addition of EPDM resulted in diminished performance in other mechanical properties, as previously discussed. This reduction in stiffness is expected to worsen with increasing EPDM content due to the increasing dominance of composite ductility. These findings suggest that, while LLB reinforcement at 50 wt.% enhances stiffness and interfacial

adhesion—facilitated by MA and DCP—the elastomeric network structure of the composite remains intact under processing conditions, contributing to improved impact strength in inherently rigid WPCs. This transition from brittle (low-impact) to ductile (high-impact) behavior is further corroborated by the shift in glass transition temperature (Tg), as evidenced by the dynamic mechanical thermal analysis (DMTA) and differential scanning calorimetry (DSC) results presented in Sections 3.4 and 3.5. In MMBS-modified composites, polybutadiene particles are finely dispersed within the polystyrene matrix, while the stiffer methyl methacrylate segments enhance both stiffness and strength while concurrently facilitating impact energy absorption. These findings align with the observations of Mengeloglu et al. [57], who reported that incorporating MMBS into rigid wood-fiber composites improved impact performance by functioning as an elastomeric adhesive between PVC particles, effectively preventing brittle crack propagation.

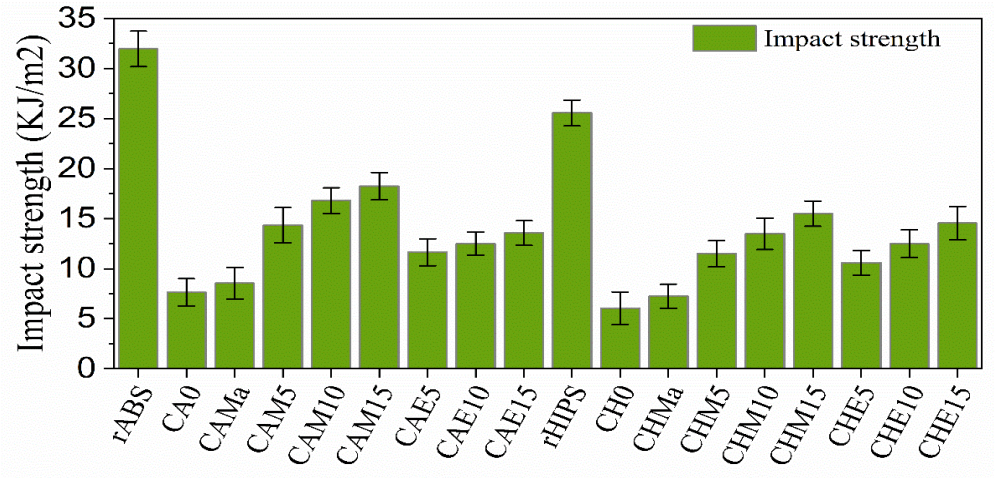

Figure 6. 4 Impact strength of WPCs based on the rABS and rHIPS

6.3.2 Water uptake of formulated WPCs

Water absorption in WPCs predominantly occurs in the outer layers and gradually decreases toward the core attributed to the hydrophilic and porous nature of lignocellulosic fibers, resulting in overall weight gain of WPCs thereby influencing the composite's overall moisture resistance. As illustrated in **Figure 6.5** a and b, significant variations in water absorption were observed with increasing MMBS and EPDM content at 5%, 10%, and 15% in both composite systems remaining lower than those of the uncoupled samples including a substantial reduction in %WA was also observed when compared to composites formulated solely with MA and DCP. The water

absorption trend followed a linear increase during the first week of immersion, after which the rate of absorption gradually slowed. After one month of complete water immersion, no significant variations in %WA were detected, indicating a close stage of the saturation equilibrium. In rABS-based WPCs, the %WA decreased as MMBS content increased to 5%, 10%, and 15% at a constant MA and DCP loading. This resulted in %WA reductions to 5.48% ± 0.28 (C_AM_5), 4.06% ± 0.35 (C_AM_{10}), and 5.12% ± 0.29 (C_AM_{15}), corresponding to decreases of 53.63%, 65.65%, and 56.69%, respectively, compared to the uncoupled CA_0 (11.82%). Similarly, reductions of 44%, 58.2%, and 47.86% were observed compared to C_AM_a (9.82%). Likewise, rABS-based WPCs containing EPDM exhibited significant reductions in %WA of 54.4% (C_AE_5), 64.21% (C_AE_{10}), and 65.9% (C_AE_{15}) with EPDM contents of 5%, 10%, and 15%, respectively, compared to CA_0. When compared to CAMA, the reductions were 45.1%, 56.92%, and 58.96%, respectively. These findings indicates the excellent water-repellent properties of both MMBS and EPDM, which synergistically enhance both impact toughness and moisture resistance in the composite. The increased EPDM content likely improves flowability and enhances the rubber coating of LLB particles, thereby reducing voids in the bulk matrix and minimizing discontinuities at interfacial regions. This effect is further corroborated by the representative fractured SEM morphology analysis, as discussed in section 3.7.

A similar trend was observed in rHIPS-based composites, which demonstrated even greater reductions in %WA over 30 days of water immersion in their coupled formulations. The %WA of uncoupled CH_0 composites reached 10.85%, while reductions of 49.95% (C_HM_5), 63.01% (C_HM_{10}), and 65.1% (C_HM_{15}) were observed when MMBS content varied at 5%, 10%, and 15%, respectively. Corresponding reductions of 55.3% (C_HE_5), 61.2% (C_HE_{10}), and 61.38% (C_HE_{15}) were recorded when EPDM content was varied at the same levels, maintaining a constant MA and DCP loading across all formulations. These results indicate that rHIPS-based composites exhibit superior resistance to water uptake in their coupled formulations containing both MMBS and EPDM. The enhanced resistance in rHIPS composites is attributed to the improved rubber coating effect, particularly from EPDM, which provides greater moisture protection compared to rABS composites.

In both rABS- and rHIPS-based coupled composites, interfacial adhesion is significantly enhanced due to hydrophobic matrix encapsulation and polarity modification. This effect is

primarily facilitated by maleic anhydride, which interacts with the hydrophilic hydroxyl groups of lignocellulosic fibers, thereby reducing the number of free hydroxyl sites available for water absorption and improving interphase compatibility. Additionally, the hydrophobic polymer matrix, crosslinked with DCP, interacts with the nonpolar regions of impact modifiers, further enhancing moisture resistance. This mechanism minimizes void formation within the composite interface, preventing further water penetration and reducing %WA in hydrophilic LLB particles as similarly reported in previous studies [56].

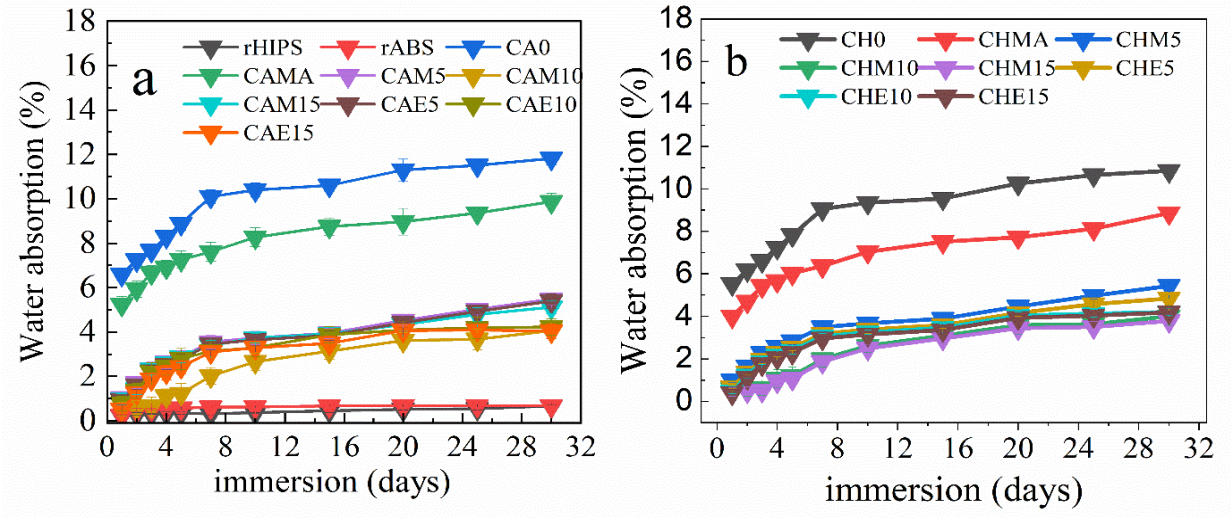

Figure 6. 5 Water uptakes of WPCs based on the rABS (a) and rHIPS matrices (b)

6.3.3 Dynamic Mechanical properties of WPCs

The compatibility and interphase modifications among the blend components of LLB-reinforced WPCs were evaluated using DMTA, considering both the storage modulus (**Figure 6.6a**) and tan δ curves (**Figure 6.6b**). The analysis was conducted on representative rABS-based and rHIPS-based composites, each assessed at 10% MMBS (C_AM_{10} and C_HM_{10}) and EPDP (C_AE_{10} and C_HE_{10}), along with the unreinforced matrix (rABS and rHIPS), respective uncoupled composites (CA_0 and CH_0), and composite samples containing only DCP and MA (C_AMa and C_HMa). The storage modulus, which represents the energy stored during elastic deformation and serves as an indicator of a material's elastic properties, exhibited a notable enhancement in MMBS-containing composites. Specifically, C_AM_{10} (4542.8 MPa) and C_HMA_{10} (2883.3 MPa) demonstrated significantly higher storage modulus values compared to the EPDM-based composites C_HE_{10} (2170 MPa) and C_AE_{10} (2587 MPa). This discrepancy is attributed to the increased elastomeric

segment of EPDM in the rubbery phase, which reduces stiffness and results in lower E′ values across the entire temperature range. Nonetheless, these values remained higher than those of the unreinforced rHIPS (1837 MPa) and rABS (2062 MPa) at the onset of thermal stress. This enhancement in mechanical properties may be attributed to increased molecular chain entanglement during melting and blending, as well as the reinforcing effect of LLB particles. Similarly, the damping curves (tan δ) presented in Figure 6b indicate a shift in the glass transition temperature (Tg). The Tg of C_AM_{10} and C_AE_{10} shifted to higher temperatures relative to the Tg of rABS (104.6°C), while the Tg of C_HE_{10} and C_HM_{10} shifted to higher temperatures compared to the Tg of rHIPS (98.3°C). This shift, accompanied by a corresponding increase in storage modules at elevated temperatures, suggests enhanced interfacial interactions. The presence of stiffening amorphous chains near fibrous particles, along with bulky pendant groups such as benzene rings and highly cross-linked polymer chains, restricts molecular mobility and rotational motion, thereby increasing Tg [30,73]. These findings indicate that both MMBS and EPDM impact modifiers effectively contribute to the formation of a strong interfacial structure and uniform distribution of LLB particles. In contrast, uncoupled composites (CH_0 and CA_0) did not exhibit a Tg shift to higher temperatures, instead remaining below the Tg of their respective unreinforced matrices. This behavior is indicative of weak interfacial bonding within the composite molecular chains, where reinforcement is primarily governed by mechanical interlocking rather than strong chemical interactions, leading to reduced deformation

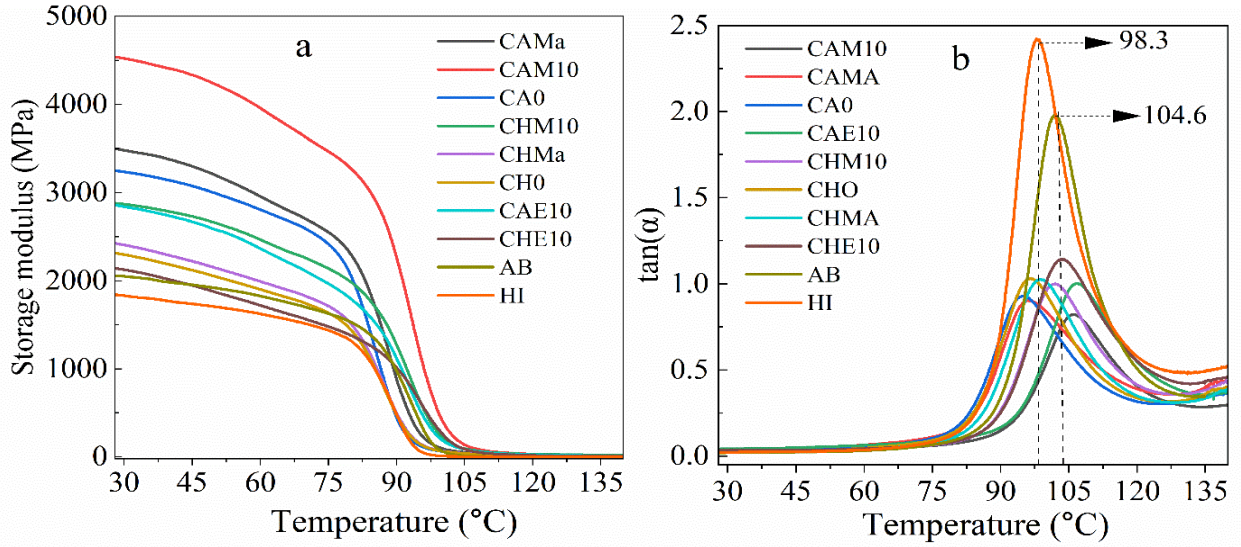

Figure 6. 6 Storage modulus (a) and damping factors (b) characteristics of the WOCS based on the rABS and rHIPS

6.3.4 Thermal Stability and Degradation of WPCs

TGA and DSC thermographs of representative WPCs samples and matrices are presented in **Figure 6.7a** and **6.7b**, respectively, with the corresponding data summarized in **Table 6.2**. As depicted in Figure 7a, the degradation onset temperature, determined at 5% mass loss ($T_{5\%}$), was used to evaluate the initial thermal decomposition. Additionally, the temperatures corresponded to 50% mass loss ($T_{50\%}$), 25% remaining mass ($T_{75\%}$), the maximum degradation temperature (T_{max}) before 600°C, and the percentage of residue at 700°C were analyzed. These parameters were assessed across four distinct pyrolytic regions within the temperature range of 40–700°C. Furthermore, the glass transition temperature (T_g) was determined from the DSC curves, specifically from the endothermic phase illustrated in **Figure 6.7b**. The thermal decomposition of rHIPS and recycled rABS commenced at $T_{5\%}$ values of 362.9°C and 348.1°C, respectively. The primary degradation phase occurred within the temperature ranges of 362–451.9°C and 419.7–459.8°C for rHIPS and rABS, respectively. Both materials continued degrading until reaching region III, where residual masses of 5% and 7% remained, respectively. Beyond this point, only minor degradation was observed, with final pyrolytic residues of 3.05% for rHIPS and 3.48% for rABS. These findings are consistent with prior studies which typically occurred between 300–450°C, corresponds to the structural decomposition of ABS, followed by a second minor degradation phase around 450–480°C, attributed to the decomposition of residual material [269].

Similarly, LLB particles exhibited a $T_{5\%}$ around 225°C, primarily due to the release of moisture, low-molecular-weight volatile compounds, and amorphous hemicellulose. The major degradation phase in region II, with a mass loss of 67.3% between 206–372°C, is primarily associated with the decomposition of hemicellulose and cellulose [56]. The subsequent degradation in region III, extending up to 700°C, is attributed to lignin decomposition, which exhibits high thermal stability, persisting up to 600°C, as well as the oxidative decomposition of the carbonized residue, ultimately forming a charring residue of 13.73%.

As illustrated in **Figure 6.7b**, the thermal degradation patterns of WPC samples involve multiple degradation phases across regions I to IV. In region I minimal degradation occurred, while regions

II and III feature dominant transition phases, with active pyrolysis shifting towards higher temperatures compared to the degradation profile of pristine LLB particles, which primarily degrade within region II. This shift is likely due to the encapsulation of LLB particles within the polymer matrix, delaying the decomposition of cellulose and lignin. This encapsulation facilitates char carbonization and results in the highest peak intensity in region III, along with an increased T_{max} in this region, coinciding with the major degradation phase of the unreinforced matrices.

The incorporation of impact modifiers, specifically MMBS and EPDM), along with DCP and MA, significantly improved the thermal stability of the modified WPC samples compared to their unmodified counterparts. This enhancement is attributed to the superior thermal stability and improved interfacial compatibility of LLB particles, facilitated by the grafted MA [55]. Notably, in region III, the T_{max} values for composite samples C_AM_{10} and C_AE_{10}, with 10% filler loading shows an increase of around 8.2°C and 5.2°C compared with their uncoupled counterparts (CA_0, 477.5°C). Similarly, T_{max} values for C_HM_{10} and C_HE_{10} demonstrated an increase of 13.7°C and 10°C compared to CH_0 as summarized in **Table 6.2**. A similar trend was observed for $T_{50\%}$, where C_AM_{10} and C_AE_{10} exhibited increases of 11.6°C and 7.4°C, respectively, over CA_0. Likewise, C_HM_{10} and C_HE_{10} displayed 27.7°C and 24.7°C higher $T_{50\%}$ values compared to CH_O (408.4°C). The composites C_AM_a, C_AM_{10}, C_AE_{10}, C_HM_a, C_HM_{10}, and C_HE_{10} demonstrated higher thermal stability, with temperature shifts of 77.7°C, 87.3°C, 83.1°C, 71.8°C, 100.5°C, and 77.5°C, respectively, compared to pristine $T_{50\%}$, of LLB particles.

However, the inherently high carbonization and charring abilities of LLB particles contributed to the stable $T_{25\%}$ values in region IV and beyond. Nevertheless, at a 10 wt.% filler content, $T_{25\%}$ values showed significant increases compared to their uncoupled pristine matrices, with MMBS-containing composites demonstrating superior stability. This suggests improved thermal stability due to enhanced cross-linking within the composite system, particularly in regions II and III. The impact modifiers played a crucial role in improving the thermal stability of LLB and uncoupled composites by facilitating effective matrix encapsulation and enhancing interfacial compatibility.

Correspondingly, the DSC thermographs in **Figure 6.7b** were primarily used to evaluate the glass Tg of rABS, rHIPS, and their respective WPC composites. Recycled ABS and rHIPS exhibited prominent Tg without due to their amorphous nature, as indicated by noticeable changes in heat flow around 100°C. The Tg values for rABS and rHIPS were observed at 104.8°C and 98.3°C,

respectively. However, rABS displayed a minor endothermic peak at 133°C, corresponding to the acrylonitrile transition, as reported in previous studies. Similarly, in rHIPS, the presence of polyolefin impurities was detected in the endothermic curves at approximately 120°C and 160°C, corresponding to PE and PP fractions, respectively [56,270] These impurities likely originated from the recycling process, with PE potentially introduced as a color masterbatch component and PP possibly incorporated due to incorrect material separation. However, these impurities did not significantly alter the material properties; instead, they may have positively influenced the composite system, particularly through synergistic interactions with impact modifiers such as EPDM. The presence of EPDM and MMBS in 10 wt.% composite samples led to a gradual increase in Tg values. The Tg of rHIPS-based composites increased from 98.3°C to 106.4°C (C_HM_{10}) and 107.5°C (C_HE_{10}), while for rABS-based composites, it increased from 104.8°C to 113.5°C (C_AE_{10}) and 117.8°C (C_AM_{10}). This shift to higher Tg values is likely due to restricted polymer chain segment mobility, attributed to LLB particle reinforcement and strong interfacial adhesion, which synergistically resulted in more rigid and compact polymer chains, thereby increasing Tg in the composite blends [269].

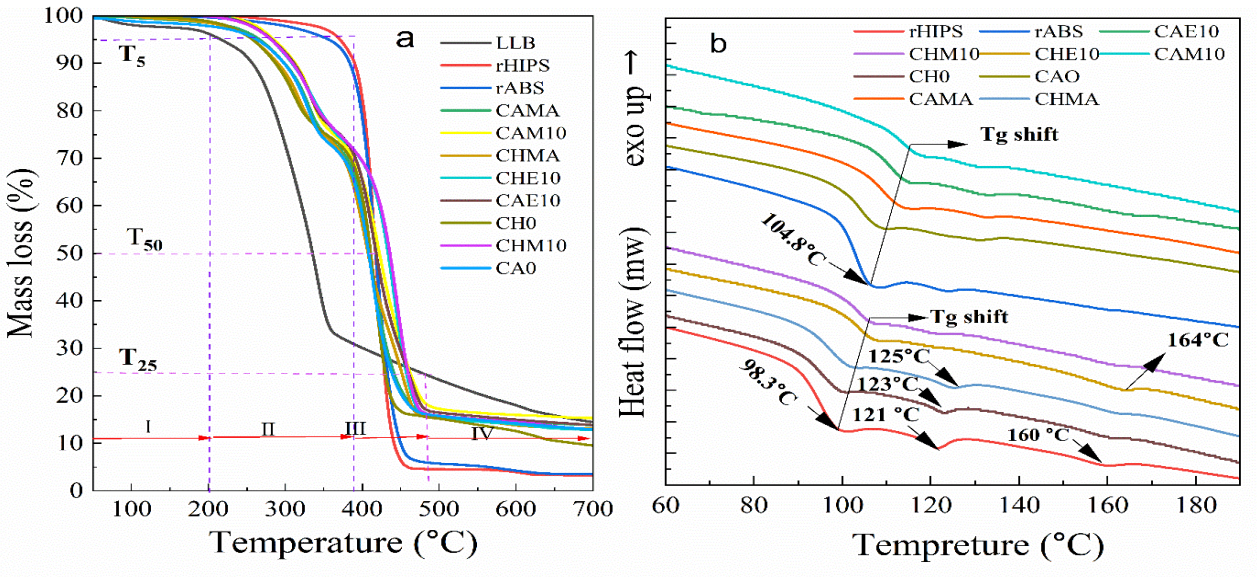

Figure 6. 7 TGA (a) and DSC (b) thermograph representatives WPC samples and matrices

Table 6. 2 Refined data of TGA and DSC curves of representatives' WPCs and matrices

Sample ID	$T_{5\%}$ (°C)	$T_{50\%}$ (°C)	T_{max} (°C)	$T_{75\%}$	Residue at 700°C	Tg from DSC curves (°C)

LLB	225.8	335.6	-	495.7	13.73	-
rHIPS	362.9	411.9	451.9	429.6	3.05	98.3
rABS	348.1	419.7	459.8	432.8	3.48	104.8
CA_0	258.6	405.3	477.4	437.5	13.1	106.8
C_AM_a	263.4	413.3	479.8	440.6	13.2	110.5
C_AM_{10}	273.8	422.9	485.6	462.5	15.3	113.5
C_AE_{10}	277.5	418.7	482.6	460.3	13.6	117.8
CH_0	256.9	408.4	466.8	430.9	10.5	98.9
C_HM_a	260.5	407.4	471.8	451.6	12.01	99.61
C_HM_{10}	278.0	436.0	480.5	459.0	13.1	106.4
C_HE_{10}	276.4	433.1	476.8	455.9	12.8	107.5

6.3.5 Characterizations of chemical bonds

Representative FTIR spectra of the uncoupled samples (CA_0 and CH_0), the coupled and modified WPC samples (C_AE_{10}, C_AM_{10}, C_HM_{10}, and C_HE_{10}), and their individual components (unreinforced matrices rABS, rHIPS, LLB, MA, and DCP) are shown in **Figure 6.8**. The group of spectra on the left (**Figure 6.8a**) presents the rHIPS-based composites, while the group on the right (**Figure 6.8b**) shows the rABS-based composites. Composite samples containing 10% MMBS and EPDM display modified composite interphases compared to the uncoupled samples, as evidenced by differences in their FTIR spectral regions. For instance, in the rABS matrix, the nitrile group –CN peaks at 2237.51 cm^{-1} (triple bond) and 1468 cm^{-1} (double bond) were altered in the WPC samples (C_AH_{10} and C_AM_{10}) compared to the neat rABS and CAMA samples, indicating chemical interactions with the coupling and impact modifiers [271]. Similarly, the peak near 1050 cm^{-1}, attributed to C–O symmetric stretching in cellulose and hemicellulose [56], was also noticeably affected. Furthermore, the broad O–H stretching peak near 3350 cm^{-1}[73], characteristic of lignocellulose, was significantly reduced across the WPC samples, particularly in C_AM_{10}, C_AE_{10}, C_HM_{10}, and C_HE_{10}. This reduction suggests that original –OH groups were involved in the formation of new bonds or interactions. These new interactions likely involve hydrogen bonds formed by nucleophilic substitution between the –OH groups of the LLB cell wall and the carbonyl groups of the MA coupling agent [56], as supported by the reduced carbonyl peak intensity of MA at 1733 cm^{-1} in the coupled composites. Additionally, C–C bond vibrations in

MA were observed at 822 cm^{-1}. Characteristic peaks attributed to C=C stretching of butadiene (1640 cm^{-1}), C=O stretching of ester groups in methyl methacrylate (1732 cm^{-1}), and the monosubstituted benzene ring of styrene (698 cm^{-1}) [75] were also present in the WPCs. These observations suggest the formation of graft copolymers during in situ melt compatibilization. Moreover, some changes were noticed in the unreinforced polymer in the areas of aliphatic C–H asymmetric and symmetric stretching at 2920 cm^{-1} and 2852 cm^{-1} (2960–2830 cm^{-1}), aromatic C–H stretching at 3026 cm^{-1} and 3062 cm^{-1} (3060–3025 cm^{-1}), C–C aromatic stretching at 1603 cm^{-1}, CH_2 deformation within the aromatic C=C ring at 1452 cm^{-1} and 1492 cm^{-1}, and C–H bending in CH_2 at 697 cm^{-1} and 757 cm^{-1} (900–675 cm^{-1}) [56].

These spectral changes were more pronounced in the coupled WPC samples, especially those containing MMBS likely due to enhanced interactions between the coupling agents and the composite systems. Additionally, although bands below 1460 cm^{-1} generally originate from various carbohydrate and lignin vibrations, the band between 1030–1050 cm^{-1}, associated with both cellulose and lignin [255], appeared narrower and less intense in the coupled composites compared to LLB. This narrowing most likely reflects interactions of the impact modifiers, facilitated by DCP-induced crosslinking, leading to improved interphase compatibility and mechanical interlocking. These interactions ultimately contribute to better composite properties, as discussed earlier, and improved morphologies, as revealed by SEM analysis.

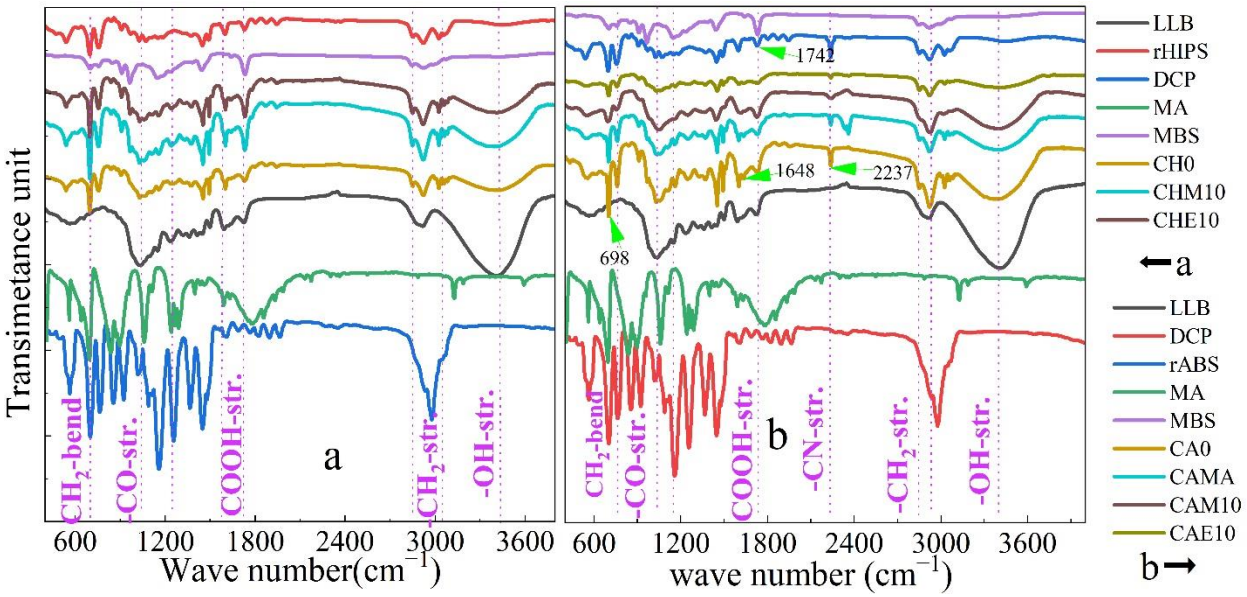

Figure 6. 8 FTIR Spectra of representatives WPCS based on the rHIPS (a) and rABS (b)

6.3.6 SEM morphology

SEM is widely used to examine the polymer phase distribution and surface morphology of materials. SEM images of representative samples obtained following impact strength tests include uncoupled composites (CA_0 and CH_0) shown in **Figure 6. 9**; the MA/DCP-modified composites (C_AM_A and C_HM_A), captured at two locations for comparison, shown in **Figure 6. 10** ; and the reinforced coupled WPCs (C_AM10, C_AE_{10}, C_HM_{10}, and C_HE_{10}), captured at one location, shown in **Figure 6. 11**. The morphology of the uncoupled composites (**Figure 6.9a–d**) reveals weak reinforcement by LLB particles, as indicated by the extensive presence of particle pull-out holes within the layered structures, significant debonding leading to the removal of LLB particles, formation of large voids, and poor interfacial homogeneity. **Figures 6.8c and 6.d** clearly demonstrate severe debonding, as evidenced by the presence of large cavities dispersed by voids across the fractured surfaces. Moreover, **Figures 6.9a and b** reveal a clearly visible interface between the continuous and dispersed phases, indicating poor compatibility. Conversely, the SEM images of the coupled composites demonstrate that the LLB particles were significantly embedded within the polymer matrix. This effect was particularly pronounced in the composites containing 10 wt. % reinforcement, as well as in the C_AM_a (**Figure 6.10e, f**) and C_HMa (Figure **6.10 g, h**) samples, albeit to a lesser extent. In addition, the interface between the distributed and continuous phases appeared blurred, suggesting improved compatibility. Moreover, the fracture surfaces in **Figures 11i–l** exhibit well-bonded particles, a uniform distribution of tearing ridges, and compact polymer coatings that remained intact after impact testing, suggesting the formation of an immobilized viscous layer that flows over the surface cracks and fills them. **Figures 6.11i**,**j** show minimal voids, gaps, or signs of particle pull-out, confirming the improved impact resistance of the coupled composites, and **Figures 6.11k,** l further indicate enhanced interfacial adhesion between the LLB particles and polymer matrix, as evidenced by the breakage matrix bound surfaces and LLB particles during impact, along with tearing edges including effective rubber coatings (**Figure 6.11of l**). The observed surface morphology reflects a tearing-dominated failure mechanism rather than particle pull-out, unlike **Figures 6.9a–b**. The improved particle–matrix interaction leads to enhanced mechanical and thermal properties compared to those of uncoupled composites, enabling more efficient stress transfer from the matrix to the reinforcement. These results are consistent with those of previous studies [26,31,32] and are further supported by the observed improvements in the mechanical performance and

hydrophobicity of the coupled composites. Uniform particle dispersion, achieved through the synergistic use of impact modifiers and interfacial modifiers such as DCP and MA, confirms their effectiveness in developing WPCs with favorable mechanical strength and better dimensional stability.

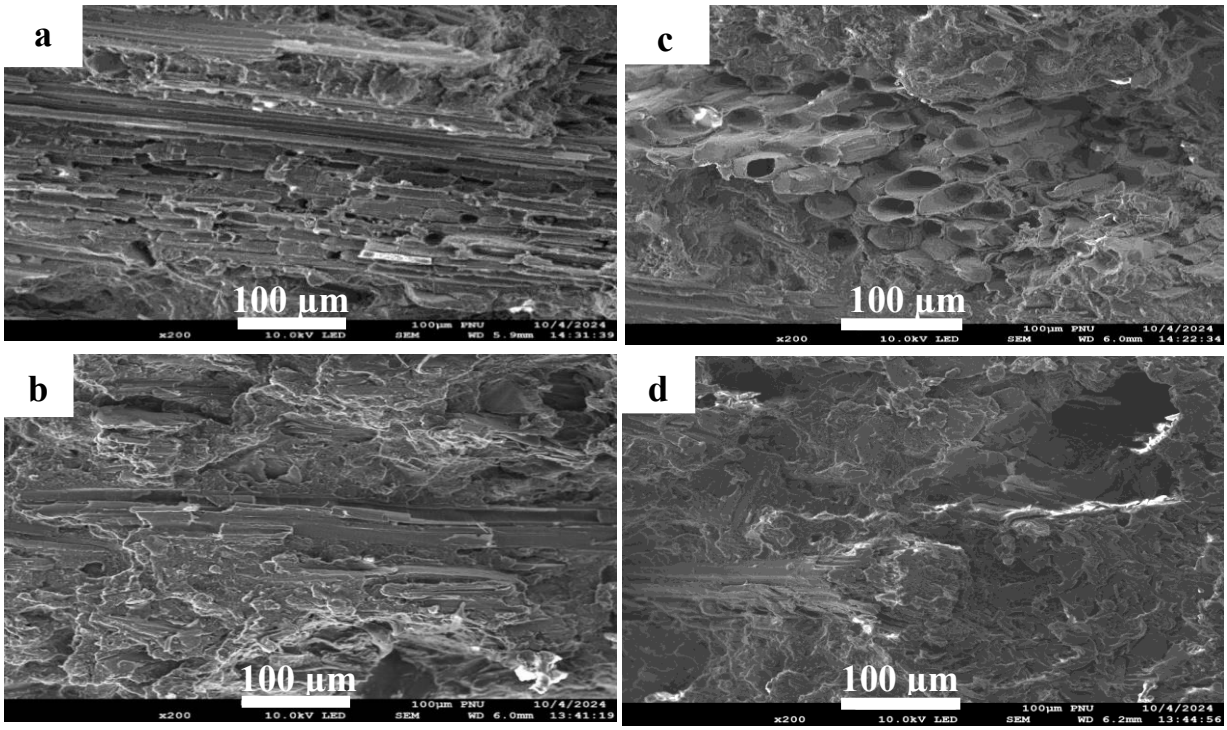

Figure 6. 9 CA_0 (a,b) and CH_0 (c d) two different sites

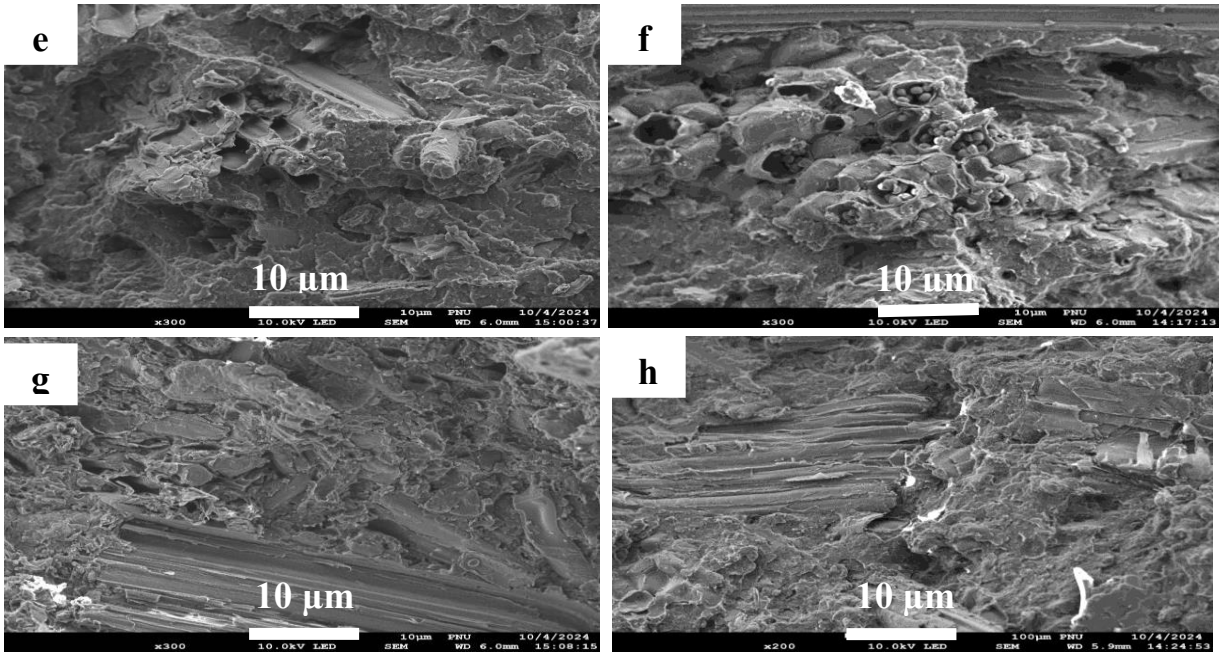

Figure 6. 10 the C_AM_a (e,f) and C_HM_a (g,h) composite morphology at two different sites

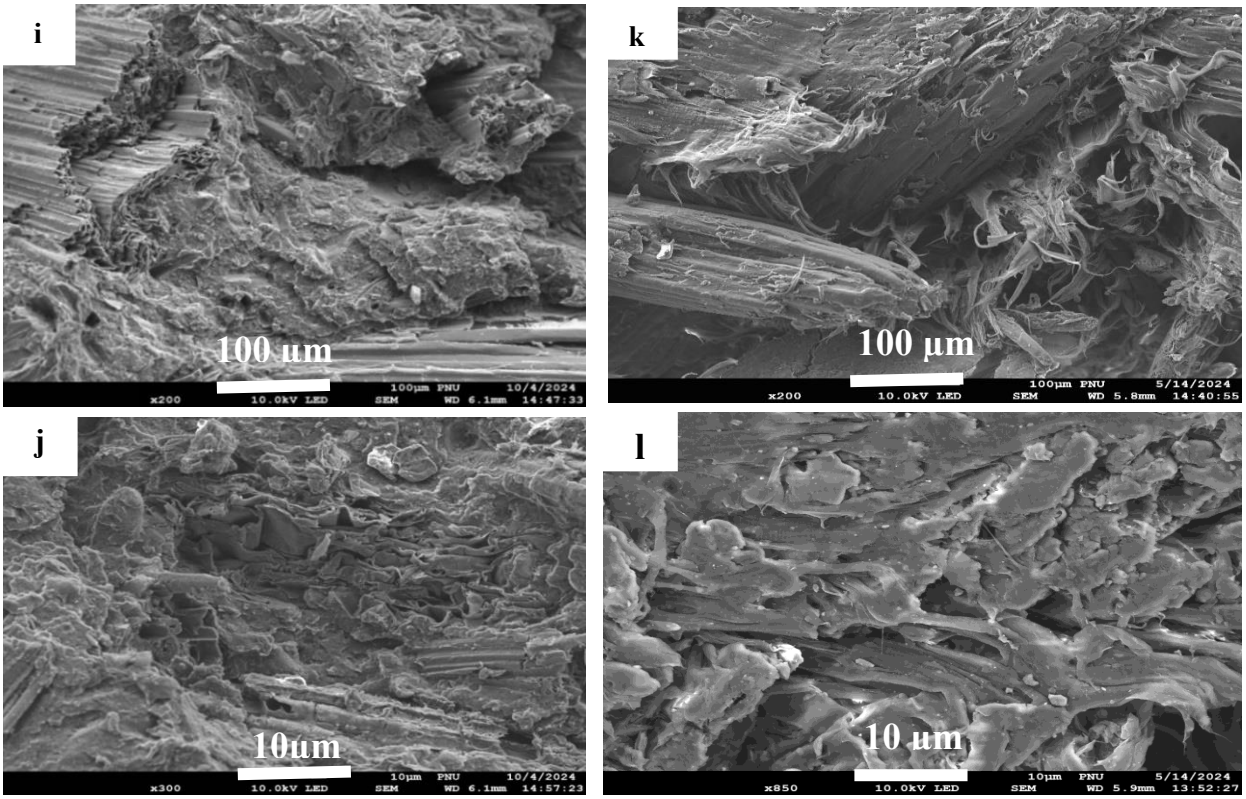

Figure 6. 11 C_AM_{10} (i), C_AE_{10} (j), C_HM_{10} (k) and C_HE_{10}(l) composite morphology

6.3 Chapter Summary

In this study, novel high-performance WPCs were developed using recycled ABS and HIPS from electronic waste as polymer matrices, reinforced with LLB particles reinforcement. Multipurpose MMBS and EPDM were employed as impact modifiers, while MA and DCP were applied through in situ reactive melt compatibilization, resulting in significantly improved interfacial adhesion, strength, and toughness.

The effects of varying impact modifier concentrations (5–15 wt.%) were systematically evaluated while maintaining constant MA and DCP contents. The composites exhibited notable improvements in mechanical properties, thermal stability, dimensional stability, and water resistance. MMBS-modified rABS composites displayed superior tensile and flexural strength, modulus of rupture, and storage modulus, with optimal performance achieved at 10 wt.% MMBS, 1 wt.% DCP, and 0.5 wt.% MA. The rABS-based composites reached a maximum flexural strength of 74.5 MPa, representing a 32.2% improvement over unreinforced matrices, while

rHIPS-based composites showed up to 45.4% enhancement, highlighting the effectiveness of crosslinking and uniform LLB dispersion.

Increasing EPDM content slightly reduced stiffness and strength but markedly improved impact strength, toughness, dimensional stability, water resistance, and thermal stability. The highest impact performance was observed for 15 wt.% MMBS (18.25 KJ/m²) and 15 wt.% EPDM (14.56 KJ/m²), with the high LLB content preserving stiffness while promoting a transition from brittle to ductile behavior, as confirmed by shifts in glass transition temperatures from DMTA and DSC analyses.

Overall, this study demonstrates that carefully tailored incorporation of impact modifiers below 10 wt.% in rABS- and rHIPS-based composites achieves an optimal balance of stiffness and toughness. The resulting WPCs outperform conventional polyolefin-based composites in mechanical strength, dimensional stability, and water resistance, offering promising lightweight, durable, and cost-effective alternatives for building applications such as decking, wall panels, floors, and interior finishes. Furthermore, this work supports circular economy by recycling E-waste-derived polymers, promoting sustainable and eco-friendly composite development while retaining and prolonging valuable rABS and rHIPS in the product lifecycle.

CHAPTER SEVEN

General conclusion and recommendations

7.1 Conclusion

This study explored the development of novel WPCs by utilizing a diverse range of multicomponent recycled thermoplastics sourced from municipal solid waste. These included post-consumer recycled PE fractions (rLLDPE, rMDPE, rHDPE) and electronic waste fractions (rPS, rHIPS, and rABS), which were reinforced with Ethiopian indigenous LLB particles as the novel reinforcements. The research focused on evaluating the formulation and combined performance of these WPCs, particularly those produced through polyblend system and in situ melt compatibilization techniques.

The compositional characterization of the indigenous Ethiopian lowland bamboo (LLB) biomass revealed a high cellulose content (57.16 wt.%), along with lignin (14.29 wt.%) and hemicellulose (25.94 wt.%). This relatively high cellulose fraction compared to many other bamboo species highlights the potential of LLB as a sustainable and effective alternative to conventional wood fibers in WPC formulations. Furthermore, the presence of residual elements (Ti, Ba, Cl, Zn, Pd, Hg, Br, and Cr VI) and PAHs in the recycled thermoplastic fractions remained below threshold limits implying suitability as secondary raw materials for WPC production.

WPCs produced from recycled polyethylene polyblends—rLLDPE, rMDPE, and rHDPE—reinforced with LLB particles and compatibilized with MAPP exhibited significantly enhanced interfacial strength. The ultimate tensile strength TS and flexural strength decreased with increasing LLB particle content from 40% to 60%, with optimal mechanical performance observed at 40% loading due to improved melt flow and matrix encapsulation in the PE polyblend-based WPCs. Nevertheless, even at higher LLB loadings (60%), the incorporation of MAPP effectively preserved considerable mechanical integrity. In contrast, flexural modulus and tensile modulus increased with higher LLB content across all formulations, with only minimal variations attributed to the MAPP compatibilizer. Furthermore, WPCs formulated from an equal-melt blend composition of MAPP-coupled rLLDPE, rMDPE, and rHDPE (EM) exhibited unexpectedly improved performance despite the inherent immiscibility of the components. This

improvement was attributed to thermally induced chemical coupling, which enhanced compatibility and facilitated the efficient dispersion of bamboo particles, thereby promoting mechanical interlocking and effective blending of the less mechanically robust rLLDPE with rMDPE and rHDPE. Notably, the impact strength of EM-based WPCs increased by 23.4–44.2% compared to rHDPE-based matrices and by 18.5–28.6% relative to rMDPE-based composites, while maintaining desirable mechanical and thermal properties. These enhancements demonstrate a consistent improvement in toughness due to the EM matrix, resulting from the synergistic effect of incorporating flexible rLLDPE components. Thermal stability also showed significant improvement in EM-based WPCs, benefiting from the inherently high thermal resistance of the rHDPE matrix.

WPCs developed from LLB particles, rHDPE, rPS, and their equal blends demonstrated significantly enhanced interfacial strength through in-situ reactive compounding with MAPP and DCP. This approach improved interphase integrity via thermal and chemical crosslinking, leading to chemical interactions and mechanical interlocking of fibers. Although ultimate tensile and flexural strengths declined with higher LLB loadings across both particle size ranges (<0.5 mm and 0.5–1 mm), broader particle size distributions helped maintain overall performance. In contrast, tensile and flexural modulus demonstrates increasing trends. Coupled and crosslinked composites outperformed their uncoupled and unblended counterparts with particles size fractions below 500μm performs better properties across all formulations. Similarly Impact strength improved significantly with DCP and MAPP additions in equal blend WPCs which are collective compatibility and shared toughness and ductility of rHDPE. Dynamic mechanical analysis showed higher storage modulus and lower damping for composites with <0.5 mm particles, with a shift in tanδ peak to higher temperatures and retention of stiffness below Tg equally justifying the better interface with the particle size distributions below 0.5mm. Similarly, thermal stability from TGA and endothermic melting point from DSC increased significantly with the coupled WPCs implying uniform particle dispersion and improved interfacial adhesion with better nucleation in WPCs produced from small size particles distribution of less than 0.5mm than the larger size ranging from 0.5mm to 1mm.

WPCs formulated using an equal-weight blend of rHDPE and rPS as the polymer matrix, reinforced with 50 wt.% LLB particles varied at 3% 5% 7% and 10% (wt.%) for both SEBS-g-

MA and MAPP and crosslinked with DCP revealed a notable improvement in toughness with increasing levels of both compatibilizers. However, SEBS-g-MA showing the most pronounced effect at all respective compositions attributed to the flexible ethylene-butylene segments within its structure. In contrast, MAPP combined with DCP resulted superior tensile strength, flexural properties, and storage modulus compared to uncoupled composites. These properties improved from 3% to 5% MAPP content, followed by a decline at higher concentrations, indicating that the optimal performance was achieved with 5% MAPP and 1% DCP (wt.). For SEBS-g-MA, the best balance of tensile, flexural, and storage modules was observed at 3% combined with 1% DCP. Mechanical tests demonstrated MAPP's strong effectiveness in enhancing tensile and flexural strength, while SEBS-g-MA provided synergistic improvements in impact strength and interfacial compatibility for the rPS/rHDPE-based WPCs. Additionally, water absorption and thermal dimensional stability improved significantly with higher SEBS-g-MA content but decreased with increasing MAPP content. These findings suggest that SEBS-g-MA-based composites are better suited for applications requiring enhanced dimensional stability, moisture resistance, and resilience to sudden impacts, whereas MAPP-based composites are more appropriate for applications demanding higher stiffness and mechanical strength.

High-performance WPCs formulated using rABS and rHIPS, both sourced from electronic waste, as the polymer matrices with 50 wt.% LLB particles with inclusion of EPDM and MMBS contents varied at 5%, 10%, and 15% (wt. based) with fixed MA (0.5 wt.%) and DCP (1 wt.%) revealed substantial improvements in mechanical strength, thermal and dimensional stability, and water resistance showing MMBS superior compatibility with both matrices, particularly enhancing tensile strength, flexural strength, modulus of rupture, and storage modulus. Recycled ABS-based composites consistently outperformed rHIPS-based ones, with the optimal formulation identified at 10% MMBS, 1% DCP, and 0.5 % MA—beyond which mechanical properties declined. At this optimal composition, rABS-based composites achieved a maximum flexural strength peak of 70.5 MPa, reflecting a 32.2% increase over the unmodified matrix. Similarly, rHIPS-based composites showed up to a 45.4% improvement in flexural strength, underscoring the effectiveness of crosslinking and uniform dispersion of LLB particles. While increasing EPDM content resulted in a slight decrease in tensile and flexural properties, it led to notable gains in impact strength, toughness, dimensional stability, resistance to water absorption and thermal degradation—making EPDM-based composites especially suitable for long-lasting outdoor applications like

decking. Similarly, the impact strength was highly dependent on both type and concentration of impact modifiers. MMBS-modified rABS composites exhibited a 52% increase in impact resistance, whereas EPDM-based composites achieved a 48.76% gain. The highest impact values peaks were recorded at 15 wt.% MMBS of C_AM_{15} (18.25 kJ/m²), followed by C_HM_{15} (15.5 kJ/m²), and finally C_HH_{15} (14.56 kJ/m²). The high LLB content contributed to maintaining overall composite stiffness, while the synergistic effect of MA and DCP enhanced interfacial bonding, promoting a transition from brittle to ductile behavior as evidenced by changes Tg evaluated by both DMTA and DSC. These demonstrate the critical role of impact modifiers in tailoring the mechanical, thermal, and moisture-resistant properties of WPCs. An optimal balance between toughness and stiffness can be achieved by fine-tuning MMBS and EPDM concentrations within rABS and rHIPS matrices up to 10wt.% of both EPDM and MMBS.

In conclusion, WPCs formulated from recycled thermoplastics and Ethiopian LLB particles present a sustainable and practical alternative to conventional wood and polyolefin-based composites. The application of in-situ reactive melt compatibilization—facilitated by coupling agents and crosslinkers—led to significant improvements in interfacial adhesion, mechanical strength, thermal stability, and moisture resistance. These composites met key minimum requirements of international standards (ISO 178, ASTM D6109, ASTM D7032) for flexural and tensile properties, with optimal performance achieved at 40–60% wood fiber or polymer content. The resulting materials are most probably well-suited for use in affordable housing, particularly in non-load-bearing applications such as interior architectural elements, decking, wall cladding, ceiling boards, furniture, and insulation panels while simultaneously transforming plastic waste into eco-friendly, cost-effective building materials. It also reduces reliance on virgin polymers and minimizes the need for energy-intensive fiber processing, thereby contributing to circular economy goals.

7. 2 Future Recommendation

The following key areas are recommended for future research to advance the development and application of WPCs. First, large-scale production requires evaluating the performance of formulated WPCs under diverse environmental conditions—such as moisture, UV exposure, and temperature fluctuations—to ensure durability and long-term reliability in real-world applications like flooring, decking, and cladding. Findings on reactive melt compatibilization are

recommended to be repeated into industrial-scale processes (e.g., extrusion and injection molding) specifically for equal blend ratios of both matric and LLB reinforcements, which necessitates optimizing processing parameters including temperature, pressure, screw speed, and residence time to maintain consistent compatibilization reactions at larger scales to better assess the effects of realistic processing conditions.

Further investigations, such as shear rheological studies, are needed to explore the relationship between rheology and morphology, as well as to assess the life cycle assessments of WPCs developed via reactive melt compatibilization. For scale-up studies, a wide range of experimental variables must be considering optimizing extrusion systems with respect to particle size distribution, degradation behavior, retention characteristics, barrel temperature profiles (feeding, melting, mixing, forming), cooling rates, screw speed, and extruder design configurations.

Additionally, benchmarking the various fractions of thermoplastic waste and identifying specific target applications can help unlock the full potential of WPCs. Similarly, effective recycling of the thermoplastic using advanced technologies for sorting and processing secondary raw materials to ensure quality and purity should be investigated. Further research should also address the effects of recycled thermoplastics on long-term durability, as well as investigate suitable coatings to mitigate any residual odors observed with WPCs made from recycled materials.

References

[1] Chen, L., Msigwa, G., Yang, M. et al. Strategies to achieve a carbon neutral society: a review. Environ Chem Lett 20, 2277–2310 (2022). https://doi.org/10.1007/s10311-022-01435-8.

[2] O. Faruk, A.K. Bledzki, H.P. Fink, M. Sain, Biocomposites reinforced with natural fibers: 2000-2010, Prog. Polym. Sci. 37 (2012) 1552–1596. https://doi.org/10.1016/j.progpolymsci.2012.04.003.

[3] L. Teuber, V.S. Osburg, W. Toporowski, H. Militz, A. Krause, Wood polymer composites and their contribution to cascading utilisation, J. Clean. Prod. 110 (2016) 9–15. https://doi.org/10.1016/j.jclepro.2015.04.009.

[4] K. D. Ayana , CS. Ha, A.Y Ali, Comprehensive overview of wood polymer composite : Formulation and technology , properties , interphase modification , and characterization, Sustain. Mater. Technol. 40 (2024) e00983. https://doi.org/10.1016/j.susmat.2024.e00983.

[5] G. Schiller, J. Roscher, Impact of urbanization on construction material consumption: A global analysis, J. Ind. Ecol. 27 (2023) 1021–1036. https://doi.org/10.1111/jiec.13392.

[6] M. Nodehi, V.M. Taghvaee, Applying Circular Economy to Construction Industry through Use of Waste Materials: A Review of Supplementary Cementitious Materials, Plastics, and Ceramics, Circ. Econ. Sustain. 2 (2022). https://doi.org/10.1007/s43615-022-00149-x.

[7] M.G. Kibria, N.I. Masuk, R. Safayet, H.Q. Nguyen, M. Mourshed, Plastic Waste: Challenges and Opportunities to Mitigate Pollution and Effective Management, Springer International Publishing, 2023. https://doi.org/10.1007/s41742-023-00507-z.

[8] KD Ayana, AY Ali, C-S Ha, Wood Polymer Composites Based on the Recycled Polyethylene Blends from Municipal Waste and Ethiopian Indigenous Bamboo (Oxytenanthera abyssinica) Fibrous Particles Through Chemical Coupling Crosslinking. Polymers. 16(21)(2024) 2982. https://doi.org/10.3390/polym16212982.

[9] Q. Zhang, D. Zhang, H. Xu, W. Lu, X. Ren, H. Cai, H. Lei, E. Huo, Y. Zhao, M. Qian, X. Lin, E.M. Villota, W. Mateo, Biochar filled high-density polyethylene composites with excellent properties: Towards maximizing the utilization of agricultural wastes, Ind. Crops Prod. 146 (2020) 112185. https://doi.org/10.1016/j.indcrop.2020.112185.

[10] L.P. Dos Santos, E. Trombetta, T.S. Flores-Sahagun, K.G. Satyanarayana, Effect of domestic compatabilizer on the performance of polypropylene-sawdust composites, J. Compos. Mater. 50 (2016) 1353–1365. https://doi.org/10.1177/0021998315591046.

[11] J. Geldermann, L.M. Kolbe, A. Krause, C. Mai, H. Militz, V.S. Osburg, A. Schöbel, M. Schumann, W. Toporowski, S. Westphal, Improved resource efficiency and cascading utilisation of renewable materials, J. Clean. Prod. 110 (2016) 1–8. https://doi.org/10.1016/j.jclepro.2015.09.092.

[12] Y.M. Song, Q.W. Wang, G.P. Han, H.G. Wang, H. Gao, Effects of two modification methods on the mechanical properties of wood flour/recycled plastic blends composites: Addition of thermoplastic elastomer SEBS-g-MAH and in-situ grafting MAH, J. For. Res. 21 (2010) 373–378. https://doi.org/10.1007/s11676-010-0084-1.

[13] A.S. Mohammed, M. Meincken, Properties of low-cost WPCs made from alien invasive trees and rLDPE for interior use in social housing, Polymers (Basel). 13 (2021). https://doi.org/10.3390/polym13152436.

[14] J. Andrzejewski, M. Barczewski, D. Czarnecka-Komorowska, T. Rydzkowski, K. Gawdzińska, V.K. Thakur, Manufacturing and characterization of sustainable and recyclable wood-polypropylene biocomposites: Multiprocessing-properties-structure relationships, Ind. Crops Prod. 207 (2024). https://doi.org/10.1016/j.indcrop.2023.117710.

[15] V. Kumar, L. Tyagi, S. Sinha, Wood flour-reinforced plastic composites: A review, Rev. Chem. Eng. 27 (2011) 253–264. https://doi.org/10.1515/REVCE.2011.006.

[16] U. Qasim, M. Ali, T. Ali, R. Iqbal, F. Jamil, Biomass derived Fibers as a Substitute to Synthetic Fibers in Polymer Composites, ChemBioEng Rev. 7 (2020) 193–215. https://doi.org/10.1002/cben.202000002.

[17] A. Manral, P. Kumar Bajpai, F. Ahmad, R. Joshi, Processing of sustainable thermoplastic based biocomposites: A comprehensive review on performance enhancement, J. Clean. Prod. 316 (2021) 128068. https://doi.org/10.1016/j.jclepro.2021.128068.

[18] A. Karimah, M.R. Ridho, S.S. Munawar, D.S. Adi, Ismadi, R. Damayanti, B. Subiyanto, W. Fatriasari, A. Fudholi, A review on natural fibers for development of eco-friendly bio-composite: characteristics, and utilizations, J. Mater. Res. Technol. 13 (2021) 2442–2458. https://doi.org/10.1016/j.jmrt.2021.06.014.

[19] N. Ehiosu, S. Rusnakova, A. Ebele, R. Olabanji, S. Onyedekachi, A. Nosakhare, A comprehensive review of natural fiber reinforced Polymer composites as emerging materials for sustainable applications, Appl. Mater. Today 43 (2025) 102666. https://doi.org/10.1016/j.apmt.2025.102666.

[20] M.A. Hubbe, W. Grigsby, From nanocellulose to wood particles: A review of particle size vs. the properties of plastic composites reinforced with cellulose-based entities, BioResources 15 (2020) 2030–2081. https://doi.org/10.15376/biores.15.1.2030-2081.

[21] E.O. Olakanmi, M.J. Strydom, Critical materials and processing challenges affecting the interface and functional performance of wood polymer composites (WPCs), Mater. Chem. Phys. 171 (2016) 290–302. https://doi.org/10.1016/j.matchemphys.2016.01.020.

[22] A.H. Elsheikh, H. Panchal, S. Shanmugan, T. Muthuramalingam, A.M. El-Kassas, B. Ramesh, Recent progresses in wood-plastic composites: Pre-processing treatments, manufacturing techniques, recyclability and eco-friendly assessment, Clean. Eng. Technol. 8 (2022) 100450. https://doi.org/10.1016/j.clet.2022.100450.

[23] S.R. Mousavi, M.H.Zamani, S.Estaji, et al. Mechanical properties of bamboo fiber-reinforced polymer composites: a review of recent case studies, J Mater Sci 57 (2022), 3143–316. https://doi.org/10.1007/s10853-021-06854-6

[24] M.M.A. Nassar, K.I. Alzebdeh, T. Pervez, N. Al-Hinai, A. Munam, Progress and challenges in sustainability, compatibility, and production of eco-composites: A state-of-art review, J. Appl. Polym. Sci. 138 (2021). https://doi.org/10.1002/app.51284.

[25] S. Migneault, A. Koubaa, P. Perré, B. Riedl, Effects of wood fiber surface chemistry on strength of wood-plastic composites, Appl. Surf. Sci. 343 (2015) 11–18. https://doi.org/10.1016/j.apsusc.2015.03.010.

[26] K.D. Ayana, M. De Angelis, G. Schmidt, A. Krause, A.Y. Ali, Valorization of Potential Post-Consumer Polyethylene (PE) Plastics Waste and Ethiopian Indigenous Highland Bamboo (EHB) for Wood Plastic Composite (WPC): Experimental Evaluation and Characterization, Fibers 10 (2022) 85. https://doi.org/10.3390/fib10100085.

[27] H. Hong, H. Liao, H. Zhang, H. He, T. Liu, D. Jia, Significant improvement in performance of recycled polyethylene/wood flour composites by synergistic compatibilization at multi-scale interfaces, Compos. Part A Appl. Sci. Manuf. 64 (2014) 90–98. https://doi.org/10.1016/j.compositesa.2014.04.022.

[28] C. Zárate-Pérez, R. Ramírez-Aguilar, E.A. Franco-Urquiza, C. Sánchez-Alvarado, The Role of Coupling Agents in the Mechanical and Thermal Properties of Polypropylene/Wood Flour Composites, Macromol 3 (2023) 65–78. https://doi.org/10.3390/macromol3010006.

[29] H. Gao, Y. Xie, R. Ou, Q. Wang, Grafting effects of polypropylene/polyethylene blends with maleic anhydride on the properties of the resulting wood-plastic composites, Compos. Part A Appl. Sci. Manuf. 43 (2012) 150–157. https://doi.org/10.1016/j.compositesa.2011.10.001.

[30] G. Chen, A. Gupta, T.H. Mekonnen, Silane-modified wood fiber filled EPDM bio-composites with improved thermomechanical properties, Compos. Part A Appl. Sci. Manuf. 159 (2022) 107029. https://doi.org/10.1016/j.compositesa.2022.107029.

[31] M. Ghorbani, N. Poorzahed, S.M. Amininasab, Morphological, physical, and mechanical properties of silanized wood-polymer composite, J. Compos. Mater. 54 (2020) 1403–1412. https://doi.org/10.1177/0021998319881493.

[32] Y. Xie, C.A.S. Hill, Z. Xiao, H. Militz, C. Mai, Silane coupling agents used for natural fiber/polymer composites: A review, Compos. Part A Appl. Sci. Manuf. 41 (2010) 806–819. https://doi.org/10.1016/j.compositesa.2010.03.005.

[33] A. Shavandi, M.A. Ali, Graft polymerization onto wool fibre for improved functionality, Prog. Org. Coatings 130 (2019) 182–199. https://doi.org/10.1016/j.porgcoat.2019.01.054.

[34] M. Dun, H. Fu, J. Hao, W. Shan, W. Wang, Tailoring flexible interphases in bamboo fiber-reinforced linear low-density polyethylene composites, Compos. Part A Appl. Sci. Manuf. 150 (2021) 106606. https://doi.org/10.1016/j.compositesa.2021.106606.

[35] L. Du, Y. Li, S. Lee, Q. Wu, Water absorption properties of heat-treated bamboo fiber and high density polyethylene composites, BioResources 9 (2014) 1189–1200. https://doi.org/10.15376/biores.9.1.1189-1200.

[36] Y. Martinez Lopez, J.B. Paes, D. Gustave, F.G. Gonçalves, F.C. Méndez, A.C. Theodoro Nantet, Production of wood-plastic composites using cedrela odorata sawdust waste and recycled thermoplastics mixture from post-consumer products - A sustainable approach for cleaner production in Cuba, J. Clean. Prod. 244 (2020). https://doi.org/10.1016/j.jclepro.2019.118723.

[37] R.M. Abhilash, G.S. Venkatesh, S.S. Chauhan, Development of bamboo polymer

composites with improved impact resistance, Polym. Polym. Compos. 29 (2021) S464–S474. https://doi.org/10.1177/09673911211009369.

[38] Y. Wang, M. Zou, K. Gao, W. Guo, G. Wang, Q. Tang, Effects of surface modification on the physical, mechanical, and thermal properties of bamboo-polypropylene composites, BioResources 15 (2020) 6230–6243. https://doi.org/10.15376/biores.8.3.6230-6243.

[39] C. Wang, J. Mei, L. Zhang, High-added-value biomass-derived composites by chemically coupling post-consumer plastics with agricultural and forestry wastes, J. Clean. Prod. 284 (2021) 124768. https://doi.org/10.1016/j.jclepro.2020.124768.

[40] S.A. Bahari, W. Grigsby, A. Krause, Thermal stability of processed PVC/bamboo blends: effect of compounding procedures, Eur. J. Wood Wood Prod. 75 (2017) 147–159. https://doi.org/10.1007/s00107-016-1148-5.

[41] S.A. Bahari, A. Krause, Utilizing Malaysian bamboo for use in thermoplastic composites, J. Clean. Prod. 110 (2016) 16–24. https://doi.org/10.1016/j.jclepro.2015.03.052.

[42] L.P. Fonseca, W.R. Waldman, M.A. De Paoli, ABS composites with cellulose fibers: Towards fiber-matrix adhesion without surface modification, Compos. Part C Open Access 5 (2021) 100142. https://doi.org/10.1016/j.jcomc.2021.100142.

[43] B. Tansel, From electronic consumer products to e-wastes: Global outlook, waste quantities, recycling challenges, Environ. Int. 98 (2017) 35–45. https://doi.org/10.1016/j.envint.2016.10.002.

[44] P.G.C. Nayanathara Thathsarani Pilapitiya, A.S. Ratnayake, The world of plastic waste: A review, Clean. Mater. 11 (2024) 100220. https://doi.org/10.1016/j.clema.2024.100220.

[45] R. Geyer, J.R. Jambeck, K.L. Law, Production, use, and fate of all plastics ever made, Sci. Adv. 3 (2017) 25–29. https://doi.org/10.1126/sciadv.1700782.

[46] D. Rajasekaran, P.K. Maji, Recycling of waste PP and crumb rubber together by use of self-healing ionomer as process compatibilizer, J. Mater. Cycles Waste Manag. 23 (2021) 1058–1070. https://doi.org/10.1007/s10163-021-01194-8.

[47] Y. Miao, A. von Jouanne, A. Yokochi, Current technologies in depolymerization process and the road ahead, Polymers (Basel). 13 (2021) 1–17. https://doi.org/10.3390/polym13030449.

[48] S.M. Al-Salem, P. Lettieri, J. Baeyens, Recycling and recovery routes of plastic solid

waste (PSW): A review, Waste Manag. 29 (2009) 2625–2643. https://doi.org/10.1016/j.wasman.2009.06.004.

[49] Plastics recycling and waste management in the US - ScienceDirect, (n.d.). https://www.sciencedirect.com/science/article/abs/pii/S092134499900049X (accessed March 23, 2021).

[50] O.A. Oumer, K. Dagne, T. Feyissa, K. Tesfaye, J. Durai, M.Z. Hyder, Genetic diversity, population structure, and gene flow analysis of lowland bamboo [Oxytenanthera abyssinica (A. Rich.) Munro] in Ethiopia, Ecol. Evol. 10 (2020) 11217–11236. https://doi.org/10.1002/ece3.6762.

[51] A. Anjulo, Y. Mulatu, B. Kidane, S. Reza, A. Getahun, S. Mulat, M. Abere, U. Teshome, Oxytenanthera abyssinica A. Rich. Munro species-site suitability matching in Ethiopia, Adv. Bamboo Sci. 1 (2022) 100001. https://doi.org/10.1016/j.bamboo.2022.100001.

[52] A. Anjulo, Y. Mulatu, B. Kidane, S. Reza, A. Getahun, S. Mulat, M. Abere, U. Teshome, Oxytenanthera abyssinica A. Rich. Munro species-site suitability matching in Ethiopia, Adv. Bamboo Sci. 1 (2022) 100001. https://doi.org/10.1016/j.bamboo.2022.100001.

[53] F. Bakala, T. Bekele, T. Woldeamanuel, E. Auch, Value Chain Analysis of Lowland Bamboo Products: The Case of Homosha District, Northwestern Ethiopia, 6 (2016) 1–15.

[54] Z. Mekonnen, A. Worku, T. Yohannes, M. Alebachew, D. Teketay, H. Kassa, Bamboo resources in Ethiopia: Their value chain and contribution to livelihoods, Ethnobot. Res. Appl. 12 (2014) 511–524. https://doi.org/10.17348/era.12.0.511-524.

[55] K.D. Ayana, A.Y. Ali, C.S. Ha, Wood polymer composite (WPC) formulation from Ethiopian indigenous lowland bamboo particles and post-consumer plastic blends: synergetic and dual effects of both coupling agent and organic crosslinking catalyst. Macromol. Res. 33(2025) 479–496. https://doi.org/10.1007/s13233-024-00347-6.

[56] K.D. Ayana, C. Ha, A.Y. Ali, Property optimization of wood polymer composites (WPC) formulated from recycled thermoplastic blends and bamboo particles reinforcements by cross-linking coupling agent and initiator catalyst, Compos. Interfaces 32(9) (2025) 1–23. https://doi.org/10.1080/09276440.2025.2467689.

[57] F. Mengeloglu, L.M. Matuana, J.A. King, Effects of impact modifiers on the properties of rigid PVC/wood-fiber composites, J. Vinyl Addit. Technol. 6 (2000) 153–157. https://doi.org/10.1002/vnl.10244.

[58] Limited, W.P. Wood Polymer Composites (WPCs); Woodhead Publishing Limited: Sawston, UK, 2008.

[59] J.A. Simão, J.M. Marconcini, L.H. Capparelli Mattoso, A.R. Sanadi, Effect of SEBS-MA and MAPP as coupling agent on the thermal and mechanical properties in highly filled composites of oil palm fiber/PP, Compos. Interfaces 26 (2019) 699–709. https://doi.org/10.1080/09276440.2018.1530916.

[60] S.K. Yeh, C.C. Hsieh, H.C. Chang, C.C.C. Yen, Y.C. Chang, Synergistic effect of coupling agents and fiber treatments on mechanical properties and moisture absorption of polypropylene-rice husk composites and their foam, Compos. Part A Appl. Sci. Manuf. 68 (2015) 313–322. https://doi.org/10.1016/j.compositesa.2014.10.019.

[61] W. Dokmai, T. Ratanawilai, Improved mechanical, thermal, and flame-retardant properties of hybrid composites with different recycled plastics, Polym. Bull. 81 (2024) 8119–8139. https://doi.org/10.1007/s00289-023-05089-6.

[62] C.H. Chen, C.L. Chiang, W.J. Chen, M.Y. Shen, The effect of mbs toughening for mechanical properties of wood-plastic composites under environmental ageing, Polym. Polym. Compos. 26 (2018) 45–57. https://doi.org/10.1177/096739111802600106.

[63] D. Basalp, F. Tihminlioglu, S.C. Sofuoglu, F. Inal, A. Sofuoglu, Utilization of Municipal Plastic and Wood Waste in Industrial Manufacturing of Wood Plastic Composites, Waste and Biomass Valorization 11 (2020) 5419–5430. https://doi.org/10.1007/s12649-020-00986-7.

[64] M. Dun, H. Fu, J. Hao, W. Shan, W. Wang, Tailoring flexible interphases in bamboo fiber-reinforced linear low-density polyethylene composites, Compos. Part A Appl. Sci. Manuf. 150 (2021) 106606. https://doi.org/10.1016/j.compositesa.2021.106606.

[65] K.B. Adhikary, S. Pang, M.P. Staiger, Dimensional stability and mechanical behaviour of wood-plastic composites based on recycled and virgin high-density polyethylene (HDPE), Compos. Part B Eng. 39 (2008) 807–815. https://doi.org/10.1016/j.compositesb.2007.10.005.

[66] K.L. Yam, B.K. Gogoi, C.C. Lai, S.E. Selke, Composites from compounding wood fibers with recycled high density polyethylene, Polym. Eng. Sci. 30 (1990) 693–699. https://doi.org/10.1002/pen.760301109.

[67] S.E. Selke, I. Wichman, Wood fiber/polyolefin composites, Compos. Part A Appl. Sci.

Manuf. 35 (2004) 321–326. https://doi.org/10.1016/j.compositesa.2003.09.010.

[68] K. Jayaraman, D. Bhattacharyya, Mechanical performance of woodfibre-waste plastic composite materials, Resour. Conserv. Recycl. 41 (2004) 307–319. https://doi.org/10.1016/j.resconrec.2003.12.001.

[69] F. Gu, P. Hall, N.J. Miles, Performance evaluation for composites based on recycled polypropylene using principal component analysis and cluster analysis, J. Clean. Prod. 115 (2016) 343–353. https://doi.org/10.1016/j.jclepro.2015.12.062.

[70] W. Tang, J. Xu, Q. Fan, W. Li, H. Zhou, T. Liu, C. Guo, R. Ou, X. Hao, Q. Wang, Rheological behavior and mechanical properties of ultra-high-filled wood fiber/polypropylene composites using waste wood sawdust and recycled polypropylene as raw materials, Constr. Build. Mater. 351 (2022) 128977. https://doi.org/10.1016/j.conbuildmat.2022.128977.

[71] L. Chotirat, K. Chaochanchaikul, N. Sombatsompop, On adhesion mechanisms and interfacial strength in acrylonitrile-butadiene-styrene/wood sawdust composites, Int. J. Adhes. Adhes. 27 (2007) 669–678. https://doi.org/10.1016/j.ijadhadh.2007.02.001.

[72] P.Y. Kuo, S.Y. Wang, J.H. Chen, H.C. Hsueh, M.J. Tsai, Effects of material compositions on the mechanical properties of wood-plastic composites manufactured by injection molding, Mater. Des. 30 (2009). https://doi.org/10.1016/j.matdes.2009.03.012.

[73] Ghorbani, M.; Poorzahed, N.; Amininasab, S.M. Morphological, physical, and mechanical properties of silanized wood-polymer composite. J. Compos. Mater. 2020, 54, 1403–1412.

[74] S. Yang, J. Jiang, W. Duan, S. Bai, Q. Wang, Production of sustainable wood-plastic composites from the nonmetals in waste printed circuit boards: Excellent physical performance achieved by solid-state shear milling, Compos. Sci. Technol. 200 (2020) 108411. https://doi.org/10.1016/j.compscitech.2020.108411.

[75] F. da S.M. Teixeira, A.C. de C. Peres, E.B.A.V. Pacheco, Mechanical recycling of acrylonitrile-butadiene-styrene copolymer and high impact polystyrene from waste electrical and electronic equipment to comply with the circular economy, Front. Sustain. 4 (2023). https://doi.org/10.3389/frsus.2023.1203457.

[76] Z. He, X. Zhu, J. Wang, M. Mu, Y. Wang, Comparison of CO 2 emissions from OPC and recycled cement production, Constr. Build. Mater. 211 (2019) 965–973.

https://doi.org/10.1016/j.conbuildmat.2019.03.289.

[77] J.O. Babayemi, I.C. Nnorom, O. Osibanjo, R. Weber, Ensuring sustainability in plastics use in Africa: consumption, waste generation, and projections, Environ. Sci. Eur. 31 (2019). https://doi.org/10.1186/s12302-019-0254-5.

[78] N. Mohamad, A.A. Latiff, H.E.A. Maulod, M.A. Azam, M.E.A. Manaf, A Sustainable Polymer Composite from Recycled Polypropylene Filled with Shrimp Shell Waste, Polym. - Plast. Technol. Eng. 53 (2014) 167–172. https://doi.org/10.1080/03602559.2013.843704.

[79] W. Zhang, X. Yao, S. Khanal, S. Xu, A novel surface treatment for bamboo flour and its effect on the dimensional stability and mechanical properties of high density polyethylene/bamboo flour composites, Constr. Build. Mater. 186 (2018) 1220–1227. https://doi.org/10.1016/j.conbuildmat.2018.08.003.

[80] K. Rohit, S. Dixit, A review - future aspect of natural fiber reinforced composite, Polym. from Renew. Resour. 7 (2016) 43–60. https://doi.org/10.1177/204124791600700202.

[81] K. Salasinska, J. Ryszkowska, The effect of filler chemical constitution and morphological properties on the mechanical properties of natural fiber composites, Compos. Interfaces 22 (2015) 39–50. https://doi.org/10.1080/15685543.2015.984521.

[82] M. Ramesh, L. Rajeshkumar, G. Sasikala, D. Balaji, A. Saravanakumar, V. Bhuvaneswari, R. Bhoopathi, A Critical Review on Wood-Based Polymer Composites: Processing, Properties, and Prospects, Polymers (Basel). 14 (2022) 1–35. https://doi.org/10.3390/polym14030589.

[83] S.Y. Fu, X.Q. Feng, B. Lauke, Y.W. Mai, Effects of particle size, particle/matrix interface adhesion and particle loading on mechanical properties of particulate-polymer composites, Compos. Part B Eng. 39 (2008) 933–961. https://doi.org/10.1016/j.compositesb.2008.01.002.

[84] K.L. Pickering, M.G.A. Efendy, T.M. Le, A review of recent developments in natural fibre composites and their mechanical performance, Compos. Part A Appl. Sci. Manuf. 83 (2016) 98–112. https://doi.org/10.1016/j.compositesa.2015.08.038.

[85] P.O. Akadiri, E.A. Chinyio, P.O. Olomolaiye, Design of a sustainable building: A conceptual framework for implementing sustainability in the building sector, Buildings 2 (2012) 126–152. https://doi.org/10.3390/buildings2020126.

[86] H. Zhou, W. Li, X. Hao, G. Zong, X. Yi, J. Xu, R. Ou, Q. Wang, Recycling end-of-life WPC products into ultra-high-filled, high-performance wood fiber/polyethylene composites: a sustainable strategy for clean and cyclic processing in the WPC industry, J. Mater. Res. Technol. 18 (2022) 1–14. https://doi.org/10.1016/j.jmrt.2022.02.091.

[87] H. Klee, R. Hunziker, R. van der Meer, R. Westaway, Getting the numbers right: a database of energy performance and carbon dioxide emissions for the cement industry, Greenh. Gas Meas. Manag. 1 (2011) 109–118. https://doi.org/10.1080/20430779.2011.579357.

[88] A.A. Klyosov, Wood–Plastic Composites, John Wiley & Sons, Inc., Hoboken, New Jersey., 2007.

[89] D.J. Gardner, Y. Han, L. Wang, Wood–Plastic composite technology, Curr. For. Reports 1 (2015) 139–150. https://doi.org/10.1007/s40725-015-0016-6.

[90] S. Huang, Q. Fu, L. Yan, B. Kasal, Characterization of interfacial properties between fibre and polymer matrix in composite materials – A critical review, J. Mater. Res. Technol. 13 (2021) 1441–1484. https://doi.org/10.1016/j.jmrt.2021.05.076.

[91] D.A. Jesson, J.F. Watts, The interface and interphase in polymer matrix composites: Effect on mechanical properties and methods for identification, Polym. Rev. 52 (2012) 321–354. https://doi.org/10.1080/15583724.2012.710288.

[92] M.Z.R. Khan, S.K. Srivastava, M.K. Gupta, A state-of-the-art review on particulate wood polymer composites: Processing, properties and applications, Polym. Test. 89 (2020) 106721. https://doi.org/10.1016/j.polymertesting.2020.106721.

[93] S. Khamtree, C. Srivabut, S. Khamtree, R. Kaewmai, Effects of Natural Fiber Waste, Content, and Coupling Agent on the Physical and Mechanical Properties of Wood Species–Plastic Composites as Green Materials, Fibers Polym. 25 (2024) 1391–1402. https://doi.org/10.1007/s12221-024-00493-9.

[94] E. Stanaszek-Tomal, Wood - Polymer Composites as an Alternative to the Natural Environment, IOP Conf. Ser. Mater. Sci. Eng. 603 (2019). https://doi.org/10.1088/1757-899X/603/2/022009.

[95] G.H. Doh, S.Y. Lee, I.A. Kang, Y.T. Kong, Thermal behavior of liquefied wood polymer composites (LWPC), Compos. Struct. 68 (2005) 103–108. https://doi.org/10.1016/j.compstruct.2004.03.004.

[96] V.K. Thakur, M.K. Thakur, R.K. Gupta, Review: Raw Natural Fiber-Based Polymer Composites, Int. J. Polym. Anal. Charact. 19 (2014) 256–271. https://doi.org/10.1080/1023666X.2014.880016.

[97] M.R. Sanjay, P. Madhu, M. Jawaid, P. Senthamaraikannan, S. Senthil, S. Pradeep, Characterization and properties of natural fiber polymer composites: A comprehensive review, J. Clean. Prod. 172 (2018) 566–581. https://doi.org/10.1016/j.jclepro.2017.10.101.

[98] A. Olszewski, P. Kosmela, Ł. Piszczyk, A novel approach in wood waste utilization for manufacturing of catalyst-free polyurethane-wood composites (PU-WC), Sustain. Mater. Technol. 36 (2023). https://doi.org/10.1016/j.susmat.2023.e00619.

[99] A. Hejna, K. Formela, M.R. Saeb, Processing, mechanical and thermal behavior assessments of polycaprolactone/agricultural wastes biocomposites, Ind. Crops Prod. 76 (2015) 725–733. https://doi.org/10.1016/j.indcrop.2015.07.049.

[100] F. Sliwa, N.E. El Bounia, G. Marin, F. Charrier, F. Malet, A new generation of wood polymer composite with improved thermal stability, Polym. Degrad. Stab. 97 (2012) 496–503. https://doi.org/10.1016/j.polymdegradstab.2012.01.023.

[101] İ.H. Başboğa, İ. Atar, K. Karakuş, F. Mengeloğlu, Determination of Some Technological Properties of Injection Molded Pulverized-HDPE Based Composites Reinforced with Micronized Waste Tire Powder and Red Pine Wood Wastes, J. Polym. Environ. 28 (2020) 1776–1794. https://doi.org/10.1007/s10924-020-01726-7.

[102] A. Fazli, T. Stevanovic, D. Rodrigue, Recycled HDPE/Natural Fiber Composites Modified with Waste Tire Rubber: A Comparison between Injection and Compression Molding, Polymers (Basel). 14 (2022). https://doi.org/10.3390/polym14153197.

[103] J. Zhang, A. Koubaa, D. Xing, H. Wang, F. Wang, X.M. Wang, Q. Wang, Flammability, thermal stability, and mechanical properties of wood flour/polycarbonate/polyethylene bio-based composites, Ind. Crops Prod. 169 (2021) 113638. https://doi.org/10.1016/j.indcrop.2021.113638.

[104] Kristiina Oksman Niska and Mohini Sain, ed., Wood-polymer composites, Woodhead Publishing Limited, Sawston, UK, 2008.

[105] M. Hyvärinen, M. Ronkanen, T. Kärki, The effect of the use of construction and demolition waste on the mechanical and moisture properties of a wood-plastic composite,

Compos. Struct. 210 (2019) 321–326. https://doi.org/10.1016/j.compstruct.2018.11.063.

[106] P. Sormunen, I. Deviatkin, M. Horttanainen, T. Kärki, An evaluation of thermoplastic composite fillers derived from construction and demolition waste based on their economic and environmental characteristics, J. Clean. Prod. 280 (2021). https://doi.org/10.1016/j.jclepro.2020.125198.

[107] A. Keskisaari, T. Kärki, Utilization of Industrial Wastes from Mining and Packaging Industries in Wood-Plastic Composites, J. Polym. Environ. 26 (2018) 1504–1510. https://doi.org/10.1007/s10924-017-1052-z.

[108] T. Mishra, P. Mandal, A.K. Rout, D. Sahoo, A state-of-the-art review on potential applications of natural fiber-reinforced polymer composite filled with inorganic nanoparticle, Compos. Part C Open Access 9 (2022) 100298. https://doi.org/10.1016/j.jcomc.2022.100298.

[109] Y. Ma, H. He, B. Huang, H. Jing, Z. Zhao, In situ fabrication of wood flour/nano silica hybrid and its application in polypropylene-based wood-plastic composites, Polym. Compos. 41 (2020) 573–584. https://doi.org/10.1002/pc.25389.

[110] H. Khanjanzadeh, H. Pirayesh, A. Salari, Long term hygroscopic characteristics of polypropylene based hybrid composites with and without organo-modified clay, Eur. J. Wood Wood Prod. 71 (2013) 211–218. https://doi.org/10.1007/s00107-012-0661-4.

[111] M.B.S. Nunes, A.F.F. Farias, E.S. Medeiros, J.E. Oliveira, I.M.G. Santos, L.H. Carvalho, A.S.F. Santos, The effect of clay organophilization on wood plastic composite (WPC) based on recycled high density polyethylene (HDPE) and coir fiber, Prog. Rubber, Plast. Recycl. Technol. 37 (2021) 394–411. https://doi.org/10.1177/14777606211019404.

[112] K. Karakuş, D. Aydemir, A. Öztel, G. Gunduz, F. Mengeloglu, Nanoboron nitride-filled heat-treated wood polymer nanocomposites: Comparison of different multicriteria decision-making models to predict optimum properties of the nanocomposites, J. Compos. Mater. 51 (2017) 4205–4218. https://doi.org/10.1177/0021998317699984.

[113] H.F. Ahangarkolaei, M. Mashkour, D. Rasouli, Superparamagnetic wood-polypropylene nanocomposite made using magnetic wood flour with a nanoparticle-free surface, J. Appl. Polym. Sci. 140 (2023). https://doi.org/10.1002/app.53531.

[114] H.S. Kim, B.H. Lee, S.W. Choi, S. Kim, H.J. Kim, The effect of types of maleic anhydride-grafted polypropylene (MAPP) on the interfacial adhesion properties of bio-

flour-filled polypropylene composites, Compos. Part A Appl. Sci. Manuf. 38 (2007) 1473–1482. https://doi.org/10.1016/j.compositesa.2007.01.004.

[115] J.D. Megiatto, C.G. Silva, E.C. Ramires, E. Frollini, Thermoset matrix reinforced with sisal fibers: Effect of the cure cycle on the properties of the biobased composite, Polym. Test. 28 (2009) 793–800. https://doi.org/10.1016/j.polymertesting.2009.07.001.

[116] V.K. Thakur, M.K. Thakur, Processing and characterization of natural cellulose fibers/thermoset polymer composites, Carbohydr. Polym. 109 (2014) 102–117. https://doi.org/10.1016/j.carbpol.2014.03.039.

[117] M.S. Salit, M. Jawaid, N. Bin Yusoff, M.E. Hoque, Manufacturing of natural fibre reinforced polymer composites, Manuf. Nat. Fibre Reinf. Polym. Compos. (2015) 1–383. https://doi.org/10.1007/978-3-319-07944-8.

[118] A. Ares, R. Bouza, S.G. Pardo, M.J. Abad, L. Barral, Rheological, mechanical and thermal behaviour of wood polymer composites based on recycled polypropylene, J. Polym. Environ. 18 (2010) 318–325. https://doi.org/10.1007/s10924-010-0208-x.

[119] S. Park, W. Shou, L. Makatura, W. Matusik, K. (Kelvin) Fu, 3D printing of polymer composites: Materials, processes, and applications, Matter 5 (2022) 43–76. https://doi.org/10.1016/j.matt.2021.10.018.

[120] N. Singh, D. Hui, R. Singh, I.P.S. Ahuja, L. Feo, F. Fraternali, Recycling of plastic solid waste: A state of art review and future applications, Compos. Part B Eng. 115 (2017) 409–422. https://doi.org/10.1016/j.compositesb.2016.09.013.

[121] L.K. Ncube, A.U. Ude, E.N. Ogunmuyiwa, R. Zulkifli, I.N. Beas, An overview of plasticwaste generation and management in food packaging industries, Recycling 6 (2021) 1–25. https://doi.org/10.3390/recycling6010012.

[122] D.K.A. Barnes, F. Galgani, R.C. Thompson, M. Barlaz, Accumulation and fragmentation of plastic debris in global environments, Philos. Trans. R. Soc. B Biol. Sci. 364 (2009) 1985–1998. https://doi.org/10.1098/rstb.2008.0205.

[123] P.F. Sommerhuber, T. Wang, A. Krause, Wood-plastic composites as potential applications of recycled plastics of electronic waste and recycled particleboard, J. Clean. Prod. 121 (2016) 176–185. https://doi.org/10.1016/j.jclepro.2016.02.036.

[124] S. Hangargi, A. Swamy, R.G. Raj, M. Aruna, R. Venkatesh, S. Madhu, S. Al Obaid, S.A. Alharbi, M.A. Kalam, Enhancement of Kevlar fiber-polypropylene composite by the

inclusions of cotton stalk and granite particle: characteristics study, Biomass Convers. Biorefinery (2023). https://doi.org/10.1007/s13399-023-04817-2.

[125] W.A.A. Sadik, A.G.M. El Demerdash, R. Abbas, A. Bedir, Effect of Nanosilica and Nanoclay on the Mechanical, Physical, and Morphological Properties of Recycled Linear Low Density Polyethylene/Rice Husk Composites, J. Polym. Environ. 29 (2021) 1600–1615. https://doi.org/10.1007/s10924-020-01983-6.

[126] Y. Lei, Q. Wu, Wood plastic composites based on microfibrillar blends of high density polyethylene/poly(ethylene terephthalate), Bioresour. Technol. 101 (2010) 3665–3671. https://doi.org/10.1016/j.biortech.2009.12.069.

[127] V. Lahtela, T. Kärki, A study on the effect of construction and demolition waste (CDW) plastic fractions on the moisture and resistance to indentation of wood-polymer composites (WPC), J. Compos. Sci. 5 (2021) 1–7. https://doi.org/10.3390/jcs5080205.

[128] Y.C. Chiou, M.Y. Shen, C.L. Chiang, Y.L. Li, W.M. Lai, Effects of Environmental Aging on the Durability of Wood-Flour Filled Recycled PET/PA6 Wood Plastic Composites, J. Polym. Environ. 30 (2022) 1300–1313. https://doi.org/10.1007/s10924-021-02268-2.

[129] P.F. Sommerhuber, J. Welling, A. Krause, Substitution potentials of recycled HDPE and wood particles from post-consumer packaging waste in Wood-Plastic Composites, Waste Manag. 46 (2015) 76–85. https://doi.org/10.1016/j.wasman.2015.09.011.

[130] O. Bijaisoradat, M. Luttapreecha, H. Manuspiya, Eco composites with synergistic combinations of natural rubber latex and wood flour toughened recycled HDPE, Mater. Today Commun. 25 (2020) 101483. https://doi.org/10.1016/j.mtcomm.2020.101483.

[131] P. Noorunnisa Khanam, M.A. AlMaadeed, Improvement of ternary recycled polymer blend reinforced with date palm fibre, Mater. Des. 60 (2014) 532–539. https://doi.org/10.1016/j.matdes.2014.04.033.

[132] P.K.P.K. Aggarwal, S. Chauhan, N. Raghu, S. Karmarkar, G.M.M. Shashidhar, Mechanical properties of bio-fibers-reinforced high-density polyethylene composites: Effect of coupling agents and bio-fillers, J. Reinf. Plast. Compos. 32 (2013) 1722–1732. https://doi.org/10.1177/0731684413500545.

[133] C.A. Echeverria, F. Pahlevani, V. Sahajwalla, Valorisation of discarded nonwoven polypropylene as potential matrix-phase for thermoplastic-lignocellulose hybrid material

engineered for building applications, J. Clean. Prod. 258 (2020). https://doi.org/10.1016/j.jclepro.2020.120730.

[134] V. Çavuş, F. Mengeloğlu, Effect of wood particle size on selected properties of neat and recycled wood polypropylene composites, BioResources 15 (2020) 3427–3442. https://doi.org/10.15376/biores.15.2.3427-3442.

[135] R.F. Khedr, H.H. Elnahas, Preparation of wood plastic composite from flax fibers and post consumed polystyrene foam based on environmental and economical scales, J. Thermoplast. Compos. Mater. (2023). https://doi.org/10.1177/08927057231187526.

[136] R. Tewari, M.K. Singh, S. Zafar, Utilization of forest and plastic wastes for composite manufacturing using microwave-assisted compression molding for low load applications, J. Polym. Res. 28 (2021). https://doi.org/10.1007/s10965-021-02778-6.

[137] Jafar Ghaje Beigloo; Habibollah Khademi Eslam; Amir Hooman Hemmasi; Behzad Bazyar and Ismaeil Ghasemi, Thermal Properties and Morphology of Nanocomposite Made of Recycled High Density Polyethylene and Wood Flour, BioResources 12 (2017) 1382–1394.

[138] H. Rangavar, H.R. Taghiyari, A. Oromiehie, T. Gholipour, A. Safarpour, Effects of nanoclay on physical and mechanical properties of wood-plastic composites, Wood Mater. Sci. Eng. 12 (2017) 211–219. https://doi.org/10.1080/17480272.2016.1156743.

[139] S. Haq, R. Srivastava, Wood Polypropylene (PP) Composites Manufactured by Mango Wood Waste with Virgin or Recycled PP : Mechanical , Morphology , Melt Flow Index and Crystalline Behaviour, J. Polym. Environ. (2016). https://doi.org/10.1007/s10924-016-0845-9.

[140] A.K. Gupta, M. Biswal, S. Mohanty, S.K. Nayak, Mechanical and thermal degradation behavior of sisal fiber (SF) reinforced recycled polypropylene (RPP) composites, Fibers Polym. 15 (2014) 994–1003. https://doi.org/10.1007/s12221-014-0994-1.

[141] M.J. Taufiq, M.R. Mansor, Z. Mustafa, Characterisation of wood plastic composite manufactured from kenaf fibre reinforced recycled-unused plastic blend, Compos. Struct. 189 (2018) 510–515. https://doi.org/10.1016/j.compstruct.2018.01.090.

[142] D. Friedrich, Thermoforming of wood-plastic composites: a compolytics-approach translating combined polymer and policy analyses into industrial design principles, Int. J. Adv. Manuf. Technol. 124 (2023) 3533–3551. https://doi.org/10.1007/s00170-022-

10760-9.

[143] A. Ashori, Wood-plastic composites as promising green-composites for automotive industries!, Bioresour. Technol. 99 (2008) 4661–4667. https://doi.org/10.1016/j.biortech.2007.09.043.

[144] S.K.S.-K. Yeh, K.J.K.-J. Kim, R.K. Gupta, Synergistic effect of coupling agents on polypropylene-based wood-plastic composites, J. Appl. Polym. Sci. 127 (2013) 1047–1053. https://doi.org/10.1002/app.37775.

[145] R. Porebska, A. Rybak, B. Kozub, R. Sekula, Polymer matrix influence on stability of wood polymer composites, Polym. Adv. Technol. 26 (2015) 1076–1082. https://doi.org/10.1002/pat.3535.

[146] T. Gurunathan, S. Mohanty, S.K. Nayak, A review of the recent developments in biocomposites based on natural fibres and their application perspectives, Compos. Part A Appl. Sci. Manuf. 77 (2015) 1–25. https://doi.org/10.1016/j.compositesa.2015.06.007.

[147] L. Mohammed, M.N.M. Ansari, G. Pua, M. Jawaid, M.S. Islam, A Review on Natural Fiber Reinforced Polymer Composite and Its Applications, Int. J. Polym. Sci. 2015 (2015). https://doi.org/10.1155/2015/243947.

[148] X. Li, M. Yang, W. Zhang, K. Chen, C. Wang, High concentration acid-induced discoloration polymeric dyes fabricated with UV-curable azobenzene-lignin-based waterborne polyurethane, Int. J. Biol. Macromol. 182 (2021) 1953–1965. https://doi.org/10.1016/j.ijbiomac.2021.05.173.

[149] S. Wang, W. Liu, D. Yang, X. Qiu, Highly Resilient Lignin-Containing Polyurethane Foam, Ind. Eng. Chem. Res. 58 (2019) 496–504. https://doi.org/10.1021/acs.iecr.8b05072.

[150] B. Zhao, Y. Ni, K. Chen, Z. Lin, Z. Jia, H. Qiu, Double-shell lignin microcapsules were prepared by one - step method for fabric coatings with UV resistance and durable antibacterial activity, Prog. Org. Coatings 179 (2023) 107518. https://doi.org/10.1016/j.porgcoat.2023.107518.

[151] P. Saha, S. Chowdhury, D. Roy, B. Adhikari, J.K. Kim, S. Thomas, A brief review on the chemical modifications of lignocellulosic fibers for durable engineering composites, Polym. Bull. 73 (2016) 587–620. https://doi.org/10.1007/s00289-015-1489-y.

[152] F. Luis, G. Moncayo, Lignocellulosic Polymer Composites, Scrivener Publishing and

John Wiley & Sons, Inc, Hoboken, NJ,USA, 2015. https://doi.org/10.1002/9781118773949.

[153] G. Portal, Conversion of Lignocellulosic Biomass to Nanocellulose: Structure and Chemical Process, Appl. Thermolumin. Dosim. 852745443 (1981) 97–122.

[154] A. Sharma, M. Thakur, M. Bhattacharya, T. Mandal, S. Goswami, Commercial application of cellulose nano-composites – A review, Biotechnol. Reports 21 (2019) e00316. https://doi.org/10.1016/j.btre.2019.e00316.

[155] B. Hünnekens, G. Avramidis, G. Ohms, A. Krause, W. Viöl, H. Militz, Impact of plasma treatment under atmospheric pressure on surface chemistry and surface morphology of extruded and injection-molded wood-polymer composites (WPC), Appl. Surf. Sci. 441 (2018) 564–574. https://doi.org/10.1016/j.apsusc.2018.01.294.

[156] L. Sobczak, R. Welser, O. Brüggemann, A. Haider, Polypropylene (PP)-based wood polymer composites: Performance of five commercial maleic anhydride grafted PP coupling agents, J. Thermoplast. Compos. Mater. 27 (2014) 439–463. https://doi.org/10.1177/0892705712447806.

[157] J.Z. Lu, A. Professor, H.S. McNabb, J. Professor, Society of Wood Science and Technology State-of-the-Art Review CHEMICAL COUPLING IN WOOD FIBER AND POLYMER COMPOSITES: A REVIEW OF COUPLING AGENTS AND TREATMENTS' Qinglin W u t, Wood Fiber Sci. 32 (2000) 88–104.

[158] J.Z. Lu, Q. Wu, H.S. McNabb, Chemical coupling in wood fiber and polymer composites: A review of coupling agents and treatments, Wood Fiber Sci. 32 (2000) 88–104.

[159] M.S. Anbupalani, C.D. Venkatachalam, R. Rathanasamy, Influence of coupling agent on altering the reinforcing efficiency of natural fibre-incorporated polymers – A review, J. Reinf. Plast. Compos. 39 (2020) 520–544. https://doi.org/10.1177/0731684420918937.

[160] X. Hao, J. Xu, H. Zhou, W. Tang, W. Li, Q. Wang, R. Ou, Interfacial adhesion mechanisms of ultra-highly filled wood fiber/polyethylene composites using maleic anhydride grafted polyethylene as a compatibilizer, Mater. Des. 212 (2021) 110182. https://doi.org/10.1016/j.matdes.2021.110182.

[161] T.-H. Yang, S.-Y. Leu, T.-H. Yang, S.-F. Lo, Optimized material composition to improve the physical and mechanical properties of extruded wood-plastic composites (WPCs),

Constr. Build. Mater. 29 (2012) 120–127. https://doi.org/10.1016/j.conbuildmat.2011.09.013.

[162] S.K. Yeh, S. Agarwal, R.K. Gupta, Wood-plastic composites formulated with virgin and recycled ABS, Compos. Sci. Technol. 69 (2009) 2225–2230. https://doi.org/10.1016/j.compscitech.2009.06.007.

[163] Q. Wang, Z. Xiao, W. Wang, Y. Xie, Coupling pattern and efficacy of organofunctional silanes in wood flour-filled polypropylene or polyethylene composites, J. Compos. Mater. 49 (2015) 677–684. https://doi.org/10.1177/0021998314525065.

[164] S. Chauhan, P. Aggarwal, A. Karmarkar, The effectiveness of m-TMI-grafted-PP as a coupling agent for wood polymer composites, J. Compos. Mater. 50 (2016) 3515–3524. https://doi.org/10.1177/0021998315622050.

[165] A. Karmarkar, S.S. Chauhan, J.M. Modak, M. Chanda, Mechanical properties of wood-fiber reinforced polypropylene composites: Effect of a novel compatibilizer with isocyanate functional group, Compos. Part A Appl. Sci. Manuf. 38 (2007) 227–233. https://doi.org/10.1016/j.compositesa.2006.05.005.

[166] T. Liu, Q. Wang, Y. Xie, S. Lee, Q. Wu, Effects of use of coupling agents on the properties of microfibrillar composite based on high-density polyethylene and polyamide-6, Polym. Bull. 71 (2014) 685–703. https://doi.org/10.1007/s00289-013-1086-x.

[167] Y. Li, Effect of coupling agent concentration, fiber content, and size on mechanical properties of wood/HDPE composites, Int. J. Polym. Mater. Polym. Biomater. 61 (2012) 882–890. https://doi.org/10.1080/00914037.2011.617338.

[168] S.A. Bahari, A. Krause, Bamboo Particles-Polyvinyl Chloride Composites: Analysis of Particles Size Distribution and Composites Performance, J. Mater. Sci. Res. 6 (2017) 1. https://doi.org/10.5539/jmsr.v6n2p1.

[169] M. Kociszewski, C. Gozdecki, A. Wilczyński, S. Zajchowski, J. Mirowski, Effect of industrial wood particle size on mechanical properties of wood-polyvinyl chloride composites, Eur. J. Wood Wood Prod. 70 (2012) 113–118. https://doi.org/10.1007/s00107-011-0531-5.

[170] A. Akdogan, A.S. Vanli, Material characterization of different-dimensioned wood particle-reinforced polymer composites, J. Thermoplast. Compos. Mater. 26 (2013)

1237–1248. https://doi.org/10.1177/0892705713484743.

[171] M.E. Golmakani, T. Wiczenbach, M. Malikan, R. Aliakbari, V.A. Eremeyev, Investigation of wood flour size, aspect ratios, and injection molding temperature on mechanical properties of wood flour/polyethylene composites, Materials (Basel). 14 (2021). https://doi.org/10.3390/ma14123406.

[172] A. Ashori, A. Nourbakhsh, Reinforced polypropylene composites: Effects of chemical compositions and particle size, Bioresour. Technol. 101 (2010) 2515–2519. https://doi.org/10.1016/j.biortech.2009.11.022.

[173] H. Xu, Y. Yang, L. Li, B. Liu, X. Fu, X. Yang, Y. Cao, Mechanical Properties Variation in Wood—Plastic Composites with a Mixed Wood Fiber Size, Materials (Basel). 16 (2023) 5801. https://doi.org/10.3390/ma16175801.

[174] M. Li, Y. Pu, V.M. Thomas, C.G. Yoo, S. Ozcan, Y. Deng, K. Nelson, A.J. Ragauskas, Recent advancements of plant-based natural fiber–reinforced composites and their applications, Compos. Part B Eng. 200 (2020). https://doi.org/10.1016/j.compositesb.2020.108254.

[175] J.L. Thomason, J.L. Rudeiros-Fernández, A review of the impact performance of natural fiber thermoplastic composites, Front. Mater. 5 (2018) 1–18. https://doi.org/10.3389/fmats.2018.00060.

[176] T.T.L. Doan, S.L. Gao, E. Mäder, Jute/polypropylene composites I. Effect of matrix modification, Compos. Sci. Technol. 66 (2006) 952–963. https://doi.org/10.1016/j.compscitech.2005.08.009.

[177] S. Kazemi Najafi, Use of recycled plastics in wood plastic composites - A review, Waste Manag. 33 (2013) 1898–1905. https://doi.org/10.1016/j.wasman.2013.05.017.

[178] N.E. Marcovich, M.A. Villar, Thermal and mechanical characterization of linear low-density polyethylene/wood flour composites, J. Appl. Polym. Sci. 90 (2003) 2775–2784. https://doi.org/10.1002/app.12934.

[179] A. Nourbakhsh, B. V. Kokta, A. Ashori, A. Jahan-Latibari, Effect of a novel coupling agent, polybutadiene isocyanate, on mechanical properties of wood-fiber polypropylene composites, J. Reinf. Plast. Compos. 27 (2008) 1679–1687. https://doi.org/10.1177/0731684407087377.

[180] N.I.N. Haris, M.Z. Hassan, R.A. Ilyas, M.A. Suhot, S.M. Sapuan, R. Dolah, R.

Mohammad, M.R.M. Asyraf, Dynamic mechanical properties of natural fiber reinforced hybrid polymer composites: a review, J. Mater. Res. Technol. 19 (2022) 167–182. https://doi.org/10.1016/j.jmrt.2022.04.155.

[181] S.A. Bahari, W.J. Grigsby, A. Krause, Flexural Properties of PVC/Bamboo Composites under Static and Dynamic-Thermal Conditions: Effects of Composition and Water Absorption, Int. J. Polym. Sci. 2017 (2017). https://doi.org/10.1155/2017/2717848.

[182] F. Tian, L. Chen, X. Xu, Dynamical mechanical properties of wood-high density polyethylene composites filled with recycled rubber, J. Bioresour. Bioprod. 6 (2021) 152–159. https://doi.org/10.1016/j.jobab.2021.02.007.

[183] C. Berger, B.D. Mattos, S.C. Amico, J.A. de Farias, R. Coldebella, D.A. Gatto, A.L. Missio, Production of sustainable polymeric composites using grape pomace biomass, Biomass Convers. Biorefinery (2020). https://doi.org/10.1007/s13399-020-00966-w.

[184] Y. Zhou, D. Hui, Y. Wang, M. Fan, Nanomechanical and dynamic mechanical properties of rubber-wood-plastic composites, Nanotechnol. Rev. 11 (2021) 167–175. https://doi.org/10.1515/ntrev-2022-0002.

[185] Y. Zhou, Y. Wang, M. Fan, Incorporation of tyre rubber into wood plastic composites to develop novel multifunctional composites: Interface and bonding mechanisms, Ind. Crops Prod. 141 (2019). https://doi.org/10.1016/j.indcrop.2019.111788.

[186] N. Saba, M. Jawaid, O.Y. Alothman, M.T. Paridah, A review on dynamic mechanical properties of natural fibre reinforced polymer composites, Constr. Build. Mater. 106 (2016) 149–159. https://doi.org/10.1016/j.conbuildmat.2015.12.075.

[187] B. Effah, A. Van Reenen, M. Meincken, Characterisation of the Interfacial Adhesion of the Different Components in Wood–Plastic Composites with AFM, Springer Sci. Rev. 3 (2015) 97–111. https://doi.org/10.1007/s40362-015-0032-8.

[188] J. Coates, Interpretation of Infrared Spectra, A Practical Approach, Encycl. Anal. Chem. (2006) 1–23. https://doi.org/10.1002/9780470027318.a5606.

[189] Q. Yu, Y. Wang, H. Ye, Y. Sheng, Y. Shi, M. Zhang, W. Fan, R. Yang, C. Xia, S. Ge, Preparation and properties of wood plastic composites with desirable features using poplar and five recyclable plastic wastes, Appl. Sci. 11 (2021). https://doi.org/10.3390/app11156838.

[190] S. Park, J.O. Baker, M.E. Himmel, P.A. Parilla, D.K. Johnson, Cellulose crystallinity

index: Measurement techniques and their impact on interpreting cellulase performance, Biotechnol. Biofuels 3 (2010). https://doi.org/10.1186/1754-6834-3-10.

[191] U. Meekum, A. Khongrit, Toughening of wood-plastic composites based on silane/peroxide macro crosslink poly(propylene) systems, BioResources 13 (2018) 1678–1695. https://doi.org/10.15376/biores.13.1.1678-1695.

[192] K.C. Krause, P. Sauerbier, T. Koddenberg, A. Krause, Utilization of recycled material sources for wood-polypropylene composites: Effect on internal composite structure, particle characteristics and physico-mechanical properties, Fibers 6 (2018). https://doi.org/10.3390/fib6040086.

[193] N.R.R. Royan, A.B. Sulong, N.Y. Yuhana, R.S. Chen, M.H. Ab Ghani, S. Ahmad, UV/O3 treatment as a surface modification of rice husk towards preparation of novel biocomposites, PLoS One 13 (2018) 1–17. https://doi.org/10.1371/journal.pone.0197345.

[194] X. Ye, H. Wang, K. Zheng, Z. Wu, H. Zhou, K. Tian, Z. Su, X. Tian, The interface designing and reinforced features of wood fiber/polypropylene composites: Wood fiber adopting nano-zinc-oxide-coating via ion assembly, Compos. Sci. Technol. 124 (2016) 1–9. https://doi.org/10.1016/j.compscitech.2015.12.016.

[195] X. Hao, J. Sun, C. Chen, H. Zhou, Y. Li, W. Li, Q. Wang, R. Ou, Dimensional stability improvements of waste wood flour/HDPE composites via carbon black network embedding, Constr. Build. Mater. 299 (2021) 123955. https://doi.org/10.1016/j.conbuildmat.2021.123955.

[196] P. Sauerbier, R. Köhler, G. Renner, H. Militz, Plasma treatment of polypropylene-based wood-plastic composites (WPC): Influences of working gas, Polymers (Basel). 12 (2020). https://doi.org/10.3390/POLYM12091933.

[197] R. Rajan, J. Näkki, R. Layek, E. Rainosalo, Wood plastic composites with improved electrical and thermal conductivity, Wood Sci. Technol. 55 (2021) 719–739. https://doi.org/10.1007/s00226-021-01275-9.

[198] M. Malakani, B. Bazyar, M. Talaiepour, A.H. Hemmasi, I. Ghasemi, Effect of acetylation of wood flour and MAPP content during compounding on physical properties, decay resistance, contact angle, and morphology of polypropylene/wood flour composites, BioResources 10 (2015) 2113–2129. https://doi.org/10.15376/biores.10.2.2113-2129.

[199] J. Hong, Z. Wang, L. Li, C. Guo, Value-added utilization of corncob hydrolysis residues:

Preparation of reinforced wood-plastic composite with highly water resistance and decay resistance, Ind. Crops Prod. 195 (2023) 116497. https://doi.org/10.1016/j.indcrop.2023.116497.

[200] G.S. Oporto, D.J. Gardner, G. Bernhardt, D.J. Neivandt, Characterizing the mechanism of improved adhesion of modified wood plastic composite (WPC) surfaces, J. Adhes. Sci. Technol. 21 (2007) 1097–1116. https://doi.org/10.1163/156856107782105954.

[201] C. Lazrak, B. Kabouchi, M. Hammi, A. Famiri, M. Ziani, Structural study of maritime pine wood and recycled high-density polyethylene (HDPEr) plastic composite using Infrared-ATR spectroscopy, X-ray diffraction, SEM and contact angle measurements, Case Stud. Constr. Mater. 10 (2019) e00227. https://doi.org/10.1016/j.cscm.2019.e00227.

[202] K.P. Črešnar, M. Bek, T. Luxbacher, M. Brunčko, L.F. Zemljič, Insight into the surface properties of wood fiber-polymer composites, Polymers (Basel). 13 (2021). https://doi.org/10.3390/polym13101535.

[203] S. Sharma, V. Sharma, S. Chatterjee, Contribution of plastic and microplastic to global climate change and their conjoining impacts on the environment - A review, Sci. Total Environ. 875 (2023) 162627. https://doi.org/10.1016/j.scitotenv.2023.162627.

[204] K. Xu, Y. Wen, X. Xu, Melt flow ratio: A way to identify the type of polyethylene, Adv. Ind. Eng. Polym. Res. 6 (2023) 79–82. https://doi.org/10.1016/j.aiepr.2022.08.001.

[205] T.R. Walker, L. Fequet, Current trends of unsustainable plastic production and micro(nano)plastic pollution, TrAC - Trends Anal. Chem. 160 (2023) 116984. https://doi.org/10.1016/j.trac.2023.116984.

[206] P.M. Subramanian, Plastics recycling and waste management in the US, Resour. Conserv. Recycl. 28 (2000) 253–263. https://doi.org/10.1016/S0921-3449(99)00049-X.

[207] K. Formela, M. Kurańska, M. Barczewski, Recent Advances in Development of Waste-Based Polymer Materials: A Review, Polymers (Basel). 14 (2022). https://doi.org/10.3390/polym14051050.

[208] J. Singh, I. Ordoñez, Resource recovery from post-consumer waste: important lessons for the upcoming circular economy, J. Clean. Prod. 134 (2016) 342–353. https://doi.org/10.1016/j.jclepro.2015.12.020.

[209] L.M. Alsarhan, A.S. Alayyar, N.B. Alqahtani, N.H. Khdary, Circular carbon economy (Cce): A way to invest co2 and protect the environment, a review, Sustain. 13 (2021).

https://doi.org/10.3390/su132111625.

[210] L. Sobczak, R. Welser, O. Brüggemann, A. Haider, Polypropylene (PP)-based wood polymer composites: Performance of five commercial maleic anhydride grafted PP coupling agents, J. Thermoplast. Compos. Mater. 27 (2014) 439–463. https://doi.org/10.1177/0892705712447806.

[211] M. Kaseem, K. Hamad, F. Deri, Y.G. Ko, Material properties of polyethylene/wood composites: A review of recent works, Polym. Sci. - Ser. A 57 (2015) 689–703. https://doi.org/10.1134/S0965545X15070068.

[212] A. Hejna, M. Przybysz-Romatowska, P. Kosmela, Ł. Zedler, J. Korol, K. Formela, Recent advances in compatibilization strategies of wood-polymer composites by isocyanates, Wood Sci. Technol. 54 (2020) 1091–1119. https://doi.org/10.1007/s00226-020-01203-3.

[213] D. Lorenz, N. Erasmy, Y. Akil, B. Saake, A new method for the quantification of monosaccharides, uronic acids and oligosaccharides in partially hydrolyzed xylans by HPAEC-UV/VIS, Carbohydr. Polym. 140 (2016) 181–187. https://doi.org/10.1016/j.carbpol.2015.12.027.

[214] M. Wang, R. Li, G. Chen, S. Zhou, X. Feng, Y. Chen, M. He, D. Liu, T. Song, H. Qi, Highly Stretchable, Transparent, and Conductive Wood Fabricated by in Situ Photopolymerization with Polymerizable Deep Eutectic Solvents, ACS Appl. Mater. Interfaces 11 (2019) 14313–14321. https://doi.org/10.1021/acsami.9b00728.

[215] BAuA, Product Safety Commission (AfPS) GS Specification Testing and assessment of polycyclic aromatic hydrocarbons (PAHs) in the course of awarding the GS mark - Specification pursuant to article 21 (1) no . 3 of the Product Safety Act (ProdSG) – Manage, (2014) 1–12.

[216] J. Wolksa, Safeguarding the environment - XRF analysis of heavy metals in polyethylene, Plast. Addit. Compd. 7 (2005) 36–39. https://doi.org/10.1016/S1464-391X(05)00334-X.

[217] H. Fink, U. Panne, M. Theisen, R. Niessner, T. Probst, X. Lin, Determination of metal additives and bromine in recycled thermoplasts from electronic waste by TXRF analysis, Fresenius. J. Anal. Chem. 368 (2000) 235–239. https://doi.org/10.1007/s002160000392.

[218] G.W. Curtzwiler, M. Schweitzer, Y. Li, S. Jiang, K.L. Vorst, Mixed post-consumer

recycled polyolefins as a property tuning material for virgin polypropylene, J. Clean. Prod. 239 (2019) 117978. https://doi.org/10.1016/j.jclepro.2019.117978.

[219] A. Prasad, A quantitative analysis of low density polyethylene and linear low density polyethylene blends by differential scanning calorimetery and fourier transform infrared spectroscopy methods, Polym. Eng. Sci. 38 (1998) 1716–1728. https://doi.org/10.1002/pen.10342.

[220] D. Li, L. Zhou, X. Wang, L. He, X. Yang, Effect of crystallinity of polyethylene with different densities on breakdown strength and conductance property, Materials (Basel). 12 (2019). https://doi.org/10.3390/ma12111746.

[221] F.E. Hanana, D. Rodrigue, Effect of particle size, fiber content, and surface treatment on the mechanical properties of maple-reinforced LLDPE produced by rotational molding, Polym. Polym. Compos. 29 (2021) 343–353. https://doi.org/10.1177/0967391120916602.

[222] D.G. Dikobe, A.S. Luyt, Thermal and mechanical properties of PP/HDPE/wood powder and MAPP/HDPE/wood powder polymer blend composites, Thermochim. Acta 654 (2017) 40–50. https://doi.org/10.1016/j.tca.2017.05.002.

[223] M. Bengtsson, M. Le Baillif, K. Oksman, Extrusion and mechanical properties of highly filled cellulose fibre-polypropylene composites, Compos. Part A Appl. Sci. Manuf. 38 (2007) 1922–1931. https://doi.org/10.1016/j.compositesa.2007.03.004.

[224] S. Migneault, A. Koubaa, P. Perré, Effect of fiber origin, proportion, and chemical composition on the mechanical and physical properties of wood-plastic composites, J. Wood Chem. Technol. 34 (2014) 241–261. https://doi.org/10.1080/02773813.2013.869604.

[225] M. Poletto, J. Dettenborn, M. Zeni, A.J. Zattera, Characterization of composites based on expanded polystyrene wastes and wood flour, Waste Manag. 31 (2011) 779–784. https://doi.org/10.1016/j.wasman.2010.10.027.

[226] X. Cai, B. Riedl, M. Bouaziz, Lignocellulosic composites with grafted polystyrene interfaces, Compos. Interfaces 12 (2005) 25–39. https://doi.org/10.1163/1568554053542124.

[227] M. Chakkour, M. Ould Moussa, I. Khay, M. Balli, T. Ben Zineb, Effects of humidity conditions on the physical, morphological and mechanical properties of bamboo fibers composites, Ind. Crops Prod. 192 (2023) 116085.

https://doi.org/10.1016/j.indcrop.2022.116085.

[228] C. Dolza, E. Fages, E. Gonga, J. Gomez-Caturla, R. Balart, L. Quiles-Carrillo, Development and characterization of environmentally friendly wood plastic composites from biobased polyethylene and short natural fibers processed by injection moulding, Polymers (Basel). 13 (2021). https://doi.org/10.3390/polym13111692.

[229] Y. Guo, S. Zhu, Y. Chen, D. Li, Thermal properties of wood-plastic composites with different compositions, Materials (Basel). 16 (2019). https://doi.org/10.3390/ma12060881.

[230] K.S. Chun, S. Husseinsyah, F.N. Azizi, Characterization and Properties of Recycled Polypropylene/Coconut Shell Powder Composites: Effect of Sodium Dodecyl Sulfate Modification, Polym. - Plast. Technol. Eng. 52 (2013) 287–294. https://doi.org/10.1080/03602559.2012.749282.

[231] K.P. Pramoda, Q.F. Lim, S. Chen, Synergistic effects of fillers on recycled polystyrene composites, Polym. Bull. 75 (2018) 1185–1195. https://doi.org/10.1007/s00289-017-2085-0.

[232] M.A. López Manchado, M. Arroyo, J. Biagiotti, J.M. Kenny, Enhancement of Mechanical Properties and Interfacial Adhesion of PP/EPDM/Flax Fiber Composites Using Maleic Anhydride as a Compatibilizer, J. Appl. Polym. Sci. 90 (2003) 2170–2178. https://doi.org/10.1002/app.12866.

[233] M. Alzerreca, M. Paris, O. Boyron, D. Orditz, G. Louarn, O. Correc, Mechanical properties and molecular structures of virgin and recycled HDPE polymers used in gravity sewer systems, Polym. Test. 46 (2015) 1–8. https://doi.org/10.1016/j.polymertesting.2015.06.012.

[234] M. Poletto, Effects of the coupling agent structure on the adhesion of recycled polystyrene wood flour composites: Thermal degradation kinetics and thermodynamics parameters, J. Compos. Mater. 50 (2016) 3291–3299. https://doi.org/10.1177/0021998315618250.

[235] S. Hwang, Y. Han, D.J. Gardner, Morphological characteristics of spray dried cellulose nanofibers produced using various wood pulp feedstocks and their effects on polypropylene composite properties, Compos. Part B Eng. 268 (2024) 111093. https://doi.org/10.1016/j.compositesb.2023.111093.

[236] Y. Karaduman, M.M.A. Sayeed, L. Onal, A. Rawal, Viscoelastic properties of surface modified jute fiber/polypropylene nonwoven composites, Compos. Part B Eng. 67 (2014) 111–118. https://doi.org/10.1016/j.compositesb.2014.06.019.

[237] V.G. Geethamma, G. Kalaprasad, G. Groeninckx, S. Thomas, Dynamic mechanical behavior of short coir fiber reinforced natural rubber composites, Compos. Part A Appl. Sci. Manuf. 36 (2005) 1499–1506. https://doi.org/10.1016/j.compositesa.2005.03.004.

[238] A. Sakamoto, M. Tasumi, Symmetry of the benzene ring and its normal vibrations: The "breathing" mode is not always a normal vibration of a benzene ring, J. Raman Spectrosc. 52 (2021) 2282–2291. https://doi.org/10.1002/jrs.6131.

[239] Y. Horikawa, S. Hirano, A. Mihashi, Y. Kobayashi, S. Zhai, J. Sugiyama, Prediction of Lignin Contents from Infrared Spectroscopy: Chemical Digestion and Lignin/Biomass Ratios of Cryptomeria japonica, Appl. Biochem. Biotechnol. 188 (2019) 1066–1076. https://doi.org/10.1007/s12010-019-02965-8.

[240] X. Zhang, F. Wang, L.M. Keer, Influence of surface modification on the microstructure and thermo-mechanical properties of bamboo fibers, Materials (Basel). 8 (2015) 6597–6608. https://doi.org/10.3390/ma8105327.

[241] H. Ahmad, E. Rostami-Tapeh-Esmaeil, D. Rodrigue, The effect of chemical crosslinking on the properties of Rotomolded high density polyethylene, J. Appl. Polym. Sci. 141 (2024) 1–15. https://doi.org/10.1002/app.54744.

[242] J. Liu, J. Liu, Characterization of maleic anhydride/styrene melt-grafted random copolypropylene and its impact on crystallization and mechanical properties of isotactic polypropylene, Polym. Bull. 76 (2019) 4369–4387. https://doi.org/10.1007/s00289-018-2609-2.

[243] L. Haile, Study of Recycling of Waste High Impact Polystyrene (PS-HI) and Polystyrene with Flame Retardant Additives (PS-FR) Co-Polymers, J. Text. Sci. Fash. Technol. 7 (2021) 1–11. https://doi.org/10.33552/jtsft.2021.07.000666.

[244] F. Guo, X. Zhang, R. Yang, L. Salmén, Y. Yu, Hygroscopicity, degradation and thermal stability of isolated bamboo fibers and parenchyma cells upon moderate heat treatment, Cellulose 28 (2021) 8867–8876. https://doi.org/10.1007/s10570-021-04050-y.

[245] D. Liu, J. Song, D.P. Anderson, P.R. Chang, Y. Hua, Bamboo fiber and its reinforced composites: Structure and properties, Cellulose 19 (2012) 1449–1480.

https://doi.org/10.1007/s10570-012-9741-1.

[246] K. Sheng, S. Zhang, S. Qian, C.A. Fontanillo Lopez, High-toughness PLA/Bamboo cellulose nanowhiskers bionanocomposite strengthened with silylated ultrafine bamboo-char, Compos. Part B Eng. 165 (2019) 174–182. https://doi.org/10.1016/j.compositesb.2018.11.139.

[247] Y. Wang, Y. Shi, W. Shao, Y. Ren, W. Dong, F. Zhang, L.Z. Liu, Crystallization, structures, and properties of different polyolefins with similar grafting degree of maleic anhydride, Polymers (Basel). 12 (2020). https://doi.org/10.3390/polym12030675.

[248] Q. Zhang, M.U. Khan, X. Lin, H. Cai, H. Lei, Temperature varied biochar as a reinforcing filler for high-density polyethylene composites, Compos. Part B Eng. 175 (2019) 107151. https://doi.org/10.1016/j.compositesb.2019.107151.

[249] S. Luo, C. Lv, L. Chang, W. Guo, Enhancing Crystallization and Toughness of Wood Flour/Polypropylene Composites via Matrix Crystalline Modification: A Comparative Study of Two β-Nucleating Agents, Polymers (Basel). 14 (2022). https://doi.org/10.3390/polym14173561.

[250] N. Ayrilmis, M. Taşdemir, T. Akbulut, Water absorption and mechanical properties of PP/HIPS hybrid composites filled with wood flour, Polym. Compos. 38 (2017). https://doi.org/10.1002/pc.23647.

[251] A.F. Carrera, Coupling Agent Usage in the Preparation of Cellulose Nanofibril (CNF) - and Cellulose Nanocrystal (CNC) -Based Nanocomposites, in: A.D. Hanieh Kargarzadeh, Ishak Ahmad, Sabu Thomas (Ed.), Handb. Nanocellulose Cellul. Nanocomposites, wiley, 2017: pp. 335–364. https://doi.org/https://doi.org/10.1002/9783527689972.ch10.

[252] H. Zhou, W. Li, X. Hao, G. Zong, X. Yi, J. Xu, R. Ou, Q. Wang, Recycling end-of-life WPC products into ultra-high- filled , high-performance wood fiber / polyethylene composites : a sustainable strategy for clean and cyclic processing in the WPC industry, J. Mater. Res. Technol. 18 (n.d.) 1–14. https://doi.org/10.1016/j.jmrt.2022.02.091.

[253] Z.M.O. Rzayev, Graft Copolymers of Maleic Anhydride and Its Isostructural Analogues : High Performance Engineering Materials, 2011.

[254] O. Hosseinaei, S. Wang, A.A. Enayati, T.G. Rials, Effects of hemicellulose extraction on properties of wood flour and wood-plastic composites, Compos. Part A Appl. Sci. Manuf.

43 (2012) 686–694. https://doi.org/10.1016/j.compositesa.2012.01.007.

[255] D.M. Panaitescu, Z. Vuluga, M. Ghiurea, M. Iorga, C. Nicolae, R. Gabor, Influence of compatibilizing system on morphology, thermal and mechanical properties of high flow polypropylene reinforced with short hemp fibers, Compos. Part B Eng. 69 (2015) 286–295. https://doi.org/10.1016/j.compositesb.2014.10.010.

[256] I. Debbah, R. Krache, N. Aranburu, M. Fernández, A. Etxeberria, Effect of SEBS-g-MAH addition on the mechanical, rheological, and morphological properties of polycarbonate/acrylonitrile–butadiene–styrene blends, J. Elastomers Plast. 50 (2018) 611–633. https://doi.org/10.1177/0095244317753652.

[257] H. Gao, Q.-W. Wang, H.-G. Wang, Y.-M. Song, Properties of highly filled wood fiber-maleic anhydride grafted thermoplastic blends composites, 2010. https://doi.org/10.4028/www.scientific.net/AMR.113-116.1856.

[258] H. Ismail, L. Mega, H.P.S. Abdul Khalil, Effect of a silane coupling agent on the properties of white rice husk ash-polypropylene/natural rubber composites, Polym. Int. 50 (2001) 606–611. https://doi.org/10.1002/pi.673.

[259] R. Sonnier, E. Leroy, L. Clerc, A. Bergeret, J.M. Lopez-Cuesta, A.S. Bretelle, P. Ienny, Compatibilizing thermoplastic/ground tyre rubber powder blends: Efficiency and limits, Polym. Test. 27 (2008) 901–907. https://doi.org/10.1016/j.polymertesting.2008.07.003.

[260] S. Chandgude, S. Salunkhe, In state of art: Mechanical behavior of natural fiber-based hybrid polymeric composites for application of automobile components, Polym. Compos. 42 (2021) 2678–2703. https://doi.org/10.1002/pc.26045.

[261] C. Arslan, M. Dogan, The effects of fiber silane modification on the mechanical performance of chopped basalt fiber/ABS composites, J. Thermoplast. Compos. Mater. 33 (2020) 1449–1465. https://doi.org/10.1177/0892705719829515.

[262] D. Kusić, U. Božič, M. Monzón, R. Paz, P. Bordón, Thermal and mechanical characterization of banana fiber reinforced composites for its application in injection molding, Materials (Basel). 13 (2020). https://doi.org/10.3390/MA13163581.

[263] L. Ma, H. He, C. Jiang, L. Zhou, Y. Luo, D. Jia, Effect of alkali treatment on structure and mechanical properties of acrylonitrile-butadiene-styrene/bamboo fiber composites, J. Macromol. Sci. Part B Phys. 51 (2012) 2232–2244. https://doi.org/10.1080/00222348.2012.669688.

[264] O. Ozenc, M.A. Dundar, D.E. Sahin, Examination of compressive and flexural behaviors of acrylonitrile-butadiene-styrene filled with hemp fiber particles, J. Thermoplast. Compos. Mater. 37 (2024). https://doi.org/10.1177/08927057231186326.

[265] S.R. Scagliusi, E.C.L. Carvalho, A.B. Lugão, Introduction to the Study of Mechanical Properties of Terpolymer PP/EPDM Mixtures, J. Res. Updat. Polym. Sci. 10 (2021) 1–8. https://doi.org/10.6000/1929-5995.2021.10.1.

[266] S-Y. Leu, T-H. Yang, S-F Lo, Te-Hsin Yang, Optimized material composition to improve the physical and mechanical properties of extruded wood-plastic composites (WPCs), Constr. Build. Mater. 29 (2012) 120–127. https://doi.org/10.1016/j.conbuildmat.2011.09.013.

[267] E. Kuram, Rheological, mechanical and morphological properties of acrylonitrile butadiene styrene composite filled with sunflower seed (Helianthus annuus L.) husk flour, J. Polym. Res. 27 (2020). https://doi.org/10.1007/s10965-020-02211-4.

[268] J.F., Horta, F.J. Simões, Mateus, A. Study of Wood-Plastic Composites with Reused High Density Polyethylene and Wood Sawdust. Procedia Manuf. 2016, 12, 221–229, 2017

[269] W. Zhang, X.Yao, S.Khanal, S. Xu, A novel surface treatment for bamboo flour and its effect on the dimensional stability and mechanical properties of high density polyethylene/bamboo flour composites, Constr. Build. Mater. 86(1) (2018) 1220–1227. https://doi.org/10.1016/j.conbuildmat.2018.08.003

[270] K.M.M. Billah, F.A.R. Lorenzana, N.L. Martinez, S. Chacon, R.B. Wicker, D. Espalin, Thermal analysis of thermoplastic materials filled with chopped fiber for large area 3D printing, Solid Free. Fabr. 2019 Proc. 30th Annu. Int. Solid Free. Fabr. Symp. - An Addit. Manuf. Conf. SFF 2019 (2019) 892–898.

[271] S.Y. Fu, X.Q. Feng, B. Lauke, Y.W. Mai. Effects of particle size, particle/matrix interface adhesion and particle loading on mechanical properties of particulate-polymer composites, Compos. Part B Eng. 2008;39: 933–961. https://doi.org/10.1016/j.compositesb.2008.01.002..